Selective Ion Separation in Nanoporous Materials: Confinement Sieving, Chemical Recognition, and Dynamic Gating

Journal:	*SCIENCE CHINA Materials*
Manuscript ID	SCMs-2026-1729.R1
Manuscript Type:	Review
Date Submitted by the Author:	29-Jul-2026

Complete List of Authors:	Dai, Chaoyang Xu, Zhicheng Luo, Hao Zhou, Tianyang Shao, Yinzi Wu, Tianhao XIE, Linghai; Nanjing University of Posts and Telecommunications Feng, Quanyou; Nanjing University of Posts and Telecommunications,

Keywords:	selective ion separation, nanoporous materials, confinement sieving, chemical recognition, dynamic gating
Speciality:	Adsorption and Separation Materials

SCHOLARONE MANUSCRIPTS

Point-by-point response to reviewers

We would like to express our gratitude to the Editor and Reviewers for their insightful feedback on our manuscript. In light of their valuable comments, we have carefully revised the paper, aiming to incorporate their suggestions effectively. These revisions are detailed below.

Reviewer #1: This review article provides a comprehensive and timely overview of the application of nanoporous materials for isovalent ion separation.

It is well-structured and highlights both current progresses, challenges and future research directions. However, a major revision is needed prior to being accepted for publication at SCIENCE CHINA Materials.

We sincerely thank you for your positive assessment and valuable suggestions.

1. The introduction session should more specifically define this review's unique contribution compared to other reviews on isovalent ion separation. Is it the specific focus on MOFs, COFs materials? Other nanoporous materials such as biochar should also be included in this review.

We sincerely thank you for your insightful and constructive comment. In response, we have substantially revised the Introduction to more clearly articulate the unique contribution of this Review. Rather than introducing another material-based classification of ion-separation systems, the Review adopts the sequential ion transport process as a unified conceptual framework to systematically compare the separation mechanisms across diverse nanoporous materials. Specifically, the revised Introduction discusses size- and solvation-based sieving, chemical recognition, and dynamic gating from the perspectives of pore entry and solvation reorganization, interfacial partitioning and ion–site interactions, intrapore migration, and outlet-side release. We believe that this transport-process-oriented framework provides a more general and mechanistic perspective for understanding and comparing selective ion separation across diverse nanoporous platforms.

In addition, following your valuable suggestion, we have considerably broadened the scope of materials covered in this Review. Beyond MOFs and COFs, the revised manuscript now includes zeolites and other inorganic molecular sieves, two-dimensional materials (e.g., graphene oxide and MXenes), microporous polymer membranes, ion-exchange membranes, biomimetic nanochannels, organic–inorganic composites, functionalized porous carbons, and biochars. In particular, biochar has now been explicitly incorporated into the Introduction, Table 2, Section 2.2, Section 3.3, and

For Review Only

Table 4. Moreover, to improve the scientific rigor of the discussion, we distinguish among surface complexation, ion exchange, intrapore retention, and mineral-phase-induced precipitation as different ion-removal mechanisms, rather than attributing the overall removal capacity solely to specific adsorption.

The corresponding revisions have been incorporated into the Introduction, Table 2, Section 2.2, Section 3.3, and Table 4, and are highlighted in yellow in the revised manuscript.

2. Section 2 provides an excellent overview on three separation mechanisms: size sieving, chemical recognition and dynamic gating. A valuable addition would be a discussion on how these three mechanisms interact and potentially compete in real, multi-ion separations, and whether there are models attempting to predict performance based on these interactions.

We thank you for this valuable comment. We agree with this suggestion and have added a dedicated Section 2.4, "Synergy among Multiple Mechanisms." The three mechanisms are no longer treated as independent categories. Instead, the revised section discusses three principal forms of coupling:

(1) coupling among geometric confinement, confined-solvent structure, and interfacial affinity within the same pore domain;

(2) spatial division of function among different structural regions, such as an entrance-gating layer followed by low-resistance internal transport pathways; and

(3) ion-ion coupling arising from multi-ion occupancy, co-ion/counter-ion migration, and electroneutrality constraints.

We also discuss situations in which these mechanisms counteract, rather than reinforce, one another. For example, a reduced entry barrier may be offset by slow intrapore diffusion, while strong chemical recognition may lead to kinetic retention when outlet-side release is hindered. The dominant rate-limiting step may also shift among interfacial partitioning, intrapore migration, and ion release as salinity and site occupancy change.

To address the modeling aspect, we have substantially expanded Section 4.2 to cover explicit-solvent free-energy calculations, competitive multi-ion occupancy, molecular dynamics, classical density functional theory approaches, coupled Poisson-Nernst-Planck/Navier–Stokes models, and membrane- and device-scale transport models. Rather than claiming a condition-independent universal selectivity model, we now emphasize that local free energies, partitioning, diffusion, multicomponent friction, and

For Review Only

process boundary conditions must be quantitatively integrated and independently validated under different feed compositions, membrane thicknesses, and continuous-flow conditions.

The corresponding revisions have been incorporated into the Section 2.4 and Section 4.2, and are highlighted in yellow in the revised manuscript.

3. A significant weakness of this article is the reliance solely on reproduced figures from other researchers in the literature. A high-impact review should include original, self-created schematic diagrams summarizing the core mechanisms and material strategies, plus a comprehensive table comparing the performance, advantages, and limitations of different nanoporous materials types/strategies.

We sincerely thank you for this valuable suggestion. In response to this comment, we have added an original schematic Figure 2, which integrates partial ion desolvation, pore entry, the operando effective aperture, and the corresponding performance regimes associated with excessively narrow, optimal, excessively wide, and defect-containing channels. Rather than representing a specific material system, this figure provides a unified mechanistic framework to illustrate size- and solvation-dependent ion sieving.

We have also reconstructed Figure 1a to present publication trends and introduced Figure 6 to conceptually clarify the comparability boundaries among different performance metrics and testing modes. For panels adapted from previous studies, the captions have been revised to consistently indicate “adapted from” the corresponding references, and the sources of all reproduced or adapted panels have been carefully checked.

In addition, five tables with distinct purposes have been incorporated into the revised manuscript:

Table 1 compares different ion-pair classes, their physicochemical characteristics, dominant mechanisms, and potential confounding factors;

Table 2 summarizes the structures, representative performance, advantages, and limitations of major nanoporous material platforms;

Table 3 provides quantitative comparisons of membrane and nanochannel performance together with the corresponding testing conditions;

Table 4 compares selective adsorbents in terms of competitive capture, kinetics, and regeneration performance;

Table 5 summarizes continuous operation performance, performance evolution, post-

For Review Only

operation characterization evidence, product metrics, and energy requirements.

Changes in the manuscript: Figure 2, Figure 6, and Tables 1–5 have been added or revised accordingly.

4. The overall structure is solid. However, the ultimate goal of such a comprehensive review is to provided guidance for future research in this area. It is suggested to put forward more specific and implementable future directions, not only for NF membranes, but also for adsorptive nanoporous materials.

We sincerely thank you for this valuable suggestion. We have adopted this recommendation and distributed more actionable future directions across the mechanistic understanding, performance evaluation, and validation levels, rather than limiting them to a general statement in the concluding section.

For membranes and nanochannels, we now recommend the simultaneous reporting of absolute fluxes for target and competing ions, mixed-feed selectivity, membrane thickness, and effective area, followed by validation under high-salinity conditions, varying ion ratios, continuous-flow operation, and module-scale scenarios. For adsorptive materials, we emphasize the need to move beyond single-component maximum adsorption capacity toward the evaluation of competitive working capacity, breakthrough capacity, accessible-site utilization, mass transfer after shaping, product concentration, and regenerant consumption per unit amount recovered.

Regarding operational stability, we recommend evaluating cumulative treatment load rather than relying solely on operating time or cycle number. We further highlight the importance of assessing wet-state structural integrity, functional-site retention, flux/capacity retention, product purity, recovery, energy consumption, and chemical inputs within a consistent evaluation boundary. In Section 4, we additionally propose constraining models with operando observations, validating predictions beyond calibration conditions, and applying active learning to identify the next experiments with the greatest mechanistic or design value.

Changes in the manuscript: Sections 3.1–3.4 and Sections 4.1–4.3 have been added or revised accordingly.

Reviewer #2: This Review discusses nanoporous materials for ion separation from the perspectives of size sieving, chemical recognition, dynamic gating, in situ/operando characterization, and data-guided materials design. The attempt to organize the literature according to transport processes rather than merely according to material classes is potentially valuable. The proposed “space–time–data” framework may also provide a useful conceptual structure for connecting pore/interface design,

For Review Only

dynamic transport observation, and computational optimization.

However, the manuscript in its present form has a fundamental inconsistency in scope. Although the title and central premise emphasize isovalent ion separation, a substantial fraction of the discussion, including several key examples and figures, concerns Li^+/Mg^{2+} separation, which is heterovalent rather than isovalent. This conceptual inconsistency affects the classification of mechanisms and the conclusions drawn throughout the manuscript. In addition, the Review remains largely descriptive, with insufficient quantitative benchmarking and limited critical differentiation from existing reviews. Several figures, tables, terminology choices, and mechanistic statements also require careful correction.

I therefore recommend major revision before the manuscript can be considered for publication in Science China Materials.

We sincerely thank you for your positive comments and valuable suggestions.

1. The definition and scope of "isovalent ion separation" must be fundamentally reconsidered.

The manuscript defines isovalent ions using examples such as K^+/Na^+ and Mg^{2+}/Ca^{2+}. However, many of the principal examples subsequently discussed are based on Li^+/Mg^{2+} separation, including the COF membrane, NP-MXene membrane, crown-ether-functionalized MXene membrane, salt-lake lithium extraction, and several stability cases.

Li^+ and Mg^{2+} do not have identical valence states. Therefore, Li^+/Mg^{2+} separation cannot be classified as isovalent ion separation. Moreover, electrostatic exclusion, Donnan effects, charge density, and ion–surface interactions can differ substantially between monovalent and divalent ions, making Li^+/Mg^{2+} separation mechanistically distinct from Li^+/Na^+, Na^+/K^+, Mg^{2+}/Ca^{2+}, or lanthanide-lanthanide separation.

The authors are suggested to follow either one of the following approaches:

- strictly restrict the Review to genuinely isovalent ion pairs and substantially revise the literature coverage; or

- broaden the title and central scope to "selective ion separation", "chemically similar ion separation", or "nanoconfined separation of competing ions", and explicitly distinguish isovalent and heterovalent systems.

A dedicated classification table should be added, separating at least:

For Review Only

- monovalent/monovalent pairs, such as Li^+/Na^+ and Na^+/K^+;
- divalent/divalent pairs, such as Mg^{2+}/Ca^{2+};
- heterovalent pairs, especially Li^+Mg^{2+};
- chemically similar multivalent ions, such as rare-earth ions.

Without resolving this issue, the title and central conclusions are scientifically misleading.

We appreciate your insightful comment and fully agree that the original definition and scope of "isovalent ion separation" require reconsideration. Accordingly, we have adopted the second option suggested by the Reviewer and broadened the scope of this Review to selective ion separation, with ion systems carefully classified according to their valence relationships.

The revised title is: **Selective Ion Separation in Nanoporous Materials: Confinement Sieving, Chemical Recognition, and Dynamic Gating.**

The revised Abstract and Introduction now explicitly distinguish four categories of ion separation systems:

(1) isovalent monovalent ion pairs, such as Li^+/Na^+ and Na^+/K^+;

(2) isovalent divalent ion pairs, such as Mg^{2+}/Ca^{2+} and Co^{2+}/Ni^{2+};

(3) heterovalent ion pairs, particularly Li^+/Mg^{2+};

(4) chemically similar isovalent multivalent ions, such as adjacent lanthanides.

We have added Table 1 to compare the physicochemical differences, dominant separation factors, and major confounding factors among these four classes. In addition, Section 3.2 has been reorganized into separate subsections covering heterovalent ions, isovalent monovalent ions, and isovalent multivalent ions. Importantly, Li^+/Mg^{2+} separation examples are no longer used to directly interpret the mechanisms of isovalent ion separation. Instead, we explicitly clarify that the high selectivity observed in heterovalent systems is often strongly affected by Donnan partitioning, charge density, and electrostatic exclusion, and therefore should not be regarded as direct evidence for precise size-selective recognition.

Changes in the manuscript: The title and Abstract have been revised; Table 1 has been added; and Sections 3.2.1–3.2.3 have been reorganized accordingly.

2. A quantitative benchmarking section is essential.

For Review Only

The Review repeatedly emphasizes the selectivity – permeability trade-off, but it does not provide a systematic quantitative comparison across materials. At present, isolated values are quoted under different feed compositions, membrane thicknesses, driving forces, test modes, and definitions of selectivity. Such values cannot be compared directly. Some of the following items may be compared together:

- ion pair and valence relationship;
- membrane/material type;
- membrane thickness and effective area;
- feed composition and competing-ion ratio;
- concentration and pH;
- temperature;
- driving force;
- test configuration, such as diffusion, pressure-driven, electrically driven, or concentration-gradient transport;
- ion flux or permeance;
- selectivity definition;
- operation duration;
- test in real or simulated feed;
- original reference.

A selectivity – flux or selectivity – permeance plot would also be valuable, provided that the authors normalize or clearly group data according to testing conditions. Otherwise, the discussion of the trade-off remains qualitative.

We sincerely thank you for this valuable suggestion. We fully agree that isolated numerical values without clearly defined testing conditions and evaluation criteria may hinder meaningful comparison among different materials. Accordingly, we have added a dedicated Section 3.1, entitled “Performance Metrics, Testing Modes, and Comparability Boundaries”, to clarify the physical meanings of selectivity, flux, permeability, rejection, and ionic conductivity. In this section, we further distinguish single-salt and mixed-salt tests, diffusion-based and pressure-/electrically driven transport, as well as electrical current and molar flux, to establish clearer comparison

For Review Only

boundaries. Figure 6 has been added to illustrate the distinction between ideal selectivity and true mixed-feed selectivity, and to demonstrate how feed concentration, competing ions, and testing configurations influence the interpretation of separation performance.

In addition, Table 3 has been added to provide a condition-resolved quantitative comparison of representative reported systems, including:

(1) ion systems and valence relationship;

(2) material types and membrane thicknesses/effective areas;

(3) feed compositions and testing conditions;

(4) testing modes and driving forces;

(5) absolute flux or permeation performance;

(6) selectivity definitions and corresponding values;

(7) operation duration and the use of real or simulated feeds; and

(8) original references.

For adsorbent-based systems and long-term operation studies, Tables 4 and 5 have also been revised to include additional practical performance parameters, such as working capacity, kinetics, regeneration methods, continuous-flow validation, performance stability, product metrics, and energy consumption.

We have carefully considered constructing a universal selectivity-permeability plot. However, the driving forces, selectivity definitions, and transport quantities reported in different studies are often physically incompatible, and forced normalization would create a potentially misleading ranking. We therefore perform rigorous quantitative comparison only when the ion system, feed, driving force, and metric definition are sufficiently consistent; otherwise, the data are used only to compare trends or orders of magnitude.

Changes have been made in Section 3.1, Figure 6, and Tables 3–5 of the revised manuscript.

3. The treatment of chemical recognition should distinguish adsorption selectivity from membrane transport selectivity.

The manuscript sometimes implies that stronger binding to a target ion leads to higher permeation. However, strong binding can increase membrane partitioning while

For Review Only

decreasing diffusivity and delaying desorption. In other systems, the strongly bound ion may be retained rather than preferentially transported.

The authors should formulate the discussion using a solution − diffusion or partition − diffusion framework. This framework would clarify why stronger ion − ligand affinity does not necessarily produce higher permeability and why selective capture, selective transport, and selective release must be distinguished.

Site saturation, binding-site density, cooperative binding, competitive displacement, and regeneration kinetics may also be discussed.

uld become an actionable design strategy rather than a general outlook on AI.

Note: The final sentence above is reproduced verbatim from the decision letter, in which it appears truncated.

To address the identifiable substantive points in this comment, we have reorganized Section 2.2 accordingly. In the revised manuscript, we explicitly clarify that chemical recognition primarily affects ion partitioning into the membrane phase, whereas preferential partitioning does not necessarily lead to preferential permeation. Within a simplified concentration-gradient-driven partition–diffusion framework that neglects electromigration and cross-component coupling, the ion flux is expressed as:

$$J_i = \frac{K_i D_i}{\ell} \Delta c_i$$

As discussed in the revised text, strengthening ion-site interactions may increase the partition coefficient K_i; however, it may also prolong the residence time of ions, reduce the intramembrane diffusion coefficient D_i, and increase the dissociation resistance during release from the membrane. Accordingly, the revised manuscript clearly distinguishes among intramembrane enrichment, selective retention, and preferential transmembrane transport.

In addition, we have added a new Section 3.3, entitled “Selective Adsorption and Ion Capture,” which adopts a capture–dissociation–intrapore diffusion–release framework and separately discusses:

(1) equilibrium affinity and site utilization;

(2) competitive occupancy and working capacity;

(3) intrapore mass transfer and material-shaping effects; and

(4) release and reversible capture.

Within this section, we also discuss site saturation, binding-site density, competitive

For Review Only

displacement, cooperative effects associated with neighbouring sites and multi-ion occupancy, the distinction between maximum and working capacities, breakthrough capacity, desorption conditions, product-stream concentration, and regenerant consumption. Furthermore, we distinguish the completion of a single capture–release cycle in Section 3.3 from long-term regeneration stability, which is discussed separately in Section 3.4.

We have also addressed the discernible request for an actionable data-guided design strategy in Section 4.3. The revised text specifies a workflow that retains condition-complete data objects, uses physically informed structural representations, applies grouped validation and uncertainty analysis, and uses active learning to select experiments under previously untested materials and feed conditions. Corresponding changes have been made in Sections 2.2, 3.3, and 4.3 of the revised manuscript.

4. Operational stability and practical relevance require clearer benchmarks.

The Review appropriately emphasizes realistic feeds, fouling, swelling, and long-term operation. However, “long-term stability” is used without a consistent definition. Tests lasting several hours or seven days should not automatically be treated as evidence of industrial durability.

Some of the following issues are suggested to discuss in this section:

- continuous-flow rather than static diffusion tests;
- membrane area and module configuration;
- repeated regeneration cycles;
- flux and selectivity retention;
- structural and chemical analysis after operation;
- real-brine or realistic multi-component feeds;
- resistance to pH changes, organic matter, colloids, and multivalent-ion precipitation;
- energy consumption and recovery ratio.

A distinction should also be made among material stability, membrane structural stability, functional-site stability, and process-level performance stability.

We sincerely thank you for this valuable comment. We have accepted this suggestion and added a comprehensive Section 3.4, “Operational Stability and Process Performance.” Stability is now explicitly categorized into four levels:

For Review Only

(1) chemical stability of the material;

(2) structural stability of pores, membrane – support interfaces, and particles;

(3) stability of functional sites, fixed charges, and responsive units; and

(4) process-performance stability in terms of product purity, recovery, productivity, and energy consumption.

Section 3.4.1 explains that operating time and cycle number alone do not adequately represent actual stability. Treatment volume per unit area, cumulative target-ion transport, the number of bed volumes, regeneration count, and pressure or electric-field history should also be reported. We also explicitly distinguish the evidence provided by static diffusion or batch adsorption tests from that obtained using continuous-flow membrane cells, fixed-bed systems, and cyclic electrochemical devices.

Section 3.4.2 addresses selectivity drift caused by high salinity, pH variation, organic matter, colloids, and scaling precursors. Section 3.4.3 emphasizes that post-operation changes in wet-state structure, surface charge, pore-size distribution, component leaching, residual occupying ions, and functional-group state should be correlated with flux and selectivity drift. Section 3.4.4 distinguishes single-cycle desorption from long-term functional recovery. Section 3.4.5 further discusses membrane area, flow distribution, module defects, fixed-bed channeling, product purity, recovery, energy consumption, and chemical inputs.

Table 5 now includes dedicated columns for “Operation/Load,” “Performance Retention or Drift,” “Regeneration/Fouling/Post-operation Evidence,” “Product and Energy Metrics,” and “Evidence Boundary,” thereby avoiding the direct interpretation of several hours or days of laboratory operation as evidence of industrial stability.

Changes have been made in Section 3.4 and Table 5 of the revised manuscript.

5. The figure – caption does not match the content of Figure 7.

We sincerely thank you for identifying this inconsistency. We have carefully rechecked and revised the complete caption of Figure 7 to ensure consistency between the caption and the corresponding figure panels, including the materials, testing systems, and interpretation of each dataset.

In the revised Figure 7:

Figures 7a and 7b correspond to OSARIP polyamide nanofiltration membranes and present the effects of mean pore size on water permeance, Li^{+} and Mg^{2+} rejection,

For Review Only

Li^+/Mg^{2+} selectivity, and ion permeability.

Figures 7c and 7d correspond to COF-EOx/PAN membranes and present salt permeances, Li^+/Mg^{2+} selectivity in binary $LiCl/MgCl_2$ feed solutions, and mixed-feed permeances normalized against the corresponding single-salt values.

The order of the examples in the main text, panel labels, and reference numbers has also been carefully checked and corrected for consistency.

Changes in the manuscript: Figure 7, its caption, and the associated discussion in Section 3.2.1 have been revised accordingly.

6. The bibliometric methodology should be provided for Figure 1

We appreciate your valuable suggestion. We have revised the caption of Figure 1 to provide detailed information on the bibliometric methodology, including the database, search date, publication time range, document types, primary search terms, duplicate-removal procedure, and the partial-year nature of the 2026 data.

Changes in Figure 1 caption of the manuscript have been made accordingly.

7. The Review should cover genuinely important isovalent-ion pairs more comprehensively.

We sincerely appreciate your valuable comment. In response to this suggestion, we have substantially expanded the discussion of important isovalent-ion systems in the revised manuscript.

For isovalent monovalent ions, a dedicated Section 3.2.2 has been added to discuss Li^+/Na^+, Li^+/K^+, and Na^+/K^+ separation systems, including randomly oriented COF membranes, KcsA-inspired channels, crown-ether-pillared angstrom-scale channels, and amino-acid-functionalized COF membranes with pH-switchable Na^+/K^+ selectivity. We have also explicitly clarified the direction of separation by discussing whether the target ion is preferentially transported or retained and enriched through the removal of competing ions.

For isovalent divalent and multivalent ions, Section 3.2.3 has been expanded to cover Mg^{2+}/Ca^{2+}, representative transition-metal-ion systems (including Cu^{2+}/M^{2+} and Co^{2+}/Ni^{2+}), and adjacent lanthanide ions. These discussions focus on the recognition of intact hydration structures, competitive coordination, transformation of solution species, ligand-exchange kinetics, and preorganized multidentate binding sites.

In addition, Table 1 has been revised to separately classify isovalent monovalent,

For Review Only

isovalent divalent, and chemically similar isovalent multivalent ions. Figure 8 has also been updated to integrate representative examples of isovalent monovalent ion transport and coordination–diffusion coupling mechanisms in isovalent divalent-ion separation. The corresponding changes have been made in Table 1, Sections 3.2.2 and 3.2.3, and Figure 8 of the revised manuscript.

For Review Only

Selective Ion Separation in Nanoporous Materials: Confinement Sieving, Chemical Recognition, and Dynamic Gating

Chaoyang Dai[2], Zhicheng Xu[1], Hao Luo[3], Tianyang Zhou[2], Yinzi Shao[4], Haotian Wu[1], Linghai Xie[1]* and Quanyou Feng[1]*

1 State Key Laboratory of Flexible Electronics, Institute of Advanced Materials, Centre for Molecular Systems and Organic Devices, Nanjing University of Posts & Telecommunications, 9 Wenyuan Road, Nanjing 210023, China

2 College of Electronic and Optical Engineering & College of Flexible Electronics (Future Technology), Nanjing University of Posts and Telecommunications, 9 Wenyuan Road, Nanjing 210023, China

3 School of Communications and Information Engineering, Nanjing University of Posts and Telecommunications, 9 Wenyuan Road, Nanjing 210023, China

4 Xuzhou University of Technology, 2 Lishui Road, Xuzhou 221018, China

* Corresponding authors (email: iamlhxie@njupt.edu.cn; iamqyfeng@njupt.edu.cn)

Abstract: Selective ion separation is important for resource recovery, water treatment, lithium extraction from salt lakes, and nuclear-waste management. However, differences among ions in size, solvation structure, and coordination behaviour are often extremely limited, while the separation process is further influenced by valence, interfacial charge, and competing ions. Nanoporous materials possess tunable subnanometre channels and chemically active interfaces, enabling regulation of ion entry, solvation reorganization, interfacial partitioning, intrapore migration, and release. This Review examines three mechanisms—size- and solvation-based sieving, chemical recognition, and dynamic gating—from the perspective of confined transport and ion–pore interactions, and compares their roles and coupling relationships in systems involving isovalent monovalent ions, isovalent divalent ions, heterovalent ions, and chemically similar multivalent ions. On this basis, selective adsorption, intramembrane enrichment, and transmembrane transport are further distinguished, and the effects of selectivity definitions, ion flux, feed composition, driving force, and operating time on performance evaluation are discussed. Existing studies continue to face three major challenges: limited comparability of performance data obtained under different testing conditions, a lack of direct evidence for ion solvation, site occupancy, and migration under operating conditions, and insufficient functional stability in complex feeds and during long-term operation. To address these issues, this Review summarizes advances in in situ/operando characterization, multiscale simulation, and data-driven methods, and proposes a research framework that connects wet-state pore structures, interfacial chemistry, transport kinetics, and process performance, thereby providing guidance for the development of nanoporous separation materials with high selectivity, high flux, and long-term stability.

Keywords: selective ion separation; nanoporous materials; confinement sieving; chemical recognition; dynamic gating

1. Introduction

Selective ion separation is a fundamental process in lithium extraction from salt lakes, seawater desalination, critical-metal recovery, water treatment, and nuclear-waste management.[1–4] In contrast to the separation of gases or neutral molecules, ion transport depends not only on geometric size but also on solvation structure, valence, charge density, coordination preference, and interfacial potential. In systems containing multiple competing ions, these factors are mutually coupled and vary with salinity, composition, and external driving force, making it difficult to establish a simple one-to-one correspondence between material structure and separation outcome.[5–9]

The physicochemical basis of separation differs among ion systems. Isovalent monovalent ions, such as Li^+/Na^+ and Na^+/K^+, have the same charge and similar sizes, and the exploitable differences arise primarily from solvation strength, desolvation penalties, and weak ion–pore-wall interactions.[5–7,10] For isovalent divalent ions, such as Mg^{2+}/Ca^{2+} and Co^{2+}/Ni^{2+}, coordination number, coordination geometry, and ligand-exchange kinetics contribute in addition to the above factors.[5,7,11] For heterovalent ion pairs such as Li^+/Mg^{2+}, electrostatic partitioning, Donnan exclusion, and differences in charge density generally make more pronounced contributions.[3,5,11] Selectivities obtained for ions with different valence relationships therefore cannot be explained using the same mechanism, and a high separation factor in a heterovalent system cannot simply be regarded as evidence of precise size recognition or specific coordination. Chemically similar multivalent ions, such as adjacent lanthanides, impose an even greater requirement on materials to distinguish subtle differences in coordination and desolvation.[12]

Nanoporous materials provide a unique space in which these factors can be regulated. Their pore entrances and channels can be reduced to the subnanometre scale, while the charge, polarity, coordination sites, and wettability of the pore walls can be tuned through compositional design or postsynthetic modification.[5,8,9,11,13] As an ion approaches and enters a pore from the feed side, its solvation shell may be compressed, reorganized, or partially removed. Once inside the confined space, the ion further undergoes interfacial partitioning, transient binding, intrapore diffusion, and release at the outlet. The structural requirements imposed on a material differ across these transport stages: narrowing the pore entrance may amplify differences in desolvation between ions, but it also increases the entry resistance of the target ion; interfacial interactions, meanwhile, affect both intramembrane partitioning and subsequent migration. Macroscopic selectivity is therefore determined by the continuous sequence of ion entry, partitioning, migration, and release, rather than being a direct mapping of pore size, surface charge, or binding constant.

The relevant material platforms have expanded from zeolites and inorganic molecular sieves with relatively fixed pore sizes to metal–organic frameworks and covalent organic frameworks with programmable pore structures and interfacial chemistry, as well as two-dimensional materials such as graphene oxide and MXenes with tunable interlayer spacing and surface terminations.[10,11,14,15] Microporous polymer membranes, ion-exchange membranes, biomimetic nanochannels, and organic–inorganic composite membranes have further diversified the available pore architectures.[8,9,16] Amorphous porous materials, including functionalized porous carbons and biochars, provide platforms for ion adsorption and capture that are jointly governed by heterogeneous pore structures and surface sites.[17,18] The continued expansion of material systems has broadened the design space, but has not automatically yielded transferable rules across material classes: similar nominal pore sizes can produce different ion-transport sequences, while the

same recognition group may promote target-ion enrichment during adsorption yet create difficult-to-release trapped states during membrane transport.[5,8,9,13]

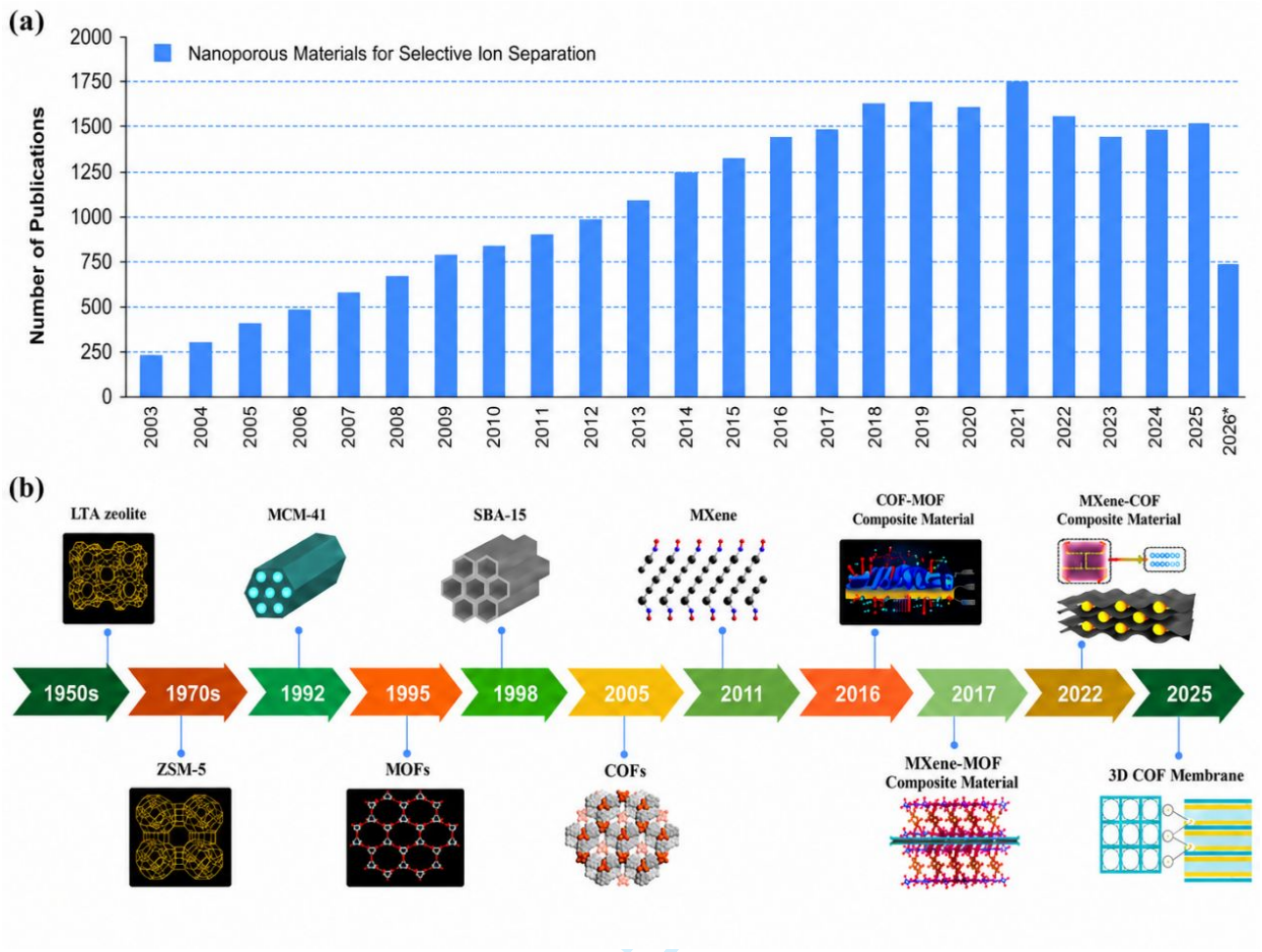


Figure 1 Publication trends and evolution of nanoporous platforms for selective ion transport.
(a) Annual number of publications related to nanoporous materials for selective ion transport from 2003 to 2026. Records were retrieved from the Web of Science Core Collection on 26 July 2026 using a topic search combining terms related to nanoporous materials, nanoporous membranes, nanochannels, ion sieving, selective ion transport, and selective ion separation. The timespan was restricted to 2003–2026, and only Articles and Reviews were included. Duplicate records were removed before annual counting. The 2026 value represents a partial-year count. (b) Selected milestones illustrating the expansion from rigid inorganic molecular sieves to chemically programmable frameworks, two-dimensional nanochannels and hybrid membranes. The evolution of material platforms is accompanied by a transition from predominantly geometric exclusion to coupled regulation of pore confinement, interfacial recognition and dynamic transport. All third-party images reproduced in this figure were used with permission.

Existing reviews on selective ion separation have generally focused on particular material platforms, target-ion systems, or application scenarios, for example by separately summarizing the structural design of framework materials, two-dimensional membranes, polymer membranes, and ion-exchange membranes, or by concentrating on processes such as lithium extraction from salt lakes, seawater resource recovery, and heavy-metal recovery.[3,5,13,19–23] These studies have systematically reviewed advances in material preparation and performance. However, pore size, interfacial charge, coordination sites, and responsive behaviour are usually discussed within their respective material systems, making it difficult to address several mechanistic questions shared across material classes: why channels with similar nominal pore sizes exhibit different transport sequences; why increasing ion affinity may simultaneously enhance enrichment and reduce permeation; and why an external stimulus may regulate total flux without necessarily improving the selectivity of a target ion over competing ions.

The distinctive feature of this Review is not the introduction of another material classification, but the use of interconnected physicochemical steps in the ion-separation process as a common analytical scale for cross-comparing different nanoporous materials. Specifically, size- and solvation-based sieving, chemical recognition, and dynamic gating are reconsidered in terms of pore entry and solvation reorganization, interfacial partitioning and ion–site interactions, intrapore migration, and release, with particular emphasis on their synergy, competition, and shifts in the dominant mechanism under multicomponent conditions. Pore size, surface charge, and functional sites are thus no longer treated as mutually independent material parameters, but are placed within the same transport process to examine where they act and how they affect subsequent steps.

Within this process-oriented framework, this Review undertakes three tasks. First, ion systems are distinguished according to valence relationship and solution speciation, including isovalent monovalent, isovalent divalent, heterovalent, and chemically similar multivalent ions. Second, selective adsorption, intramembrane partitioning, and steady-state transmembrane transport are differentiated to avoid using equilibrium affinity to directly explain dynamic separation. Third, mechanistic interpretations are placed under specific feed compositions, driving forces, membrane thicknesses, and operating times, and are tested using operando characterization, multiscale simulation, and data-driven methods. The central concern is not the ranking of material performance, but where ion differences are amplified,

how different mechanisms cooperate or counteract one another, and what evidence is sufficient to support cross-material comparison and extrapolation across operating conditions.

2. Selective Ion-Transport Mechanisms

On the basis of the ion differences summarized in Table 1, existing regulatory strategies can be classified according to the principal controlled state variable into size- and solvation-based sieving, chemical recognition, and dynamic gating.[5,11,13,24] Size- and solvation-based sieving focuses on the effects of pore-entry constraints and confined-solvent structure on ion entry. Chemical recognition alters interfacial partitioning, residence, and migration through coordination, electrostatic, and supramolecular interactions. Dynamic gating uses reversible changes in pore size, charge, conformation, or wettability to reorganize transport pathways in response to external stimuli or ion occupancy. This classification describes the variables that primarily control selectivity, rather than assigning different materials to mutually exclusive categories.

In practice, the three mechanisms are generally coupled within the same pore. Narrowing a pore entrance not only amplifies differences in desolvation but also alters charge screening and site accessibility, while interfacial chemistry and gating state jointly regulate ion partitioning, intrapore migration, and solvent organization. In mixed electrolytes, competitive occupancy, counter-ion migration, and ion–ion correlations further alter the relative contribution of each mechanism. Actual separation behaviour therefore arises from synergy and competition among mechanisms and from their transitions with feed composition and operating state.[5,7–9,11,13,24–26]

On this basis, mechanistic attribution must address at least three questions: which state variable establishes a difference between the target and competing ions, at which transport step that difference predominantly acts, and whether the available evidence can exclude alternative explanations such as charge exclusion, transient adsorption, structural swelling, or defect-mediated bypass transport. Table 1 accordingly compares the key physicochemical contrasts, principal separation bases, and common confounding factors for different ion systems. The following sections first discuss the three fundamental mechanisms separately and then analyse how they cooperate or constrain one another under multicomponent conditions.[5,9,13,24]

Table 1. Representative ion-pair classes and dominant physicochemical factors governing selective ion separation

Ion-pair class	Representative ion pairs	Key physicochemical contrasts	Dominant separation factors	Major confounding factors
Isovalent monovalent ion pairs	Li^+/Na^+, Li^+/K^+, Na^+/K^+	Solvation strength and exchange kinetics; effective solvated size; weak coordination preferences	Pore-entry partial desolvation; confined-solvent reorganization; subtle differences in ion–pore affinity and in-pore mobility	Wet-state pore size and swelling; surface charge and electrical double layers; non-selective defects; concentration-dependent ion correlations
Isovalent divalent ion pairs	Mg^{2+}/Ca^{2+}, Co^{2+}/Ni^{2+}, Cu^{2+}/Zn^{2+}	Solvation thermodynamics; preferred coordination number and geometry; ligand-exchange kinetics; solution speciation	Coupled desolvation and coordination; competitive site occupancy; preorganized or multidentate recognition	pH-dependent hydrolysis and complexation; precipitation; counterion effects; site saturation
Heterovalent ion pairs	Li^+/Mg^{2+}, Na^+/Mg^{2+}, K^+/Mg^{2+}	Valence and charge density; solvation free energy; effective solvated size	Donnan partitioning and exclusion; coupled electrostatic and size/solvation discrimination; specific ion–interface interactions	Ionic-strength screening; concentration polarization; co-ion coupling and electroneutrality constraints; pH-dependent surface charge
Chemically similar isovalent multivalent ions	Adjacent lanthanide pairs, such as La^{3+}/Pr^{3+}, Nd^{3+}/Sm^{3+} and Dy^{3+}/Ho^{3+}	Picometre-scale differences in ionic radius; coordination number and geometry; solvation and ligand-exchange thermodynamics	Preorganized multidentate or cooperative coordination; size-matched confinement; reversible binding under competitive conditions	Hydrolysis and solution speciation; competing ligands and trace impurities; slow exchange and kinetic trapping; limited site capacity

2.1 Size- and Solvation-Based Sieving

Size sieving is often understood as geometric matching between pore size and ion size. However, ions approaching a nanopore entrance are generally solvated rather than transported as bare ions. In aqueous media, entry into a confined space is often accompanied by compression, reorganization, or partial removal of the hydration shell.[5–7,9,11,13,26] Bare-ion radius, solvated diameter, and crystallographic pore size therefore provide only preliminary references; actual selectivity depends on how pore-entry confinement alters the solvation free energy and entry kinetics of different ions.

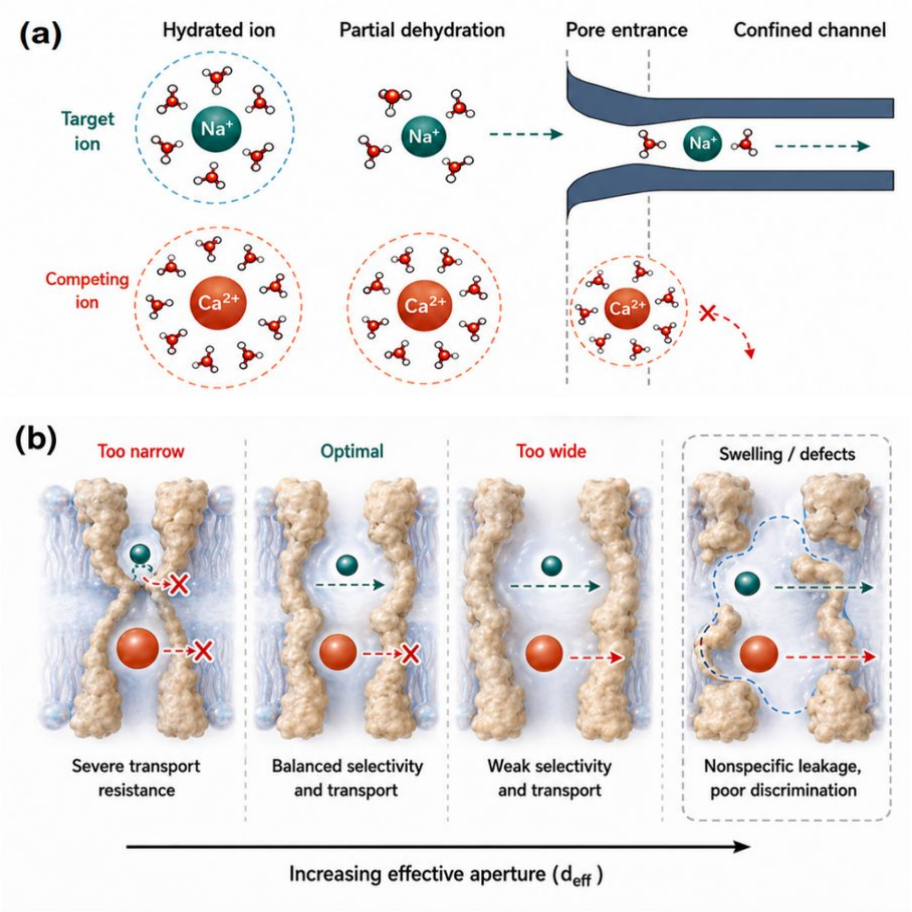


Figure 2 Size- and solvation-dependent ion transport through nanoporous channels.

(a) Schematic illustration of ion dehydration and pore entry. (b) Conceptual influence of the effective pore aperture on ion-separation performance.

Figure 2a summarizes this process. The target ion reduces its effective size through partial desolvation and enters the confined channel after overcoming the pore-entry barrier. A competing ion that must incur a higher solvation-reorganization penalty is more likely to be blocked at the entrance. The sieving boundary is not a fixed geometric cut-off, but a "soft boundary" jointly determined by ion-solvation strength, solvent-exchange kinetics, pore-entry morphology, and pore-wall chemistry.[6,7,9,11,14,15,26] Even when the nominal solvated size exceeds the pore aperture, an ion may still pass through, although its entry rate may vary markedly with the cost of solvation reorganization. Size sieving therefore amplifies not the difference in bare-ion radii, but the difference in the ease with which ions reorganize their solvation structures under confinement.

This understanding also changes the definition of pore size. Many nanoporous materials are not rigid under operating conditions. Lamellar membranes may swell through solvent adsorption and ion intercalation; flexible frameworks may undergo local deformation upon guest occupancy; and terminal groups, solvent content, and external mechanical constraints may alter the actual accessible space. At the same time, grain boundaries, interlayer misalignment, and nonselective defects may create bypass pathways around the designed pore entrance.[9,14,15] The parameter directly relevant to ion separation is therefore not the dry-state mean pore size, but the operando effective pore aperture, d_{eff}, jointly determined by channel geometry, solvent occupancy, ion loading, and structural flexibility.

Figure 2b further illustrates the nonmonotonic relationship between effective pore aperture and separation performance. When the aperture is too narrow, both target and competing ions experience high transport resistance; geometric exclusion is strengthened, but at the cost of a substantial loss in flux. Within an appropriate aperture range, the target ion can undergo the necessary solvation reorganization and enter the channel, whereas the competing ion remains subject to a higher barrier, thereby balancing selectivity and transport rate. When the aperture becomes too wide, solvation differences between ions can no longer be effectively amplified, and selectivity weakens accordingly.[5,9,14,15,27] If swelling or defects create nonselective bypass pathways, competing ions may circumvent local bottlenecks even when the nominal pore size satisfies the sieving requirement, reducing macroscopic selectivity.

Selectivity established at the pore entrance, however, does not necessarily persist throughout the transport process. In atomically thin pores, the local entry barrier may account for most of the total resistance. In channels of finite length, ions must additionally undergo confined diffusion, solvent-shell exchange, ion–pore-wall friction, and transient adsorption. As the transport distance increases, intrapore resistance may gradually exceed entry resistance, causing the same pore aperture to produce different rate-limiting steps at different membrane thicknesses. Size-sieving performance must therefore be evaluated together with selective-layer thickness and the actual migration distance.[5,7,25–27]

The division of roles between entrance sieving and intrapore migration also provides a physical basis for "narrow-entrance–wide-channel" structures. Local subnanometre bottlenecks amplify differences in ion solvation, whereas relatively spacious internal cavities reduce subsequent migration resistance. High selectivity does not require the entire channel to retain an extremely small diameter. On the contrary, if the entire transport pathway remains strongly confined, selectivity obtained at the entrance may be offset by excessive intrapore resistance.[10,25–27] A more rational design concentrates precise sieving at a limited number of critical bottlenecks while maintaining continuous, low-resistance migration after entry.

At the subnanometre scale, geometric confinement is further coupled to pore-wall chemistry and confined-solvent structure.[7,9,11,24–26] Moderate ion–pore-wall interactions can stabilize a partially desolvated target ion and compensate for the energetic cost of pore entry, whereas excessively strong interactions create deep energy wells, prolong residence times, and impede release. Pore-wall polarity and wettability also influence the density, orientation, and connectivity of the confined solvent. Moderately ordered solvent structures may support directional migration, whereas excessive confinement or local dewetting disrupts the continuous solvent network required for transport. Pore-size optimization therefore cannot be considered independently of interfacial chemistry and the state of the confined solvent.

The design target of size- and solvation-based sieving should accordingly shift from nominal pore size to matching among the operando effective aperture, the cost of solvation reorganization, and intrapore migration resistance.[5,9,11,13,24–27] Mechanistic interpretation should likewise not rely solely on dry-state pore size and an endpoint separation factor, but should combine evidence from swelling behaviour, membrane thickness, interfacial chemistry, steady-state flux, and solvation state or activation energy to determine whether selectivity is established at pore entry or limited by subsequent intrapore migration.

2.2 Chemical Recognition

When differences in ion size and solvation are insufficient to establish a clear sieving boundary, pore-wall chemistry provides another important route to selectivity. Coordination groups, fixed charges, macrocyclic hosts, and molecularly imprinted sites can exploit subtle differences among ions in donor-atom preference, coordination number, geometric configuration, and ligand-exchange kinetics to alter their relative stability at pore entrances and within pores. The objective of chemical recognition, however, is not to bind the target ion as strongly as possible, but to establish a sufficiently pronounced relative advantage under competitive conditions that can be continuously propagated. If the interaction is too weak, the partitioning difference between target and competing ions remains limited; if it is too strong, the ion may become trapped at a local site, causing "selective recognition" to manifest as retention rather than preferential transport.[8,24,28–30]

This also means that the binding constant of a ligand in a homogeneous solution cannot directly represent its recognition ability inside a nanopore.[11,24,28,29] Before contacting a site, an ion has often already undergone hydration-shell reorganization, pore entry, and local configurational adjustment. Once inside the pore, site orientation and accessibility, cooperative effects from neighbouring groups, confined-solvent structure, and local potential further reshape the coordination environment. The same functional group may therefore exhibit entirely different ion preferences when placed in pores of different sizes, frameworks, or solvent states. Effective recognition is never an isolated property of a functional group, but a local state jointly formed by the ion, site, pore, and solvent.

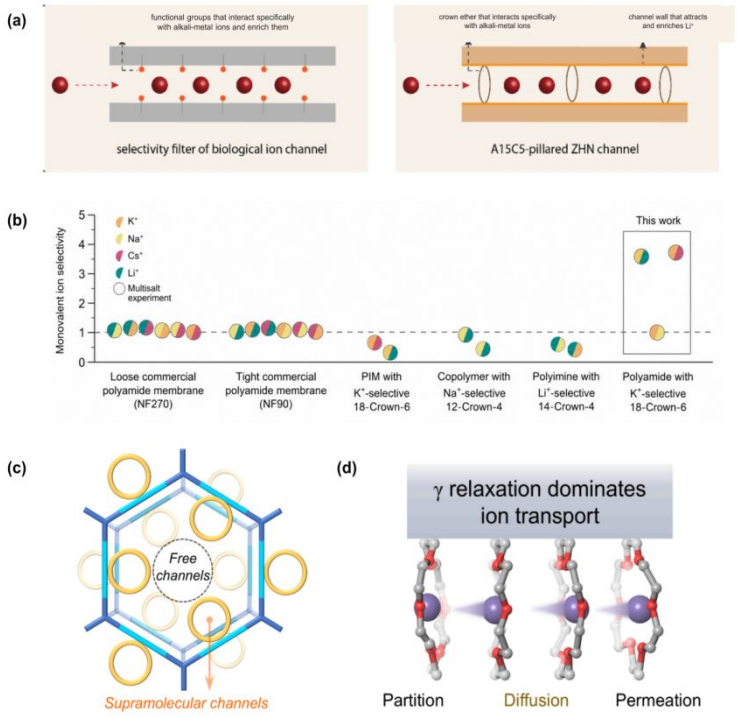


Figure 3 Chemical recognition under confinement and its translation into selective ion transport.

(a) Schematic comparison between the selectivity filter of a biological ion channel and an angstrom-scale ZHN channel pillared with 1-aza-15-crown-5 (A15C5). Specific functional groups in the biological channel and crown-ether units in the artificial channel promote local enrichment through ion–site interactions. In the artificial system, chemical recognition is further coupled with angstrom-scale confinement to regulate pore entry and intrapore partitioning. Adapted from Ref. [28]. (b) Monovalent-ion selectivity of commercial polyamide membranes and crown-ether-based polymer membranes. NF270 and NF90 are commercial membranes without crown-ether recognition units, whereas the remaining membranes incorporate crown ethers with distinct ion-affinity preferences; symbols outlined in grey denote measurements under multisalt feed conditions. The comparison illustrates that both the chemical identity of the recognition unit and its organization within the membrane influence whether preferential affinity is translated into macroscopic transport selectivity. Adapted from Ref. [29]. (c) Compartmentalized dual-channel architecture of 18C6-COF. Continuously aligned 18-crown-6 units form supramolecular recognition channels alongside framework-defined free channels, illustrating the spatial division between selective binding and low-resistance transport domains. Adapted from Ref. [30]. (d) Ion migration coupled to the conformational dynamics of 18-crown-6. Ion partitioning is followed by intrapore diffusion and transmembrane permeation. The original study proposes that γ-relaxation of the crown-ether units enables bound ions to migrate without complete detachment from the recognition sites, thereby mitigating kinetic trapping associated with strong ion–pore interactions. Adapted from Ref. [30].

The biomimetic channel shown in Figure 3a provides a direct illustration of this confinement effect. Biological ion channels regulate local ion enrichment and passage through ordered functional groups within their selectivity filters, whereas the A15C5-pillared ZHN angstrom-scale channel places crown-ether recognition and geometric confinement within the same transport region. Pore-entry constraints determine the solvation state in which the ion approaches the macrocyclic site, while stabilization by the crown ether can compensate for part of the entry penalty. Selectivity here arises neither from simple size exclusion nor from the binding of a free ion by a bulk-solution ligand, but from the combined effects of solvation reorganization, spatial matching, and ion–site interactions.[24,28]

For transmembrane separation, chemical recognition generally first alters ion partitioning into the membrane phase, but preferential partitioning does not necessarily imply preferential permeation. Within a simplified partition–diffusion picture that neglects electromigration and cross-component coupling, the concentration-gradient-driven ion flux can be expressed as

$$J_i = \frac{K_i D_i}{\ell} \Delta c_i$$

where K_i is the partition coefficient of ion i between the membrane phase and the external solution, D_i is its effective diffusion coefficient within the membrane, and ℓ is the thickness of the selective layer. Strengthening ion–site interactions generally favours an increase in K_i, but may also prolong residence time, reduce D_i, and increase the dissociation resistance at the outlet. Intramembrane enrichment, selective retention, and preferential permeation therefore correspond to different process outcomes. Chemical affinity can be translated into steady-state transmembrane selectivity only through intrapore migration and outlet-side release.[8,24,29,30]

The comparison between conventional polyamide membranes and crown-ether-containing polymer membranes in Figure 3b further demonstrates that a recognition unit provides only a potential chemical preference, rather than a predetermined ion-transport sequence.[24,29] Macrocycle size, site orientation and accessibility, selective-layer thickness, degree of crosslinking, and polymer free volume all affect whether a target ion can continue to migrate after entering the membrane phase. Under mixed-salt conditions, competitive occupancy and ion correlations may further alter the affinity sequence established in single-salt experiments. Macroscopic selectivity therefore cannot be explained solely by the solution binding ability of a crown ether towards a given ion, but depends on how recognition sites are embedded within an effectively percolated transport network.

The spatial organization of sites is critical for coordinating affinity and mobility. Isolated high-affinity sites readily create deep energy wells, requiring the ion to undergo complete dissociation, resolvation, and rebinding at every forward step, thereby accumulating transport resistance. If recognition sites are continuously arranged at suitable intervals along the migration direction, ions may instead undergo relay-like transport through exchange between adjacent sites.[24,30] In the 18C6-COF shown in Figure 3c, supramolecular channels formed by continuous crown-ether units are placed alongside framework-defined free channels, allowing selective partitioning and low-resistance migration to be assigned to different pore domains. This spatial division of function offers a more effective design strategy than merely increasing site density.

Conformational motion of the recognition units themselves may also alter the relationship between binding and migration. As shown in Figure 3d, the original study associated ion transport in 18C6-COF with the γ-relaxation of crown ethers, proposing that bound ions could move along the channel without completely leaving the recognition environment, thereby reducing the energetic cost of repeated dissociation, rehydration, and rebinding.[30] Similar site-exchange, conformation-assisted migration, or multi-ion pushing processes may enable strong local recognition to coexist with rapid long-range transport. A high flux alone, however, is insufficient to establish such a synergistic mechanism; corroborating evidence from intrapore occupancy, concentration dependence, relaxation timescales, and molecular motion is also required.

Adsorptive nanoporous materials follow a different process logic. They do not require the target ion to continuously traverse the material, but instead preferentially occupy sites under competitive conditions and are subsequently released by changing the solution conditions. Adsorption selectivity should therefore be understood along a "capture–dissociation–intrapore diffusion–release" pathway. Higher affinity can improve the capture of low-concentration target ions, but may also impede subsequent desorption. Even after an ion has dissociated from a site, it must still return to the bulk phase through a tortuous pore network. For functionalized porous carbons and biochars, apparent removal may simultaneously involve ion exchange, surface complexation, and mineral-phase-induced precipitation or coprecipitation; total adsorption therefore cannot be directly equated with specific recognition by predefined sites.[12,18] Quantitative comparisons of working capacity, fixed-bed mass transfer, and regeneration performance are discussed further in Section 3.3.

Recognition sites are also not static structures with unlimited capacity and invariant interactions.[12,24,30] At low occupancy, target ions may preferentially enter high-affinity regions. As these sites gradually become saturated, additional ions shift towards lower-affinity sites or nonselective pores, changing the apparent selectivity. If the site density is too low, the chemical preference cannot extend throughout the material; if it is too high, overlapping fields from adjacent sites may create a continuous kinetic trap. More meaningful control variables are therefore the matching among site density, spatial spacing, conformational flexibility, and binding–dissociation rates.

Competing ions can alter pathways through a continuous recognition channel by displacement, cooperative occupancy, and electrostatic coupling. Moderate multi-ion occupancy may drive ions further along the pathway, whereas occupation of a critical site by a competing ion may interrupt relay transport.[3,11,24,30] In heterovalent systems such as Li^+/Mg^{2+}, Donnan partitioning, charge screening, and electroneutrality constraints coexist with coordination interactions, requiring mechanistic attribution to be supported by multiple, mutually corroborating forms of evidence.

Recognition sites must therefore be organized into a percolated and exchangeable transport network before a local chemical preference can be translated into membrane transport or selective capture. If the conformation, accessibility, or local potential of the sites changes reversibly in response to an external stimulus or ion occupancy, static recognition further transitions into dynamic gating.[24,28–30]

2.3 Dynamic Gating

Size- and solvation-based sieving and chemical recognition are generally established within relatively fixed pore structures and interfacial chemistries, whereas dynamic gating further introduces a temporal dimension.[16] Applied potential, pH, light, or ion occupancy can alter pore-entry geometry, surface potential, chain conformation, wetting state, and the accessibility of recognition sites, allowing the same channel to exhibit different transport

states during operation.[13,31–34] Dynamic gating is therefore not simply the mechanical opening and closing of a pore, but a reversible reorganization of the energy barriers associated with ion entry, interfacial partitioning, and intrapore migration. In addition to changes in the charge or conformation of solid pore walls, dynamic liquid films can serve as reconfigurable transport boundaries. Cation valence can trigger transitions between channel states by regulating interfacial electrostatic interactions and liquid-film morphology, demonstrating that feed ions themselves can act as gating signals.[35]

The ability of a material to respond to a stimulus does not necessarily mean that it possesses a selective-separation function. If a state transition causes the fluxes of all ions to change approximately in parallel, the structure more closely resembles a tunable nanofluidic valve. Genuine selective gating requires the change in material state to affect the target and competing ions asymmetrically, so that their relative partitioning or migration sequence changes reversibly.[13,31–34] In other words, the significance of gating for separation is determined not by the magnitude of the change in total ionic current, but by whether the altered transport state amplifies the initially limited physicochemical differences between ions.

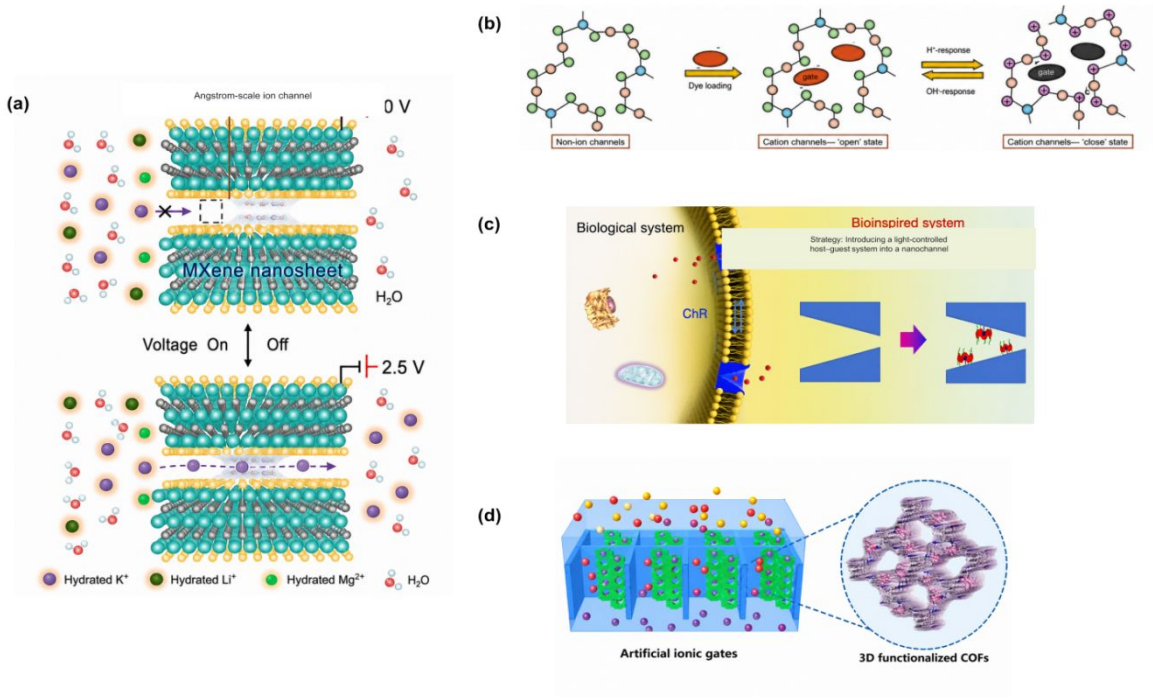


Figure 4 Dynamically gated ion transport triggered by external stimuli and ion occupancy.

(a) Voltage gating in angstrom-scale MXene–PDA channels. Switching the applied potential from 0 to 2.5 V reorganizes the intrachannel ion distribution and migration state, enabling high-flux, K^+-preferential transport through the combined regulation of voltage gating and cation charge density. Adapted from Ref. [31]. (b) TASK2-inspired pH-responsive polymeric nanochannels. Loading of an anionic dye converts the nonionic channel into an open, cation-selective state. The H^+ response induces amino-group protonation and ionic crosslinking, accompanied by changes in chain conformation and channel-wall charge, thereby switching the channel to a closed state; the process is reversed by the OH^- response. Adapted from Ref. [32]. (c) A light-controlled host–guest nanochannel inspired by channelrhodopsin. Incorporation of photoresponsive host–guest units into a conical nanochannel allows light to reversibly regulate ion transport by altering the interfacial assembly state and chemical environment of the channel wall. Adapted from Ref. [33]. (d) Ion-triggered gating in crown-ether-functionalized three-dimensional COFs. Coordination of Li^+ with 12-crown-4 recognition sites changes the ion-transport state of the pore, translating static chemical recognition into adaptive gating triggered by ion occupancy. Adapted from Ref. [34].

Externally driven gating operates primarily by changing the charge state and local structure of the channel. Potential control can rapidly reorganize the intrapore ion distribution and alter interactions between charged interfaces and ions of different valence. In the angstrom-scale MXene–PDA channels shown in Figure 4a, the applied potential and cation charge density jointly affect the competitive transport of K^+, Li^+, and Mg^{2+}, indicating that electrochemical gating can regulate not only transport rate but also the occupancy relationship among ions within the channel.[31] The applied potential, however, often plays two simultaneous roles: it changes the pore-wall state and directly drives ion migration. If these effects are not distinguished, the observed current change may contain contributions from surface charging, electromigration, and concentration polarization, and cannot be attributed entirely to gating itself.

A pH response more closely couples interfacial charge to channel conformation.[32] Protonation or deprotonation not only changes fixed-charge density, but may also induce ionic crosslinking, chain contraction or swelling, and changes in intrapore water content. TASK2-inspired polymer channels switch between states of different pore size and charge through precisely these coupled changes, as shown in Figure 4b. Such systems offer the advantage of simultaneously controlling geometric confinement and electrostatic partitioning, but their interpretation is also more complex because changes in pH alter metal-ion hydrolysis, complexation, and solution speciation. Material response must be distinguished from changes in feed chemistry to determine whether the observed change in selectivity originates from channel gating or from a change in the chemical form of the ions in solution.

By contrast, photoresponsiveness provides a noncontact mode of regulation with relatively high spatial and temporal resolution.[33] Introducing photoisomerizable or host–guest assembly units at pore entrances and pore walls can regulate local steric hindrance, surface charge, and the recognition environment without directly changing the transmembrane driving force. The biomimetic nanochannel in Figure 4c uses light to control the interfacial assembly state and thereby alter ion transport. The effectiveness of this design depends strongly on the location of the responsive unit. If the conformational change occurs in a region remote from

the principal transport pathway, even a pronounced spectroscopic response may have little effect on separation. A molecular-scale structural change can be translated into observable ion selectivity only when it acts directly on a pore-entry bottleneck or a continuous migration pathway.

In addition to external stimuli, ions themselves may trigger changes in the channel state.[34] The crown-ether-functionalized three-dimensional COF in Figure 4d uses coordination between Li^+ and 12-crown-4 sites to alter the intrapore transport environment, converting ion recognition into feedback regulation driven by occupancy. Such adaptive gating lies at the boundary between chemical recognition and dynamic regulation. If target-ion binding merely enhances local adsorption or intramembrane enrichment, the process remains static recognition. Genuine ion-triggered gating occurs only when site occupancy further changes the effective pore size, pore-wall potential, conformational state, or migration barrier experienced by subsequent ions. Its distinctive feature is that feed composition is no longer merely the object of separation, but also participates in determining the transport state of the material itself.

In practical multicomponent systems, the gating state is generally not an idealized "open" or "closed" condition, but a series of intermediate states jointly determined by ion concentration, competitive occupancy, and charge screening.[31,32,34,36] As salt concentration increases, compression of the electrical double layer may weaken charge gating. As recognition sites become saturated, ion-triggered feedback may level off. A competing ion that preferentially occupies a responsive site may even reverse the direction of gating. The timescale of gating is equally important. If the response is too slow, the material state cannot follow changes in the feed; if recovery is too slow, pronounced memory effects and path dependence emerge. Dynamic selectivity therefore depends on temporal matching between ion transport and material-state transitions, rather than solely on static differences between two steady states.

Effective gating must act at a pore entrance, narrow bottleneck, or principal recognition region, and must exert an asymmetric, reversible, and temporally matched influence on the target and competing ions. Its evaluation should simultaneously consider ion-pair selectivity, response and recovery times, hysteresis, and cyclic drift, rather than relying only on the magnitude of a conformational change or the on/off ratio of total current. Dynamic gating can thus be understood as the state-dependent and temporally ordered reconfiguration of confinement sieving and chemical recognition.[13,31–34]

2.4 Synergy among Multiple Mechanisms

Size- and solvation-based sieving, chemical recognition, and dynamic gating are three analytical dimensions for identifying the origin of selectivity, rather than mutually isolated transport mechanisms. In an actual nanopore, an ion approaches the pore entrance from the bulk phase and subsequently undergoes solvation reorganization, interfacial partitioning, intrapore migration, and outlet-side release. Pore size, interfacial chemistry, and channel state often act simultaneously at several of these stages. A selective advantage established at one stage can be translated into the final separation outcome only if it persists through subsequent stages. A reduction in the entry barrier may be offset by slow intrapore diffusion, while high intramembrane affinity may manifest as retention if release is hindered. The essence of multimechanism coupling is therefore not the addition of more structural units or functional groups, but the coordination of the location, strength, and direction of different effects along the transport pathway so that they jointly favour the target ion rather than counteracting one another at different stages.[5,8,9,11,13,24–26,30] This process-oriented understanding is also the central feature that distinguishes this Review from literature surveys organized by material class.

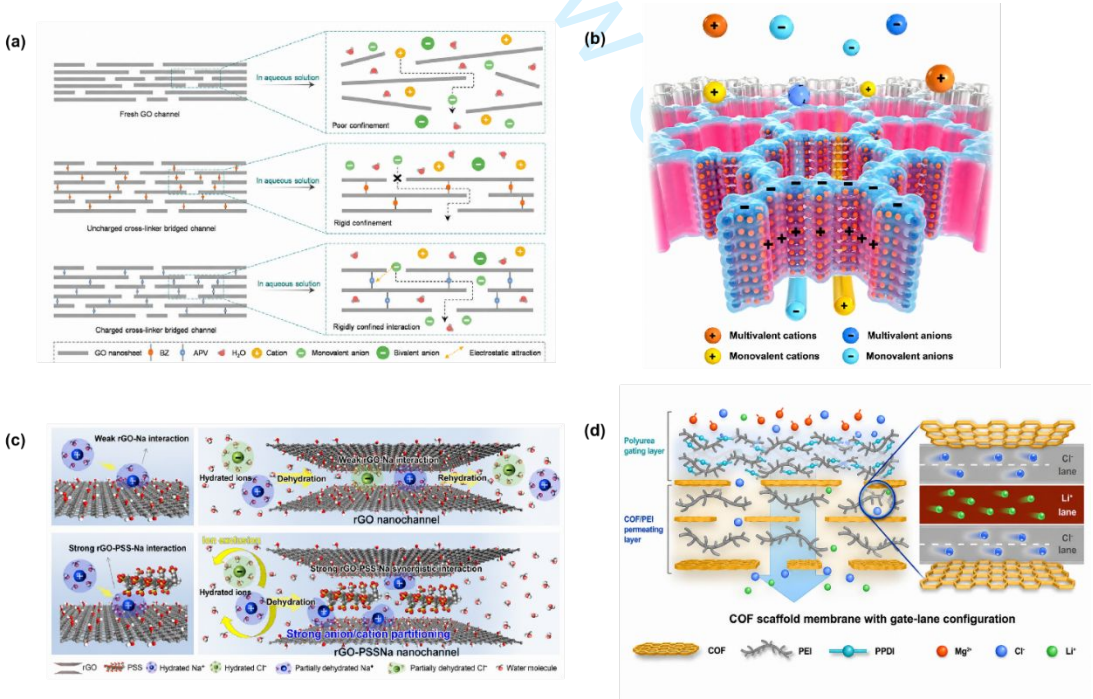


Figure 5 Spatial coupling of separation mechanisms and multicomponent ion transport in nanoporous membranes.

(a) Coupling of rigid confinement and ion–channel affinity in GO channels. Charged cross-linkers suppress swelling while compensating ion-dehydration penalties, thereby improving anion discrimination. Adapted from Ref. [37]. (b) Molecular-packing-regulated screening of cations and anions. Ordered charge environments and ion–π interactions in two-dimensional COFs differentiate monovalent and multivalent ions. Adapted from Ref. [38]. (c) Electrostatic-induced intrachannel partitioning and decoupling of anion–cation co-transport. PSSNa promotes partial Na^+ dehydration and confined enrichment, increasing the spatial partitioning difference between cations and anions. Adapted from Ref. [39]. (d) Hierarchical coupling of a gating layer and lane-separated pathways. The polyurea surface layer restricts Mg^{2+} entry, whereas the COF/PEI interior forms preferential Li^+ and Cl^- transport lanes, highlighting the roles of ion competition, counter-ion migration, and electroneutrality in mixed-salt selectivity. Adapted from Ref. [40].

A typical form of coupling occurs within a pore domain in which confinement and interfacial interactions coexist. Geometric constraints force the ion hydration shell to compress or reorganize, but also increase the cost of entering the pore. Moderate ion–pore-wall interactions can stabilize this transition state and partly compensate for the energetic penalty of solvation reorganization. The crosslinked GO membrane shown in Figure 5a suppresses aqueous swelling by fixing adjacent nanosheets while using charged crosslinking structures to regulate interactions between anions and the channel.[37] The hydration shells of different anions consequently undergo different degrees of configurational reorganization, and selectivity arises from the combined effects of rigid confinement, confined-water structure, and interfacial affinity rather than from pore size or electrostatics alone. Importantly, this synergy exists within an appropriate interaction window: insufficient confinement fails to amplify ion differences, whereas excessively strong interactions may create deep local energy wells and hinder subsequent migration.

Spatial organization inside the channel likewise determines whether chemical interactions can be translated into sustained transport selectivity. Isolated or disordered sites may enhance local adsorption but do not necessarily affect ion migration along a percolated pathway. Oriented COFs provide a different situation: face-to-face arrangement and interlayer packing of the building units organize aromatic π systems and their local potentials along the transport direction, allowing multiple relatively weak ion–π interactions to be amplified through spatial cooperation and thereby differentiating the partitioning and migration of monovalent and multivalent ions, as shown in Figure 5b.[38] This result demonstrates that selectivity is governed not only by the chemical identity or number of recognition groups, but also by their position relative to the pore entrance and transport direction. Even at identical material composition and nominal pore size, changes in orientation, packing, and grain-boundary state can reconstruct the interfacial environment actually experienced by the ions.

Different effects can also cooperate through spatial division of function rather than through colocalized superposition. If the entire transport pathway retains extremely small pores or strong binding, suppression of competing-ion migration is generally accompanied by increased resistance to target-ion transport. Hierarchical structures allow the selective bottleneck to be concentrated at the pore entrance or within a local membrane layer, while subsequent regions provide lower-resistance migration. In the gate–lane architecture shown in Figure 5d, a surface polyurea layer restricts Mg^{2+} entry, whereas internal COF/PEI regions provide suitable transport environments for Li^{+} and Cl^{-}, respectively.[40] Entry exclusion of the competing ion, intrapore migration of the target ion, and charge compensation by the counter-ion are thus no longer assigned entirely to the same structure. This “entrance gating–internal transport” design shows that mechanistic synergy does not require every pore region to possess all functions simultaneously; rather, the responsibilities of different regions must be spatially defined so that selectivity established at the entrance is not consumed by subsequent transport resistance.

When the feed contains multiple salts, coupling extends from ion–pore interactions to ion–ion interactions. Recent studies further emphasize that ion association under nanoconfinement is not a secondary correction restricted to high-concentration conditions, but may directly alter intrapore partitioning, correlations in ion migration, and ultimately the sequence of precision separation.[41] Because of electroneutrality constraints, the target ion cannot always be treated as an independently migrating component; local enrichment of competing ions, co-ions, and counter-ions may all change the transport sequence. In the ArGO–PSSNa membrane shown in Figure 5c, interlayer confinement and the affinity of sulfonate groups for Na^{+} confine cations within the nanochannels and increase the difference in intrapore partitioning between Na^{+} and Cl^{-}. Dynamic correlations between cations and anions are thereby weakened, suppressing their original cooperative transmembrane transport. By contrast, the gate–lane membrane provides coordinated but spatially separated pathways for Li^{+} and Cl^{-}, making counter-ion migration part of the mechanism that sustains target-ion transport. These apparently opposite strategies reveal the same principle: selectivity is determined not only by target-ion entry and diffusion, but also by how a material reconstructs the local composition and correlated motion of the entire electrolyte.[39,40]

Competitive effects exhibit a pronounced dependence on composition. In an oriented COF membrane, interfacial occupancy by monovalent cations can restrict multivalent cations from approaching the pore wall, thereby enhancing cation sieving. For anions, analogous competition may instead weaken the interfacial partitioning of strongly binding species.[30,38–40] As salt concentration and site occupancy change, the rate-limiting step may also shift from interfacial partitioning to intrapore migration or release.

Dynamic gating adds state dependence to the above spatial coupling, allowing entrance sieving, interfacial partitioning, and intrapore migration to change jointly with an external stimulus or ion occupancy. The gating state can alter the final ion-pair selectivity only if it acts on the actual rate-limiting step.[31–34]

Overall, multimechanism synergy is achieved mainly through confinement–interface coupling within the same pore domain, division of function among different structural regions, and multi-ion occupancy coupled with counter-ion migration. Its effectiveness should be judged by whether the net transport advantage of the target ion in a mixed feed can be retained successively through pore entry, intrapore migration, and outlet-side release, rather than inferred directly from a single pore size, site affinity, or static structural parameter.[24,25,30,37–40] The corresponding quantitative cross-scale description is discussed further in Section 4.

3. Ion-Separation Performance of Nanoporous Materials

The preceding mechanistic analysis shows that nanopores can establish selectivity at different stages of ion entry, partitioning, migration, and release. Mechanistic plausibility, however, does not directly establish superior separation performance. The same separation factor may arise from enhanced target-ion transport or merely from stronger inhibition of a competing ion, while similar fluxes or rejection values may carry different physical meanings because of differences in feed composition, driving force, membrane thickness, or testing mode.[42–44] This section therefore does not repeat the discussion of local mechanisms themselves, but instead examines the performance metrics, testing boundaries, and quantitative comparability of different nanoporous materials, and analyses how material-level selectivity is translated into actual separation outcomes.

Different nanoporous materials derive selective separation from different structural bases. Rigid crystalline channels provide relatively well-defined size constraints; framework materials allow pore size and interfacial chemistry to be tuned within ordered channels; two-dimensional lamellar materials offer short transport pathways and flexible control over interlayer spacing; and polymer membranes have advantages in processing and module integration. For adsorbent materials such as porous carbons and biochars, performance depends more strongly on heterogeneous pore structures, surface sites, and their reversible

occupancy under competitive conditions. These material classes differ substantially in design freedom, applicable processes, and failure modes, and cannot be ranked simply according to maximum selectivity or capacity values reported under different conditions.[5,13,19–21,42,43] Table 2 accordingly summarizes the key structural features, representative separation performance, advantages, and limitations of the principal material platforms.

Table 2. Comparison of major nanoporous material platforms for selective ion separation

Material platform	Key structural features	Representative performance	Main advantages	Main limitations	Refs.
Zeolites and inorganic molecular sieves	Rigid, uniform subnanometre pores; tunable framework charge	Preferential H^+ transport over VO^{2+}, Cr^{2+} and Fe^{2+} through ZSM-5	Well-defined apertures; low transport resistance	Limited chemical tunability; difficult defect-free fabrication	[45]
MOFs	Programmable pore windows, nodes and linkers	Mono-/divalent conductance difference of approximately 10^3	Coupled control of pore size and interfacial chemistry	Predominantly micro-/nanoscale demonstrations; defect and scale-up issues	[26]
COFs	Ordered channels; tunable stacking, orientation and functionality	K^+/Al^{3+} and NO_3^-/PO_4^{3-} selectivities of 214 and 451	High structural programmability; continuous recognition sites	Strong sensitivity to stacking, orientation and grain boundaries	[38]
Two-dimensional lamellar materials, including GO and MXenes	Tunable wet-state spacing, terminal groups and surface charge	Cl^-/SO_4^{2-} selectivity of 125 in a GO membrane	Thin selective layers; facile crosslinking and functionalization	Swelling, restacking and long-term structural evolution	[37]
Microporous polymers and ion-exchange membranes	Dynamic free volume; tunable fixed charges and functionalities	Monovalent-ion/Mg^{2+} selectivity above 100 in an electrodialysis stack	Processable, scalable and module-compatible	Hydration-induced swelling; broad pore-size distributions	[9,27,46]
Biomimetic and artificial nanochannels	Ångström-scale apertures; precisely positioned recognition sites	K^+/Li^+ selectivity of approximately 364	High precision for isovalent ions; explicit mechanisms	Small effective area; difficult device integration	[28,47]
Functionalized porous carbons and biochars	Heterogeneous pores; diverse surface groups and mineral phases	Cd^{2+} and Cu^{2+} capacities of 29.9 and 34.1 mg g^{-1} for HFO–biochar	Low cost; compatible with adsorption and fixed beds	Limited intrinsic selectivity; heterogeneous and complex mechanisms	[18,48]
Composite and hierarchical porous architectures	Spatially separated gating, scaffold and transport domains	True Li^+/Mg^{2+} selectivity of 231.9 at 11.5 L m^{-2} h^{-1} bar^{-1}	Potential mitigation of the selectivity–permeability trade-off	Complex fabrication; interfacial defects and durability concerns	[40]

Note: This table provides an overview of the structural characteristics and representativeness of different material platforms and is not intended for quantitative ranking across ion systems or testing modes.

3.1 Performance Metrics, Testing Modes, and Comparability Boundaries

Compared with mechanistic classification, performance comparison among nanoporous materials is more susceptible to the testing method and metric definition. Existing studies commonly describe material performance in terms of selectivity, ion flux, permeability, rejection, or ionic conductivity, although these metrics correspond to different physical processes. Selectivity emphasizes relative transport between the target and competing ions; flux reflects the absolute amount transported per unit area; and rejection is more commonly used to describe retention of an individual component under pressure-driven conditions. Even when the same term is used, values reported in different studies may derive from single-salt diffusion, mixed-salt separation, membrane-potential calculations, or electrically driven transport. Comparing such data outside their specific testing boundaries often causes differences arising from experimental conditions to be misidentified as intrinsic differences in material performance.[42–44]

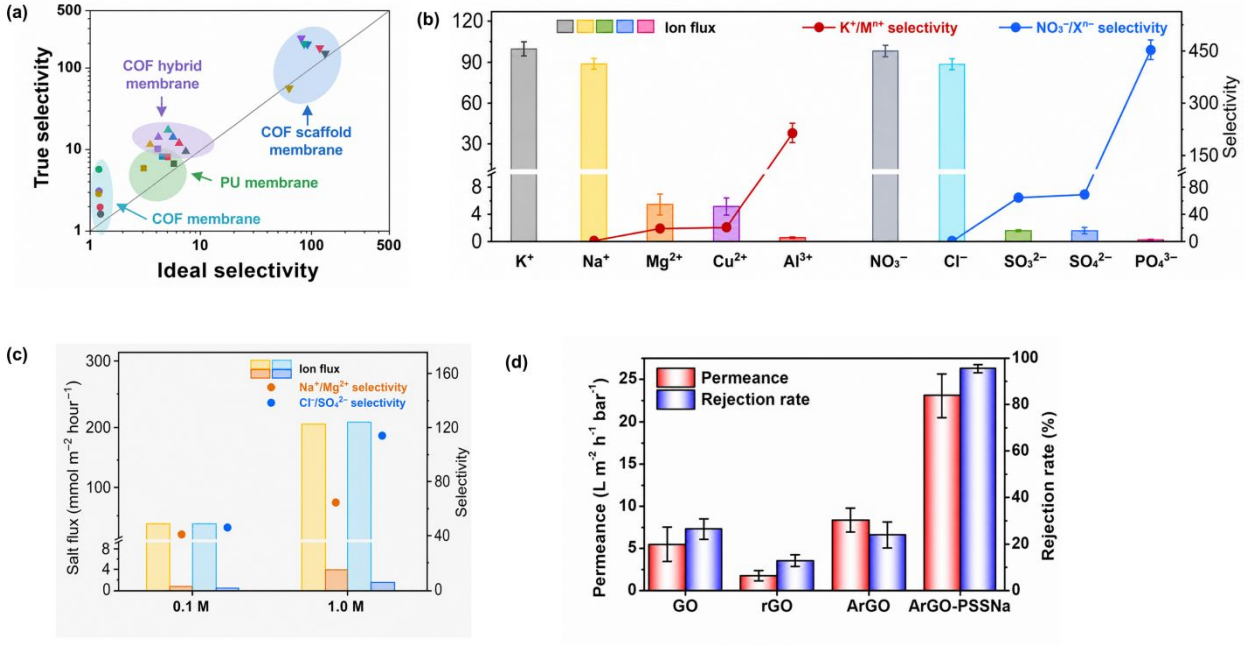


Figure 6 Effects of performance metrics and testing conditions on the interpretation of selective ion separation.

(a) Comparison of ideal selectivity with true selectivity measured in mixed feeds, showing that single-salt performance does not directly predict multicomponent separation. Adapted from Ref. [40]. (b) Ion fluxes and K^+/M^{n+} and NO_3^-/X^{n-} selectivities of a COF-170/PAN membrane under 0.1 M single-salt conditions. Adapted from Ref. [38]. (c) Fluxes and selectivities in equimolar ternary mixtures of NaCl, Na_2SO_4 and $MgCl_2$ at 0.1 and 1.0 M, illustrating the effects of competitive partitioning and ion–ion interactions. Adapted from Ref. [38]. (d) Water permeance and NaCl rejection of GO, rGO, ArGO and ArGO-PSSNa membranes at 5 bar using a 5 mM NaCl feed. Adapted from Ref. [39].

Single-salt experiments are suitable for identifying the potential transport preference of a material for individual ions, whereas multicomponent feeds reorganize the membrane composition through competitive occupancy, ionic strength, counter-ion migration, and electroneutrality constraints. In the gate–lane membrane shown in Figure 6a, the true Li^+/Mg^{2+} selectivity reached 231.9, exceeding the ideal selectivity of 80.5 derived from single-salt results, indicating that ion-mixing effects can further amplify selectivity in certain systems.[40] Figures 6b and 6c further show that coexisting ions and total salt concentration can alter both the sequence and magnitude of Na^+/Mg^{2+} and Cl^-/SO_4^{2-} selectivity.[38] Single-salt results therefore characterize potential preference, whereas mixed-salt data describe actual separation under a specified composition.[42–44]

The driving force determines the physical process represented by a performance metric. Concentration-gradient experiments primarily reflect intramembrane partitioning and diffusion; pressure-driven measurements additionally involve water-flow entrainment, convective mass transfer, and concentration polarization; and electrically driven transport is governed by electromigration and ion transference numbers. Water permeability and rejection, diffusion flux, relative permeability inferred from membrane potential, and single-pore current are therefore not equivalent performance quantities. Comparisons must also specify ion system, feed composition, pH, temperature, membrane thickness, effective area, and testing duration, because these conditions determine the relative contributions of entry resistance, intrapore migration, defect-mediated bypass transport, and transient effects.[42–44]

Accordingly, rigorous quantitative comparisons are made here only when the ion system, feed conditions, driving force, and metric definition are essentially consistent. Other data are used to assess trends or orders of magnitude,[42,43] and are discussed separately according to single-salt versus mixed-salt feeds, diffusion versus pressure-driven transport, and electrical-current versus molar-flux measurements. Figure 6 defines the boundaries of comparison rather than ranking materials.

3.2 Performance Comparison of Membranes and Nanochannels

After metric definitions and testing boundaries have been clarified, the performance of membranes and nanochannels must still be interpreted in the context of the specific ion system. Ion valence, hydration characteristics, and coordination chemistry determine the differences that a material can exploit, and also influence how the separation factor is generated and what process value it carries. The following discussion is organized according to heterovalent ions, isovalent monovalent ions, and isovalent multivalent ions, while simultaneously considering the absolute transport of target and competing ions, the direction of selectivity, and performance retention in mixed feeds.

3.2.1 Heterovalent-Ion Separation

Li^+/Mg^{2+} is the most extensively studied heterovalent cation-separation system. Because the two ions differ substantially in valence, charge density, and hydration characteristics, a high separation factor is relatively easy to establish, although its origin is not always the same. The polyamide nanofiltration membranes shown in Figures 7a and 7b narrow the pore-size distribution so that most pore entrances lie between the effective sizes of Li^+ and Mg^{2+}. As the mean pore size decreases, Mg^{2+} rejection approaches completion while Li^+ retains negative rejection, causing Li^+/Mg^{2+} selectivity to increase sharply.[49] Ion-permeability measurements further show that Li^+ permeability remains broadly similar, whereas Mg^{2+} permeability decreases by more than three orders of magnitude. The performance enhancement here arises primarily from strong inhibition of the competing ion, rather than sustained acceleration of Li^+ transport. At the same time, negative Li^+ rejection in a mixed-salt system is also affected by the transmembrane potential and electroneutrality coupling, and the resulting selectivity cannot therefore be attributed entirely to a static pore-size difference.

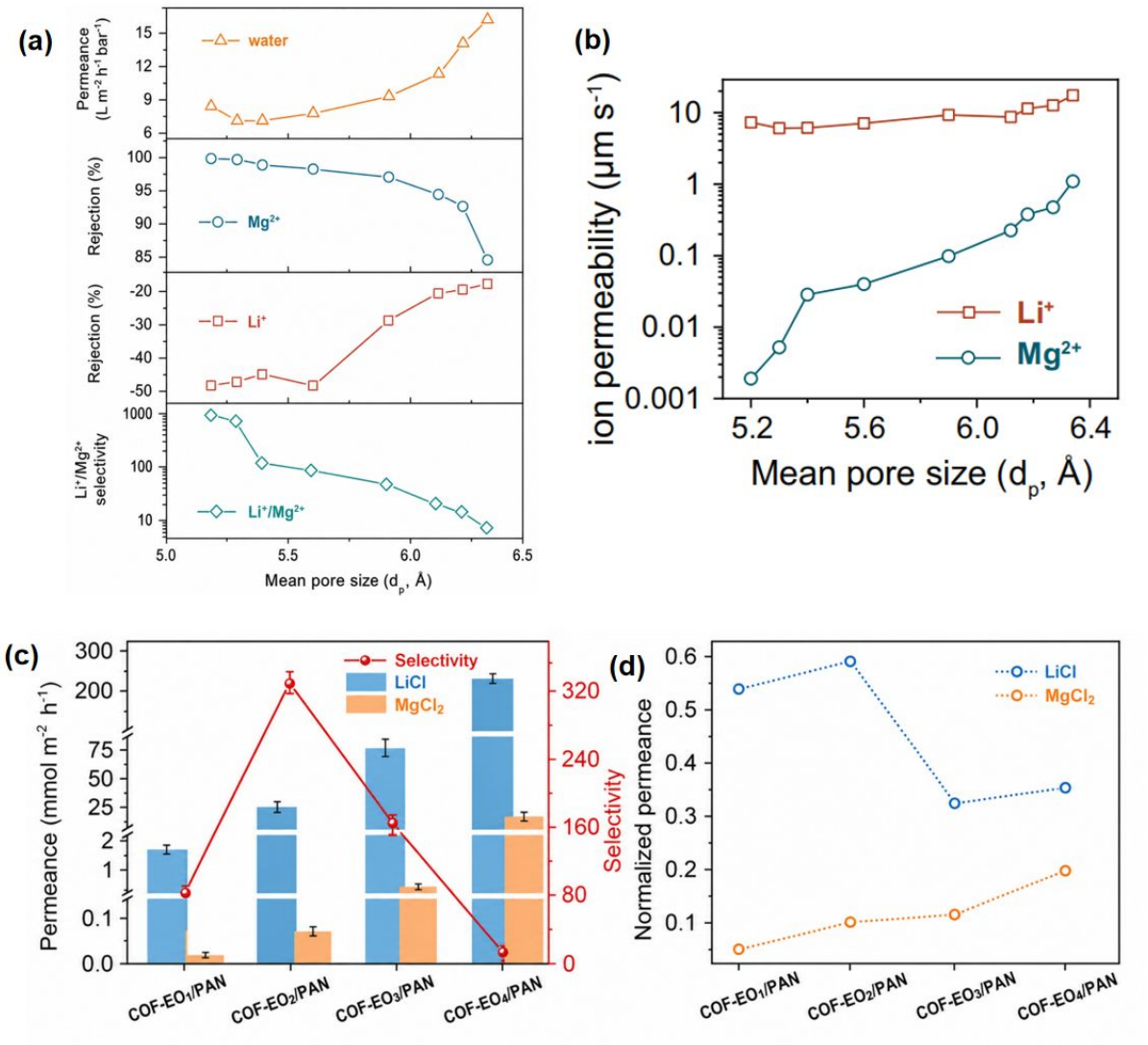


Figure 7 Distinct origins of selectivity in heterovalent ion separation.

(a,b) Effects of the mean pore size of polyamide nanofiltration membranes on water permeance, Li^+ and Mg^{2+} rejection, Li^+/Mg^{2+} selectivity, and ion permeability. Decreasing pore size preferentially suppresses Mg^{2+} transport, thereby increasing selectivity. Adapted from Ref. [49]. (c,d) Salt permeances and Li^+/Mg^{2+} selectivity of COF-EOx/PAN membranes in binary $LiCl/MgCl_2$ feeds, together with permeances normalized to the corresponding single-salt values. Intrapore solvation and mixed-ion competition jointly reshape the relative transport of Li^+ and Mg^{2+}. Adapted from Ref. [50].

Intrapore chemistry provides another regulatory route. In Figures 7c and 7d, the COF-EOx/PAN membranes tune local solvation ability inside the pores by changing the length of oligomeric ether chains.[50] $LiCl/MgCl_2$ selectivity exhibits a pronounced nonmonotonic dependence on ether-chain length. Moderate ion–pore-wall interactions favour Li^+ partitioning and migration while imposing higher resistance on Mg^{2+}. Further enhancement of the channel's solvating ability, however, also increases Mg^{2+} permeation, thereby reducing selectivity. Changes in binary-mixture permeance relative to single-salt results further demonstrate that Li^+ and Mg^{2+} do not traverse the membrane independently. Local solvation, competitive occupancy, and counter-ion migration jointly reconstruct the intrapore composition, such that true selectivity cannot be obtained simply by dividing the two single-salt permeabilities.

Similar principles apply to anion systems. An ionized polymer of intrinsic microporosity restricts the pore window to a range between the hydrated and Stokes diameters of the anions and introduces quaternary ammonium sites to promote migration of partially dehydrated monovalent anions, achieving Cl^-/CO_3^{2-} and Cl^-/SO_4^{2-} selectivities of 106 and 82, respectively.[27] This performance depends simultaneously on subnanometre confinement and fixed charge and cannot be regarded as simple size cut-off. More instructively, conventional valence-based trends can be reversed through specific interactions. When hydrated manganese oxide is incorporated into a cation-exchange membrane, phosphate migrates continuously along reversible outer-sphere complexation sites; its flux is increased 27-fold relative to that through the unmodified membrane, and phosphate is transported preferentially over sulfate, nitrate, and chloride.[8] This result demonstrates that a higher valence does not necessarily correspond to lower permeability. Provided that binding remains reversible and is matched to a continuous diffusion pathway, chemical recognition can promote rather than impede target-ion transport.

Acid–base-pair engineering in ion-exchange membranes provides another route to heterovalent-ion separation. Moderately sulfonated polybenzimidazole membranes form contracted ionic clusters and hydrophilic domains with restricted connectivity, thereby imposing a higher migration barrier on Mg^{2+} than on Li^+. The resulting SP45 membrane exhibits a Li^+/Mg^{2+} selectivity of 48.1 at 2 mA cm^{-2} and limits selectivity decay to less than 10% over multiple mixed-salt cycles.[51] This result shows that ionic-cluster dimensions, hydrophilic-domain connectivity, and local acid–base interactions can jointly regulate the partitioning and migration of heterovalent ions without relying entirely on geometric pore-size cut-off.

Overall, heterovalent ions already exhibit substantial differences in charge and hydration, allowing many membranes to attain high apparent selectivity. Such values, however, are also particularly likely to obscure their origin: some systems genuinely improve target-ion transport, whereas others merely achieve nearly complete rejection of the competing ion.[42,43,49,50] Evaluation of heterovalent-ion membranes should therefore not stop at the separation factor, but should simultaneously examine the absolute fluxes of the target and competing ions and determine whether the difference persists under mixed-salt conditions.

3.2.2 Isovalent Monovalent-Ion Separation

When the valence difference disappears, electrostatic exclusion cannot directly distinguish Li^+, Na^+, and K^+, and selectivity depends more strongly on subtle differences among solvation reorganization, the operando pore aperture, and ion–site interactions. Under these conditions, high selectivity generally does not arise from one exceptionally large barrier, but from the accumulation of multiple local sieving or recognition events along the transport pathway.

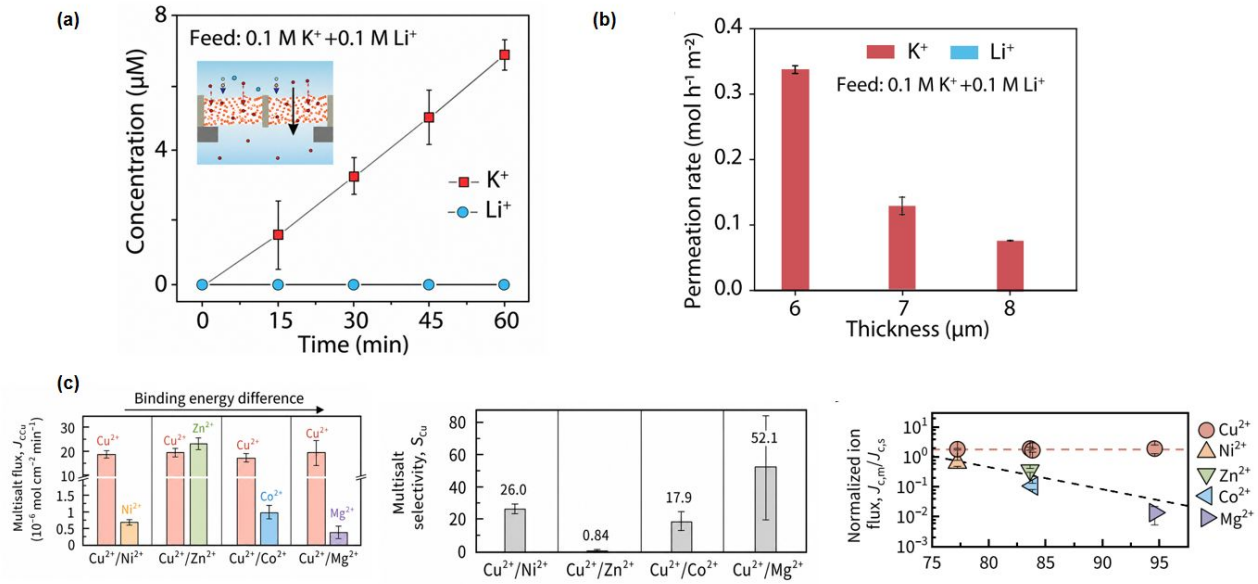


Figure 8 Transport direction, thickness effects, and coordination contrasts in isovalent ion separation.
(a,b) Transmembrane transport of K^+ and Li^+ from a mixed feed and its dependence on membrane thickness. K^+ permeates continuously while Li^+ is largely retained, and the K^+ permeation rate decreases with increasing membrane thickness. Adapted from Ref. [52]. (c,d) Ion fluxes and Cu^{2+} selectivities in mixed feeds containing Cu^{2+} and another divalent cation, together with the dependence of normalized flux on the difference in ligand-binding energy. A larger binding-energy contrast mainly suppresses transport of the competing ion, while the Cu^{2+} flux remains comparatively stable, indicating that selectivity arises from asymmetric partitioning–diffusion coupling rather than a simple enhancement of target-ion flux by stronger binding. Adapted from Ref. [53].

The randomly oriented COF membrane shown in Figures 8a and 8b adopts a separation direction different from the commonly pursued "preferential permeation of Li^+".[52] Narrow, randomly oriented channels and preferential interactions of sulfonate groups with Na^+ and K^+ allow K^+ to permeate continuously, while Li^+ is largely retained on the feed side. The product is therefore not a Li^+-containing permeate; rather, Li^+ is retained and enriched by removing competing ions. When the membrane thickness increases from 6 to 8 μm, K^+ permeation decreases markedly while Li^+ remains nearly impermeable, showing that increasing the transport distance can preserve the direction of sieving but directly reduces the processing rate. Random orientation in this system creates channels between two extremes: parallel-oriented pores are too wide to provide selectivity, whereas vertically oriented structures have such high resistance that they permit almost no ion passage.

Biomimetic channels further demonstrate that subtle differences can be amplified through preorganized sites. KcsA-type artificial channels use cation–π and electrostatic interactions within subnanometre cages to achieve a K^+ transport rate of 94.4 mmol m^{-2} h^{-1}, with K^+/Li^+ and K^+/Na^+ selectivities of 363 and 31, respectively.[47] Crown-ether-pillared angstrom-scale channels exploit intrapore enrichment and host–guest recognition to achieve high effective Li^+/Na^+ selectivity in artificial seawater containing only 25 μM Li^+.[28] These examples show that preorganized sites can amplify small free-energy differences between isovalent ions in different transport directions. Because channel area, driving mode, and measured quantities vary substantially, however, these values are more suitable for comparing mechanisms and trends than for direct ranking against macroscopic pressure-driven membranes.

The selectivity sequence within the same material is also not necessarily fixed.[42–44] An amino-acid-functionalized COF membrane can switch between Na^+ selectivity and K^+ selectivity with changing pH because protonation alters the relative interactions between the ions and coordination sites.[54] This further demonstrates that free-energy differences among isovalent monovalent ions are generally small, and that minor changes in intrapore water structure, site state, or solution conditions can alter the final transport sequence.

3.2.3 Isovalent Multivalent-Ion Separation

The differentiation of isovalent multivalent ions depends more strongly than that of heterovalent ions on the coupling between the local coordination environment and mass transport. Cu^{2+}, Ni^{2+}, Co^{2+}, Zn^{2+}, Mg^{2+}, and Ca^{2+} have the same or similar charge states, making it difficult to establish a stable selectivity sequence solely through Donnan exclusion. The exploitable differences arise more often from hydration-shell structure, coordination geometry, ligand-exchange kinetics, and solution speciation. Selectivity in these systems therefore does not necessarily originate from direct discrimination of bare-ion dimensions at the pore entrance, but may develop progressively through hydration recognition, competitive coordination, or species transformation.

The ultrathin polymer selective layer shown in Figures 8c and 8d uses iminodiacetate sites to amplify differences in binding among divalent transition-metal ions.[53] In mixed feeds containing Cu^{2+} and another divalent cation, the Cu^{2+} flux changes only modestly, whereas the competing-ion flux decreases substantially as the difference between its binding energy and that of Cu^{2+} increases, raising Cu^{2+}/M^{2+} selectivity from approximately unity to several tens. The increase in selectivity arises primarily from the relative disadvantage of the competing ion in intramembrane partitioning and diffusion, rather than from sustained promotion of Cu^{2+} migration by stronger binding. This result also demonstrates that equilibrium affinity can be translated into an advantage in transmembrane transport only when the selective layer is sufficiently thin, the sites form a continuous pathway, and ions can exchange and be released rapidly.

The Mg^{2+}/Ca^{2+} system further demonstrates that ion recognition does not necessarily require complete removal of the hydration shell. The two ions have the same valence, but Mg^{2+} has a higher charge density and a more rigid first hydration shell. The selective site of the biological Mg^{2+} channel MgtE binds Mg^{2+} approximately 500 times more strongly than Ca^{2+}, with corresponding half-maximal response concentrations of 27.7 ± 3.7 μM and 12.2 ± 1.9 mM, respectively.[55] Structural analysis shows that the site does not directly coordinate bare Mg^{2+}, but recognizes its intact hydration geometry through a water-mediated hydrogen-bonding network. Although this result cannot be used as a direct comparison of macroscopic membrane fluxes, it provides an important design benchmark: for isovalent ions such as Mg^{2+} and Ca^{2+}, selectivity may arise either from different dehydration penalties or from matching of a particular hydration geometry within the pore. In other words, retaining and reorganizing the hydration shell may sometimes be more effective than further narrowing the pore.

Co^{2+}/Ni^{2+} illustrates another route.[56] Because their hydrated sizes and conventional coordination properties are highly similar, direct differentiation using a fixed pore size generally yields only limited contrast. Altering the solution coordination environment can amplify their species-level differences before membrane entry. At high Cl^- concentration, Ni^{2+} primarily forms the positively charged species $[Ni(H_2O)_5Cl]^+$, whereas Co^{2+} forms the negatively charged $[CoCl_4]^{2-}$ complex. Coupling these oppositely charged coordination species with electrodialysis yields a maximum Ni^{2+}/Co^{2+} separation selectivity of 370.70; when applied to leachates from NCM and NCA batteries, the selectivities remain 90.60 and 109.42, respectively. Similarly, oriented COF membranes with tunable intrapore sulfonic-acid-group contents have been used for EDTA-assisted $Ni^{2+}/Co^{2+}/Mn^{2+}$ separation by balancing permeation of free M^{2+} ions against rejection of negatively charged M–EDTA complexes.[57] These results show that such high selectivity does not arise from intrinsic recognition of bare Co^{2+} and Ni^{2+} by the material, but is jointly constructed through solution coordination, species charge, and intramembrane migration. This strategy can substantially amplify otherwise limited ionic differences, but its performance depends more strongly on ligand concentration, counter-ion composition, and complexation equilibria.

Adjacent lanthanide ions extend this challenge to an even finer scale. The continuous and subtle radius changes produced by lanthanide contraction, together with highly similar hydration and coordination chemistry, mean that conventional surface ligands often yield separation factors of only a few units. For porous zirconia modified with aminomethylenephosphonic-acid ligands, the separation factors for adjacent Ce^{3+}/La^{3+} and Yb^{3+}/Tm^{3+} in an equimolar mixture containing all lanthanides are only 2.3 ± 0.4 and 2.7 ± 0.1, respectively.[58] More notably, the Lu^{3+}/La^{3+} separation factor of the same material is 87.4 ± 9.8 in a multicomponent mixture but decreases to 29.8 ± 2.7 in a binary solution, demonstrating that competitive occupancy can markedly alter apparent selectivity and that a single binary system may not represent partitioning in an actual rare-earth mixture.

Further preorganization of intrapore coordination sites can greatly amplify these subtle differences. The ion-microporous ATZ-BTC-Zn framework uses size-matched exchangeable cations and a high density of “nanotrap pockets” to attain a Ce^{3+}/La^{3+} separation factor of 543 in a binary system and a factor of 908 for the adjacent light rare-earth pair La^{3+}/Nd^{3+}.[59] These values, however, describe partition selectivity in equilibrium adsorption or ion exchange rather than steady-state transmembrane permeation. Their significance lies in demonstrating that regular pore cavities can amplify extremely small free-energy differences among lanthanide ions through the combined effects of coordination geometry, site density, and local charge. Whether this advantage can be further translated into continuous transport still depends on sufficiently rapid intrapore diffusion and ion release.

These cases show that isovalent multivalent-ion separation has at least three distinct origins. Mg^{2+}/Ca^{2+} separation more strongly reflects recognition of hydration geometry and confined-water structure; Co^{2+}/Ni^{2+} separation can use solution coordination to convert subtle chemical differences into pronounced charge differences; and separation of adjacent lanthanides relies on preorganized multidentate sites and competitive occupancy to amplify continuous variations in coordination free energy. Binding strength, EC_{50}, adsorption separation factor, and membrane-transport selectivity should therefore not be placed in a single ranking. A more meaningful question is whether the free-energy difference established during ion entry or partitioning can survive competitive occupancy in a mixed feed and be retained during subsequent migration and release.

3.2.4 Cross-System Understanding of Ion-Separation Performance

Across the above systems, high membrane selectivity is generated primarily through two pathways. The first is inhibition of competing ions, in which pore-entry confinement, a higher desolvation penalty, or unfavourable coordination preferentially reduces the partitioning and migration of nontarget ions. The second is promotion of the target ion, in which continuous hydrated pathways, reversible recognition sites, or low-resistance transport pathways enhance target-ion entry and diffusion. The first route readily produces a high separation factor but does not necessarily improve target-ion productivity. The second is more favourable for maintaining flux, but is generally more sensitive to site-exchange rates, channel connectivity, and feed composition.[8,24,42,47,49,50,52–54]

The relative importance of these two routes differs among ion systems. Heterovalent ions exhibit relatively pronounced differences in charge, hydration, and Donnan partitioning and can therefore often be separated with high selectivity by suppressing competing ions. Isovalent monovalent ions have smaller physicochemical differences, requiring accumulation through channel orientation, repeated recognition, and transport distance. Isovalent multivalent ions require coordination thermodynamics, species forms, and exchange kinetics to be mutually matched. The so-called selectivity–flux trade-off is therefore not a single empirical upper bound shared by all materials, but the system-specific distribution of resistance among pore entry, partitioning, intrapore migration, and release.[42,43]

Table 3. Quantitative ion-separation performance of representative ion-selective membranes and nanochannels

Ion system	Material/membrane thickness and area	Feed and conditions	Mode and driving force	Flux/permeation performance	Selectivity definition and value	Duration and feed realism	Refs.
Li^+/Mg^{2+} heterovalent cations	OSARIP polyamide NF membrane; selective layer ≈55 nm; effective area 7.1 × 10^{-4} m^2	Binary LiCl/$MgCl_2$; total salt 2000 ppm; Mg/Li mass ratio 20:1; 25 °C	Cross-flow pressure filtration; 4 bar; 50 L h^{-1}	Li^+ permeability ≈10 μm s^{-1}; Mg^{2+} rejection 99.82%; Li^+ rejection −48.35%	S=(1−RLi)/(1−RMg); 828 at 20:1; maximum 4147 at Mg/Li=60:1	Stabilized ≥30 min; simulated brine; high-salinity and multicomponent tests also reported	[49]
Li^+/Na^+, Li^+/K^+, Li^+/Mg^{2+}, Li^+/Ca^{2+}	Rigid nonporous crystalline NCM-1 membrane; submillimetre bulk thickness (0.6 mm variant also tested); area NR	Single salts or five-cation mixture, 0.1 M each; natural low-grade brine also tested	Electrically driven; 3 V; HCl receiver	Single-salt Li^+ flux 575.8 mmol m^{-2} h^{-1}; approximately halved in mixed salts	Flux-normalized separation factor; mixed-feed Li/Na 1325.2, Li/K 13695.9, Li/Mg 25283.7, Li/Ca 14048.2	13 cycles with natural brine; post-operation fissures and Na^+ insertion observed	[60]
Na^+/Mg^{2+} and Cl^-/SO_4^{2-}	Oriented COF-170/PAN composite; COF layer ≈170 nm; area NR	Ternary NaCl/Na_2SO_4/$MgCl_2$, 0.1 or 1 M each	Concentration-gradient diffusion; −1 V also applied	NaCl flux ≈90 mmol m^{-2} h^{-1} in 0.1 M single-salt test; total flux increased ≈6-fold at −1 V	Relative ion-flux ratio; at 0.1 M ternary feed Cl/SO_4=64 and Na/Mg=39; at 1 M, 113 and 45	30 min ternary test; 3 h artificial-seawater test; simulated feeds	[38]
Cl^-/SO_4^{2-} heterovalent anions	APV-crosslinked GO laminate; channel ≈7 Å; thickness and area NR	0.1 M NaCl/Na_2SO_4 mixture; flow 20 mL min^{-1}	Continuous-flow electrodialysis; 6 mA cm^{-2}	Cl^- transport rate 2.74 mol m^{-2} h^{-1}	S=(JCl/CCl)/(JSO4/CSO4); Cl/SO_4=125	108 h continuous test; 10-cycle test; simulated mixed feed	[37]
Li^+/Mg^{2+} heterovalent cations	COF scaffold gate–lane composite NF membrane; thickness and area NR	Binary salt with Mg/Li mass ratio 50; concentration, pH and temperature NR	Pressure-driven nanofiltration	Permeance 11.5 L m^{-2} h^{-1} bar^{-1}	True selectivity 231.9; ideal selectivity 80.5; Li^+ enrichment 120.2%	Duration NR; simulated high-Mg/Li brine	[40]
Cu^{2+}/Ni^{2+}, Zn^{2+}, Co^{2+}, Mg^{2+} homovalent divalent	$(PDMAA/PAH)_{3.5}$ ultrathin coordinating polymer membrane; thickness and area NR	0.1 M $CuCl_2$ + 0.1 M competing salt; pH 3.6; 25±0.1 °C	Concentration-gradient diffusion; DI-water receiver	Cu^{2+} flux ≈(17–20)×10^{-9} mol cm^{-2} min^{-1}; competing-ion flux decreases with binding-energy contrast	Multisalt $S_i(Cu/M_j)$; Cu/Ni=26.0, Cu/Zn=0.84, Cu/Co=17.9, Cu/Mg=52.1	Steady multisalt tests; simulated binary feeds	[53]
K^+/Li^+ and Na^+/Li^+ homovalent monovalent	Randomly oriented sulfonated COF/AAO membrane; COF layer 6–8 μm; area NR	KCl+LiCl or NaCl+LiCl, 0.1 M each; 0.1 mM–0.1 M and seawater also tested	Passive diffusion; DI-water receiver	K^+ or Na^+ permeated continuously; Li^+ remained below detection over 60 min; permeation decreased with thickness	Permeation-rate ratio; finite selectivity not assigned because Li^+ was below detection	60 min; five-cation mixtures and seawater validation	[52]

Note: Selectivity definitions and testing conditions are specified for each entry. NR, not reported.

For Review Only

3.3 Selective Adsorption and Ion Capture

The fundamental distinction between selective adsorption and membrane transport is that the target ion need not continuously traverse the material. Instead, it is preferentially transferred into the solid phase and subsequently forms a recoverable product stream through desorption or regeneration. Adsorption performance should therefore not be judged solely by single-component equilibrium capacity, but by the actual capture ability of the material under competitive feed conditions and by whether enrichment in the solid phase can be further translated into effective recovery.[61–66]

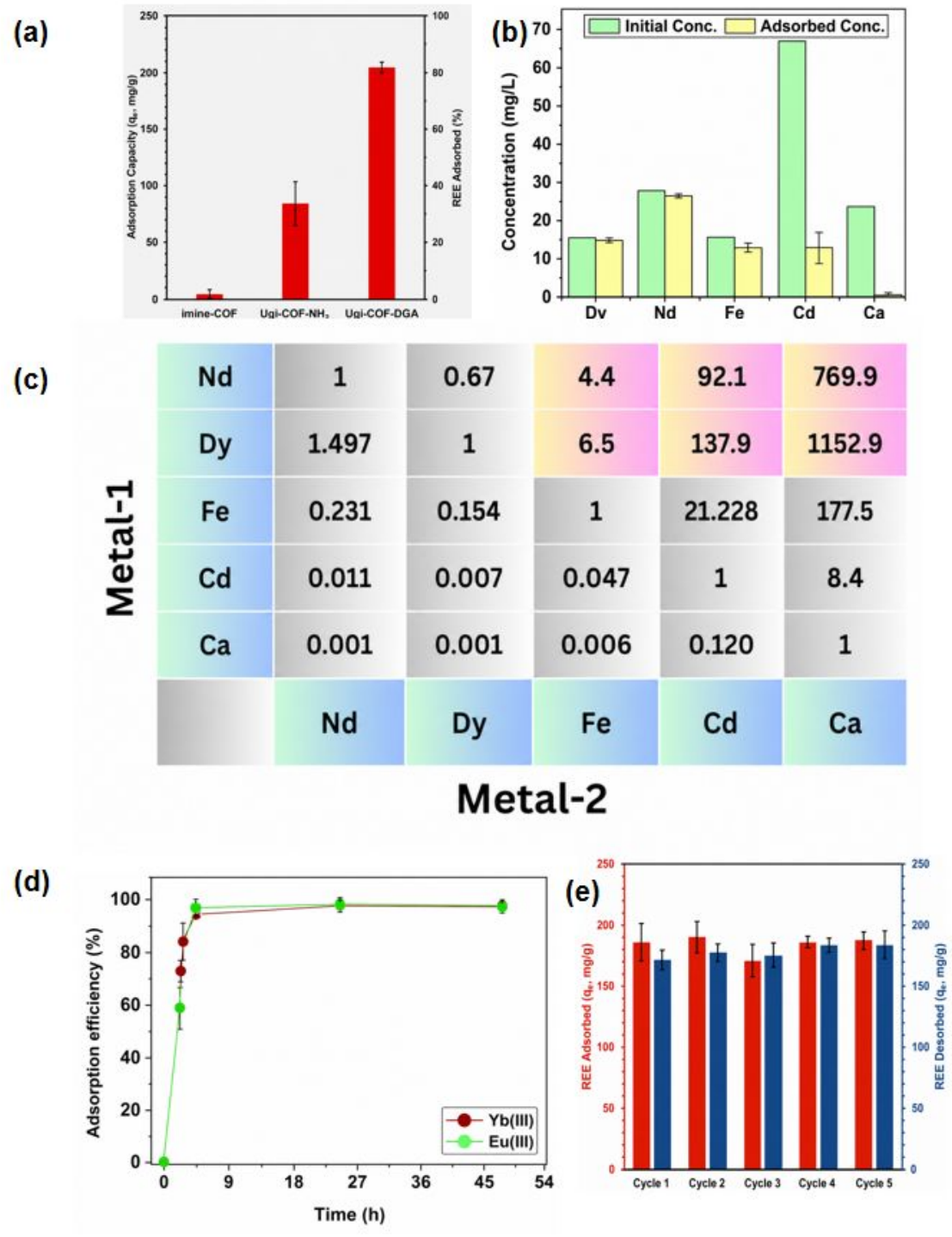


Figure 9 Selective ion capture from site construction to competitive separation and reversible release.

(a) Nd^{3+} adsorption capacities of different COFs, showing the enhanced rare-earth capture enabled by DGA recognition sites. Adapted from Ref. [61]. (b,c) Initial and adsorbed metal concentrations and pairwise separation factors of CA-BNMG-1 composite beads in simulated mine wastewater, demonstrating preferential capture of Dy^{3+} and Nd^{3+} in the presence of abundant competing ions. Adapted from Ref. [62]. (d) Time-dependent adsorption efficiencies for Yb^{3+} and Eu^{3+}, reflecting the kinetic accessibility of selective sites in the shaped beads. Adapted from Ref. [62]. (e) The capacity variation of Ugi-COF-DGA during five Nd^{3+} adsorption-desorption cycles demonstrates that the captured ions can be released, providing preliminary evidence of site reversibility. Adapted from Ref. [61].

3.3.1 Equilibrium Affinity and Site Utilization

In nanoporous adsorbents, specific surface area and functional-group density are commonly the first parameters used to explain increases in capacity, but neither has a simple positive correlation with selectivity. A large volume of nonselective pores may increase total adsorption without necessarily increasing the partition advantage of the target ion over competing components. Conversely, a small number of geometrically and chemically well-defined sites may contribute little to the total capacity while determining final product purity. High capacity and high selectivity therefore often originate from different types of sites and must be distinguished.

The COF system shown in Figure 9a illustrates this distinction.[61] For otherwise similar frameworks, introduction of diglycolamide coordination units produces a substantially higher Nd^{3+} adsorption capacity than in the imine and aminated control materials. The key is not simply an increase in oxygen-containing groups, but the creation of a local chemical environment better suited to rare-earth coordination, converting otherwise poorly utilized intrapore space into accessible recognition sites. Similar strategies are widely used with macrocyclic receptors, ion-imprinted cavities, and preorganized multidentate ligands, which amplify small free-energy differences among ions by constraining coordination geometry and the local solvation state.

The presence of a site, however, does not mean that the site can be effectively utilized. Excessive functionalization may simultaneously reduce pore volume and pore-entry size, thereby limiting access to internal sites. Adsorbed ions may also obstruct subsequent mass-transfer pathways, causing the theoretical site density to become increasingly decoupled from actual utilization. Site design should therefore report not only functional-group content but also the fraction of accessible sites, utilization per unit time, and how utilization changes with ion loading.

For biochars and mineral composite adsorbents, the problem is more complex.[18,48,66] Apparent removal may simultaneously arise from surface complexation, ion exchange, dissolution–reprecipitation of mineral phases, and micropore retention, and some heavy metals may enter the solid phase as precipitates or reduction products. Assigning the entire concentration difference between the liquid and solid phases to “selective adsorption” would overestimate the contribution of material recognition sites. Reliable interpretation requires speciation analysis, mass balance, and post-adsorption solid-state characterization to distinguish reversible binding, structural ion exchange, and irreversible phase transformation.

3.3.2 Competitive Occupancy and Working Capacity

Selective sites never operate in isolation in a practical feed. Even when high-abundance competing ions have weaker affinity for the material, mass action may cause them to occupy large numbers of nonselective regions. The target ion must progressively displace them through more favourable coordination or desolvation. Multicomponent adsorption is therefore not a simple superposition of several single-component isotherms, but an occupancy process that continuously reorganizes with time and site saturation.

Figures 9b and 9c show that reporting the separation factor alone is insufficient for evaluating competitive capture.[62] CA-BNMG-1 composite beads retain high adsorption of Dy^{3+} and Nd^{3+} in simulated mining wastewater, while solid-phase enrichment of high-concentration Cd^{2+} and Ca^{2+} is markedly weaker. Pairwise separation factors further indicate a substantial preference for rare-earth ions over common competing metals. The magnitude of the separation factor, however, must be interpreted together with the absolute amount captured. If competing-ion adsorption approaches zero but target-ion uptake is also very low, an extremely high ratio does not mean that the material has sufficient treatment capacity. By contrast, a material with a moderate separation factor but stable working capacity under highly competitive conditions may offer greater process value.

Competition does not necessarily reduce selectivity. Weakly bound ions may initially occupy external surfaces or low-energy sites and then be progressively displaced by target ions. Certain coexisting ions may also change the surface potential, coordination form of the target ion, or intrapore water structure, thereby increasing target-ion partitioning. Competitive adsorption therefore depends on concentration ratio, binding sequence, and displacement kinetics and cannot be predicted solely from a static ranking of binding energies. The same material may even exhibit different selectivity sequences in short- and long-duration tests: early data are governed by external-surface mass transfer, whereas later behaviour gradually shifts towards deep-pore diffusion and site displacement.

This distinction also reveals the difference between “maximum capacity” and “working capacity”.[43,62–66] Maximum equilibrium capacity describes the total amount accommodated by a material at high concentration and after sufficient equilibration. Competitive working capacity represents the fraction actually utilized when the target ion is at low abundance and competing ions are present in large excess. For continuous treatment, breakthrough capacity is closer to practical performance than either quantity because it is directly constrained by the width of the mass-transfer zone, feed velocity, and the allowable leakage concentration. Existing adsorption studies still overemphasize maximum capacity in single-salt systems, while mixed-salt working capacity and breakthrough behaviour remain comparatively underreported, creating one of the most common sources of superficial superiority in comparisons among materials.

3.3.3 Intrapore Mass Transfer and Shaping Effects

Even if the target ion thermodynamically favours entry into a material, the sites may not be fully utilized within a finite time. To reach an intrapore recognition site from the bulk solution, an ion must undergo external-film mass transfer, pore-entry partitioning, intrapore diffusion, and local ligand exchange. High resistance at any one of these steps can confine high affinity to the local surface rather than translating it into overall working capacity.

In Figure 9d, the adsorption of Yb^{3+} and Eu^{3+} by shaped MOF particles increases rapidly at first and then gradually reaches a plateau.[62] This result indicates that polymer coating does not completely block access of rare-earth ions to internal sites, although several hours are still required to approach equilibrium. Material shaping therefore has a characteristic dual effect. On the one hand, macroscopic particles facilitate recovery, packing, and flow operation. On the other hand, the binder phase and longer diffusion pathways increase internal mass-transfer resistance. Rapid adsorption and high capacity observed in powder materials are generally redistributed after granulation, membrane formation, or fixed-bed packing: part of the capacity may be lost through site occlusion, while another part becomes more usable because of improved structural stability and fluid contact.

A high site density may also cause preferential surface occupancy, pore-entry crowding, and underutilization of deep sites. In materials containing multidentate ligands or ion-imprinted cavities, ligand exchange may itself become rate limiting.

For Review Only

Adsorption time should therefore be shortened by optimizing pore hierarchy, particle size, and the spatial distribution of sites, while perturbations in particle size, flow rate, and temperature should be used to distinguish the relative contributions of external mass transfer, intrapore diffusion, and ligand exchange.

Biochar systems further illustrate the strong influence of target-ion speciation on mass transfer.[66] Natural organic matter may form large complexes with metal ions, reducing the probability that they enter micropores. Electrolytes and multivalent cations may in turn alter the aggregation state of organic matter through charge screening or bridging, causing apparent adsorption to vary by orders of magnitude among different water matrices. “Pore-size matching” therefore refers not only to a comparison between material pore size and the dimensions of bare or hydrated ions, but also to the actual complexes, ion pairs, and colloidal forms present in the feed.

Analysis of adsorption kinetics should likewise not stop at fitting empirical models. Pseudo-first-order or pseudo-second-order equations can describe the time dependence of concentration but cannot by themselves establish reaction control or a chemisorption mechanism. More informative approaches to identifying the actual limiting step include varying particle size, stirring rate, temperature, and flow rate, or using time-resolved characterization to track the evolution of solution species and solid-state sites. For continuous-flow systems, the shape of the breakthrough curve often provides more information than the equilibration time in a batch test because it simultaneously reflects site affinity, intrapore diffusion, and movement of the mass-transfer zone.[62,64,65]

3.3.4 Release and Reversible Capture

The adsorption process does not end when capacity reaches a plateau. Enrichment in the solid phase can be translated into a recoverable product stream only if the target ion can be selectively, concentratedly, and controllably released from the material. Recognition sites therefore need to operate within an appropriate reversible-affinity window: sufficiently strong to resist competitive occupancy under feed conditions, but able to dissociate rapidly under regeneration conditions. Interactions that are too weak cannot establish selectivity, whereas excessively strong binding shifts the separation bottleneck from capture to desorption.

In Figure 9e, Ugi-COF-DGA retains similar uptake and release amounts over five Nd^{3+} adsorption–desorption cycles, indicating preliminary reversibility of its coordination sites.[61] The system, however, uses relatively concentrated nitric acid for elution. Near-complete desorption first establishes that Nd^{3+} can be released from the material, but does not by itself demonstrate that regeneration is mild, efficient, or low in resource consumption. Desorption efficiency should be reported together with eluent composition and concentration, liquid-to-solid ratio, elution volume, target-ion concentration in the eluate, and structural retention of the material after cycling.

Final desorption efficiency is also insufficient for evaluating resource-recovery value. A large volume of dilute eluate may release most of the target ion but negate the enrichment achieved during adsorption. High ionic strength or competitive ligands may simultaneously release coexisting components and reduce product purity. More process-relevant metrics include release rate, elution-peak width, enrichment factor, recovery purity, complete mass balance, and reagent consumption per unit amount recovered.[61–65] A system with high adsorption selectivity but producing a highly dilute product stream may have less practical value than a material with slightly lower selectivity that can release the target ion in concentrated form.

A small number of adsorption–desorption cycles can provide preliminary evidence of reversible release, but should not be used to establish long-term regeneration stability. Whether selective sites, pore structures, and material composition are continuously retained during cycling, and whether the chemical and energy inputs required to restore separation function increase with cycle number, are questions of operational stability and are discussed in Section 3.4.

Overall, the process performance of selective adsorption is jointly controlled by equilibrium partitioning, competitive occupancy, intrapore mass transfer, and reversible release. Equilibrium capacity has a clear separation and recovery significance only when the target ion can occupy effective sites in a complex feed, establish sufficient working capacity within a practical residence time, and be released as a product stream of reasonable concentration and purity.

For Review Only

Table 4. Quantitative performance of representative nanoporous adsorbents for competitive ion capture

Target/competing ions	Adsorbent and selective site	Feed, pH and temperature	Capacity or partition metric	Competitive selectivity/working performance	Kinetics and testing mode	Desorption, regeneration and limitation	Refs.
Nd^{3+}; REE capture	DGA-postfunctionalized Ugi-COF; multidentate diglycolic-acid sites	50 ppm $Nd(NO_3)_3$; 10 mg in 50 mL; pH ≈6; 25 °C	qe≈203 mg g^{-1} under the stated condition; Langmuir qmax≈656 mg g^{-1}	Predominantly single-component capacity; no real-feed competitive working capacity	20 h batch equilibration; rapid initial uptake	Desorption with 2.0 M HNO_3; uptake/release largely retained over five cycles; strong-acid demand remains a process burden	[61]
Nd^{3+}, Dy^{3+}, Yb^{3+}, Eu^{3+}; Cd^{2+}, Ca^{2+}, Fe^{3+} and others	CA-BNMG-1 MOF/cellulose-acetate macrobeads; imidazole-N sites	Simulated mine wastewater/e-waste leachate; pH 5; 25 °C	Yb^{3+} and Eu^{3+} adsorption efficiencies ≈95–100%; absolute uptake feed-dependent	In simulated mine water: Nd/Cd=92.1, Dy/Cd=137.9, Nd/Ca=769.9, Dy/Ca=1152.9	24 h batch tests; Yb/Eu approach equilibrium within hours	Mild acid elution; >95% uptake retained over cycles; Cu leaching <1%; fixed-bed evidence remains limited	[62]
Tb^{3+} and multiple REEs; broad non-REE background	Lanmodulin-functionalized magnetic nanoparticles; protein recognition sites	Synthetic competition tests, coal-fly-ash leachate and geothermal brine	Tb adsorption activity 6.01±0.11 μmol g^{-1}	REE selectivity retained against diverse non-REEs; 967-fold increase in REE purity	Fast batch uptake; magnetic recovery	>90% desorption; ≈95% activity retained after eight cycles; relatively low gravimetric capacity	[63]
Y^{3+}, Gd^{3+}, Dy^{3+}; K^{+}, Mn^{2+}, Ca^{2+}, Mg^{2+}	ZIF-8; imidazole-N and hydrolysis-assisted REE–O interactions	Real REE-mining wastewater; pH and temperature as reported	Kd: Y 4.02×10^4, Gd 7.8×10^4, Dy 6.8×10^4 mL g^{-1}	Competing-ion Kd only 239–396 mL g^{-1}, giving orders-of-magnitude partitioning advantage	Batch adsorption plus 7 h column test	>40% desorption of heavy REEs; >40% column recovery; recovery remains below what equilibrium partitioning alone suggests	[64]
Li^{+}; Na^{+} and other brine ions	P-PAA granulated LMO; hierarchical pores and PAA carboxyl groups facilitate Li^{+} transfer	Real Puguang gas-field brine with high Na salts and organic contaminants	Li^{+} capacity 12.9 mg g^{-1}; Kd=1391.3 mL g^{-1}	Li/Na separation factor 718; Li recovery ≈98.4–98.5% from real brine	Granular adsorption with kinetic and intraparticle-transport analysis	No obvious salt crystals/internal cracks after extended cyclic use; cumulative bed volumes and regenerant consumption need fuller reporting	[65]
Hg(II); Cl^{-}, NO_3^{-}, Ca^{2+}, Na^{+} and NOM	Wood-based SWP700 biochar; sulfur-containing intraparticle sites	Hg-contaminated water; NOM up to 46.2 mg L^{-1}; varied ionic backgrounds; 48 h	log Kd=0.8–4.4 in complex matrices, spanning >3 orders of magnitude	Not a conventional ion-pair selectivity metric; NOM limits pore access, whereas Cl^{-} and Ca^{2+} can restore capture through speciation and bridging	48 h batch tests; speciation modelling plus EXAFS	Desorption/reuse not reported; demonstrates that real-water chemistry can reshape apparent capture performance	[66]

Note: maximum equilibrium capacity, competitive working capacity, distribution coefficient and breakthrough capacity are physically distinct. Single-component qmax values should not be used to infer practical recovery without competitive-feed or continuous-flow evidence.

3.4 Operational Stability and Process Performance

Peak flux, selectivity, or adsorption capacity obtained by selective ion-separation materials in ideal feeds and short-duration tests does not automatically extend to continuous operation. In an actual process, the material must withstand high ionic strength, compositional fluctuations, foulant deposition, mechanical loading, and repeated cleaning or regeneration. The resulting reconstruction of pore structure, changes in interfacial charge, and deactivation of recognition sites may gradually erode the initially established selective advantage. Operational stability should therefore be understood as sustained retention of the origin of selectivity and its corresponding separation function under practical conditions, rather than as preservation of material appearance or a single performance metric.

Such functional retention involves several interconnected but nonequivalent levels. Chemical stability concerns whether the framework, polymer chains, metal nodes, or active phase undergo hydrolysis, dissolution, or leaching. Structural stability concerns changes in operando pore size, interlayer spacing, membrane–support interfaces, and particle morphology. Functional-site stability involves irreversible occupancy, drift in protonation state, ligand loss, and response fatigue. These changes must ultimately be evaluated through target-ion flux, competing-ion leakage, working capacity, product purity, and recovery.[43,67–75] Structural preservation is only a necessary condition for stable operation; process-level stability can be discussed only when both separation function and process output are retained.

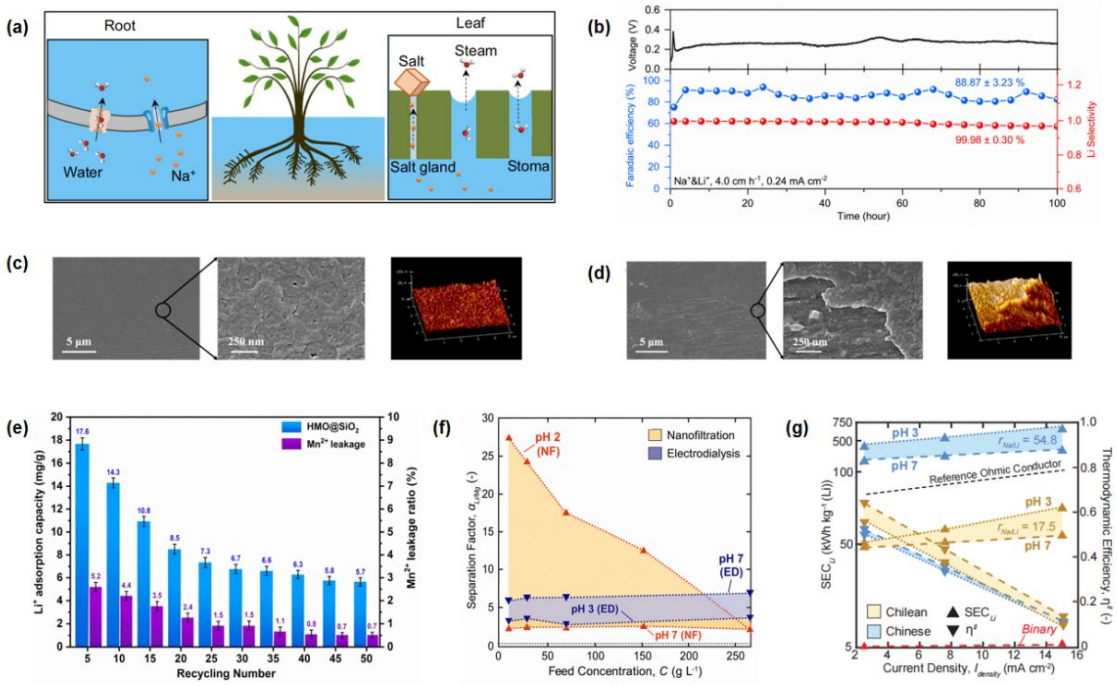


Figure 10 Multilevel assessment of operational stability and process performance in selective ion separation.
(a) A mangrove-inspired root–leaf transport architecture coupling selective ion exclusion at the root with evaporation-driven water transport at the leaf, illustrating the translation of material function into an integrated separation process. Adapted from Ref. [67]. (b) Operating voltage, Faradaic efficiency, and Li^+ selectivity during 100 h of continuous lithium extraction from a mixed Na^+/Li^+ feed, showing that operational stability requires the simultaneous retention of driving conditions, transport efficiency, and selectivity. Adapted from Ref. [68]. (c,d) FESEM and AFM images of CEM 0 and CEM 409 membranes, revealing surface roughening, delamination, and defect development under hypersaline-brine exposure and linking performance drift to structural degradation. Adapted from Ref. [69]. (e) The Li^+ working capacity and Mn^{2+} dissolution rate of HMO@SiO_2 over 50 adsorption-desorption cycles indicate that the apparent cycle plateau may be accompanied by initial capacity loss and active phase depletion. Adapted from Ref. [70]. (f) Li^+/Mg^{2+} separation factors of nanofiltration and electrodialysis as functions of feed concentration and pH, illustrating the coupled effects of ionic strength, interfacial charge, and operating mode on apparent selectivity. Adapted from Ref. [71]. (g) Specific energy consumption per unit Li recovered (SECLi) and second-law efficiency (ηII) as functions of current density for Chilean and Chinese salt-lake brines, revealing the energetic penalty associated with maintaining ion selectivity under hypersaline conditions. Adapted from Ref. [72].

3.4.1 From Operating Time to Cumulative Load

Existing studies often summarize stability using operating duration or cycle number, but neither metric represents the actual treatment load borne by the material. The same 100 h of operation may correspond to cumulative transported amounts differing by several orders of magnitude because of differences in membrane area, feed concentration, flow rate, and target-ion flux. Similarly, tens of cycles in low-concentration batch adsorption cannot be equated with operation of a fixed bed treating tens of bed volumes near breakthrough. Stability is therefore better described jointly by time and cumulative load, including treated volume per unit area, cumulative target-ion transport, number of bed volumes, regeneration count, and pressure or electric-field history.

Figure 10b shows the synchronous evolution of operating voltage, Faradaic efficiency, and Li^+ selectivity during continuous lithium extraction.[68] The value of this result lies not merely in operation for 100 h, but in the simultaneous tracking of several mutually constraining metrics. Voltage reflects device resistance and driving requirements, Faradaic efficiency measures charge utilization, and selectivity describes relative transport of the target and competing ions. Even when total current or target-ion flux remains stable, a gradual increase in competing-ion leakage indicates deterioration of separation function. Conversely, preservation of selectivity may be achieved at the cost of continuously increasing voltage and energy consumption. “Stability” should therefore not mean that an individual curve

remains approximately horizontal, but that the relationships among critical performance metrics do not undergo substantive drift within a specified load range.

Different testing modes also provide markedly different levels of stability evidence.[43,68–70] Static diffusion cells and batch adsorption are suitable for excluding rapid dissolution or initial deactivation of the material, but poorly reproduce concentration polarization, propagation of the mass-transfer zone, foulant accumulation, and local precipitation in continuous processes. Continuous-flow membrane cells, fixed beds, and cyclic electrochemical devices reveal performance evolution more realistically, but their effective area, flow-channel geometry, loading, and operating boundaries must still be specified. Long-duration laboratory operation can establish durability under a particular set of conditions, but cannot be directly extrapolated to module lifetime or replace validation using real feeds and enlarged systems.

3.4.2 Complex Feeds and Selectivity Drift

High-salinity backgrounds, organic ligands, colloids, and scaling precursors in practical feeds simultaneously alter target-species speciation, interfacial state, and mass-transfer resistance, causing selectivity to be reordered during operation.[71] The challenge posed by complex feeds is therefore not merely the presence of more competing ions, but also the temporal evolution of material state and the dominant transport mechanism.

Increasing ionic strength first compresses the electrical double layer and weakens Donnan exclusion, causing heterovalent-ion separation that relies on fixed charge to progressively lose its advantage. In Figure 10f, the nanofiltration membrane achieves a high Li^+/Mg^{2+} separation factor at low pH and low feed concentration, but selectivity decreases substantially as salt concentration increases. Electrodialysis, by contrast, maintains a relatively stable separation factor over a broader concentration range. This difference does not imply that electrodialysis is intrinsically unaffected by high salinity; rather, it shows that different processes depend differently on interfacial charge, transference number, and external driving force. Material performance cannot therefore be compared independently of feed concentration and mode of operation. An electrostatic mechanism dominant in a dilute system may be reconstructed by charge screening, ion correlations, and concentration polarization at high salinity.

The influence of pH likewise extends beyond regulation of surface charge.[72] It also changes metal-ion hydrolysis, complexation, and precipitation equilibria, as well as the protonation state of coordination sites. An increase in removal observed in some systems may arise because the target ion forms an insoluble phase or a complex that is more readily rejected, rather than because the affinity of a recognition site genuinely increases. Such speciation changes are particularly likely to confound selective adsorption with phase transformation for rare-earth, transition-metal, and uranyl ions. Complex-feed tests therefore need to combine solution speciation with characterization of solid products. Otherwise, apparent “resistance to pH fluctuations” may simply mean that similar endpoint concentrations are maintained through different chemical processes rather than through preservation of the same separation mechanism.

Organic matter and colloids exert more dualistic effects.[66,69] On the one hand, they may cover pore entrances or functional sites and reduce flux and working capacity. On the other hand, the resulting fouling layer may itself introduce new charge- and size-sieving effects, more strongly obstructing competing ions and temporarily increasing apparent selectivity. Such an apparent “performance improvement” does not indicate a superior material state, but may mean that the original selective layer has been replaced by an uncontrolled secondary mass-transfer layer.[75] Flux decline, selectivity increase, or capacity retention in a complex feed therefore cannot be interpreted in isolation, but must be assessed together with foulant-layer composition, reversible cleanability, and recovery of selectivity after cleaning.

3.4.3 Structural Degradation and Post-Operation Evidence

Performance degradation during operation generally arises from changes occurring at multiple scales. Lamellar membranes may undergo swelling, compaction, or nanosheet misalignment; polyelectrolyte selective layers may reorganize under high-salinity and multivalent-ion conditions; and delamination or nonselective bypass pathways may develop at the interface between a selective layer and its support. Adsorbent particles may experience abrasion, pulverization, pore blockage, and dissolution of active components. These changes do not necessarily occur synchronously and may not all be visible by conventional dry-state characterization.

The pronounced roughening, delamination, and defect formation observed on the membrane surfaces in Figures 10c and 10d under high-salinity conditions[69] demonstrate that long-term performance changes can be directly traced to structural degradation of the selective layer. The converse, however, is not valid: the absence of visible cracks does not prove preservation of transport pathways. Minor swelling of subnanometre pores, a decrease in fixed-charge density, or changes in local wettability may substantially alter ion partitioning while leaving the macroscopic morphology largely unchanged. For isovalent-ion separation that depends on precise pore size and coordination environments, such subtle changes may be more consequential than complete collapse of the framework.

Functional-site deactivation may also precede structural failure. Once high-affinity sites are irreversibly occupied by competing ions or impurities, total adsorption capacity may still be maintained by a large population of nonselective sites; capacity retention therefore does not necessarily mean selectivity retention.[9] A similar problem exists in membrane systems: total ionic conductivity may change only slightly even though the local coordination sites originally responsible for the target-ion advantage have undergone hydrolysis, screening, or reorganization. Stability evaluation should therefore target the origin of selectivity itself rather than merely determine whether the material remains porous or retains ion-exchange capacity.

The purpose of post-operation characterization is to establish this causal relationship. PXRD can determine whether long-range structural order is retained, but cannot prove that pore-entry dimensions and site chemistry remain stable. SEM can identify macroscopic defects, but provides little information on wet-state swelling or local coordination changes. More persuasive evidence should correlate changes in wet-state structure, surface charge, pore-size distribution, component leaching, residual occupying ions, and functional-group state before and after operation with performance drift. Characterization methods should be selected according to the hypothesized failure mechanism rather than applied as a routine collection of spectra.

3.4.4 Regeneration and Recovery of Function

Regeneration here refers not merely to eluting the target ion from the material, but to whether the material can recover and continuously retain its original separation function after desorption or cleaning. Section 3.3 considers whether a single capture–release process can be closed; this section examines whether the selective sites, mass-transfer pathways, and material

structure continue to operate in the same manner after the process is repeated. A high single-cycle desorption efficiency therefore proves only that the ion can be released, not that the material possesses long-term regeneration stability.

Regeneration conditions themselves may become an important source of material degradation. Strong acids or bases promote dissociation of target ions but may also cause ligand hydrolysis, metal-node leaching, and dissolution of inorganic active phases. Elution using high salt concentrations or competing ligands may be milder, but may leave new counterbalancing ions within the pores and alter the partition sequence in the next cycle. For membrane materials, chemical cleaning can remove a fouling layer but may simultaneously change the charge density, wetting state, and interfacial integrity of the selective layer. Regeneration is therefore not a neutral recovery step, but an additional chemical and structural perturbation experienced by the material in every cycle.

In Figure 10e, the Li^+ adsorption capacity of HMO@SiO_2 decreases rapidly during the initial cycles and then approaches a lower plateau, while Mn^{2+} continues to leach.[70] Such a result cannot simply be summarized as "the material remains usable after 50 cycles". The later plateau may indicate that the more soluble or highly active fraction was consumed during the early cycles, leaving the remaining material in a new, lower-performance steady state. A more meaningful analysis should quantify the working-capacity and selectivity losses between the first cycle and the steady-state regime, and identify the origin of performance decay through leaching of active components, mass loss, and post-operation structural changes.

Performance metrics after regeneration should directly correspond to the original source of selectivity. Adsorbents should report competitive working capacity, retention of target/competing-ion selectivity, loss of active components, and eluent consumption per unit amount recovered. Membrane materials should simultaneously measure target-ion flux, competing-ion leakage, selectivity, and structural changes after cleaning. Dynamic-gating materials should track switching amplitude, response time, hysteresis, and baseline drift. Separation function can be considered recovered only when these mechanism-relevant metrics are restored.[61–65]

The objective of regeneration is therefore not to return the system completely to its initial state after every cycle, but to keep it within a functional window that satisfies requirements for product purity, recovery, and productivity at acceptable material, chemical, and energy inputs. Evaluation should accordingly shift from cycle count to the decay of selectivity with cumulative load, while simultaneously quantifying the reagent and energy costs required to restore separation function.

3.4.5 Module Scale-Up and Process Boundaries

When a material is transferred from a small membrane coupon or powder to a continuous device, the factors controlling separation change. The biomimetic root–leaf architecture shown in Figure 10a extends local selective channels into a process coupling evaporation, transport, and salt management.[67] Such integrated designs can use spatial division of function to reduce the burden on a single separation layer, but also introduce new stability boundaries, including salt crystallization at the evaporation interface, ion backflow between functional regions, blockage of capillary channels, and unequal ageing rates among components. Conceptual process integration is genuinely superior to a single material unit only when these interfaces can operate cooperatively over the long term.

As membrane area increases, the probability of local defects increases, and a small number of bypass pathways may dominate competing-ion transport across the entire module. Velocity distributions and concentration polarization within the flow channel also invalidate the uniform mass-transfer conditions of laboratory membrane coupons. Fixed-bed scale-up faces nonuniform packing, channeling, particle compaction, and increased pressure drop.[43,75] Scale-up is therefore not a linear extrapolation of flux per unit area or capacity per unit mass, but a new problem involving coupled structure and fluid flow. Whether the material retains selectivity in a module must be evaluated in terms of effective area, flow distribution, stage recovery, and product composition.

Process stability is further constrained by the energy and material inputs required to maintain separation performance.[71] Figures 10f and 10g jointly reveal the intrinsic coupling between selectivity and energy efficiency under high-salinity conditions. As feed concentration increases, compression of the electrical double layer and weakening of Donnan exclusion cause the Li^+/Mg^{2+} separation factor of nanofiltration to decrease continuously. Electrodialysis can partly maintain differences in ion migration by increasing current density, but this increases the specific energy consumption per unit Li recovered and correspondingly decreases second-law efficiency, with the trade-off strongly dependent on brine composition.[72] Compensating for declining material selectivity by increasing the external driving force therefore does not eliminate the separation limitation, but may simply shift the bottleneck from intramembrane transport to system-level energy consumption. Operational stability should consequently consider not only whether selectivity is retained, but also whether the marginal energy required to maintain target purity and recovery continues to rise with feed concentration and operating load.

The endpoint of operational evaluation should therefore extend beyond the post-membrane solution concentration or ion loading on an adsorbent to include product purity, target-ion recovery, enrichment factor, regeneration-liquid volume, and net energy consumption per unit product. Pretreatment, pumping, cleaning, regeneration, concentration of eluates, and waste-liquid treatment all form part of the actual system boundary.[73] A material-level performance advantage is translated into a process advantage only when high selectivity produces a stable product stream at module scale and the energy, chemicals, and material replenishment required to maintain that state remain within a reasonable range.

For acidic battery leachates, the positively charged PA-TAG polyamide membrane expands ion-transport channels and enhances rejection of divalent cations, achieving a relative volumetric lithium recovery of 48.2% from a simulated feed. After two-stage nanofiltration, the Li^+/M^{2+} mass ratio in the second-stage permeate reaches 53.35, 445 times that of the feed.[76] This case demonstrates that process value depends not only on the rejection or separation factor of a single membrane stage, but also on whether the cascade configuration can translate differences in ion transport into an improved product-stream composition.

Overall, module scale-up places material selectivity under the combined constraints of flow-field distribution, defect statistics, energy consumption, and material circulation.[74] Process validation should centre on a stable product stream and simultaneously report product purity, target-ion recovery, productivity, cumulative treatment load, and energy and chemical inputs per unit product. Together, these metrics define the boundary within which material-level performance is converted into engineering process value.

Table 5. Operational stability and process-level validation of representative selective ion-separation systems

System and configuration	Feed and scale information	Operation/load	Performance retention or drift	Regeneration/fouling/post-operation evidence	Product and energy metrics	Evidence boundary	Refs.
PEI/PS-DVB monovalent-selective ion-exchange membrane	Real Llullaillaco salt-lake brine; TDS up to 409 g L^{-1}; membrane area NR	Exposure/operation up to 30 d	K^+/Mg^{2+} permselectivity decreased from 16.60 to 5.67	FESEM/AFM showed roughening, delamination and defects; charge functionality declined as ions disrupted PEI–PS-DVB ionic crosslinks	Product purity and energy not reported	High-value failure analysis, but not a complete industrial module test	[69]
Redox-couple electrodialysis (RCE) for continuous Li extraction	Li/Na or Li/K brine; linear flow 4.0 cm h^{-1}; current density 0.24 mA cm^{-2}	>100 h continuous operation; ≈0.25 V	Faradaic efficiency 88.87%; Li selectivity 0.9954 (≈99.54%)	Voltage and efficiency monitored over time; limited post-operation structural evidence	Specific energy 1.1 kWh $kgLi^{-1}$	Laboratory continuous device; effective area and real-brine load require scale-up validation	[68]
LSTH ceramic-membrane redox-mediated electrodialysis	Simulated Atacama, Taijinar and Bonneville brines plus seawater; area NR	50 h continuous simulated-seawater test; 5 V	Extraction rate retained 83% of its initial value; charge efficiency ≈60%; product Li purity >99%	Rate loss mainly attributed to declining feed Li concentration; limited structural-aging evidence	7–320 mmol m^{-2} h^{-1}; 0.14–0.34 kWh mol^{-1} depending on feed	Broad simulated resources, but real-seawater and long-term ceramic-interface validation remain needed	[73]
Rigid crystalline NCM-1 membrane for direct lithium extraction	Natural low-grade brine with large excesses of Na^+, K^+, Mg^{2+} and Ca^{2+}	Electrically driven; 13 repeated cycles	Li^+ flux 128–250 mmol m^{-2} h^{-1}; high separation factors retained across cycles	Feed-facing side developed fissures; XRD indicated Na^+ insertion associated with $NaGe_2(PO_4)_3$	Energy per unit Li not reported; direct extraction claimed within <10 h	Real-brine and post-operation evidence reveal the structural-lifetime risk of brittle inorganic membranes	[60]
Rigidly confined APV@GO anion-selective membrane	0.1 M $NaCl/Na_2SO_4$; 20 mL min^{-1}	108 h continuous-flow ED at 6 mA cm^{-2}; separate 10-cycle test	Cl^- flux 2.74 mol m^{-2} h^{-1} and Cl/SO_4 selectivity 125; APV@GO retained performance, whereas pristine GO retained only 26% selectivity after 10 cycles	Retention linked to swelling-resistant channels; quantitative post-operation chemistry remains limited	Product purity and energy not reported	Strong continuous-flow evidence, but still based on a simplified binary feed	[37]
Millimetre HMO@SiO_2/alginate beads; continuous-flow adsorption–desorption	Simulated Da Qaidam brine: Li 330.6, Na 11882.5, K 11737.5, Ca 9613.3, Mg 18825 mg L^{-1}	50 continuous-flow adsorption/acid-desorption cycles	Li capacity fell from 17.6 to a stable ≈6.22 mg g^{-1}; later Mn dissolution averaged 1.26% per cycle	Capacity and Mn dissolution declined together over the first 25 cycles, consistent with acid-induced spinel damage; SiO_2 reduced acid dissolution	Energy and eluate-concentration costs not reported	Many cycles were demonstrated, but the large early capacity loss precludes an unqualified claim of stability	[70]
λ-MnO_2/Purolite C100 composite cation-selective membrane in ED	Simulated brine containing 1% Li; membrane area and long-term duration NR	Electrodialysis process test	Li recovery 44.5%; current efficiency 57.9%	Limited cyclic, fouling and post-operation evidence	Energy consumption 0.185 kWh mol^{-1}	Useful process-level recovery/energy data, but insufficient for long-term stability claims	[74]

Note: The "evidence boundary" column defines the scope supported by the reported tests and should not be interpreted as certification of industrial stability.

4. From Mechanistic Inference to Verifiable Design

The preceding performance analysis shows that similar fluxes, rejection values, or separation factors may correspond to different controlling steps and that endpoint performance alone cannot provide reliable mechanistic attribution.[42–44] This section therefore turns to verifiable design and discusses how operando characterization, multiscale simulation, and data-driven methods can establish testable links among microscopic states, transport processes, and macroscopic performance.

The three approaches play complementary roles. Operando characterization determines wet-state structures, solvation states, site occupancy, and local concentrations under actual feeds and driving forces. Multiscale simulation converts these states into free-energy, diffusion, and multicomponent-transport parameters and connects them to membrane, fixed-bed, and device scales. Data-driven methods integrate material structures, operating conditions, and evidence quality to identify transferable relationships, quantify predictive uncertainty, and guide subsequent experiments.[77–81] This section is therefore organized around identification of operando variables, establishment of cross-scale transfer relationships, and validation of model extrapolation, forming a feedback loop of "mechanistic hypothesis–operando observation–model testing–data updating–material design".

4.1 Operando Characterization

The central task of operando characterization is to synchronously measure the wet-state pore structure, ion solvation, site occupancy, local concentration field, and separation performance under actual feed, driving-force, and flow boundaries.[77,78] The objective is not simply to add more characterization dimensions, but to provide mutually independent experimental constraints on competing mechanisms and to determine which state variables and transport steps generate selectivity.

4.1.1 Operando Pore Structure and Effective Transport Pathways

To validate the operando effective pore aperture proposed in Section 2.1, the channel structure must be measured directly in the presence of solvent filling, ion occupancy, and the actual driving force.[9,77] The objective is no longer merely to demonstrate that a material swells or reconstructs, but to determine where the structural change occurs, its magnitude and timescale, and whether it corresponds to synchronously measured changes in flux and selectivity.

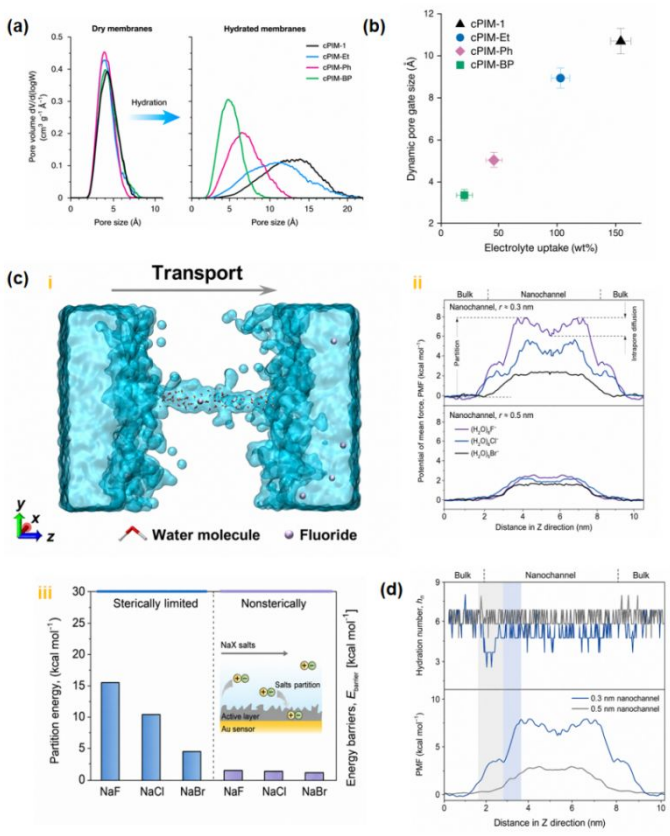


Figure 11 Hydrated pore structure and ion dehydration jointly regulate transport through subnanometre channels.

(a) Pore-size distributions of cPIM membranes in the dry and hydrated states, showing pronounced and chemistry-dependent restructuring upon hydration. Adapted from Ref. [9]. (b) Dynamic pore-gate size as a function of electrolyte uptake, demonstrating that the transport-limiting aperture cannot be inferred directly from the average dry-state pore size. Adapted from Ref. [9]. (c) Simulated water-filled polyamide nanochannels, together with the potentials of mean force and partition energies for hydrated F^-, Cl^- and Br^- transport through channels of approximately 0.3 and 0.5 nm. Strong confinement amplifies ion-dependent entry penalties, whereas these differences diminish in the wider channel. Adapted from Ref. [82]. (d) Hydration-number and free-energy profiles of F^- across the two channel sizes; the narrower channel induces more pronounced partial dehydration accompanied by a higher transport barrier. Adapted from Ref. [82].

The microporous polymer systems shown in Figures 11a and 11b illustrate this discrepancy. Different cPIM membranes exhibit similar pore-size distributions in the dry state but markedly different pore expansion and dynamic aperture sizes after hydration.[9] Increased electrolyte uptake does not simply correspond to enhanced transport. Excessive hydration enlarges percolated channels and weakens sieving, whereas insufficient hydration limits the formation of continuous aqueous pathways. The parameter more closely related to ion transport is the size and connectivity of local bottlenecks after hydration, rather than the dry-state mean pore size.

This understanding requires further differentiation among pore cavities, pore apertures, and percolated pathways. Cavities determine the local accommodation volume, apertures control the entry barrier between adjacent cavities, and percolated pathways determine whether long-range migration can persist.[9,77] These three structural features do not necessarily change synchronously in space. An unchanged mean interlayer spacing does not exclude contraction of local apertures or formation of a small number of bypass pathways; pronounced overall swelling does not mean that all transport pathways lose selectivity. For subnanometre separation, the tail of the structural distribution and local defects are often more consequential than the average structure.[9,77,83]

Operando structural analysis should therefore focus directly on effective transport pathways. In addition to wet-state pore size and interlayer spacing, the distribution of pore entrances, channel orientation, degree of percolation, and spatial location of structural changes should be examined. For responsive systems, it is further necessary to establish whether the structural response occurs at the entrance bottleneck or principal recognition region and whether its timescale is matched to ion migration. Demonstrating swelling, contraction, or conformational change alone is insufficient to support a selective-gating mechanism.[77,78]

4.1.2 Direct Evidence of Solvation and Coordination States

When an ion enters a subnanometre channel, its hydration shell generally undergoes continuous reorganization rather than an abrupt transition from a fully hydrated state to a bare ion.[5–7,82,84] Pore size, local electric field, and pore-wall chemistry jointly determine the extent of water removal, the lifetime of the coordination shell, and subsequent ion–pore-wall interactions.[82,84,85] Bulk hydrated radii and hydration free energies provide preliminary references but cannot fully describe the actual ion state under confinement.

Figures 11c and 11d show the relationship between hydration state and the free-energy pathway for anions entering polyamide nanochannels.[82] Narrower channels cause more pronounced partial desolvation and increase the free-energy costs of pore entry and intrapore migration. In wider channels, hydration-structure changes are weaker and differences in the barriers among anions decrease accordingly. Notably, water removal simultaneously changes effective charge screening and the distance over which the ion interacts with the pore wall. The consequences of desolvation are therefore not limited to a reduction in effective size, but also reconstruct subsequent electrostatic and short-range interactions.

This distinction is especially important when interpreting local spectroscopic and coordination data. A change in coordination number, a shift in a functional-group band, or intrapore ion enrichment establishes only that the local chemical environment has changed. A high intrapore concentration may reflect favourable partitioning or a long residence time; a strong coordination signal may represent a reversible transport intermediate or indicate that the ion is trapped at a high-affinity site.[24,79,82] Whether local binding is translated into steady-state migration must be assessed together with residence time, diffusion coefficient, and outlet-side release behaviour.[24,79,82,85]

For pH-sensitive or multicomponent systems, changes in solution speciation further complicate attribution. Ion hydrolysis, complexation, ion-pair formation, or local precipitation may all alter spectroscopic signals and solid-phase loading.[77,78,86,87] Without speciation analysis and a complete mass balance, a local coordination change may be mistaken for enhanced recognition by the material. Operando characterization must therefore resolve both ion state and site state and establish the temporal order in which they change.[77,78]

4.1.3 Local Concentration Fields and Transport Timescales

Steady-state flux and outlet concentration compress complex spatiotemporal processes into a single value. Interfacial enrichment, concentration polarization, transient occupancy, and propagation of a mass-transfer front may all be averaged out, causing different controlling steps to produce similar macroscopic outcomes. Time- and space-resolved measurements can recover information concealed by these global metrics.[88,89]

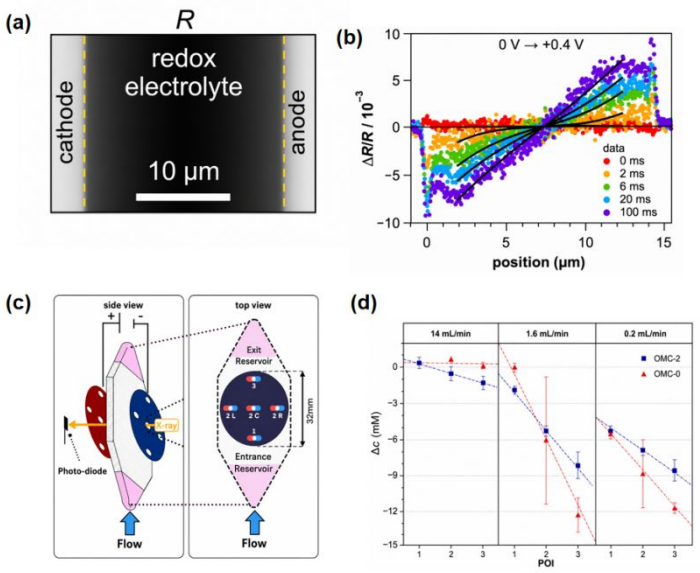


Figure 12 **Operando spatiotemporal mapping of local concentration fields during selective ion transport.**

(a) Microfluidic electrochemical channel and electrode configuration used for label-free optical imaging. Adapted from Ref. [88]. (b) Position-dependent reflectance changes at successive times following a potential step from 0 to +0.4 V, showing the millisecond-scale propagation of concentration gradients from the electrode interfaces into the electrolyte. Adapted from Ref. [88]. (c) Operando X-ray transmission cell and the measurement positions located near the inlet, centre and outlet. Adapted from Ref. [89]. (d) Final local concentration changes for two electrode materials at different flow rates, revealing pronounced axial heterogeneity and its dependence on hydrodynamic conditions. Adapted from Ref. [89].

The label-free optical imaging in Figures 12a and 12b records the evolution of ion concentration along a microfluidic channel after a potential step.[88] Concentration changes first appear near the electrodes and then propagate into the channel on the millisecond timescale, with different positions exhibiting different response amplitudes and characteristic times. Such data can distinguish interfacial response, bulk diffusion, and local accumulation, and can test whether a single diffusion model is sufficient to describe the observations. Endpoint current or average concentration, by contrast, provides only a global response and cannot locate the actual rate-limiting region.

In a flow device, the influence of local states on overall performance is even more pronounced. Operando X-ray transmission measurements in Figures 12c and 12d reveal substantial concentration differences among the inlet, centre, and outlet and show that these differences are jointly affected by flow rate and porous structure.[89] At lower flow rates, inadequate replenishment along the flow direction enlarges the axial concentration gradient, while different pore structures alter the extent of local counter-ion adsorption and release. Overall removal inferred from the outlet concentration may therefore simultaneously contain contributions from a rapid inlet response, intrapore mass-transfer limitation in the central region, and inadequate supply near the outlet.

Temporal sequence can also be used to test causality.[78,88,89] If structural changes precede selectivity drift, pore reconstruction may be a direct cause. If local ion accumulation appears first and structural changes follow, the latter are more likely to be induced by occupancy, charge accumulation, or local stress. For dynamic-gating materials, the response, migration, and recovery timescales must be measured separately. Structural differences between two steady states are insufficient to establish whether a material can switch rapidly enough under continuous feed fluctuations.

Site accessibility should also be understood within this dynamic framework. Endpoint occupancy cannot distinguish rapid enrichment at the external surface from gradual utilization of internal sites, nor can it establish whether high occupancy arises from favourable partitioning or slow dissociation. Pulse response, tracer exchange, breakthrough curves, and position-resolved concentration measurements can jointly constrain ion arrival, occupancy, displacement, and release,[77,78,88,89] thereby identifying which sites genuinely participate in effective separation.

4.1.4 Attribution Strength and Applicability Boundaries of Operando Evidence

In situ measurement generally refers to characterization of a material in a liquid phase or under an external field, although the conditions do not necessarily match those of the actual separation. Operando characterization requires the material state and separation performance to be recorded synchronously under actual feed, driving-force, and flow boundaries.[77,78] The distinction lies primarily in whether operating conditions are retained, whether structural and performance data are temporally correlated, and whether the measurements can distinguish competing mechanisms.

High-quality operando evidence must first preserve critical boundary conditions. Changes in feed composition, ion ratio, pH, pressure, current density, flow rate, or temperature may redefine the dominant transport step.[77,78] Substantially reducing salinity, eliminating flow, or changing the membrane-support configuration to accommodate a characterization cell may shift the observed system away from its actual working state. Corresponding structural and chemical signals should be acquired synchronously with target-ion flux, competing-ion leakage, or local concentration to avoid assembling data obtained from different specimens or operating stages into a single mechanistic chain.[78]

The characterization scale must also match the scale of the mechanism. An averaged scattering signal may fail to detect a small number of percolated defects, and surface-sensitive spectroscopy cannot represent the membrane interior. Second-scale temporal resolution may miss rapid solvation exchange, while nanoscale local observations may not explain concentration polarization in a millimetre-scale flow channel.[77,78] Connections among multiscale observations must be established through mass conservation, spatial correspondence, and temporal synchronization.

Interpretation of operando data is likewise constrained by measurement perturbations. Windows and probes may alter the flow field; high-energy beams can cause local heating or radiation damage; fluorescent labels may affect coordination and diffusion; and limited detection depth may overemphasize surface contributions.[78] Blank cells, measurements at different doses, label-free controls, and repeated operational tests should form part of data interpretation. Agreement among complementary methods is generally more important than the high resolution of a single instrument: scattering constrains wet-state structure, spectroscopy identifies local chemical states, imaging resolves concentration fields, and separation testing provides the overall mass balance.

Operando characterization should ultimately provide state variables that can be used for mechanistic testing and parameter constraints, rather than remaining at the level of phenomenological description. Figure 11 reveals how hydrated pore structure and solvation reorganization affect local free-energy pathways, whereas Figure 12 shows the spatially and temporally nonuniform evolution of concentration fields.[9,82,88,89] Together, these two forms of evidence constrain key factors including effective apertures, site occupancy, local migration, and boundary-layer mass transfer, thereby defining experimental boundaries for subsequent quantitative transport models.

4.2 Multiscale Simulation

The task of multiscale simulation is to convert experimentally constrained local structures and chemical states into free-energy, partitioning, diffusion, and multicomponent-migration parameters, and then determine whether these microscopic differences can continue to explain macroscopic performance when membrane thickness, feed composition, and driving force change.[79,83–87,90,91] Cross-scale connection does not mean successively inserting small-scale parameters into progressively larger models. Different models describe different physical objects, reference states, and approximations, and it is therefore first necessary to establish which parameters can be transferred across scales and which conclusions are valid only under specific boundary conditions.[79,80,83–87,90,91]

4.2.1 Local Interactions and Free-Energy Reference States

Electronic-structure calculations are suitable for comparing local coordination, proton transfer, and charge redistribution between ions and pore-wall groups, but binding energies in vacuum generally do not represent thermodynamic preference in aqueous separation.[24,79,84] Solvent competition, site protonation, counter-ion distribution, and interfacial polarization can all alter the relative stability of ions. Even when two ions exhibit a pronounced difference in binding energy in optimized configurations, the difference may be offset by desolvation penalties or configurational entropy. The basic output of local

calculations should therefore shift from a single binding energy to a free-energy difference in an explicit environment, while retaining the dependence on feed composition and chemical state

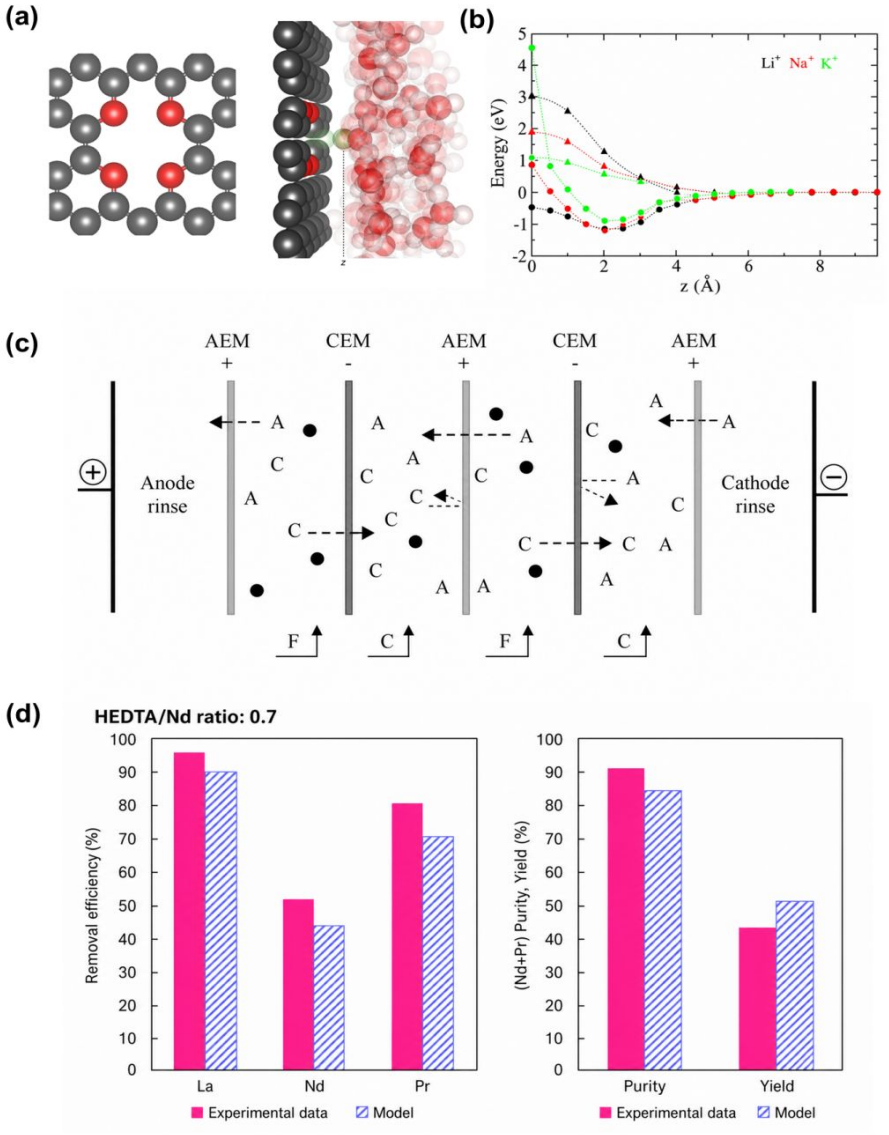


Figure 13 Multiscale modelling from molecular free energies to process-level performance.

(a) Top and side views of a crown-ether-functionalized graphene pore and the explicit-water simulation system used to calculate Li^+ translocation. Adapted from Ref. [79]. (b) Solvated energy, solvation-energy contribution and thermodynamic-integration solvation free energy for Li^+, Na^+ and K^+ along the membrane-normal coordinate, showing that ion selectivity reflects the coupled contributions of pore–ion interactions and solvent reorganization over the full transport pathway. Adapted from Ref. [79]. (c) Electrodialysis stack comprising alternating anion- and cation-exchange membranes, illustrating the partitioning and migration of anions, cations and neutral complexes across multiple compartments. Adapted from Ref. [86]. (d) Comparison of model predictions with experimental measurements at an HEDTA/Nd molar ratio of 0.7 for La, Nd and Pr removal efficiencies and for the purity and yield of the Nd+Pr product. Adapted from Ref. [87].

The first-principles framework shown in Figures 13a and 13b exemplifies this transition.[79] Machine-learning-accelerated molecular dynamics is used to explicitly represent the aqueous environment, correct capacitive effects in the finite simulation cell, and incorporate entropy and electrical-double-layer charging into the energy pathway for ions crossing a crown-ether pore. The resulting profiles for Li^+, Na^+, and K^+ are not isolated pore–ion interactions, but effective free energies jointly formed by pore chemistry, solvent reorganization, and interfacial charge. Only after microkinetics is introduced are these energetic differences translated into steady-state sieving results. Thus, even an accurately calculated free-energy profile must be embedded in a dynamic process subject to mass and charge constraints before comparable selectivities can be obtained.

Free-energy results also depend on whether the reaction coordinate represents the actual confinement process. Coordination number is convenient for describing water removal but may not reflect the geometric requirement for a hydrated complex to pass through an irregular pore entrance. Recent molecular simulations under high-salinity and high-pressure conditions show that salinity can alter cation decoordination free energies through ion association, whereas the effect of pressure is relatively limited.[84] The same study proposes that the maximum cross-sectional area of a hydrated complex can, in some cases, better represent the pore-entry constraint than the average coordination number. A potential-of-mean-force curve is therefore not a material property independent of the selected collective variable. Different migration coordinates, constraints, and reference states may yield different rate-limiting steps for the same system, and these choices and their sensitivities should be reported together with the model conclusions.

4.2.2 Molecular-Scale Transport and Multi-Ion Coupling

Molecular dynamics can resolve solvent exchange, intrapore residence, and diffusion, but barriers and diffusion coefficients obtained from single-ion trajectories are generally valid only for the corresponding concentration and occupancy state.[79,85,90] In a practical mixed feed, channel charge is compensated collectively by multiple ions, while target-ion migration is influenced by competitive occupancy, ion-pair formation, and cooperative motion. Selectivity is then no longer equal to the ratio of two independent single-ion rates, and the intrapore composition cannot be inferred directly from the bulk concentration.

Equilibrium partitioning and kinetic migration must be treated separately. Classical density-functional analysis shows that ion preference inside a nanopore can arise from coupling between excluded volume and electrostatic interactions and may vary nonmonotonically with pore size, concentration, and surface potential.[90] Such models are suitable for describing intrapore composition under multi-ion competition, but the result is an equilibrium occupancy and cannot be directly treated as a transmembrane permeation rate. Membrane-transport analysis additionally requires the mobility of each component under the corresponding occupancy state and cross-correlations among ions. Approximations based on fixed pore walls, fixed charge, and infinite dilution may underestimate structural fluctuations and collective diffusion. Conversely, indiscriminately increasing atomistic detail does not necessarily improve predictive ability, because force-field errors, finite sampling, and an excessively small simulation cell may exceed the ionic differences under investigation.

Molecular-scale models are therefore better suited to providing a set of condition-dependent quantities, including pore-entry free energy, intrapore partitioning, residence time, effective diffusion, and ion correlations, rather than a condition-independent "material selectivity".[79,84,85,90] These quantities should be cross-validated against the wet-state pore size, local coordination, and concentration distributions obtained in Section 4.1. If a simulation predicts strong enrichment of an ion inside the pore but no corresponding occupancy is observed experimentally, the protonation state, channel water content, and competing-ion settings should first be examined rather than merely adjusting the diffusion coefficient to preserve agreement with the macroscopic flux.

4.2.3 Transport Models at the Membrane and Process Scales

As the scale expands to complete membranes and flow devices, molecular free energies must be converted into partition coefficients, chemical potentials, and mobility coefficients and coupled to diffusion boundary layers, fluid transport, and potential distributions. The critical issue is not the name of the governing equation, but whether its assumptions are appropriate for the feed and membrane structure under study. Dilute-solution approximations may be used for low-concentration systems, whereas high-salinity mixtures require consideration of activity, ion association, and multicomponent friction. Homogeneous-membrane models describe average behaviour but cannot capture the disproportionate influence of a small number of large pores on competing-ion leakage.[83,86,87,91]

Pore-size-distribution models illustrate this point. Studies coupling the Poisson–Nernst–Planck and Navier–Stokes equations show that membranes with the same average pore size can exhibit different local flow rates and salt rejection because of differences in pore-size polydispersity and spatial arrangement. Cross-flow can reduce concentration polarization but cannot eliminate the loss of selectivity caused by large pores carrying a disproportionate fraction of the flow.[83] Barriers obtained from an ideal single pore therefore cannot simply be averaged according to pore number. Macroscopic flux is more accurately represented as parallel transport through different pathways weighted by flow, requiring the tail of the pore-size distribution, defect connectivity, and local hydraulic partitioning to be included in scale-up.

Process models must also explicitly represent solution species. Chelator-assisted electrodialysis of rare-earth ions provides a representative example: the species actually participating in membrane transport include free cations, charged complexes, and neutral species, whose proportions are jointly determined by pH, ligand concentration, and stability constants.[86,87] The models shown in Figures 13c and 13d connect solution selectivity, membrane selectivity, and Nernst–Planck transport, and separately validate their predictions against removal, product purity, and yield.[87] Agreement with one total concentration does not mean that the model correctly describes the flux of each species. Only when several independent process metrics are reasonably predicted are the species distribution and membrane-transport parameters sufficiently constrained.

Device-scale parameters are generally composite quantities incorporating several unresolved processes. An effective intramembrane diffusion coefficient inferred from experiments, for example, may simultaneously include pore tortuosity, interfacial partitioning, local defects, and boundary-layer resistance. After experimental calibration, a multi-ion reverse-electrodialysis model can be used to analyse flow-channel geometry and effective area, but the transferability of its parameters to new salt compositions, membrane batches, and flow states still requires independent validation.[91] Scale-up should therefore not seek to retain every microscopic parameter directly, but should identify the minimum parameter set that is both sensitive to the target output and experimentally constrainable.

4.2.4 Parameter Identifiability and Predictive Validity

Agreement between a model and experiment does not establish a unique mechanism.[86,87,91] A flux may be generated by high partitioning combined with slow diffusion or by low partitioning combined with rapid diffusion. Similar selectivity curves over a limited range of conditions do not imply that two parameter sets will have the same extrapolative behaviour. Such parameter compensation may persist even when target and competing ions are fitted simultaneously, particularly when the only observable is a steady-state outlet concentration.

An effective way to improve identifiability is to use different data types to cross-constrain the same parameter. Changes in membrane thickness can test whether bulk diffusion is dominant; feed concentration and ion ratio can constrain competitive partitioning; driving-force scans can identify assumptions of linear migration; and time-dependent responses can distinguish boundary-layer resistance from intramembrane resistance.[83,86,87,91] The operando structures, local occupancies, and concentration fields described in Section 4.1 provide independent constraints that reduce the multiplicity of solutions obtained by fitting macroscopic performance alone. Parameters should be distinguished as directly measurable physical quantities or empirical effective quantities, and the applicability range of the latter should be reported together with model results.

Validation should also shift from reproducing existing data to prediction outside the calibration conditions. Data used for parameter determination should not be reused as the principal validation set; more persuasive tests include new mixture ratios,

higher salinity, different membrane thicknesses, and continuous-flow conditions.[83,86,87,91] Systematic model bias under these conditions can expose missing species, structural changes, or transport coupling. For a material class, a shared conductivity–selectivity upper bound can provide a more stringent test than fitting an individual sample. A model that explains isolated data but not the trade-off exhibited by the material population remains of limited generality.[92]

Uncertainty should propagate across scales rather than being concealed after each modelling stage. Uncertainties in local protonation state, free energy, and pore-size distribution can be greatly amplified through exponential rate relations or flow weighting of large pores.[79,83,84] Sensitivity analysis can identify variables that merit priority measurement, while prediction intervals distinguish robust trends from parameter-dependent coincidences.[81,93] The maturity of a multiscale model ultimately depends on whether it can generate testable predictions under new conditions and specify which level of its assumptions should be revised when those predictions fail.

The value of simulation therefore lies not in adding a possible microscopic explanation to an experimental observation, but in establishing a quantitative mapping from local thermodynamics and multicomponent migration to process outputs. The cross-scale chain shown in Figure 13 can be used reliably for material screening and process design only when parameter sources are traceable, scale-conversion relationships are explicit, and predictions have been validated under independent operating conditions.[79,80,83,86,87,91,92]

4.3 Data-Driven Materials Design

Material composition, pore structure, feed chemistry, and operating parameters jointly create a design space far beyond the reach of exhaustive experiments or high-accuracy simulations.[80,81,94–96] Data-driven methods establish statistical relationships among existing experimental and computational results to screen candidate structures, identify important variables, and optimize operating conditions. Their effectiveness, however, depends on whether the data retain the specific evaluation boundaries associated with each performance value. A “material–selectivity” relationship stripped of feed composition, driving force, and testing mode can readily misidentify differences in operating conditions as intrinsic material behaviour.[81,94,95]

4.3.1 Data Objects and Independent Information Content

An independent data unit suitable for modelling should therefore contain at least four categories of information: material state, feed chemistry, operating boundary, and performance output.[81,94,95] For a membrane process, monomer structure, wet-state pore structure, surface charge, selective-layer thickness, and fabrication conditions describe the material state. The concentrations and ratios of target and competing ions, counter-ions, pH, and ionic strength define feed chemistry. Pressure, potential, flow rate, temperature, and operating time specify transport boundaries. Absolute fluxes of target and competing ions, rejection, separation factor, and energy consumption constitute the performance outputs. For adsorption, site density, material form, solid-to-liquid ratio, contact time, working capacity, elution conditions, and regeneration method must additionally be recorded. If only a material name and a single separation factor are retained, the model may incorrectly attribute differences arising from experimental boundaries to material structure.

Existing studies have demonstrated the practical impact of this problem. A database developed for ion transport through polyamide membranes contains membrane properties, ion characteristics, and operating parameters, from which a model can identify the statistical contributions of size exclusion and electrostatic interactions.[94] The study also shows, however, that inappropriate data splitting causes pronounced information leakage. Records derived from the same membrane or publication often share unreported fabrication details. Randomly assigning these records to training and test sets causes test performance to reflect recognition of related samples rather than predictive ability for new materials.

The problem is more pronounced in literature-derived adsorption data. A single lithium-ion sieve may generate many data rows at different initial concentrations, pH values, and coexisting-ion conditions, but these records do not constitute independent material samples. Grouping by source or material generally yields model performance more representative of genuine extrapolation than random splitting. Related studies further show that operating parameters can contribute more strongly to predictions of lithium adsorption than some material descriptors, indicating that a “high-capacity material” in the literature may sometimes simply have been tested under more favourable conditions.[95]

Data quality should therefore not be judged solely by the number of records. More meaningful measures include the number of independent materials, coverage of operating conditions, fraction of mixed systems, fraction of real feeds, and repeated validation across different sources.[81,94,95] Single salts, binary mixtures, and complex brines should be retained as distinct levels of evidence. Equilibrium capacity, breakthrough capacity, and post-regeneration capacity should likewise not be merged into a single label. Testing protocols and evidence quality should themselves be included as database fields, allowing a model to distinguish performance differences caused by material design from those caused by evaluation boundaries.

4.3.2 Physical Boundaries of Structural Representation and Model Interpretation

Before entering a model, a material must be converted into a machine-readable representation. For regular organic structures, molecular fingerprints, molecular graphs, and quantum-chemical descriptors can encode functional groups, local charge, and geometric features.[24,81,96] For amorphous membranes, porous composites, and defect-rich two-dimensional materials, representation solely by the monomer or ideal unit cell may omit crosslinking degree, wet-state reconstruction, and pore-size distribution.[81,96] The level of detail in the structural representation should match the prediction target: monomer descriptors may be used to screen synthetic precursors but cannot automatically represent the effective pore structure of the final membrane.

Figure 14a presents a data-driven concept for screening ion-specific sites. Candidate functional groups are first encoded as molecular graphs, fingerprints, or string representations. High-accuracy calculations on a subset then provide ion-binding data, allowing a surrogate model to be trained and used to screen a larger chemical space.[24] The rationale is to incorporate ion, site, and solvent jointly into design rather than empirically ranking classes of functional groups. The objective should likewise not be to identify the strongest-binding site. An interaction that is too weak cannot establish effective partitioning, whereas excessively strong binding may prolong residence and impede release; an appropriate site should balance selective partitioning against sustained migration.

Model interpretation can help determine whether an algorithm has learned an acceptable structural relationship. A study of polyamide nanofiltration membranes represented monomers using

molecular descriptors and fingerprints and used SHAP and partial-dependence analyses to investigate how different features affect water permeability and Li^+/Mg^{2+} selectivity.[96] Figure 14b presents both descriptor importance and the direction of correlation, avoiding the misinterpretation that "a variable frequently used by the model" means that "increasing the variable necessarily improves performance".

Interpretation remains a statistical attribution within the range of the training data. Highly correlated descriptors may substitute for one another, and the direction of a SHAP value may change with other variables and with the range of the descriptor.[81,96] Correlations of maximum partial charge, hydrophobicity, or molecular sphericity with selectivity do not mean that independently adjusting one of these parameters will reproduce the same result, because the descriptors are usually also correlated with reaction activity, crosslinked structure, and wet-state membrane morphology. The principal value of an interpretable model is to generate design hypotheses requiring further testing, rather than to replace mechanistic evidence.[81,94,96]

Hybrid physics–data models can reduce ambiguity arising from purely statistical correlations. Existing studies of ion separation have first used component and process models to generate physically consistent training data, then corrected a machine-learning surrogate with a small number of experimental results and simultaneously predicted separation efficiency and energy consumption.[80] Such frameworks are suitable for systems in which experimental samples are limited but fundamental conservation relationships are clear. Their reliability still depends on whether the underlying model includes the actual species and dominant resistances. Machine learning can correct systematic bias, but cannot automatically restore physical processes excluded from the underlying model.[80,81]

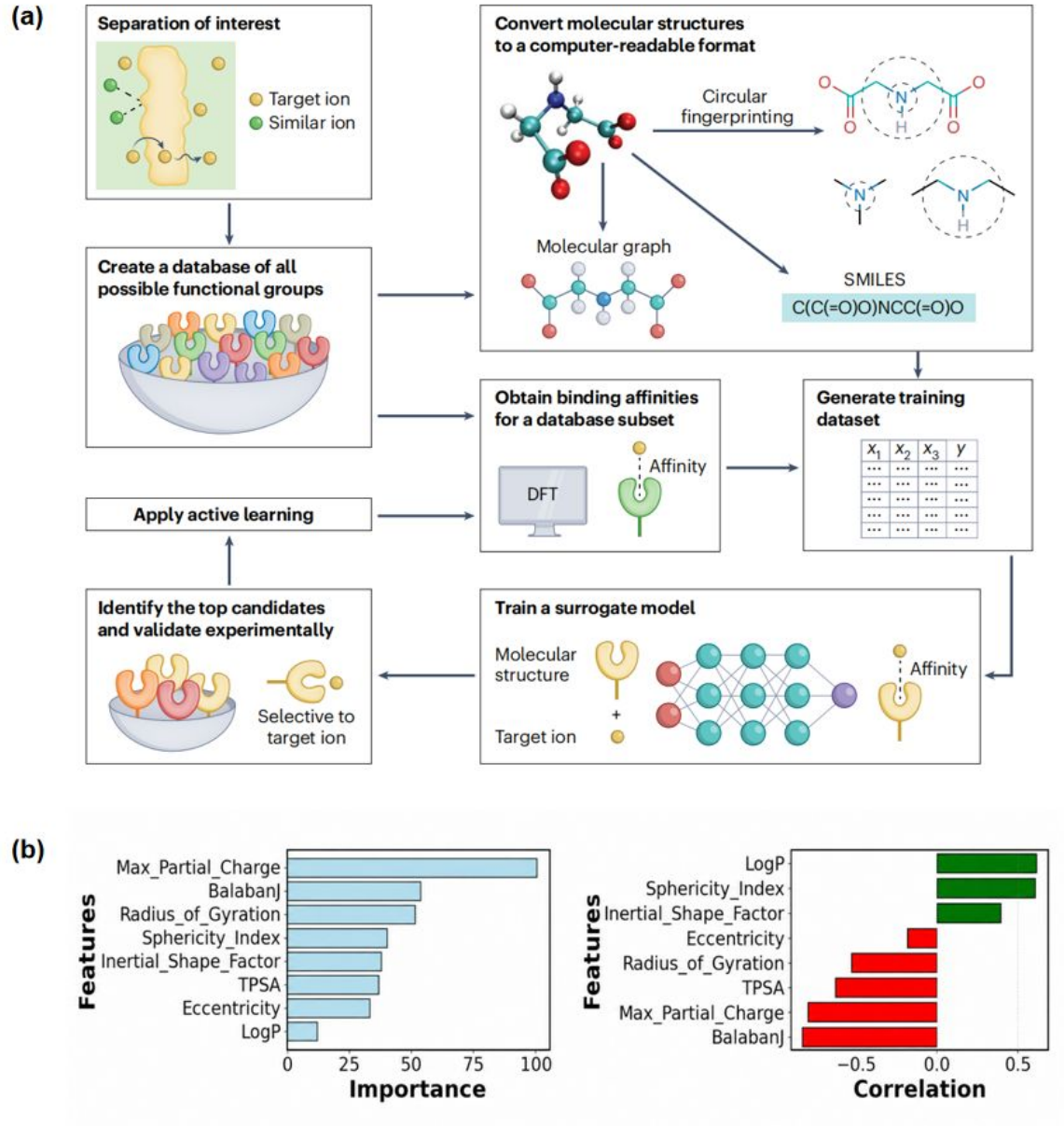


Figure 14 **Data representation and interpretable prediction for selective ion separation.**

(a) Data-driven workflow for a targeted separation problem. A library of candidate functional groups is first constructed for discriminating a target ion from similar ions. Molecular structures are then converted into machine-readable descriptors (e.g., molecular graphs, fingerprints, and SMILES), while binding affinities for a representative subset are generated by high-throughput quantum-chemical calculations to form the training set. A surrogate model is subsequently trained and iteratively refined through active learning, enabling the identification and experimental validation of top candidate binding sites. Adapted from Ref. [24]. (b) Interpretable machine-learning results for Li^+/Mg^{2+} selectivity, including the relative importance of key molecular descriptors and the direction of their correlations with selectivity. This panel highlights that the value of data-driven design lies not only in predictive accuracy, but also in identifying which structural features govern selectivity and whether they promote or suppress separation performance. Adapted from Ref. [96].

4.3.3 Candidate Screening and Multiobjective Decision-Making

An effective test of data-driven design is not whether a model can reproduce high-performing samples already present in the database, but whether it can propose candidates absent from the training set and independently verify their synthesizability and separation performance. Figure 15a presents an example in which monomers are screened by machine learning and used to fabricate polyamide membranes.[96] The candidate monomers exhibit different trade-offs between permeability and Li^+/Mg^{2+} selectivity, showing that structural screening cannot stop at a single predicted ranking. Polymerization, membrane integrity, and actual pore structure continue to affect performance beyond the molecular features represented by the model.

This also constrains the choice of optimization objectives. If only the separation factor is maximized, an algorithm may favour candidates that reduce the fluxes of both ions, but suppress the competing ion more strongly.[80,96] In adsorption systems, maximizing equilibrium capacity alone may identify high-affinity materials that are difficult to regenerate. A more rational objective set should, depending on process type, simultaneously include target-ion flux or working capacity, mixed-system selectivity, product purity and recovery, stability, and energy consumption. Because these metrics generally cannot all be optimized at a single point, candidates should be compared along a Pareto frontier rather than compressed into a composite score lacking a physical basis.

To prevent a single separation factor from obscuring the origin of performance, model outputs should separately retain the absolute flux, partition coefficient, or dynamic capacity of the target and competing ions and calculate selectivity from these values.[80,94,96] This output structure can determine whether a performance change arises from preservation of the target component, reduced leakage of the competing component, or simultaneous changes in both, and can be directly connected to the partition–diffusion and multicomponent-transport models in Section 4.2.

Failed candidates are also informative. A material predicted to perform well but found experimentally to perform poorly may expose limitations in synthetic feasibility, structural stability, or descriptor coverage. If such results are not incorporated into subsequent datasets, the model will continue to propose candidates in the same infeasible region.[81,93] Data-driven studies should therefore record negative results such as failure to form a membrane, structural collapse, low flux, and regeneration failure, rather than retaining only successful samples.

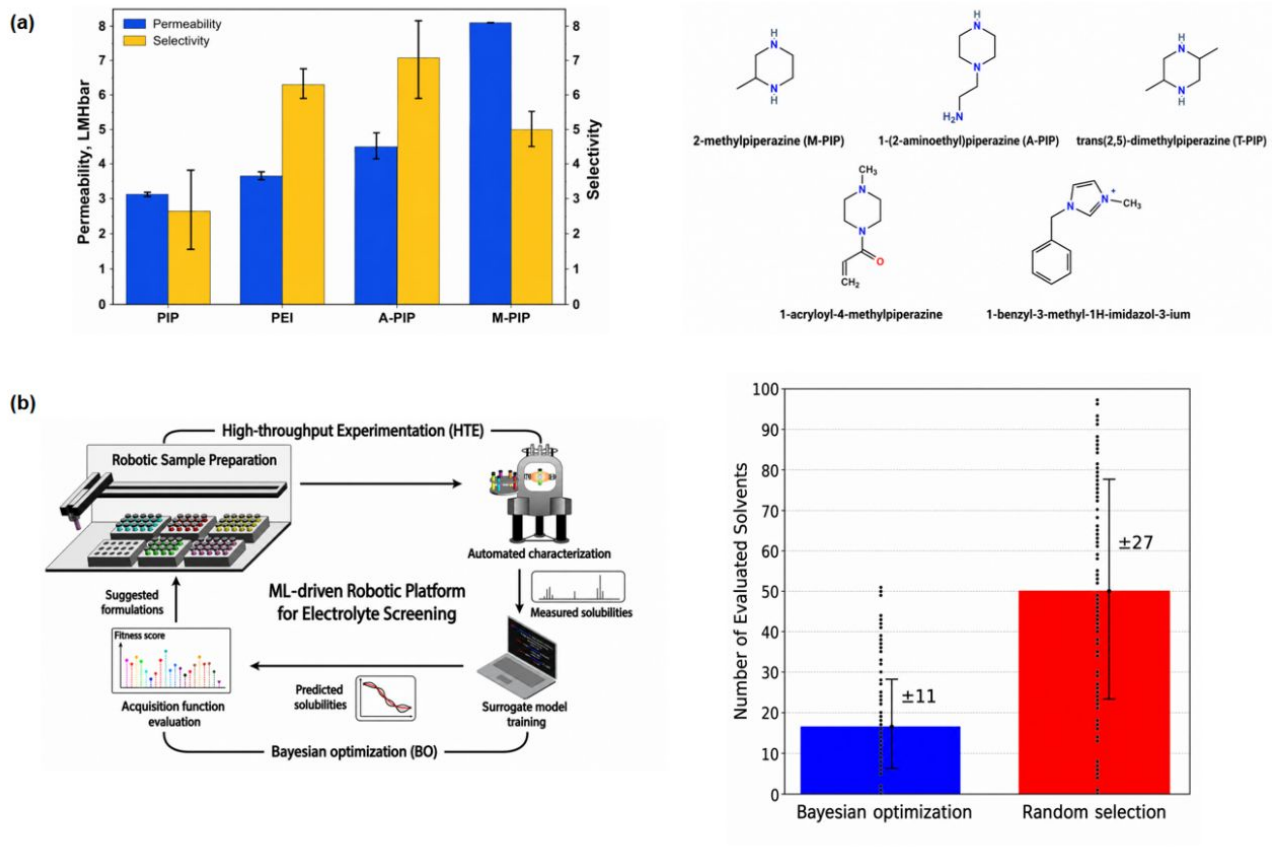


Figure 15 **Candidate validation and active-learning loops in data-guided design.**
(a) Molecular structures of machine-learning-screened monomer candidates and experimentally measured permeability and Li^+/Mg^{2+} selectivity of representative polyamide membranes. The distinct permeability–selectivity responses demonstrate that model rankings must be tested through membrane fabrication and separation experiments using previously untested chemical structures. Adapted from Ref. [96]. (b) Machine-learning-guided high-throughput experimentation and Bayesian optimization workflow. Automated preparation and characterization generate new data, while the surrogate model proposes subsequent formulations using predicted performance and uncertainty; Bayesian optimization identifies the optimum with fewer experiments than random selection. Adapted from Ref. [97].

4.3.4 Extrapolative Uncertainty and Active Learning

The principal application scenarios for selective separation generally lie outside the training distribution, including transitions from single salts to mixed salts, from low concentration to hypersaline brines, from ideal solutions to real feeds, and from small membrane coupons to continuous devices. A randomly selected test set cannot evaluate these extrapolation tasks.[81,94,95] More rigorous validation includes grouped holdout according to material family, literature source, ion system, or feed type, followed by testing of predictions for unseen chemical classes and unseen combinations of operating conditions. Systematic reviews of machine learning in membrane science likewise regard grouped validation, public availability of data and code, and explicit reporting of the training domain as basic requirements for evaluating model reproducibility and transferability.

Extrapolative predictions should also report uncertainty. A high predicted value accompanied by high uncertainty may represent a promising new structure or merely a numerical artefact far from the training data.[81,93] Distance metrics, ensemble models, and conformal prediction can be used to identify candidates outside the applicability domain, but such statistical intervals have practical meaning only when the data have been split appropriately and experimental error has been retained. The absence of failed results and long-duration operating data in the literature can also cause systematic overoptimism in predictions of performance and stability.

Active learning converts uncertainty from a risk indicator into an experimental decision variable. In the high-throughput platform shown in Figure 15b, automated experiments generate data, a surrogate model predicts candidate performance, and an acquisition function selects the next experiment by combining potential benefit and uncertainty.[97] The study concerns electrolyte formulations, and Bayesian optimization substantially reduces the number of experiments required to identify preferred candidates relative to random search; the methodology can be transferred to joint screening of separation materials and operating conditions. For ion separation, the most valuable next experiment may not be the sample with the highest predicted selectivity, but a condition that distinguishes two competing mechanisms, supplements the high-salinity region, or reduces uncertainty along the Pareto frontier.

The value of data-driven design should therefore not be assessed solely by test-set accuracy or candidate ranking, but by whether it proposes the next experiment with genuine discriminatory power. Active learning can balance potential performance, predictive uncertainty, and experimental cost, prioritizing samples and operating conditions that expand the applicability domain, distinguish competing mechanisms, or reduce uncertainty along a multiobjective frontier.[93,97] As new results are continually used to revise data representations and model assumptions, material screening can evolve from a one-off database prediction into a verifiable and updatable iterative design process.

5. Summary and Outlook

The central conclusion of this Review is that ion selectivity is a property of the transport pathway rather than an isolated function of pore size, surface charge, or binding energy.[5,13,24] Nanoconfinement can amplify limited differences in ion solvation and coordination, but a locally established advantage can be translated into a separation outcome with meaningful productivity only if it is retained through interfacial partitioning, intrapore migration, and outlet-side release.[5,9,13,24,79] Material design should therefore not stop at obtaining smaller pores or stronger sites, but should coordinate the free-energy and kinetic resistances of different transport steps.[5,13,24]

Correspondingly, performance evaluation should shift from individual maximum values to paired metrics with explicitly defined conditions.[42,43] Membranes and nanochannels should simultaneously report the absolute fluxes of target and competing ions, the selectivity definition, and performance under mixed feeds. Adsorbent materials should emphasize competitive working capacity, breakthrough behaviour, product concentration, and regenerant consumption.[42,43,61,62,65] Quantitative comparisons among materials have physical meaning only when the ion system, feed composition, driving force, and testing mode are explicitly defined.[42,43]

A deeper challenge for the field is to translate nanoscale recognition into a stable product stream under complex feeds and cumulative operating loads.[3,43,68,69,72,75] Increasing membrane area, shaping particles, and integrating devices introduce defect statistics, concentration polarization, channeling, structural wear, and additional energy consumption, preventing linear extrapolation of laboratory performance.[43,68–75] Future studies should use product purity, recovery, productivity, and cost per unit product as process endpoints, while incorporating material deactivation, cleaning and regeneration, and waste-stream treatment within the same evaluation boundary.[3,43,72,75]

Operando characterization, multiscale simulation, and data-driven methods can jointly support this transition. Experiments provide structural and chemical constraints under actual operating conditions; simulations test whether local states quantitatively explain multicomponent transport; and data-based methods identify applicability domains, organize uncertainty, and select subsequent experiments with the greatest discriminatory value.[78,79,81,94] Transferable design rules can be established only when both successful and failed results are retained and predictions are independently validated using unseen materials and operating conditions.[81,93–95,97] Nanoporous materials may thereby evolve from objects of empirical screening into quantitative separation platforms designed for specific ions, feeds, and process conditions.[5,13,24,43,79,81,93]

REFERENCES

1 Zhao Y, Gao H, Yu L, *et al*. Versatile heavy metal ion separation via biological ion-channel-inspired membranes. Nat Nanotechnol, 2026, 21: 680–688

2 Yang S, Wang Y, Pan H, *et al*. Lithium extraction from low-quality brines. Nature, 2024, 636: 309–321

3 Kim SJ, Ko SH, Kang KH, *et al*. Direct seawater desalination by ion concentration polarization. Nat Nanotechnol, 2010, 5: 297–301

4 Liu Q, Yan Z, Gao J, *et al*. Ion sieving membrane for direct seawater anti-precipitation hydrogen evolution reaction electrode. Chem Sci, 2023, 14: 11830–11839

5 Epsztein R, DuChanois RM, Ritt CL, et al. Towards single-species selectivity of membranes with subnanometre pores. Nat Nanotechnol, 2020, 15: 426–436

6 Esfandiar A, Radha B, Wang FC, *et al*. Size effect in ion transport through angstrom-scale slits. Science, 2017, 358: 511–513

7 Goutham S, Keerthi A, Ismail A, *et al*. Beyond steric selectivity of ions using ångström-scale capillaries. Nat Nanotechnol, 2023, 18: 596–601

8 Iddya A, Zarzycki P, Kingsbury R, *et al*. A reverse-selective ion exchange membrane for the selective transport of phosphates via an outer-sphere complexation–diffusion pathway. Nat Nanotechnol, 2022, 17: 1222–1228

9 Wang A, Breakwell C, Foglia F, *et al*. Selective ion transport through hydrated micropores in polymer membranes. Nature, 2024, 635: 353–358

10 Wang H, Zhai Y, Li Y, *et al*. Covalent organic framework membranes for efficient separation of monovalent cations. Nat Commun, 2022, 13: 7123

11 Mo RJ, Chen S, Huang LQ, *et al*. Regulating ion affinity and dehydration of metal-organic framework sub-nanochannels for high-precision ion separation. Nat Commun, 2024, 15: 2145

12 Hu QH, Song AM, Gao X, *et al*. Rationally designed nanotrap structures for efficient separation of rare earth elements over a single step. Nat Commun, 2024, 15: 1558
13 Shen J, Liu G, Han Y, *et al*. Artificial channels for confined mass transport at the sub-nanometre scale. Nat Rev Mater, 2021, 6: 294–312
14 Abraham J, Vasu KS, Williams CD, *et al*. Tunable sieving of ions using graphene oxide membranes. Nat Nanotechnol, 2017, 12: 546–550
15 Chen L, Shi G, Shen J, *et al*. Ion sieving in graphene oxide membranes via cationic control of interlayer spacing. Nature, 2017, 550: 380–383
16 Ma H, Wang S, Yu B, *et al*. Bioinspired nanochannels based on polymeric membranes. Sci China Mater, 2021, 64: 1320–1342
17 Chen L, Tu B, Lu X, *et al*. Unidirectional ion transport in nanoporous carbon membranes with a hierarchical pore architecture. Nat Commun, 2021, 12: 4650
18 Qiu M, Liu L, Ling Q, *et al*. Biochar for the removal of contaminants from soil and water: a review. Biochar, 2022, 4: 19
19 Werber JR, Osuji CO, Elimelech M. Materials for next-generation desalination and water purification membranes. Nat Rev Mater, 2016, 1: 16018
20 Denny MS Jr, Moreton JC, Benz L, *et al*. Metal–organic frameworks for membrane-based separations. Nat Rev Mater, 2016, 1: 16078
21 Dou H, Xu M, Wang B, *et al*. Microporous framework membranes for precise molecule/ion separations. Chem Soc Rev, 2021, 50: 986–1029
22 Srimuk P, Su X, Yoon J, *et al*. Charge-transfer materials for electrochemical water desalination, ion separation and the recovery of elements. Nat Rev Mater, 2020, 5: 517–538
23 Sheng F, Ge L, Li X, *et al*. Covalent organic framework membranes for selective ion separation. Commun Mater, 2026, 7: 33
24 Violet C, Ball A, Heiranian M, *et al*. Designing membranes with specific binding sites for selective ion separations. Nat Water, 2024, 2: 706–718
25 Zuo P, Ye C, Jiao Z, *et al*. Near-frictionless ion transport within triazine framework membranes. Nature, 2023, 617: 299–305
26 Lu J, Zhang H, Hou J, *et al*. Efficient metal ion sieving in rectifying subnanochannels enabled by metal–organic frameworks. Nat Mater, 2020, 19: 767–774
27 Tan R, Wang A, Malpass-Evans R, *et al*. Hydrophilic microporous membranes for selective ion separation and flow-battery energy storage. Nat Mater, 2020, 19: 195–202
28 Ye T, Gao H, Li Q, *et al*. Highly selective lithium transport through crown ether pillared angstrom channels. Angew Chem Int Ed, 2024, 63: e202316161
29 Villalobos LF, Zhang J, Lee J, *et al*. Ultrathin crown ether-based polyamide membrane for ion-ion separations. Nat Commun, 2026, 17: 4263
30 Li C, Li S, Zhong Y, *et al*. Supramolecular-based ion separation membranes for direct separation of concentrated mixed-salt solutions. J Am Chem Soc, 2026, 148: 6116–6124
31 Wang X, Zhang H, Wei G, *et al*. Comediation of voltage gating and ion charge in MXene membrane for controllable and selective monovalent cation separation. Sci Adv, 2024, 10: eado3998
32 Zhou S, Ai F, Song Z, *et al*. TASK2-inspired pH-gating polymeric nanochannels with multiple interconvertible permeability states by synergistic regulation of conformation and charge. Angew Chem Int Ed, 2025, 64: e202512145
33 Sun Y, Ma J, Zhang F, *et al*. A light-regulated host–guest-based nanochannel system inspired by channelrhodopsins protein. Nat Commun, 2017, 8: 260
34 Yu X, Li C, Chang J, *et al*. Gating effects for ion transport in three-dimensional functionalized covalent organic frameworks. Angew Chem Int Ed, 2022, 61: e202200820
35 Liang C, Wang D, He S, *et al*. Bioinspired cation-gated dynamic liquid film nanochannel for controlled transport of ions and molecules. Sci China Mater, 2024, 67: 2523–2531
36 Xu T, Qi H, Zhong J, *et al*. Bioinspired voltage-gated multi-state ion channels in MXene nanoconfinement for emulating synaptic plasticity. Sci China Mater, 2026, 69: 3514–3522
37 Jia R, Ji Z, Li X, *et al*. Reconfiguring hydration shells by rigidly confined interaction within graphene oxide membranes for ultra-efficient anion separation. Sci China Mater, 2026, 69: 481–491
38 Meng QW, Li J, Lai Z, *et al*. Optimizing selectivity via membrane molecular packing manipulation for simultaneous cation and anion screening. Sci Adv, 2024, 10: eado8658
39 Zhang H, Xing J, Wei G, *et al*. Electrostatic-induced ion-confined partitioning in graphene nanolaminate membrane for breaking anion–cation co-transport to enhance desalination. Nat Commun, 2024, 15: 4324
40 Zhang Z, Kong Y, Li R, *et al*. COF scaffold membrane with gate-lane nanostructure for efficient Li^+/Mg^{2+} separation. Nano-Micro Lett, 2026, 18: 126
41 Lu G, Zhao Y, Van der Bruggen B. Ion association in nanoconfinement for precision separation. Sci China Mater, 2026, 69: 2973–2974
42 Wang R, Zhang J, Tang CY, *et al*. Understanding selectivity in solute–solute separation: definitions, measurements, and comparability. Environ Sci Technol, 2022, 56: 2605–2616
43 Wang R, He R, He T, *et al*. Performance metrics for nanofiltration-based selective separation for resource extraction and recovery. Nat Water, 2023, 1: 291–300
44 Zhang J, Shocron AN, Meola V, *et al*. New methodology for characterizing ion permeability and selectivity of ion-exchange membranes. Environ Sci Technol Lett, 2025, 12: 1082–1088
45 Xu Z, Michos I, Cao Z, *et al*. Proton-selective ion transport in ZSM-5 zeolite membrane. J Phys Chem C, 2016, 120: 26386–26392
46 Ding D, Yaroshchuk A, Bruening ML. Electrodialysis through Nafion membranes coated with polyelectrolyte multilayers yields >99% pure monovalent ions at high recoveries. J Membr Sci, 2022, 647: 120294
47 Xin W, Fu J, Qian Y, *et al*. Biomimetic KcsA channels with ultra-selective K^+ transport for monovalent ion sieving. Nat Commun, 2022, 13: 1701
48 Li Y, Gao L, Lu Z, *et al*. Enhanced removal of heavy metals from water by hydrous ferric oxide-modified biochar. ACS Omega, 2020, 5: 28702–28711
49 Peng Q, Wang R, Zhao Z, *et al*. Extreme Li-Mg selectivity via precise ion size differentiation of polyamide membrane. Nat Commun, 2024, 15: 2505
50 Meng QW, Zhu X, Xian W, *et al*. Enhancing ion selectivity by tuning solvation abilities of covalent-organic-framework membranes. Proc Natl Acad Sci USA, 2024, 121: e2316716121
51 Huang D, Ge X, Chen Q, *et al*. Acid-base pairs engineering enables ultra-selective lithium-magnesium separation via sulfonated polybenzimidazole membranes. Sci China Mater, 2025, 68: 3359–3367
52 Bao S, Ma Z, Yu L, *et al*. Randomly oriented covalent organic framework membrane for selective Li^+ sieving from other ions. Nat Commun, 2025, 16: 3896
53 DuChanois RM, Heiranian M, Yang J, *et al*. Designing polymeric membranes with coordination chemistry for high-precision ion separations. Sci Adv, 2022, 8: eabm9436
54 Cao L, Chen IC, Li Z, *et al*. Switchable Na^+ and K^+ selectivity in an amino acid functionalized 2D covalent organic framework membrane. Nat Commun, 2022, 13: 7894
55 Teng X, Sheng D, Wang J, *et al*. Ion selectivity mechanism of the MgtE channel for Mg^{2+} over Ca^{2+}. iScience, 2022, 25: 105565
56 Shan W, Liang M, Zan J, *et al*. Separation of Ni and Co from lithium-ion batteries through chloride coordination and electrodialysis. Sep Purif Technol, 2025, 379: 134838
57 Xin J, Wang L, Wang X, *et al*. Selective separation of $Ni^{2+}/Co^{2+}/Mn^{2+}$ enabled by tunable intrapore sulfonic acid group content in covalent organic framework membranes via EDTA-chelation-assisted process. J Membr Sci, 2025, 732: 124252
58 Otaki M, Suominen T, Suorsa V, *et al*. The effect of phosphonates on lanthanide separation for surface-grafted porous zirconia. Mater Adv, 2023, 4: 551–560
59 Song AM, Yang MJ, Wu Z, *et al*. Efficient separation of adjacent rare earths in one step by using ion-microporous metal–organic frameworks. Adv Funct Mater, 2025, 35: 2419093
60 Fan F, Ren Y, Zhang S, et al. A bioinspired membrane with ultrahigh Li^+/Na^+ and Li^+/K^+ separations enables direct lithium extraction from brine. Adv Sci, 2024, 11: 2402898
61 Chatterjee P, Volkov A, Mi J, *et al*. Efficient capture and release of the rare-earth element neodymium in aqueous solution by recyclable covalent organic frameworks. J Am Chem Soc, 2024, 146: 20468–20476
62 Bhadane P, Dhumal P, Brun E, *et al*. Safe and sustainable by design MOF beads for selective entrapment and recovery of rare earth elements. Environ Sci Technol, 2025, 59: 16379–16391
63 Ye Q, Jin X, Zhu B, *et al*. Lanmodulin-functionalized magnetic nanoparticles as a highly selective biosorbent for recovery of rare earth elements. Environ Sci Technol, 2023, 57: 4276–4285
64 Wu R, Hong B, Xue C, *et al*. ZIF-8 used for the selective recovery of heavy rare earth elements from mining wastewater. Environ Sci Technol, 2024, 58: 9612–9623
65 Zhao M, Luan J, Zhao C, *et al*. Highly selective granulation adsorbents for lithium recovery from gas field brine: selectivity, kinetics and mechanism. Desalination, 2024, 583: 117699
66 Chaudhuri S, Sigmund G, Bone SE, *et al*. Mercury removal from contaminated water by wood-based biochar depends on natural organic

For Review Only

matter and ionic composition. Environ Sci Technol, 2022, 56: 11354–11362
67 Zhang S, Wei X, Cao X, *et al*. Solar-driven membrane separation for direct lithium extraction from artificial salt-lake brine. Nat Commun, 2024, 15: 238
68 Xu R, Xiao X, Zhang G, *et al*. Continuous lithium extraction from brine by efficient redox-couple electrodialysis. Matter, 2024, 7: 3876–3890
69 Ying J, Lin Y, Zhang Y, *et al*. Mechanistic insights into the degradation of monovalent selective ion exchange membrane towards long-term application of real salt lake brines. J Membr Sci, 2022, 652: 120446
70 Su J, Fan Q, Hu X, *et al*. Continuous flow extraction of lithium from brine using silica-coated LMO beads. Mater Adv, 2025, 6: 2202–2210
71 Foo ZH, Rehman D, Bouma AT, *et al*. Lithium concentration from salt-lake brine by Donnan-enhanced nanofiltration. Environ Sci Technol, 2023, 57: 6320–6330
72 Foo ZH, Thomas JB, Heath SM, *et al*. Sustainable lithium recovery from hypersaline salt-lakes by selective electrodialysis: transport and thermodynamics. Environ Sci Technol, 2023, 57: 14747–14759
73 Xie R, Sun D, Tang J, *et al*. Ecofriendly, highly selective lithium extraction by redox-mediated electrodialysis. ACS Cent Sci, 2024, 10: 2119–2124
74 Mojtahedi B, Askari M, Dolati A. Development of selective cationic membranes for lithium recovery from brines using electrodialysis processes. ACS Sustain Chem Eng, 2025, 13: 3107–3118
75 Foo ZH, Liu S, Kanias L, *et al*. Positively-coated nanofiltration membranes for lithium recovery from battery leachates and salt-lakes: ion transport fundamentals and module performance. Adv Funct Mater, 2024, 34: 2408685
76 Zhu Z, Qian Y, Yu W, *et al*. Positively charged polyamide membranes with expanded ion passage channels enabling exceptional lithium extraction from battery leachate. Sci China Mater, 2026, 69: 473–480
77 Petersen H, Weidenthaler C. A review of recent developments for the in situ/operando characterization of nanoporous materials. Inorg Chem Front, 2022, 9: 4244–4271
78 Prajapati A, Hahn C, Weidinger IM, *et al*. Best practices for in-situ and operando techniques within electrocatalytic systems. Nat Commun, 2025, 16: 2593
79 Bonnet N, Marzari N. Ion sieving in two-dimensional membranes from first principles. ACS Nano, 2025, 19: 8552–8560
80 Rall D, Schweidtmann AM, Kruse M, *et al*. Multi-scale membrane process optimization with high-fidelity ion transport models through machine learning. J Membr Sci, 2020, 608: 118208
81 Ignacz G, Bader L, Beke AK, *et al*. Machine learning for the advancement of membrane science and technology: A critical review. J Membr Sci, 2025, 713: 123256
82 Lu C, Hu C, Chen Z, *et al*. Dehydration-enhanced ion-pore interactions dominate anion transport and selectivity in nanochannels. Sci Adv, 2023, 9: eadf8412
83 Hsu MH, Tsou TY, Hsu JP, *et al*. Influence of pore size distribution and applied cross-flow on ion rejection and separation. Sep Purif Technol, 2025, 352: 128248
84 Schwindt NS, Epsztein R, Straub AP, *et al*. Molecular details of ion de-coordination at elevated salinity and pressure and consequences for membrane separations. J Membr Sci, 2025, 734: 124358
85 Liao S, Liu Y, Li L, *et al*. Theoretical framework for confined ion transport in two-dimensional nanochannels. Nat Commun, 2025, 16: 6675
86 Azimi G, Ding L, Mosadeghsedghi S, *et al*. Separation of rare earth elements using chelating agent-assisted electrodialysis: Phenomenological modeling and comparison with experimental data. Hydrometallurgy, 2024, 224: 106252
87 Azimi G, Mosadeghsedghi S, Dashtban Kenari SL, *et al*. Class II three-layer system phenomenological model based on limiting current density and dynamic chelation chemistry for separation of rare earth elements using electrodialysis. Sci Rep, 2024, 14: 18340
88 Utterback JK, King AJ, Belman-Wells L, *et al*. Operando label-free optical imaging of solution-phase ion transport and electrochemistry. ACS Energy Lett, 2023, 8: 1785–1792
89 Rauscher MV, Kohns R, Seyffertitz M, *et al*. Beyond global metrics in capacitive water deionization: Position-resolved ion concentration from operando X-ray transmission. Desalination, 2026, 623: 119849
90 Cui L, Liu Y, Liu H. Classical density functional analysis of ion selectivity in nanopores: The coupling between hard-sphere and electrostatic interactions. Chem Eng J, 2022, 444: 136673
91 Cho H, Kim J, Han CS. Multi-ion transport in reverse electrodialysis: A validated model for design and optimization. Desalination, 2024, 586: 117746
92 Kitto D, Kamcev J. Predicting the conductivity–selectivity trade-off and upper bound in ion-exchange membranes. ACS Energy Lett, 2024, 9: 1346–1352
93 Ren Z, Ren Z, Zhang Z, *et al*. Autonomous experiments using active learning and AI. Nat Rev Mater, 2023, 8: 563–564
94 Jeong N, Epsztein R, Wang R, *et al*. Exploring the knowledge attained by machine learning on ion transport across polyamide membranes using explainable artificial intelligence. Environ Sci Technol, 2023, 57: 17851–17862
95 Xu Z, Ding Y, Han SC, *et al*. Predicting the performance of lithium adsorption and recovery from unconventional water sources with machine learning. Water Res, 2024, 266: 122374
96 Dangayach R, Jeong N, Chen Y. Machine learning analysis and monomer screening of polyamide nanofiltration membranes for lithium separation. ACS EST Engg, 2025, 5: 3039–3050
97 Noh J, Doan HA, Job H, *et al*. An integrated high-throughput robotic platform and active learning approach for accelerated discovery of optimal electrolyte formulations. Nat Commun, 2024, 15: 2757

For review only

Acknowledgements This work was supported by the National Key R&D Program of China (2024YFB3612600), the National Natural Science Foundation of China (22375100, 22275098 and 62288102), the Basic Research Program of Jiangsu (BK20243057), and the Jiangsu Province College Students Innovation Training Program (202610293144Y).

Author contributions Chaoyang Dai contributed to conceptualization, literature curation, writing-original draft and visualization. Zhicheng Xu contributed to literature curation and writing-review and editing. Hao Luo contributed to writing-review and editing. Tianyang Zhou contributed to literature curation and visualization. Yinzi Shao contributed to writing-review and editing. Haotian Wu contributed to literature curation. Linghai Xie contributed to supervision, funding acquisition and writing-review and editing. Quanyou Feng contributed to supervision, project administration, funding acquisition and writing-review and editing. All authors have read and approved the final manuscript.

Conflict of interest The authors declare that they have no conflict of interest.

Ethical approval This review did not involve studies with human participants or animals performed by any of the authors.

AUTHOR BIOGRAPHIES



Chaoyang Dai is an undergraduate student at the College of Electronic and Optical Engineering & College of Flexible Electronics (Future Technology), Nanjing University of Posts and Telecommunications. His research interests include nanoporous materials for ion separation, machine-learning-assisted materials design and optoelectronic materials.



Linghai Xie is a professor at Nanjing University of Posts and Telecommunications (NJUPT). He received his Ph.D. degree from Fudan University in 2006 and joined the Institute of Advanced Materials of NJUPT. His research focuses on organic and polymer optoelectronic materials for organic/plastic electronics and molecular electronics.



Quanyou Feng received his Ph.D. degree from Fudan University in 2014. From 2015 to 2017, he conducted postdoctoral research at Virginia Tech. Now he is an associate professor in Institute of Advanced Material (IAM), Nanjing University of Posts and Telecommunications. His research focuses on organic/polymer wide-bandgap semiconductor materials and optoelectronic devices.

中文摘要

纳米多孔材料中的选择性离子分离：限域筛分、化学识别与动态门控

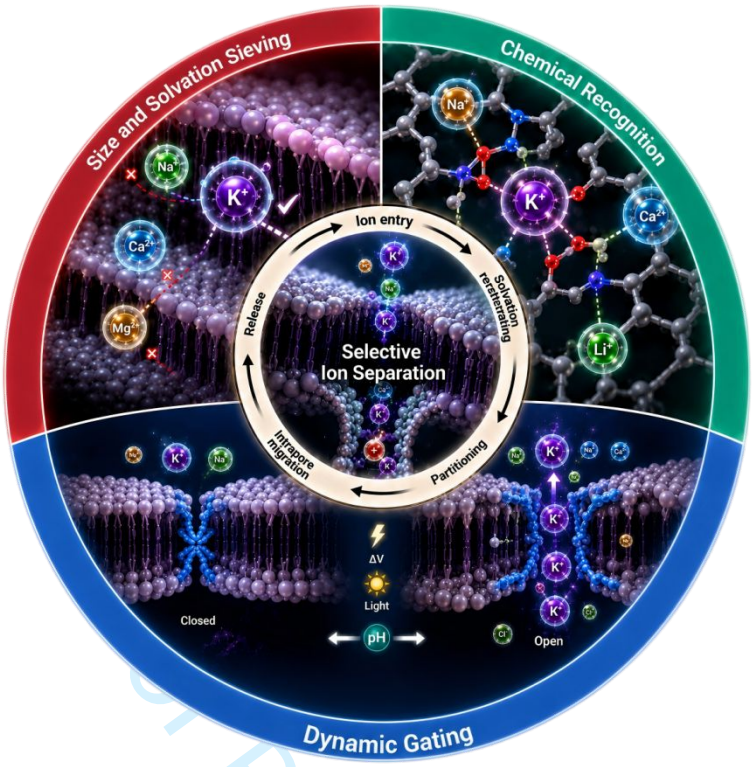
戴朝阳[2]，徐志成[1]，骆浩[3]，周天阳[2]，邵音子[4]，吴昊天[1]，解令海[1]*，冯全友[1]*

选择性离子分离对于资源回收、水处理、盐湖提锂和核废物管理具有重要意义，但不同离子在尺寸、溶剂化结构和配位行为上的差异往往十分有限，且其分离过程还受到价态、界面电荷和竞争离子共同影响。纳米多孔材料具有可调的亚纳米孔道和化学活性界面，可用于调节离子进入、溶剂化重组、界面分配、孔内迁移与释放。本文从限域传输和离子−孔道相互作用出发，综述了尺寸与溶剂化筛分、化学识别和动态门控三类机制，并比较其在同价单价、同价二价、异价及化学性质相近的多价离子体系中的作用及耦合关系。在此基础上，进一步区分选择性吸附、膜内富集与跨膜传输，讨论选择性定义、离子通量、进料组成、驱动力和运行时间对性能评价的影响。现有研究仍面临三方面问题，即不同测试条件下的性能数据缺乏可比性，运行状态下的离子溶剂化、位点占据与迁移过程缺少直接证据，以及复杂进料和长期运行中的功能稳定性不足。针对这些问题，本文总结了原位/工况表征、多尺度模拟和数据驱动方法的进展，并提出将湿态孔道结构、界面化学、传输动力学与过程性能相联系的研究思路，为发展高选择性、高通量且长期稳定的纳米多孔分离材料提供参考。

关键词：选择性离子分离；纳米多孔材料；限域筛分；化学识别；动态门控

For Review Only

Table of Contents graphic



For Review Only

Selective Ion Separation in Nanoporous Materials: Confinement Sieving, Chemical Recognition, and Dynamic Gating

Chaoyang Dai[2], Zhicheng Xu[1], Hao Luo[3], Tianyang Zhou[2], Yinzi Shao[4], Haotian Wu[1], Linghai Xie[1]* and Quanyou Feng[1]*

1 State Key Laboratory of Flexible Electronics, Institute of Advanced Materials, Centre for Molecular Systems and Organic Devices, Nanjing University of Posts & Telecommunications, 9 Wenyuan Road, Nanjing 210023, China

2 College of Electronic and Optical Engineering & College of Flexible Electronics (Future Technology), Nanjing University of Posts and Telecommunications, 9 Wenyuan Road, Nanjing 210023, China

3 School of Communications and Information Engineering, Nanjing University of Posts and Telecommunications, 9 Wenyuan Road, Nanjing 210023, China

4 Xuzhou University of Technology, 2 Lishui Road, Xuzhou 221018, China

* Corresponding authors (email: iamlhxie@njupt.edu.cn; iamqyfeng@njupt.edu.cn)

Abstract: Selective ion separation is important for resource recovery, water treatment, lithium extraction from salt lakes, and nuclear-waste management. However, differences among ions in size, solvation structure, and coordination behaviour are often extremely limited, while the separation process is further influenced by valence, interfacial charge, and competing ions. Nanoporous materials possess tunable subnanometre channels and chemically active interfaces, enabling regulation of ion entry, solvation reorganization, interfacial partitioning, intrapore migration, and release. This Review examines three mechanisms—size- and solvation-based sieving, chemical recognition, and dynamic gating—from the perspective of confined transport and ion–pore interactions, and compares their roles and coupling relationships in systems involving isovalent monovalent ions, isovalent divalent ions, heterovalent ions, and chemically similar multivalent ions. On this basis, selective adsorption, intramembrane enrichment, and transmembrane transport are further distinguished, and the effects of selectivity definitions, ion flux, feed composition, driving force, and operating time on performance evaluation are discussed. Existing studies continue to face three major challenges: limited comparability of performance data obtained under different testing conditions, a lack of direct evidence for ion solvation, site occupancy, and migration under operating conditions, and insufficient functional stability in complex feeds and during long-term operation. To address these issues, this Review summarizes advances in in situ/operando characterization, multiscale simulation, and data-driven methods, and proposes a research framework that connects wet-state pore structures, interfacial chemistry, transport kinetics, and process performance, thereby providing guidance for the development of nanoporous separation materials with high selectivity, high flux, and long-term stability.

Keywords: selective ion separation; nanoporous materials; confinement sieving; chemical recognition; dynamic gating

1. Introduction

Selective ion separation is a fundamental process in lithium extraction from salt lakes, seawater desalination, critical-metal recovery, water treatment, and nuclear-waste management.[1–4] In contrast to the separation of gases or neutral molecules, ion transport depends not only on geometric size but also on solvation structure, valence, charge density, coordination preference, and interfacial potential. In systems containing multiple competing ions, these factors are mutually coupled and vary with salinity, composition, and external driving force, making it difficult to establish a simple one-to-one correspondence between material structure and separation outcome.[5–9]

The physicochemical basis of separation differs among ion systems. Isovalent monovalent ions, such as Li^+/Na^+ and Na^+/K^+, have the same charge and similar sizes, and the exploitable differences arise primarily from solvation strength, desolvation penalties, and weak ion–pore-wall interactions.[5–7,10] For isovalent divalent ions, such as Mg^{2+}/Ca^{2+} and Co^{2+}/Ni^{2+}, coordination number, coordination geometry, and ligand-exchange kinetics contribute in addition to the above factors.[5,7,11] For heterovalent ion pairs such as Li^+/Mg^{2+}, electrostatic partitioning, Donnan exclusion, and differences in charge density generally make more pronounced contributions.[3,5,11] Selectivities obtained for ions with different valence relationships therefore cannot be explained using the same mechanism, and a high separation factor in a heterovalent system cannot simply be regarded as evidence of precise size recognition or specific coordination. Chemically similar multivalent ions, such as adjacent lanthanides, impose an even greater requirement on materials to distinguish subtle differences in coordination and desolvation.[12]

Nanoporous materials provide a unique space in which these factors can be regulated. Their pore entrances and channels can be reduced to the subnanometre scale, while the charge, polarity, coordination sites, and wettability of the pore walls can be tuned through compositional design or postsynthetic modification.[5,8,9,11,13] As an ion approaches and enters a pore from the feed side, its solvation shell may be compressed, reorganized, or partially removed. Once inside the confined space, the ion further undergoes interfacial partitioning, transient binding, intrapore diffusion, and release at the outlet. The structural requirements imposed on a material differ across these transport stages: narrowing the pore entrance may amplify differences in desolvation between ions, but it also increases the entry resistance of the target ion; interfacial interactions, meanwhile, affect both intramembrane partitioning and subsequent migration. Macroscopic selectivity is therefore determined by the continuous sequence of ion entry, partitioning, migration, and release, rather than being a direct mapping of pore size, surface charge, or binding constant.

The relevant material platforms have expanded from zeolites and inorganic molecular sieves with relatively fixed pore sizes to metal–organic frameworks and covalent organic frameworks with programmable pore structures and interfacial chemistry, as well as two-dimensional materials such as graphene oxide and MXenes with tunable interlayer spacing and surface terminations.[10,11,14,15] Microporous polymer membranes, ion-exchange membranes, biomimetic nanochannels, and organic–inorganic composite membranes have further diversified the available pore architectures.[8,9,16] Amorphous porous materials, including functionalized porous carbons and biochars, provide platforms for ion adsorption and capture that are jointly governed by heterogeneous pore structures and surface sites.[17,18] The continued expansion of material systems has broadened the design space, but has not automatically yielded transferable rules across material classes: similar nominal pore sizes can produce different ion-transport sequences, while the

same recognition group may promote target-ion enrichment during adsorption yet create difficult-to-release trapped states during membrane transport.[5,8,9,13]

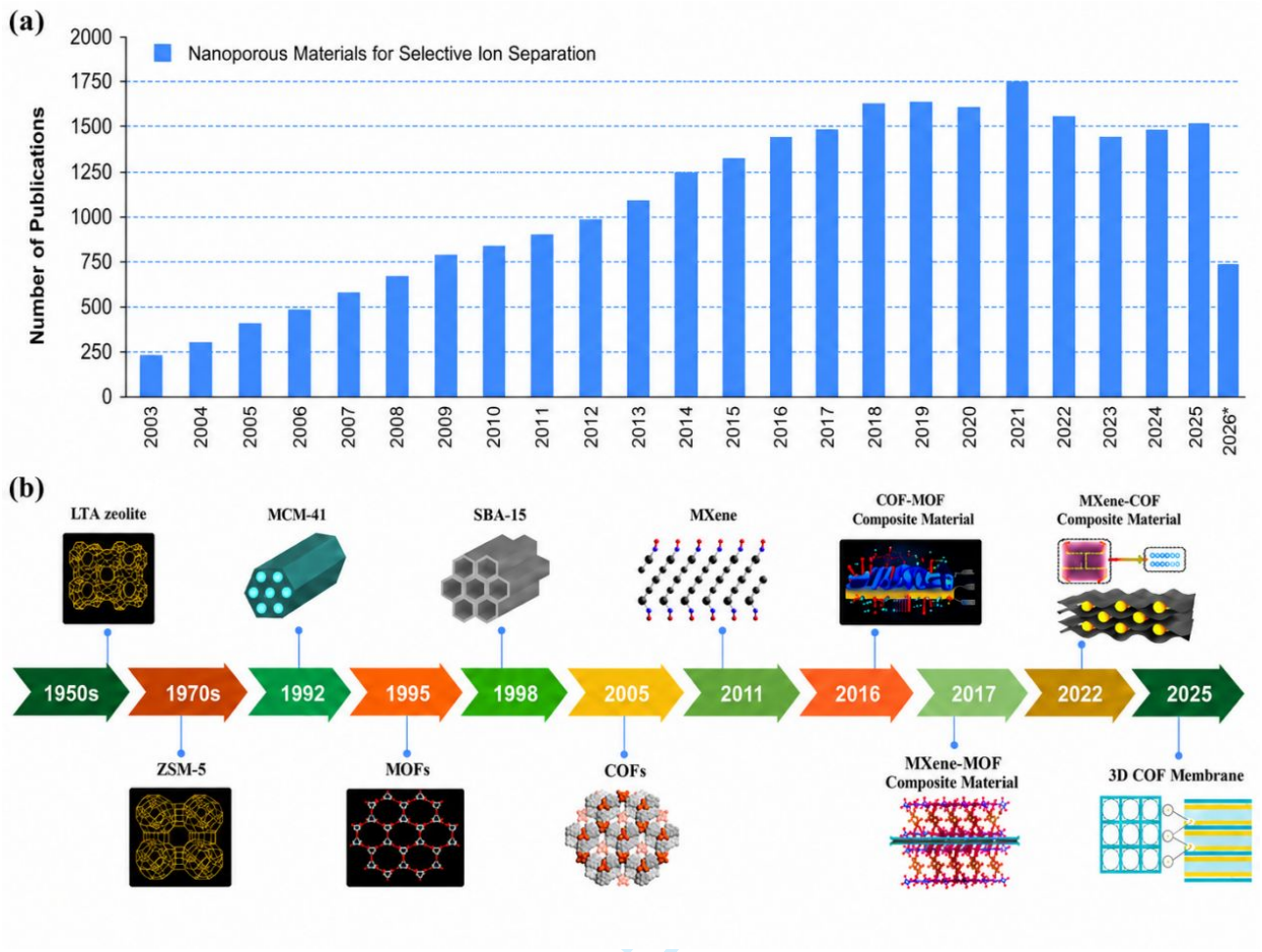


Figure 1 Publication trends and evolution of nanoporous platforms for selective ion transport.
(a) Annual number of publications related to nanoporous materials for selective ion transport from 2003 to 2026. Records were retrieved from the Web of Science Core Collection on 26 July 2026 using a topic search combining terms related to nanoporous materials, nanoporous membranes, nanochannels, ion sieving, selective ion transport, and selective ion separation. The timespan was restricted to 2003–2026, and only Articles and Reviews were included. Duplicate records were removed before annual counting. The 2026 value represents a partial-year count. (b) Selected milestones illustrating the expansion from rigid inorganic molecular sieves to chemically programmable frameworks, two-dimensional nanochannels and hybrid membranes. The evolution of material platforms is accompanied by a transition from predominantly geometric exclusion to coupled regulation of pore confinement, interfacial recognition and dynamic transport. All third-party images reproduced in this figure were used with permission.

Existing reviews on selective ion separation have generally focused on particular material platforms, target-ion systems, or application scenarios, for example by separately summarizing the structural design of framework materials, two-dimensional membranes, polymer membranes, and ion-exchange membranes, or by concentrating on processes such as lithium extraction from salt lakes, seawater resource recovery, and heavy-metal recovery.[3,5,13,19–23] These studies have systematically reviewed advances in material preparation and performance. However, pore size, interfacial charge, coordination sites, and responsive behaviour are usually discussed within their respective material systems, making it difficult to address several mechanistic questions shared across material classes: why channels with similar nominal pore sizes exhibit different transport sequences; why increasing ion affinity may simultaneously enhance enrichment and reduce permeation; and why an external stimulus may regulate total flux without necessarily improving the selectivity of a target ion over competing ions.

The distinctive feature of this Review is not the introduction of another material classification, but the use of interconnected physicochemical steps in the ion-separation process as a common analytical scale for cross-comparing different nanoporous materials. Specifically, size- and solvation-based sieving, chemical recognition, and dynamic gating are reconsidered in terms of pore entry and solvation reorganization, interfacial partitioning and ion–site interactions, intrapore migration, and release, with particular emphasis on their synergy, competition, and shifts in the dominant mechanism under multicomponent conditions. Pore size, surface charge, and functional sites are thus no longer treated as mutually independent material parameters, but are placed within the same transport process to examine where they act and how they affect subsequent steps.

Within this process-oriented framework, this Review undertakes three tasks. First, ion systems are distinguished according to valence relationship and solution speciation, including isovalent monovalent, isovalent divalent, heterovalent, and chemically similar multivalent ions. Second, selective adsorption, intramembrane partitioning, and steady-state transmembrane transport are differentiated to avoid using equilibrium affinity to directly explain dynamic separation. Third, mechanistic interpretations are placed under specific feed compositions, driving forces, membrane thicknesses, and operating times, and are tested using operando characterization, multiscale simulation, and data-driven methods. The central concern is not the ranking of material performance, but where ion differences are amplified,

how different mechanisms cooperate or counteract one another, and what evidence is sufficient to support cross-material comparison and extrapolation across operating conditions.

2. Selective Ion-Transport Mechanisms

On the basis of the ion differences summarized in Table 1, existing regulatory strategies can be classified according to the principal controlled state variable into size- and solvation-based sieving, chemical recognition, and dynamic gating.[5,11,13,24] Size- and solvation-based sieving focuses on the effects of pore-entry constraints and confined-solvent structure on ion entry. Chemical recognition alters interfacial partitioning, residence, and migration through coordination, electrostatic, and supramolecular interactions. Dynamic gating uses reversible changes in pore size, charge, conformation, or wettability to reorganize transport pathways in response to external stimuli or ion occupancy. This classification describes the variables that primarily control selectivity, rather than assigning different materials to mutually exclusive categories.

In practice, the three mechanisms are generally coupled within the same pore. Narrowing a pore entrance not only amplifies differences in desolvation but also alters charge screening and site accessibility, while interfacial chemistry and gating state jointly regulate ion partitioning, intrapore migration, and solvent organization. In mixed electrolytes, competitive occupancy, counter-ion migration, and ion–ion correlations further alter the relative contribution of each mechanism. Actual separation behaviour therefore arises from synergy and competition among mechanisms and from their transitions with feed composition and operating state.[5,7–9,11,13,24–26]

On this basis, mechanistic attribution must address at least three questions: which state variable establishes a difference between the target and competing ions, at which transport step that difference predominantly acts, and whether the available evidence can exclude alternative explanations such as charge exclusion, transient adsorption, structural swelling, or defect-mediated bypass transport. Table 1 accordingly compares the key physicochemical contrasts, principal separation bases, and common confounding factors for different ion systems. The following sections first discuss the three fundamental mechanisms separately and then analyse how they cooperate or constrain one another under multicomponent conditions.[5,9,13,24]

Table 1. Representative ion-pair classes and dominant physicochemical factors governing selective ion separation

Ion-pair class	Representative ion pairs	Key physicochemical contrasts	Dominant separation factors	Major confounding factors
Isovalent monovalent ion pairs	Li^+/Na^+, Li^+/K^+, Na^+/K^+	Solvation strength and exchange kinetics; effective solvated size; weak coordination preferences	Pore-entry partial desolvation; confined-solvent reorganization; subtle differences in ion–pore affinity and in-pore mobility	Wet-state pore size and swelling; surface charge and electrical double layers; non-selective defects; concentration-dependent ion correlations
Isovalent divalent ion pairs	Mg^{2+}/Ca^{2+}, Co^{2+}/Ni^{2+}, Cu^{2+}/Zn^{2+}	Solvation thermodynamics; preferred coordination number and geometry; ligand-exchange kinetics; solution speciation	Coupled desolvation and coordination; competitive site occupancy; preorganized or multidentate recognition	pH-dependent hydrolysis and complexation; precipitation; counterion effects; site saturation
Heterovalent ion pairs	Li^+/Mg^{2+}, Na^+/Mg^{2+}, K^+/Mg^{2+}	Valence and charge density; solvation free energy; effective solvated size	Donnan partitioning and exclusion; coupled electrostatic and size/solvation discrimination; specific ion–interface interactions	Ionic-strength screening; concentration polarization; co-ion coupling and electroneutrality constraints; pH-dependent surface charge
Chemically similar isovalent multivalent ions	Adjacent lanthanide pairs, such as La^{3+}/Pr^{3+}, Nd^{3+}/Sm^{3+} and Dy^{3+}/Ho^{3+}	Picometre-scale differences in ionic radius; coordination number and geometry; solvation and ligand-exchange thermodynamics	Preorganized multidentate or cooperative coordination; size-matched confinement; reversible binding under competitive conditions	Hydrolysis and solution speciation; competing ligands and trace impurities; slow exchange and kinetic trapping; limited site capacity

2.1 Size- and Solvation-Based Sieving

Size sieving is often understood as geometric matching between pore size and ion size. However, ions approaching a nanopore entrance are generally solvated rather than transported as bare ions. In aqueous media, entry into a confined space is often accompanied by compression, reorganization, or partial removal of the hydration shell.[5–7,9,11,13,26] Bare-ion radius, solvated diameter, and crystallographic pore size therefore provide only preliminary references; actual selectivity depends on how pore-entry confinement alters the solvation free energy and entry kinetics of different ions.

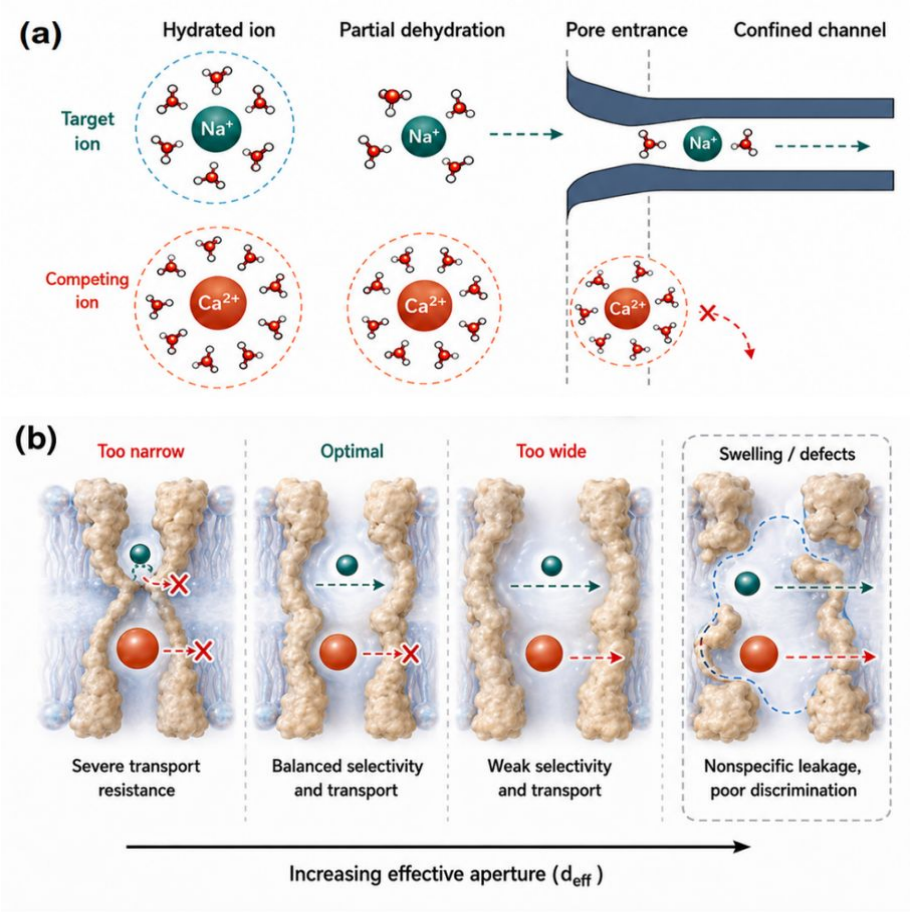


Figure 2 Size- and solvation-dependent ion transport through nanoporous channels.

(a) Schematic illustration of ion dehydration and pore entry. (b) Conceptual influence of the effective pore aperture on ion-separation performance.

Figure 2a summarizes this process. The target ion reduces its effective size through partial desolvation and enters the confined channel after overcoming the pore-entry barrier. A competing ion that must incur a higher solvation-reorganization penalty is more likely to be blocked at the entrance. The sieving boundary is not a fixed geometric cut-off, but a "soft boundary" jointly determined by ion-solvation strength, solvent-exchange kinetics, pore-entry morphology, and pore-wall chemistry.[6,7,9,11,14,15,26] Even when the nominal solvated size exceeds the pore aperture, an ion may still pass through, although its entry rate may vary markedly with the cost of solvation reorganization. Size sieving therefore amplifies not the difference in bare-ion radii, but the difference in the ease with which ions reorganize their solvation structures under confinement.

This understanding also changes the definition of pore size. Many nanoporous materials are not rigid under operating conditions. Lamellar membranes may swell through solvent adsorption and ion intercalation; flexible frameworks may undergo local deformation upon guest occupancy; and terminal groups, solvent content, and external mechanical constraints may alter the actual accessible space. At the same time, grain boundaries, interlayer misalignment, and nonselective defects may create bypass pathways around the designed pore entrance.[9,14,15] The parameter directly relevant to ion separation is therefore not the dry-state mean pore size, but the operando effective pore aperture, d_{eff}, jointly determined by channel geometry, solvent occupancy, ion loading, and structural flexibility.

Figure 2b further illustrates the nonmonotonic relationship between effective pore aperture and separation performance. When the aperture is too narrow, both target and competing ions experience high transport resistance; geometric exclusion is strengthened, but at the cost of a substantial loss in flux. Within an appropriate aperture range, the target ion can undergo the necessary solvation reorganization and enter the channel, whereas the competing ion remains subject to a higher barrier, thereby balancing selectivity and transport rate. When the aperture becomes too wide, solvation differences between ions can no longer be effectively amplified, and selectivity weakens accordingly.[5,9,14,15,27] If swelling or defects create nonselective bypass pathways, competing ions may circumvent local bottlenecks even when the nominal pore size satisfies the sieving requirement, reducing macroscopic selectivity.

Selectivity established at the pore entrance, however, does not necessarily persist throughout the transport process. In atomically thin pores, the local entry barrier may account for most of the total resistance. In channels of finite length, ions must additionally undergo confined diffusion, solvent-shell exchange, ion–pore-wall friction, and transient adsorption. As the transport distance increases, intrapore resistance may gradually exceed entry resistance, causing the same pore aperture to produce different rate-limiting steps at different membrane thicknesses. Size-sieving performance must therefore be evaluated together with selective-layer thickness and the actual migration distance.[5,7,25–27]

The division of roles between entrance sieving and intrapore migration also provides a physical basis for "narrow-entrance–wide-channel" structures. Local subnanometre bottlenecks amplify differences in ion solvation, whereas relatively spacious internal cavities reduce subsequent migration resistance. High selectivity does not require the entire channel to retain an extremely small diameter. On the contrary, if the entire transport pathway remains strongly confined, selectivity obtained at the entrance may be offset by excessive intrapore resistance.[10,25–27] A more rational design concentrates precise sieving at a limited number of critical bottlenecks while maintaining continuous, low-resistance migration after entry.

At the subnanometre scale, geometric confinement is further coupled to pore-wall chemistry and confined-solvent structure.[7,9,11,24–26] Moderate ion–pore-wall interactions can stabilize a partially desolvated target ion and compensate for the energetic cost of pore entry, whereas excessively strong interactions create deep energy wells, prolong residence times, and impede release. Pore-wall polarity and wettability also influence the density, orientation, and connectivity of the confined solvent. Moderately ordered solvent structures may support directional migration, whereas excessive confinement or local dewetting disrupts the continuous solvent network required for transport. Pore-size optimization therefore cannot be considered independently of interfacial chemistry and the state of the confined solvent.

The design target of size- and solvation-based sieving should accordingly shift from nominal pore size to matching among the operando effective aperture, the cost of solvation reorganization, and intrapore migration resistance.[5,9,11,13,24–27] Mechanistic interpretation should likewise not rely solely on dry-state pore size and an endpoint separation factor, but should combine evidence from swelling behaviour, membrane thickness, interfacial chemistry, steady-state flux, and solvation state or activation energy to determine whether selectivity is established at pore entry or limited by subsequent intrapore migration.

2.2 Chemical Recognition

When differences in ion size and solvation are insufficient to establish a clear sieving boundary, pore-wall chemistry provides another important route to selectivity. Coordination groups, fixed charges, macrocyclic hosts, and molecularly imprinted sites can exploit subtle differences among ions in donor-atom preference, coordination number, geometric configuration, and ligand-exchange kinetics to alter their relative stability at pore entrances and within pores. The objective of chemical recognition, however, is not to bind the target ion as strongly as possible, but to establish a sufficiently pronounced relative advantage under competitive conditions that can be continuously propagated. If the interaction is too weak, the partitioning difference between target and competing ions remains limited; if it is too strong, the ion may become trapped at a local site, causing "selective recognition" to manifest as retention rather than preferential transport.[8,24,28–30]

This also means that the binding constant of a ligand in a homogeneous solution cannot directly represent its recognition ability inside a nanopore.[11,24,28,29] Before contacting a site, an ion has often already undergone hydration-shell reorganization, pore entry, and local configurational adjustment. Once inside the pore, site orientation and accessibility, cooperative effects from neighbouring groups, confined-solvent structure, and local potential further reshape the coordination environment. The same functional group may therefore exhibit entirely different ion preferences when placed in pores of different sizes, frameworks, or solvent states. Effective recognition is never an isolated property of a functional group, but a local state jointly formed by the ion, site, pore, and solvent.

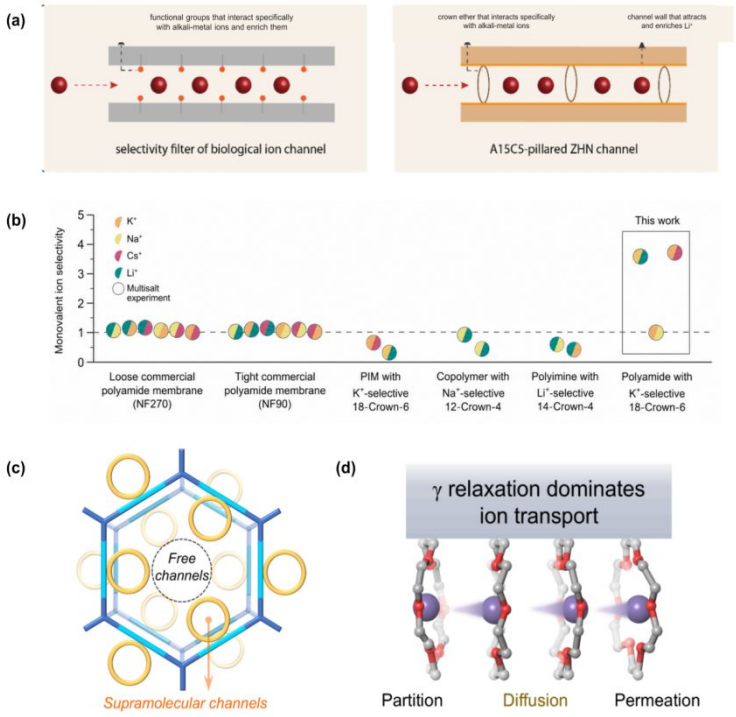


Figure 3 Chemical recognition under confinement and its translation into selective ion transport.

(a) Schematic comparison between the selectivity filter of a biological ion channel and an angstrom-scale ZHN channel pillared with 1-aza-15-crown-5 (A15C5). Specific functional groups in the biological channel and crown-ether units in the artificial channel promote local enrichment through ion–site interactions. In the artificial system, chemical recognition is further coupled with angstrom-scale confinement to regulate pore entry and intrapore partitioning. Adapted from Ref. [28]. (b) Monovalent-ion selectivity of commercial polyamide membranes and crown-ether-based polymer membranes. NF270 and NF90 are commercial membranes without crown-ether recognition units, whereas the remaining membranes incorporate crown ethers with distinct ion-affinity preferences; symbols outlined in grey denote measurements under multisalt feed conditions. The comparison illustrates that both the chemical identity of the recognition unit and its organization within the membrane influence whether preferential affinity is translated into macroscopic transport selectivity. Adapted from Ref. [29]. (c) Compartmentalized dual-channel architecture of 18C6-COF. Continuously aligned 18-crown-6 units form supramolecular recognition channels alongside framework-defined free channels, illustrating the spatial division between selective binding and low-resistance transport domains. Adapted from Ref. [30]. (d) Ion migration coupled to the conformational dynamics of 18-crown-6. Ion partitioning is followed by intrapore diffusion and transmembrane permeation. The original study proposes that γ-relaxation of the crown-ether units enables bound ions to migrate without complete detachment from the recognition sites, thereby mitigating kinetic trapping associated with strong ion–pore interactions. Adapted from Ref. [30].

The biomimetic channel shown in Figure 3a provides a direct illustration of this confinement effect. Biological ion channels regulate local ion enrichment and passage through ordered functional groups within their selectivity filters, whereas the A15C5-pillared ZHN angstrom-scale channel places crown-ether recognition and geometric confinement within the same transport region. Pore-entry constraints determine the solvation state in which the ion approaches the macrocyclic site, while stabilization by the crown ether can compensate for part of the entry penalty. Selectivity here arises neither from simple size exclusion nor from the binding of a free ion by a bulk-solution ligand, but from the combined effects of solvation reorganization, spatial matching, and ion–site interactions.[24,28]

For transmembrane separation, chemical recognition generally first alters ion partitioning into the membrane phase, but preferential partitioning does not necessarily imply preferential permeation. Within a simplified partition–diffusion picture that neglects electromigration and cross-component coupling, the concentration-gradient-driven ion flux can be expressed as

$$J_i = \frac{K_i D_i}{\ell} \Delta c_i$$

where K_i is the partition coefficient of ion i between the membrane phase and the external solution, D_i is its effective diffusion coefficient within the membrane, and ℓ is the thickness of the selective layer. Strengthening ion–site interactions generally favours an increase in K_i, but may also prolong residence time, reduce D_i, and increase the dissociation resistance at the outlet. Intramembrane enrichment, selective retention, and preferential permeation therefore correspond to different process outcomes. Chemical affinity can be translated into steady-state transmembrane selectivity only through intrapore migration and outlet-side release.[8,24,29,30]

The comparison between conventional polyamide membranes and crown-ether-containing polymer membranes in Figure 3b further demonstrates that a recognition unit provides only a potential chemical preference, rather than a predetermined ion-transport sequence.[24,29] Macrocycle size, site orientation and accessibility, selective-layer thickness, degree of crosslinking, and polymer free volume all affect whether a target ion can continue to migrate after entering the membrane phase. Under mixed-salt conditions, competitive occupancy and ion correlations may further alter the affinity sequence established in single-salt experiments. Macroscopic selectivity therefore cannot be explained solely by the solution binding ability of a crown ether towards a given ion, but depends on how recognition sites are embedded within an effectively percolated transport network.

The spatial organization of sites is critical for coordinating affinity and mobility. Isolated high-affinity sites readily create deep energy wells, requiring the ion to undergo complete dissociation, resolvation, and rebinding at every forward step, thereby accumulating transport resistance. If recognition sites are continuously arranged at suitable intervals along the migration direction, ions may instead undergo relay-like transport through exchange between adjacent sites.[24,30] In the 18C6-COF shown in Figure 3c, supramolecular channels formed by continuous crown-ether units are placed alongside framework-defined free channels, allowing selective partitioning and low-resistance migration to be assigned to different pore domains. This spatial division of function offers a more effective design strategy than merely increasing site density.

Conformational motion of the recognition units themselves may also alter the relationship between binding and migration. As shown in Figure 3d, the original study associated ion transport in 18C6-COF with the γ-relaxation of crown ethers, proposing that bound ions could move along the channel without completely leaving the recognition environment, thereby reducing the energetic cost of repeated dissociation, rehydration, and rebinding.[30] Similar site-exchange, conformation-assisted migration, or multi-ion pushing processes may enable strong local recognition to coexist with rapid long-range transport. A high flux alone, however, is insufficient to establish such a synergistic mechanism; corroborating evidence from intrapore occupancy, concentration dependence, relaxation timescales, and molecular motion is also required.

Adsorptive nanoporous materials follow a different process logic. They do not require the target ion to continuously traverse the material, but instead preferentially occupy sites under competitive conditions and are subsequently released by changing the solution conditions. Adsorption selectivity should therefore be understood along a "capture–dissociation–intrapore diffusion–release" pathway. Higher affinity can improve the capture of low-concentration target ions, but may also impede subsequent desorption. Even after an ion has dissociated from a site, it must still return to the bulk phase through a tortuous pore network. For functionalized porous carbons and biochars, apparent removal may simultaneously involve ion exchange, surface complexation, and mineral-phase-induced precipitation or coprecipitation; total adsorption therefore cannot be directly equated with specific recognition by predefined sites.[12,18] Quantitative comparisons of working capacity, fixed-bed mass transfer, and regeneration performance are discussed further in Section 3.3.

Recognition sites are also not static structures with unlimited capacity and invariant interactions.[12,24,30] At low occupancy, target ions may preferentially enter high-affinity regions. As these sites gradually become saturated, additional ions shift towards lower-affinity sites or nonselective pores, changing the apparent selectivity. If the site density is too low, the chemical preference cannot extend throughout the material; if it is too high, overlapping fields from adjacent sites may create a continuous kinetic trap. More meaningful control variables are therefore the matching among site density, spatial spacing, conformational flexibility, and binding–dissociation rates.

Competing ions can alter pathways through a continuous recognition channel by displacement, cooperative occupancy, and electrostatic coupling. Moderate multi-ion occupancy may drive ions further along the pathway, whereas occupation of a critical site by a competing ion may interrupt relay transport.[3,11,24,30] In heterovalent systems such as Li^+/Mg^{2+}, Donnan partitioning, charge screening, and electroneutrality constraints coexist with coordination interactions, requiring mechanistic attribution to be supported by multiple, mutually corroborating forms of evidence.

Recognition sites must therefore be organized into a percolated and exchangeable transport network before a local chemical preference can be translated into membrane transport or selective capture. If the conformation, accessibility, or local potential of the sites changes reversibly in response to an external stimulus or ion occupancy, static recognition further transitions into dynamic gating.[24,28–30]

2.3 Dynamic Gating

Size- and solvation-based sieving and chemical recognition are generally established within relatively fixed pore structures and interfacial chemistries, whereas dynamic gating further introduces a temporal dimension.[16] Applied potential, pH, light, or ion occupancy can alter pore-entry geometry, surface potential, chain conformation, wetting state, and the accessibility of recognition sites, allowing the same channel to exhibit different transport

For Review Only

states during operation.[13,31–34] Dynamic gating is therefore not simply the mechanical opening and closing of a pore, but a reversible reorganization of the energy barriers associated with ion entry, interfacial partitioning, and intrapore migration. In addition to changes in the charge or conformation of solid pore walls, dynamic liquid films can serve as reconfigurable transport boundaries. Cation valence can trigger transitions between channel states by regulating interfacial electrostatic interactions and liquid-film morphology, demonstrating that feed ions themselves can act as gating signals.[35]

The ability of a material to respond to a stimulus does not necessarily mean that it possesses a selective-separation function. If a state transition causes the fluxes of all ions to change approximately in parallel, the structure more closely resembles a tunable nanofluidic valve. Genuine selective gating requires the change in material state to affect the target and competing ions asymmetrically, so that their relative partitioning or migration sequence changes reversibly.[13,31–34] In other words, the significance of gating for separation is determined not by the magnitude of the change in total ionic current, but by whether the altered transport state amplifies the initially limited physicochemical differences between ions.

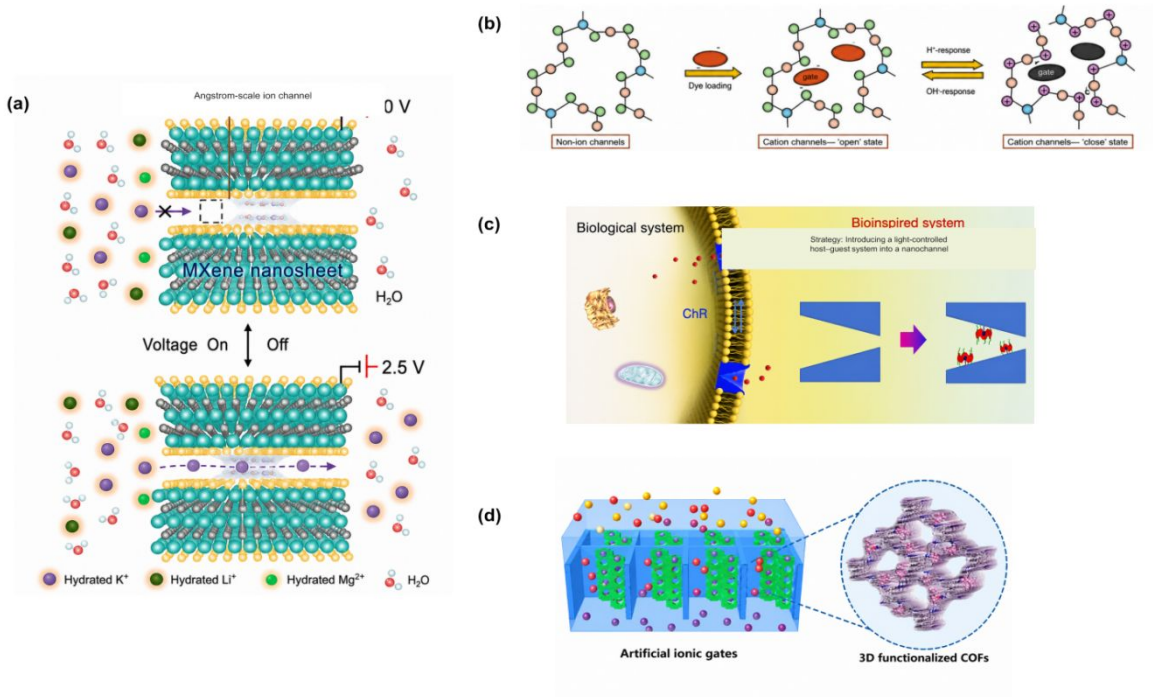


Figure 4 Dynamically gated ion transport triggered by external stimuli and ion occupancy.
(a) Voltage gating in angstrom-scale MXene–PDA channels. Switching the applied potential from 0 to 2.5 V reorganizes the intrachannel ion distribution and migration state, enabling high-flux, K^+-preferential transport through the combined regulation of voltage gating and cation charge density. Adapted from Ref. [31]. (b) TASK2-inspired pH-responsive polymeric nanochannels. Loading of an anionic dye converts the nonionic channel into an open, cation-selective state. The H^+ response induces amino-group protonation and ionic crosslinking, accompanied by changes in chain conformation and channel-wall charge, thereby switching the channel to a closed state; the process is reversed by the OH^- response. Adapted from Ref. [32]. (c) A light-controlled host–guest nanochannel inspired by channelrhodopsin. Incorporation of photoresponsive host–guest units into a conical nanochannel allows light to reversibly regulate ion transport by altering the interfacial assembly state and chemical environment of the channel wall. Adapted from Ref. [33]. (d) Ion-triggered gating in crown-ether-functionalized three-dimensional COFs. Coordination of Li^+ with 12-crown-4 recognition sites changes the ion-transport state of the pore, translating static chemical recognition into adaptive gating triggered by ion occupancy. Adapted from Ref. [34].

Externally driven gating operates primarily by changing the charge state and local structure of the channel. Potential control can rapidly reorganize the intrapore ion distribution and alter interactions between charged interfaces and ions of different valence. In the angstrom-scale MXene–PDA channels shown in Figure 4a, the applied potential and cation charge density jointly affect the competitive transport of K^+, Li^+, and Mg^{2+}, indicating that electrochemical gating can regulate not only transport rate but also the occupancy relationship among ions within the channel.[31] The applied potential, however, often plays two simultaneous roles: it changes the pore-wall state and directly drives ion migration. If these effects are not distinguished, the observed current change may contain contributions from surface charging, electromigration, and concentration polarization, and cannot be attributed entirely to gating itself.

A pH response more closely couples interfacial charge to channel conformation.[32] Protonation or deprotonation not only changes fixed-charge density, but may also induce ionic crosslinking, chain contraction or swelling, and changes in intrapore water content. TASK2-inspired polymer channels switch between states of different pore size and charge through precisely these coupled changes, as shown in Figure 4b. Such systems offer the advantage of simultaneously controlling geometric confinement and electrostatic partitioning, but their interpretation is also more complex because changes in pH alter metal-ion hydrolysis, complexation, and solution speciation. Material response must be distinguished from changes in feed chemistry to determine whether the observed change in selectivity originates from channel gating or from a change in the chemical form of the ions in solution.

By contrast, photoresponsiveness provides a noncontact mode of regulation with relatively high spatial and temporal resolution.[33] Introducing photoisomerizable or host–guest assembly units at pore entrances and pore walls can regulate local steric hindrance, surface charge, and the recognition environment without directly changing the transmembrane driving force. The biomimetic nanochannel in Figure 4c uses light to control the interfacial assembly state and thereby alter ion transport. The effectiveness of this design depends strongly on the location of the responsive unit. If the conformational change occurs in a region remote from

the principal transport pathway, even a pronounced spectroscopic response may have little effect on separation. A molecular-scale structural change can be translated into observable ion selectivity only when it acts directly on a pore-entry bottleneck or a continuous migration pathway.

In addition to external stimuli, ions themselves may trigger changes in the channel state.[34] The crown-ether-functionalized three-dimensional COF in Figure 4d uses coordination between Li^+ and 12-crown-4 sites to alter the intrapore transport environment, converting ion recognition into feedback regulation driven by occupancy. Such adaptive gating lies at the boundary between chemical recognition and dynamic regulation. If target-ion binding merely enhances local adsorption or intramembrane enrichment, the process remains static recognition. Genuine ion-triggered gating occurs only when site occupancy further changes the effective pore size, pore-wall potential, conformational state, or migration barrier experienced by subsequent ions. Its distinctive feature is that feed composition is no longer merely the object of separation, but also participates in determining the transport state of the material itself.

In practical multicomponent systems, the gating state is generally not an idealized "open" or "closed" condition, but a series of intermediate states jointly determined by ion concentration, competitive occupancy, and charge screening.[31,32,34,36] As salt concentration increases, compression of the electrical double layer may weaken charge gating. As recognition sites become saturated, ion-triggered feedback may level off. A competing ion that preferentially occupies a responsive site may even reverse the direction of gating. The timescale of gating is equally important. If the response is too slow, the material state cannot follow changes in the feed; if recovery is too slow, pronounced memory effects and path dependence emerge. Dynamic selectivity therefore depends on temporal matching between ion transport and material-state transitions, rather than solely on static differences between two steady states.

Effective gating must act at a pore entrance, narrow bottleneck, or principal recognition region, and must exert an asymmetric, reversible, and temporally matched influence on the target and competing ions. Its evaluation should simultaneously consider ion-pair selectivity, response and recovery times, hysteresis, and cyclic drift, rather than relying only on the magnitude of a conformational change or the on/off ratio of total current. Dynamic gating can thus be understood as the state-dependent and temporally ordered reconfiguration of confinement sieving and chemical recognition.[13,31–34]

2.4 Synergy among Multiple Mechanisms

Size- and solvation-based sieving, chemical recognition, and dynamic gating are three analytical dimensions for identifying the origin of selectivity, rather than mutually isolated transport mechanisms. In an actual nanopore, an ion approaches the pore entrance from the bulk phase and subsequently undergoes solvation reorganization, interfacial partitioning, intrapore migration, and outlet-side release. Pore size, interfacial chemistry, and channel state often act simultaneously at several of these stages. A selective advantage established at one stage can be translated into the final separation outcome only if it persists through subsequent stages. A reduction in the entry barrier may be offset by slow intrapore diffusion, while high intramembrane affinity may manifest as retention if release is hindered. The essence of multimechanism coupling is therefore not the addition of more structural units or functional groups, but the coordination of the location, strength, and direction of different effects along the transport pathway so that they jointly favour the target ion rather than counteracting one another at different stages.[5,8,9,11,13,24–26,30] This process-oriented understanding is also the central feature that distinguishes this Review from literature surveys organized by material class.

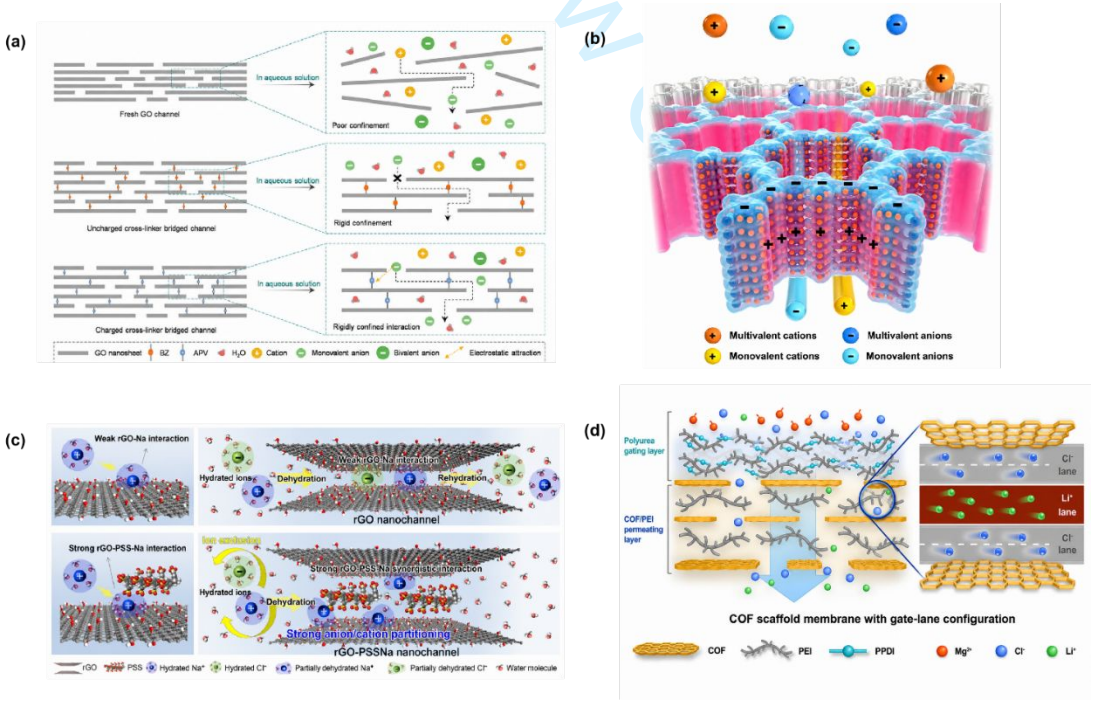


Figure 5 Spatial coupling of separation mechanisms and multicomponent ion transport in nanoporous membranes.

(a) Coupling of rigid confinement and ion–channel affinity in GO channels. Charged cross-linkers suppress swelling while compensating ion-dehydration penalties, thereby improving anion discrimination. Adapted from Ref. [37]. (b) Molecular-packing-regulated screening of cations and anions. Ordered charge environments and ion–π interactions in two-dimensional COFs differentiate monovalent and multivalent ions. Adapted from Ref. [38]. (c) Electrostatic-induced intrachannel partitioning and decoupling of anion–cation co-transport. PSSNa promotes partial Na^+ dehydration and confined enrichment, increasing the spatial partitioning difference between cations and anions. Adapted from Ref. [39]. (d) Hierarchical coupling of a gating layer and lane-separated pathways. The polyurea surface layer restricts Mg^{2+} entry, whereas the COF/PEI interior forms preferential Li^+ and Cl^- transport lanes, highlighting the roles of ion competition, counter-ion migration, and electroneutrality in mixed-salt selectivity. Adapted from Ref. [40].

A typical form of coupling occurs within a pore domain in which confinement and interfacial interactions coexist. Geometric constraints force the ion hydration shell to compress or reorganize, but also increase the cost of entering the pore. Moderate ion–pore-wall interactions can stabilize this transition state and partly compensate for the energetic penalty of solvation reorganization. The crosslinked GO membrane shown in Figure 5a suppresses aqueous swelling by fixing adjacent nanosheets while using charged crosslinking structures to regulate interactions between anions and the channel.[37] The hydration shells of different anions consequently undergo different degrees of configurational reorganization, and selectivity arises from the combined effects of rigid confinement, confined-water structure, and interfacial affinity rather than from pore size or electrostatics alone. Importantly, this synergy exists within an appropriate interaction window: insufficient confinement fails to amplify ion differences, whereas excessively strong interactions may create deep local energy wells and hinder subsequent migration.

Spatial organization inside the channel likewise determines whether chemical interactions can be translated into sustained transport selectivity. Isolated or disordered sites may enhance local adsorption but do not necessarily affect ion migration along a percolated pathway. Oriented COFs provide a different situation: face-to-face arrangement and interlayer packing of the building units organize aromatic π systems and their local potentials along the transport direction, allowing multiple relatively weak ion–π interactions to be amplified through spatial cooperation and thereby differentiating the partitioning and migration of monovalent and multivalent ions, as shown in Figure 5b.[38] This result demonstrates that selectivity is governed not only by the chemical identity or number of recognition groups, but also by their position relative to the pore entrance and transport direction. Even at identical material composition and nominal pore size, changes in orientation, packing, and grain-boundary state can reconstruct the interfacial environment actually experienced by the ions.

Different effects can also cooperate through spatial division of function rather than through colocalized superposition. If the entire transport pathway retains extremely small pores or strong binding, suppression of competing-ion migration is generally accompanied by increased resistance to target-ion transport. Hierarchical structures allow the selective bottleneck to be concentrated at the pore entrance or within a local membrane layer, while subsequent regions provide lower-resistance migration. In the gate–lane architecture shown in Figure 5d, a surface polyurea layer restricts Mg^{2+} entry, whereas internal COF/PEI regions provide suitable transport environments for Li^{+} and Cl^{-}, respectively.[40] Entry exclusion of the competing ion, intrapore migration of the target ion, and charge compensation by the counter-ion are thus no longer assigned entirely to the same structure. This “entrance gating–internal transport” design shows that mechanistic synergy does not require every pore region to possess all functions simultaneously; rather, the responsibilities of different regions must be spatially defined so that selectivity established at the entrance is not consumed by subsequent transport resistance.

When the feed contains multiple salts, coupling extends from ion–pore interactions to ion–ion interactions. Recent studies further emphasize that ion association under nanoconfinement is not a secondary correction restricted to high-concentration conditions, but may directly alter intrapore partitioning, correlations in ion migration, and ultimately the sequence of precision separation.[41] Because of electroneutrality constraints, the target ion cannot always be treated as an independently migrating component; local enrichment of competing ions, co-ions, and counter-ions may all change the transport sequence. In the ArGO–PSSNa membrane shown in Figure 5c, interlayer confinement and the affinity of sulfonate groups for Na^{+} confine cations within the nanochannels and increase the difference in intrapore partitioning between Na^{+} and Cl^{-}. Dynamic correlations between cations and anions are thereby weakened, suppressing their original cooperative transmembrane transport. By contrast, the gate–lane membrane provides coordinated but spatially separated pathways for Li^{+} and Cl^{-}, making counter-ion migration part of the mechanism that sustains target-ion transport. These apparently opposite strategies reveal the same principle: selectivity is determined not only by target-ion entry and diffusion, but also by how a material reconstructs the local composition and correlated motion of the entire electrolyte.[39,40]

Competitive effects exhibit a pronounced dependence on composition. In an oriented COF membrane, interfacial occupancy by monovalent cations can restrict multivalent cations from approaching the pore wall, thereby enhancing cation sieving. For anions, analogous competition may instead weaken the interfacial partitioning of strongly binding species.[30,38–40] As salt concentration and site occupancy change, the rate-limiting step may also shift from interfacial partitioning to intrapore migration or release.

Dynamic gating adds state dependence to the above spatial coupling, allowing entrance sieving, interfacial partitioning, and intrapore migration to change jointly with an external stimulus or ion occupancy. The gating state can alter the final ion-pair selectivity only if it acts on the actual rate-limiting step.[31–34]

Overall, multimechanism synergy is achieved mainly through confinement–interface coupling within the same pore domain, division of function among different structural regions, and multi-ion occupancy coupled with counter-ion migration. Its effectiveness should be judged by whether the net transport advantage of the target ion in a mixed feed can be retained successively through pore entry, intrapore migration, and outlet-side release, rather than inferred directly from a single pore size, site affinity, or static structural parameter.[24,25,30,37–40] The corresponding quantitative cross-scale description is discussed further in Section 4.

3. Ion-Separation Performance of Nanoporous Materials

The preceding mechanistic analysis shows that nanopores can establish selectivity at different stages of ion entry, partitioning, migration, and release. Mechanistic plausibility, however, does not directly establish superior separation performance. The same separation factor may arise from enhanced target-ion transport or merely from stronger inhibition of a competing ion, while similar fluxes or rejection values may carry different physical meanings because of differences in feed composition, driving force, membrane thickness, or testing mode.[42–44] This section therefore does not repeat the discussion of local mechanisms themselves, but instead examines the performance metrics, testing boundaries, and quantitative comparability of different nanoporous materials, and analyses how material-level selectivity is translated into actual separation outcomes.

Different nanoporous materials derive selective separation from different structural bases. Rigid crystalline channels provide relatively well-defined size constraints; framework materials allow pore size and interfacial chemistry to be tuned within ordered channels; two-dimensional lamellar materials offer short transport pathways and flexible control over interlayer spacing; and polymer membranes have advantages in processing and module integration. For adsorbent materials such as porous carbons and biochars, performance depends more strongly on heterogeneous pore structures, surface sites, and their reversible

occupancy under competitive conditions. These material classes differ substantially in design freedom, applicable processes, and failure modes, and cannot be ranked simply according to maximum selectivity or capacity values reported under different conditions.[5,13,19–21,42,43] Table 2 accordingly summarizes the key structural features, representative separation performance, advantages, and limitations of the principal material platforms.

Table 2. Comparison of major nanoporous material platforms for selective ion separation

Material platform	Key structural features	Representative performance	Main advantages	Main limitations	Refs.
Zeolites and inorganic molecular sieves	Rigid, uniform subnanometre pores; tunable framework charge	Preferential H^+ transport over VO^{2+}, Cr^{2+} and Fe^{2+} through ZSM-5	Well-defined apertures; low transport resistance	Limited chemical tunability; difficult defect-free fabrication	[45]
MOFs	Programmable pore windows, nodes and linkers	Mono-/divalent conductance difference of approximately 10^3	Coupled control of pore size and interfacial chemistry	Predominantly micro-/nanoscale demonstrations; defect and scale-up issues	[26]
COFs	Ordered channels; tunable stacking, orientation and functionality	K^+/Al^{3+} and NO_3^-/PO_4^{3-} selectivities of 214 and 451	High structural programmability; continuous recognition sites	Strong sensitivity to stacking, orientation and grain boundaries	[38]
Two-dimensional lamellar materials, including GO and MXenes	Tunable wet-state spacing, terminal groups and surface charge	Cl^-/SO_4^{2-} selectivity of 125 in a GO membrane	Thin selective layers; facile crosslinking and functionalization	Swelling, restacking and long-term structural evolution	[37]
Microporous polymers and ion-exchange membranes	Dynamic free volume; tunable fixed charges and functionalities	Monovalent-ion/Mg^{2+} selectivity above 100 in an electrodialysis stack	Processable, scalable and module-compatible	Hydration-induced swelling; broad pore-size distributions	[9,27,46]
Biomimetic and artificial nanochannels	Ångström-scale apertures; precisely positioned recognition sites	K^+/Li^+ selectivity of approximately 364	High precision for isovalent ions; explicit mechanisms	Small effective area; difficult device integration	[28,47]
Functionalized porous carbons and biochars	Heterogeneous pores; diverse surface groups and mineral phases	Cd^{2+} and Cu^{2+} capacities of 29.9 and 34.1 mg g^{-1} for HFO–biochar	Low cost; compatible with adsorption and fixed beds	Limited intrinsic selectivity; heterogeneous and complex mechanisms	[18,48]
Composite and hierarchical porous architectures	Spatially separated gating, scaffold and transport domains	True Li^+/Mg^{2+} selectivity of 231.9 at 11.5 L m^{-2} h^{-1} bar^{-1}	Potential mitigation of the selectivity–permeability trade-off	Complex fabrication; interfacial defects and durability concerns	[40]

Note: This table provides an overview of the structural characteristics and representativeness of different material platforms and is not intended for quantitative ranking across ion systems or testing modes.

3.1 Performance Metrics, Testing Modes, and Comparability Boundaries

Compared with mechanistic classification, performance comparison among nanoporous materials is more susceptible to the testing method and metric definition. Existing studies commonly describe material performance in terms of selectivity, ion flux, permeability, rejection, or ionic conductivity, although these metrics correspond to different physical processes. Selectivity emphasizes relative transport between the target and competing ions; flux reflects the absolute amount transported per unit area; and rejection is more commonly used to describe retention of an individual component under pressure-driven conditions. Even when the same term is used, values reported in different studies may derive from single-salt diffusion, mixed-salt separation, membrane-potential calculations, or electrically driven transport. Comparing such data outside their specific testing boundaries often causes differences arising from experimental conditions to be misidentified as intrinsic differences in material performance.[42–44]

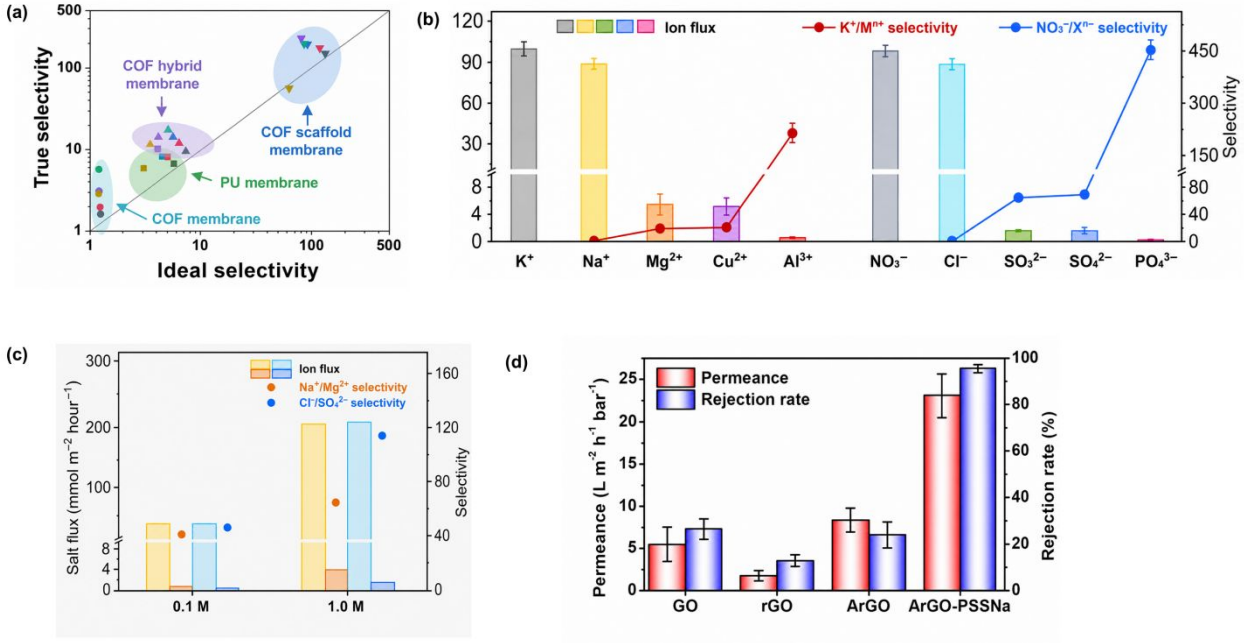


Figure 6 Effects of performance metrics and testing conditions on the interpretation of selective ion separation.

(a) Comparison of ideal selectivity with true selectivity measured in mixed feeds, showing that single-salt performance does not directly predict multicomponent separation. Adapted from Ref. [40]. (b) Ion fluxes and K^+/M^{n+} and NO_3^-/X^{n-} selectivities of a COF-170/PAN membrane under 0.1 M single-salt conditions. Adapted from Ref. [38]. (c) Fluxes and selectivities in equimolar ternary mixtures of NaCl, Na_2SO_4 and $MgCl_2$ at 0.1 and 1.0 M, illustrating the effects of competitive partitioning and ion–ion interactions. Adapted from Ref. [38]. (d) Water permeance and NaCl rejection of GO, rGO, ArGO and ArGO-PSSNa membranes at 5 bar using a 5 mM NaCl feed. Adapted from Ref. [39].

Single-salt experiments are suitable for identifying the potential transport preference of a material for individual ions, whereas multicomponent feeds reorganize the membrane composition through competitive occupancy, ionic strength, counter-ion migration, and electroneutrality constraints. In the gate–lane membrane shown in Figure 6a, the true Li^+/Mg^{2+} selectivity reached 231.9, exceeding the ideal selectivity of 80.5 derived from single-salt results, indicating that ion-mixing effects can further amplify selectivity in certain systems.[40] Figures 6b and 6c further show that coexisting ions and total salt concentration can alter both the sequence and magnitude of Na^+/Mg^{2+} and Cl^-/SO_4^{2-} selectivity.[38] Single-salt results therefore characterize potential preference, whereas mixed-salt data describe actual separation under a specified composition.[42–44]

The driving force determines the physical process represented by a performance metric. Concentration-gradient experiments primarily reflect intramembrane partitioning and diffusion; pressure-driven measurements additionally involve water-flow entrainment, convective mass transfer, and concentration polarization; and electrically driven transport is governed by electromigration and ion transference numbers. Water permeability and rejection, diffusion flux, relative permeability inferred from membrane potential, and single-pore current are therefore not equivalent performance quantities. Comparisons must also specify ion system, feed composition, pH, temperature, membrane thickness, effective area, and testing duration, because these conditions determine the relative contributions of entry resistance, intrapore migration, defect-mediated bypass transport, and transient effects.[42–44]

Accordingly, rigorous quantitative comparisons are made here only when the ion system, feed conditions, driving force, and metric definition are essentially consistent. Other data are used to assess trends or orders of magnitude,[42,43] and are discussed separately according to single-salt versus mixed-salt feeds, diffusion versus pressure-driven transport, and electrical-current versus molar-flux measurements. Figure 6 defines the boundaries of comparison rather than ranking materials.

3.2 Performance Comparison of Membranes and Nanochannels

After metric definitions and testing boundaries have been clarified, the performance of membranes and nanochannels must still be interpreted in the context of the specific ion system. Ion valence, hydration characteristics, and coordination chemistry determine the differences that a material can exploit, and also influence how the separation factor is generated and what process value it carries. The following discussion is organized according to heterovalent ions, isovalent monovalent ions, and isovalent multivalent ions, while simultaneously considering the absolute transport of target and competing ions, the direction of selectivity, and performance retention in mixed feeds.

3.2.1 Heterovalent-Ion Separation

Li^+/Mg^{2+} is the most extensively studied heterovalent cation-separation system. Because the two ions differ substantially in valence, charge density, and hydration characteristics, a high separation factor is relatively easy to establish, although its origin is not always the same. The polyamide nanofiltration membranes shown in Figures 7a and 7b narrow the pore-size distribution so that most pore entrances lie between the effective sizes of Li^+ and Mg^{2+}. As the mean pore size decreases, Mg^{2+} rejection approaches completion while Li^+ retains negative rejection, causing Li^+/Mg^{2+} selectivity to increase sharply.[49] Ion-permeability measurements further show that Li^+ permeability remains broadly similar, whereas Mg^{2+} permeability decreases by more than three orders of magnitude. The performance enhancement here arises primarily from strong inhibition of the competing ion, rather than sustained acceleration of Li^+ transport. At the same time, negative Li^+ rejection in a mixed-salt system is also affected by the transmembrane potential and electroneutrality coupling, and the resulting selectivity cannot therefore be attributed entirely to a static pore-size difference.

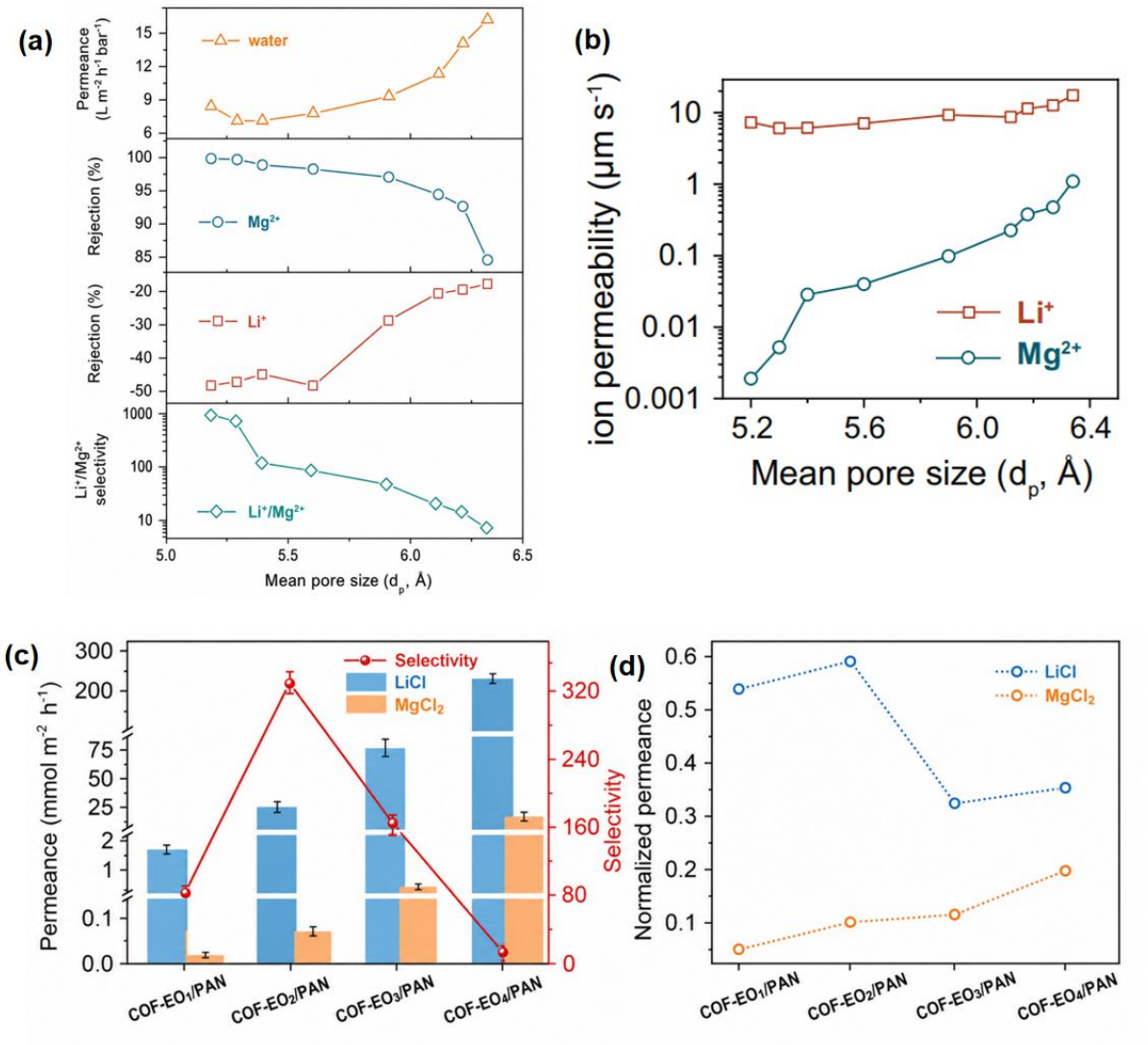


Figure 7 Distinct origins of selectivity in heterovalent ion separation.

(a,b) Effects of the mean pore size of polyamide nanofiltration membranes on water permeance, Li^+ and Mg^{2+} rejection, Li^+/Mg^{2+} selectivity, and ion permeability. Decreasing pore size preferentially suppresses Mg^{2+} transport, thereby increasing selectivity. Adapted from Ref. [49]. (c,d) Salt permeances and Li^+/Mg^{2+} selectivity of COF-EOx/PAN membranes in binary $LiCl/MgCl_2$ feeds, together with permeances normalized to the corresponding single-salt values. Intrapore solvation and mixed-ion competition jointly reshape the relative transport of Li^+ and Mg^{2+}. Adapted from Ref. [50].

Intrapore chemistry provides another regulatory route. In Figures 7c and 7d, the COF-EOx/PAN membranes tune local solvation ability inside the pores by changing the length of oligomeric ether chains.[50] $LiCl/MgCl_2$ selectivity exhibits a pronounced nonmonotonic dependence on ether-chain length. Moderate ion–pore-wall interactions favour Li^+ partitioning and migration while imposing higher resistance on Mg^{2+}. Further enhancement of the channel's solvating ability, however, also increases Mg^{2+} permeation, thereby reducing selectivity. Changes in binary-mixture permeance relative to single-salt results further demonstrate that Li^+ and Mg^{2+} do not traverse the membrane independently. Local solvation, competitive occupancy, and counter-ion migration jointly reconstruct the intrapore composition, such that true selectivity cannot be obtained simply by dividing the two single-salt permeabilities.

Similar principles apply to anion systems. An ionized polymer of intrinsic microporosity restricts the pore window to a range between the hydrated and Stokes diameters of the anions and introduces quaternary ammonium sites to promote migration of partially dehydrated monovalent anions, achieving Cl^-/CO_3^{2-} and Cl^-/SO_4^{2-} selectivities of 106 and 82, respectively.[27] This performance depends simultaneously on subnanometre confinement and fixed charge and cannot be regarded as simple size cut-off. More instructively, conventional valence-based trends can be reversed through specific interactions. When hydrated manganese oxide is incorporated into a cation-exchange membrane, phosphate migrates continuously along reversible outer-sphere complexation sites; its flux is increased 27-fold relative to that through the unmodified membrane, and phosphate is transported preferentially over sulfate, nitrate, and chloride.[8] This result demonstrates that a higher valence does not necessarily correspond to lower permeability. Provided that binding remains reversible and is matched to a continuous diffusion pathway, chemical recognition can promote rather than impede target-ion transport.

Acid–base-pair engineering in ion-exchange membranes provides another route to heterovalent-ion separation. Moderately sulfonated polybenzimidazole membranes form contracted ionic clusters and hydrophilic domains with restricted connectivity, thereby imposing a higher migration barrier on Mg^{2+} than on Li^+. The resulting SP45 membrane exhibits a Li^+/Mg^{2+} selectivity of 48.1 at 2 mA cm^{-2} and limits selectivity decay to less than 10% over multiple mixed-salt cycles.[51] This result shows that ionic-cluster dimensions, hydrophilic-domain connectivity, and local acid–base interactions can jointly regulate the partitioning and migration of heterovalent ions without relying entirely on geometric pore-size cut-off.

Overall, heterovalent ions already exhibit substantial differences in charge and hydration, allowing many membranes to attain high apparent selectivity. Such values, however, are also particularly likely to obscure their origin: some systems genuinely improve target-ion transport, whereas others merely achieve nearly complete rejection of the competing ion.[42,43,49,50] Evaluation of heterovalent-ion membranes should therefore not stop at the separation factor, but should simultaneously examine the absolute fluxes of the target and competing ions and determine whether the difference persists under mixed-salt conditions.

3.2.2 Isovalent Monovalent-Ion Separation

When the valence difference disappears, electrostatic exclusion cannot directly distinguish Li^+, Na^+, and K^+, and selectivity depends more strongly on subtle differences among solvation reorganization, the operando pore aperture, and ion–site interactions. Under these conditions, high selectivity generally does not arise from one exceptionally large barrier, but from the accumulation of multiple local sieving or recognition events along the transport pathway.

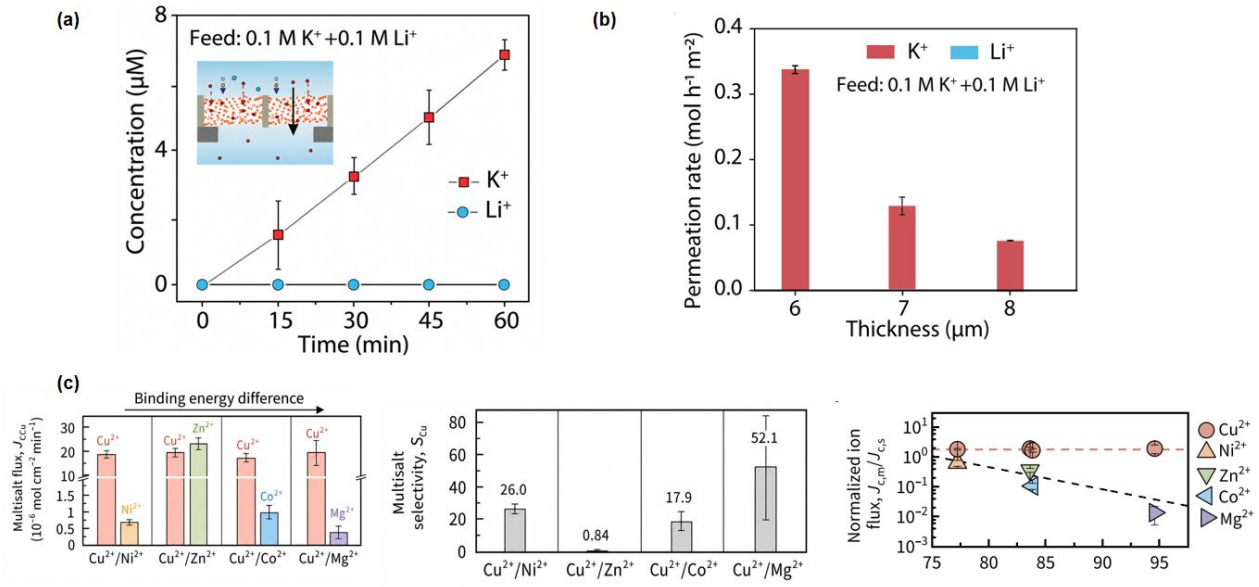


Figure 8 Transport direction, thickness effects, and coordination contrasts in isovalent ion separation.
(a,b) Transmembrane transport of K^+ and Li^+ from a mixed feed and its dependence on membrane thickness. K^+ permeates continuously while Li^+ is largely retained, and the K^+ permeation rate decreases with increasing membrane thickness. Adapted from Ref. [52]. (c,d) Ion fluxes and Cu^{2+} selectivities in mixed feeds containing Cu^{2+} and another divalent cation, together with the dependence of normalized flux on the difference in ligand-binding energy. A larger binding-energy contrast mainly suppresses transport of the competing ion, while the Cu^{2+} flux remains comparatively stable, indicating that selectivity arises from asymmetric partitioning–diffusion coupling rather than a simple enhancement of target-ion flux by stronger binding. Adapted from Ref. [53].

The randomly oriented COF membrane shown in Figures 8a and 8b adopts a separation direction different from the commonly pursued "preferential permeation of Li^+".[52] Narrow, randomly oriented channels and preferential interactions of sulfonate groups with Na^+ and K^+ allow K^+ to permeate continuously, while Li^+ is largely retained on the feed side. The product is therefore not a Li^+-containing permeate; rather, Li^+ is retained and enriched by removing competing ions. When the membrane thickness increases from 6 to 8 μm, K^+ permeation decreases markedly while Li^+ remains nearly impermeable, showing that increasing the transport distance can preserve the direction of sieving but directly reduces the processing rate. Random orientation in this system creates channels between two extremes: parallel-oriented pores are too wide to provide selectivity, whereas vertically oriented structures have such high resistance that they permit almost no ion passage.

Biomimetic channels further demonstrate that subtle differences can be amplified through preorganized sites. KcsA-type artificial channels use cation–π and electrostatic interactions within subnanometre cages to achieve a K^+ transport rate of 94.4 mmol m^{-2} h^{-1}, with K^+/Li^+ and K^+/Na^+ selectivities of 363 and 31, respectively.[47] Crown-ether-pillared angstrom-scale channels exploit intrapore enrichment and host–guest recognition to achieve high effective Li^+/Na^+ selectivity in artificial seawater containing only 25 μM Li^+.[28] These examples show that preorganized sites can amplify small free-energy differences between isovalent ions in different transport directions. Because channel area, driving mode, and measured quantities vary substantially, however, these values are more suitable for comparing mechanisms and trends than for direct ranking against macroscopic pressure-driven membranes.

The selectivity sequence within the same material is also not necessarily fixed.[42–44] An amino-acid-functionalized COF membrane can switch between Na^+ selectivity and K^+ selectivity with changing pH because protonation alters the relative interactions between the ions and coordination sites.[54] This further demonstrates that free-energy differences among isovalent monovalent ions are generally small, and that minor changes in intrapore water structure, site state, or solution conditions can alter the final transport sequence.

3.2.3 Isovalent Multivalent-Ion Separation

The differentiation of isovalent multivalent ions depends more strongly than that of heterovalent ions on the coupling between the local coordination environment and mass transport. Cu^{2+}, Ni^{2+}, Co^{2+}, Zn^{2+}, Mg^{2+}, and Ca^{2+} have the same or similar charge states, making it difficult to establish a stable selectivity sequence solely through Donnan exclusion. The exploitable differences arise more often from hydration-shell structure, coordination geometry, ligand-exchange kinetics, and solution speciation. Selectivity in these systems therefore does not necessarily originate from direct discrimination of bare-ion dimensions at the pore entrance, but may develop progressively through hydration recognition, competitive coordination, or species transformation.

The ultrathin polymer selective layer shown in Figures 8c and 8d uses iminodiacetate sites to amplify differences in binding among divalent transition-metal ions.[53] In mixed feeds containing Cu^{2+} and another divalent cation, the Cu^{2+} flux changes only modestly, whereas the competing-ion flux decreases substantially as the difference between its binding energy and that of Cu^{2+} increases, raising Cu^{2+}/M^{2+} selectivity from approximately unity to several tens. The increase in selectivity arises primarily from the relative disadvantage of the competing ion in intramembrane partitioning and diffusion, rather than from sustained promotion of Cu^{2+} migration by stronger binding. This result also demonstrates that equilibrium affinity can be translated into an advantage in transmembrane transport only when the selective layer is sufficiently thin, the sites form a continuous pathway, and ions can exchange and be released rapidly.

The Mg^{2+}/Ca^{2+} system further demonstrates that ion recognition does not necessarily require complete removal of the hydration shell. The two ions have the same valence, but Mg^{2+} has a higher charge density and a more rigid first hydration shell. The selective site of the biological Mg^{2+} channel MgtE binds Mg^{2+} approximately 500 times more strongly than Ca^{2+}, with corresponding half-maximal response concentrations of 27.7 ± 3.7 μM and 12.2 ± 1.9 mM, respectively.[55] Structural analysis shows that the site does not directly coordinate bare Mg^{2+}, but recognizes its intact hydration geometry through a water-mediated hydrogen-bonding network. Although this result cannot be used as a direct comparison of macroscopic membrane fluxes, it provides an important design benchmark: for isovalent ions such as Mg^{2+} and Ca^{2+}, selectivity may arise either from different dehydration penalties or from matching of a particular hydration geometry within the pore. In other words, retaining and reorganizing the hydration shell may sometimes be more effective than further narrowing the pore.

Co^{2+}/Ni^{2+} illustrates another route.[56] Because their hydrated sizes and conventional coordination properties are highly similar, direct differentiation using a fixed pore size generally yields only limited contrast. Altering the solution coordination environment can amplify their species-level differences before membrane entry. At high Cl^- concentration, Ni^{2+} primarily forms the positively charged species $[Ni(H_2O)_5Cl]^+$, whereas Co^{2+} forms the negatively charged $[CoCl_4]^{2-}$ complex. Coupling these oppositely charged coordination species with electrodialysis yields a maximum Ni^{2+}/Co^{2+} separation selectivity of 370.70; when applied to leachates from NCM and NCA batteries, the selectivities remain 90.60 and 109.42, respectively. Similarly, oriented COF membranes with tunable intrapore sulfonic-acid-group contents have been used for EDTA-assisted $Ni^{2+}/Co^{2+}/Mn^{2+}$ separation by balancing permeation of free M^{2+} ions against rejection of negatively charged M–EDTA complexes.[57] These results show that such high selectivity does not arise from intrinsic recognition of bare Co^{2+} and Ni^{2+} by the material, but is jointly constructed through solution coordination, species charge, and intramembrane migration. This strategy can substantially amplify otherwise limited ionic differences, but its performance depends more strongly on ligand concentration, counter-ion composition, and complexation equilibria.

Adjacent lanthanide ions extend this challenge to an even finer scale. The continuous and subtle radius changes produced by lanthanide contraction, together with highly similar hydration and coordination chemistry, mean that conventional surface ligands often yield separation factors of only a few units. For porous zirconia modified with aminomethylenephosphonic-acid ligands, the separation factors for adjacent Ce^{3+}/La^{3+} and Yb^{3+}/Tm^{3+} in an equimolar mixture containing all lanthanides are only 2.3 ± 0.4 and 2.7 ± 0.1, respectively.[58] More notably, the Lu^{3+}/La^{3+} separation factor of the same material is 87.4 ± 9.8 in a multicomponent mixture but decreases to 29.8 ± 2.7 in a binary solution, demonstrating that competitive occupancy can markedly alter apparent selectivity and that a single binary system may not represent partitioning in an actual rare-earth mixture.

Further preorganization of intrapore coordination sites can greatly amplify these subtle differences. The ion-microporous ATZ-BTC-Zn framework uses size-matched exchangeable cations and a high density of "nanotrap pockets" to attain a Ce^{3+}/La^{3+} separation factor of 543 in a binary system and a factor of 908 for the adjacent light rare-earth pair La^{3+}/Nd^{3+}.[59] These values, however, describe partition selectivity in equilibrium adsorption or ion exchange rather than steady-state transmembrane permeation. Their significance lies in demonstrating that regular pore cavities can amplify extremely small free-energy differences among lanthanide ions through the combined effects of coordination geometry, site density, and local charge. Whether this advantage can be further translated into continuous transport still depends on sufficiently rapid intrapore diffusion and ion release.

These cases show that isovalent multivalent-ion separation has at least three distinct origins. Mg^{2+}/Ca^{2+} separation more strongly reflects recognition of hydration geometry and confined-water structure; Co^{2+}/Ni^{2+} separation can use solution coordination to convert subtle chemical differences into pronounced charge differences; and separation of adjacent lanthanides relies on preorganized multidentate sites and competitive occupancy to amplify continuous variations in coordination free energy. Binding strength, EC_{50}, adsorption separation factor, and membrane-transport selectivity should therefore not be placed in a single ranking. A more meaningful question is whether the free-energy difference established during ion entry or partitioning can survive competitive occupancy in a mixed feed and be retained during subsequent migration and release.

3.2.4 Cross-System Understanding of Ion-Separation Performance

Across the above systems, high membrane selectivity is generated primarily through two pathways. The first is inhibition of competing ions, in which pore-entry confinement, a higher desolvation penalty, or unfavourable coordination preferentially reduces the partitioning and migration of nontarget ions. The second is promotion of the target ion, in which continuous hydrated pathways, reversible recognition sites, or low-resistance transport pathways enhance target-ion entry and diffusion. The first route readily produces a high separation factor but does not necessarily improve target-ion productivity. The second is more favourable for maintaining flux, but is generally more sensitive to site-exchange rates, channel connectivity, and feed composition.[8,24,42,47,49,50,52–54]

The relative importance of these two routes differs among ion systems. Heterovalent ions exhibit relatively pronounced differences in charge, hydration, and Donnan partitioning and can therefore often be separated with high selectivity by suppressing competing ions. Isovalent monovalent ions have smaller physicochemical differences, requiring accumulation through channel orientation, repeated recognition, and transport distance. Isovalent multivalent ions require coordination thermodynamics, species forms, and exchange kinetics to be mutually matched. The so-called selectivity–flux trade-off is therefore not a single empirical upper bound shared by all materials, but the system-specific distribution of resistance among pore entry, partitioning, intrapore migration, and release.[42,43]

For Peer Review Only

Table 3. Quantitative ion-separation performance of representative ion-selective membranes and nanochannels

Ion system	Material/membrane thickness and area	Feed and conditions	Mode and driving force	Flux/permeation performance	Selectivity definition and value	Duration and feed realism	Refs.
Li^+/Mg^{2+} heterovalent cations	OSARIP polyamide NF membrane; selective layer ≈55 nm; effective area 7.1×10^{-4} m^2	Binary LiCl/$MgCl_2$; total salt 2000 ppm; Mg/Li mass ratio 20:1; 25 °C	Cross-flow pressure filtration; 4 bar; 50 L h^{-1}	Li^+ permeability ≈10 μm s^{-1}; Mg^{2+} rejection 99.82%; Li^+ rejection −48.35%	S=(1−RLi)/(1−RMg); 828 at 20:1; maximum 4147 at Mg/Li=60:1	Stabilized ≥30 min; simulated brine; high-salinity and multicomponent tests also reported	[49]
Li^+/Na^+, Li^+/K^+, Li^+/Mg^{2+}, Li^+/Ca^{2+}	Rigid nonporous crystalline NCM-1 membrane; submillimetre bulk thickness (0.6 mm variant also tested); area NR	Single salts or five-cation mixture, 0.1 M each; natural low-grade brine also tested	Electrically driven; 3 V; HCl receiver	Single-salt Li^+ flux 575.8 mmol m^{-2} h^{-1}; approximately halved in mixed salts	Flux-normalized separation factor; mixed-feed Li/Na 1325.2, Li/K 13695.9, Li/Mg 25283.7, Li/Ca 14048.2	13 cycles with natural brine; post-operation fissures and Na^+ insertion observed	[60]
Na^+/Mg^{2+} and Cl^-/SO_4^{2-}	Oriented COF-170/PAN composite; COF layer ≈170 nm; area NR	Ternary NaCl/Na_2SO_4/$MgCl_2$, 0.1 or 1 M each	Concentration-gradient diffusion; −1 V also applied	NaCl flux ≈90 mmol m^{-2} h^{-1} in 0.1 M single-salt test; total flux increased ≈6-fold at −1 V	Relative ion-flux ratio; at 0.1 M ternary feed Cl/SO_4=64 and Na/Mg=39; at 1 M, 113 and 45	30 min ternary test; 3 h artificial-seawater test; simulated feeds	[38]
Cl^-/SO_4^{2-} heterovalent anions	APV-crosslinked GO laminate; channel ≈7 Å; thickness and area NR	0.1 M NaCl/Na_2SO_4 mixture; flow 20 mL min^{-1}	Continuous-flow electrodialysis; 6 mA cm^{-2}	Cl^- transport rate 2.74 mol m^{-2} h^{-1}	S=(JCl/CCl)/(JSO4/CSO4); Cl/SO_4=125	108 h continuous test; 10-cycle test; simulated mixed feed	[37]
Li^+/Mg^{2+} heterovalent cations	COF scaffold gate–lane composite NF membrane; thickness and area NR	Binary salt with Mg/Li mass ratio 50; concentration, pH and temperature NR	Pressure-driven nanofiltration	Permeance 11.5 L m^{-2} h^{-1} bar^{-1}	True selectivity 231.9; ideal selectivity 80.5; Li^+ enrichment 120.2%	Duration NR; simulated high-Mg/Li brine	[40]
Cu^{2+}/Ni^{2+}, Zn^{2+}, Co^{2+}, Mg^{2+} homovalent divalent	$(PDMAA/PAH)_{3.5}$ ultrathin coordinating polymer membrane; thickness and area NR	0.1 M $CuCl_2$ + 0.1 M competing salt; pH 3.6; 25±0.1 °C	Concentration-gradient diffusion; DI-water receiver	Cu^{2+} flux ≈(17–20)×10^{-9} mol cm^{-2} min^{-1}; competing-ion flux decreases with binding-energy contrast	Multisalt $S_i(Cu/M_j)$; Cu/Ni=26.0, Cu/Zn=0.84, Cu/Co=17.9, Cu/Mg=52.1	Steady multisalt tests; simulated binary feeds	[53]
K^+/Li^+ and Na^+/Li^+ homovalent monovalent	Randomly oriented sulfonated COF/AAO membrane; COF layer 6–8 μm; area NR	KCl+LiCl or NaCl+LiCl, 0.1 M each; 0.1 mM–0.1 M and seawater also tested	Passive diffusion; DI-water receiver	K^+ or Na^+ permeated continuously; Li^+ remained below detection over 60 min; permeation decreased with thickness	Permeation-rate ratio; finite selectivity not assigned because Li^+ was below detection	60 min; five-cation mixtures and seawater validation	[52]

Note: Selectivity definitions and testing conditions are specified for each entry. NR, not reported.

For Peer Review Only

3.3 Selective Adsorption and Ion Capture

The fundamental distinction between selective adsorption and membrane transport is that the target ion need not continuously traverse the material. Instead, it is preferentially transferred into the solid phase and subsequently forms a recoverable product stream through desorption or regeneration. Adsorption performance should therefore not be judged solely by single-component equilibrium capacity, but by the actual capture ability of the material under competitive feed conditions and by whether enrichment in the solid phase can be further translated into effective recovery.[61–66]

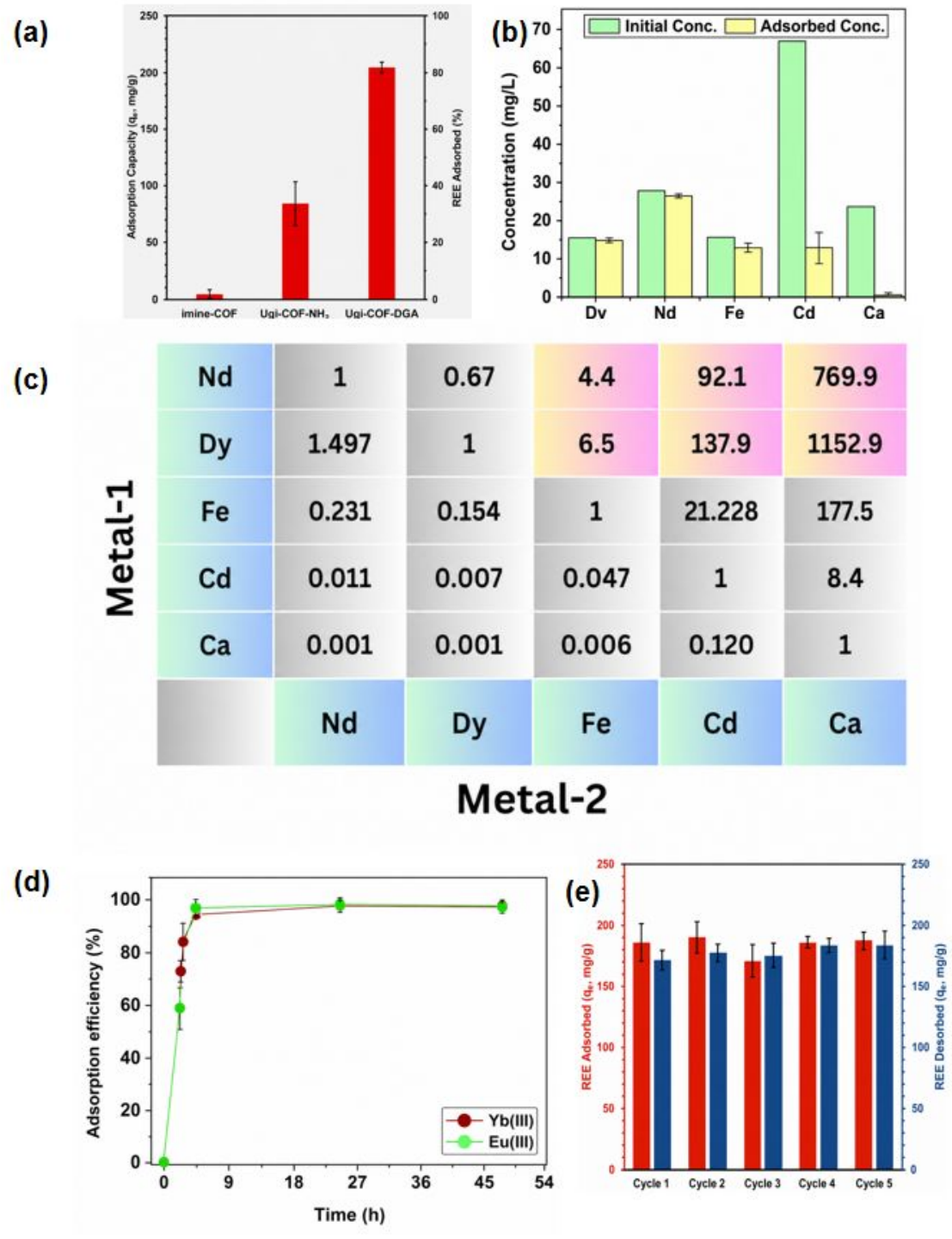


Figure 9 **Selective ion capture from site construction to competitive separation and reversible release.**

(a) Nd^{3+} adsorption capacities of different COFs, showing the enhanced rare-earth capture enabled by DGA recognition sites. Adapted from Ref. [61]. (b,c) Initial and adsorbed metal concentrations and pairwise separation factors of CA-BNMG-1 composite beads in simulated mine wastewater, demonstrating preferential capture of Dy^{3+} and Nd^{3+} in the presence of abundant competing ions. Adapted from Ref. [62]. (d) Time-dependent adsorption efficiencies for Yb^{3+} and Eu^{3+}, reflecting the kinetic accessibility of selective sites in the shaped beads. Adapted from Ref. [62]. (e) The capacity variation of Ugi-COF-DGA during five Nd^{3+} adsorption-desorption cycles demonstrates that the captured ions can be released, providing preliminary evidence of site reversibility. Adapted from Ref. [61].

3.3.1 Equilibrium Affinity and Site Utilization

In nanoporous adsorbents, specific surface area and functional-group density are commonly the first parameters used to explain increases in capacity, but neither has a simple positive correlation with selectivity. A large volume of nonselective pores may increase total adsorption without necessarily increasing the partition advantage of the target ion over competing components. Conversely, a small number of geometrically and chemically well-defined sites may contribute little to the total capacity while determining final product purity. High capacity and high selectivity therefore often originate from different types of sites and must be distinguished.

The COF system shown in Figure 9a illustrates this distinction.[61] For otherwise similar frameworks, introduction of diglycolamide coordination units produces a substantially higher Nd^{3+} adsorption capacity than in the imine and aminated control materials. The key is not simply an increase in oxygen-containing groups, but the creation of a local chemical environment better suited to rare-earth coordination, converting otherwise poorly utilized intrapore space into accessible recognition sites. Similar strategies are widely used with macrocyclic receptors, ion-imprinted cavities, and preorganized multidentate ligands, which amplify small free-energy differences among ions by constraining coordination geometry and the local solvation state.

The presence of a site, however, does not mean that the site can be effectively utilized. Excessive functionalization may simultaneously reduce pore volume and pore-entry size, thereby limiting access to internal sites. Adsorbed ions may also obstruct subsequent mass-transfer pathways, causing the theoretical site density to become increasingly decoupled from actual utilization. Site design should therefore report not only functional-group content but also the fraction of accessible sites, utilization per unit time, and how utilization changes with ion loading.

For biochars and mineral composite adsorbents, the problem is more complex.[18,48,66] Apparent removal may simultaneously arise from surface complexation, ion exchange, dissolution–reprecipitation of mineral phases, and micropore retention, and some heavy metals may enter the solid phase as precipitates or reduction products. Assigning the entire concentration difference between the liquid and solid phases to "selective adsorption" would overestimate the contribution of material recognition sites. Reliable interpretation requires speciation analysis, mass balance, and post-adsorption solid-state characterization to distinguish reversible binding, structural ion exchange, and irreversible phase transformation.

3.3.2 Competitive Occupancy and Working Capacity

Selective sites never operate in isolation in a practical feed. Even when high-abundance competing ions have weaker affinity for the material, mass action may cause them to occupy large numbers of nonselective regions. The target ion must progressively displace them through more favourable coordination or desolvation. Multicomponent adsorption is therefore not a simple superposition of several single-component isotherms, but an occupancy process that continuously reorganizes with time and site saturation.

Figures 9b and 9c show that reporting the separation factor alone is insufficient for evaluating competitive capture.[62] CA-BNMG-1 composite beads retain high adsorption of Dy^{3+} and Nd^{3+} in simulated mining wastewater, while solid-phase enrichment of high-concentration Cd^{2+} and Ca^{2+} is markedly weaker. Pairwise separation factors further indicate a substantial preference for rare-earth ions over common competing metals. The magnitude of the separation factor, however, must be interpreted together with the absolute amount captured. If competing-ion adsorption approaches zero but target-ion uptake is also very low, an extremely high ratio does not mean that the material has sufficient treatment capacity. By contrast, a material with a moderate separation factor but stable working capacity under highly competitive conditions may offer greater process value.

Competition does not necessarily reduce selectivity. Weakly bound ions may initially occupy external surfaces or low-energy sites and then be progressively displaced by target ions. Certain coexisting ions may also change the surface potential, coordination form of the target ion, or intrapore water structure, thereby increasing target-ion partitioning. Competitive adsorption therefore depends on concentration ratio, binding sequence, and displacement kinetics and cannot be predicted solely from a static ranking of binding energies. The same material may even exhibit different selectivity sequences in short- and long-duration tests: early data are governed by external-surface mass transfer, whereas later behaviour gradually shifts towards deep-pore diffusion and site displacement.

This distinction also reveals the difference between "maximum capacity" and "working capacity".[43,62–66] Maximum equilibrium capacity describes the total amount accommodated by a material at high concentration and after sufficient equilibration. Competitive working capacity represents the fraction actually utilized when the target ion is at low abundance and competing ions are present in large excess. For continuous treatment, breakthrough capacity is closer to practical performance than either quantity because it is directly constrained by the width of the mass-transfer zone, feed velocity, and the allowable leakage concentration. Existing adsorption studies still overemphasize maximum capacity in single-salt systems, while mixed-salt working capacity and breakthrough behaviour remain comparatively underreported, creating one of the most common sources of superficial superiority in comparisons among materials.

3.3.3 Intrapore Mass Transfer and Shaping Effects

Even if the target ion thermodynamically favours entry into a material, the sites may not be fully utilized within a finite time. To reach an intrapore recognition site from the bulk solution, an ion must undergo external-film mass transfer, pore-entry partitioning, intrapore diffusion, and local ligand exchange. High resistance at any one of these steps can confine high affinity to the local surface rather than translating it into overall working capacity.

In Figure 9d, the adsorption of Yb^{3+} and Eu^{3+} by shaped MOF particles increases rapidly at first and then gradually reaches a plateau.[62] This result indicates that polymer coating does not completely block access of rare-earth ions to internal sites, although several hours are still required to approach equilibrium. Material shaping therefore has a characteristic dual effect. On the one hand, macroscopic particles facilitate recovery, packing, and flow operation. On the other hand, the binder phase and longer diffusion pathways increase internal mass-transfer resistance. Rapid adsorption and high capacity observed in powder materials are generally redistributed after granulation, membrane formation, or fixed-bed packing: part of the capacity may be lost through site occlusion, while another part becomes more usable because of improved structural stability and fluid contact.

A high site density may also cause preferential surface occupancy, pore-entry crowding, and underutilization of deep sites. In materials containing multidentate ligands or ion-imprinted cavities, ligand exchange may itself become rate limiting.

For Review Only

Adsorption time should therefore be shortened by optimizing pore hierarchy, particle size, and the spatial distribution of sites, while perturbations in particle size, flow rate, and temperature should be used to distinguish the relative contributions of external mass transfer, intrapore diffusion, and ligand exchange.

Biochar systems further illustrate the strong influence of target-ion speciation on mass transfer.[66] Natural organic matter may form large complexes with metal ions, reducing the probability that they enter micropores. Electrolytes and multivalent cations may in turn alter the aggregation state of organic matter through charge screening or bridging, causing apparent adsorption to vary by orders of magnitude among different water matrices. "Pore-size matching" therefore refers not only to a comparison between material pore size and the dimensions of bare or hydrated ions, but also to the actual complexes, ion pairs, and colloidal forms present in the feed.

Analysis of adsorption kinetics should likewise not stop at fitting empirical models. Pseudo-first-order or pseudo-second-order equations can describe the time dependence of concentration but cannot by themselves establish reaction control or a chemisorption mechanism. More informative approaches to identifying the actual limiting step include varying particle size, stirring rate, temperature, and flow rate, or using time-resolved characterization to track the evolution of solution species and solid-state sites. For continuous-flow systems, the shape of the breakthrough curve often provides more information than the equilibration time in a batch test because it simultaneously reflects site affinity, intrapore diffusion, and movement of the mass-transfer zone.[62,64,65]

3.3.4 Release and Reversible Capture

The adsorption process does not end when capacity reaches a plateau. Enrichment in the solid phase can be translated into a recoverable product stream only if the target ion can be selectively, concentratedly, and controllably released from the material. Recognition sites therefore need to operate within an appropriate reversible-affinity window: sufficiently strong to resist competitive occupancy under feed conditions, but able to dissociate rapidly under regeneration conditions. Interactions that are too weak cannot establish selectivity, whereas excessively strong binding shifts the separation bottleneck from capture to desorption.

In Figure 9e, Ugi-COF-DGA retains similar uptake and release amounts over five Nd^{3+} adsorption–desorption cycles, indicating preliminary reversibility of its coordination sites.[61] The system, however, uses relatively concentrated nitric acid for elution. Near-complete desorption first establishes that Nd^{3+} can be released from the material, but does not by itself demonstrate that regeneration is mild, efficient, or low in resource consumption. Desorption efficiency should be reported together with eluent composition and concentration, liquid-to-solid ratio, elution volume, target-ion concentration in the eluate, and structural retention of the material after cycling.

Final desorption efficiency is also insufficient for evaluating resource-recovery value. A large volume of dilute eluate may release most of the target ion but negate the enrichment achieved during adsorption. High ionic strength or competitive ligands may simultaneously release coexisting components and reduce product purity. More process-relevant metrics include release rate, elution-peak width, enrichment factor, recovery purity, complete mass balance, and reagent consumption per unit amount recovered.[61–65] A system with high adsorption selectivity but producing a highly dilute product stream may have less practical value than a material with slightly lower selectivity that can release the target ion in concentrated form.

A small number of adsorption–desorption cycles can provide preliminary evidence of reversible release, but should not be used to establish long-term regeneration stability. Whether selective sites, pore structures, and material composition are continuously retained during cycling, and whether the chemical and energy inputs required to restore separation function increase with cycle number, are questions of operational stability and are discussed in Section 3.4.

Overall, the process performance of selective adsorption is jointly controlled by equilibrium partitioning, competitive occupancy, intrapore mass transfer, and reversible release. Equilibrium capacity has a clear separation and recovery significance only when the target ion can occupy effective sites in a complex feed, establish sufficient working capacity within a practical residence time, and be released as a product stream of reasonable concentration and purity.

For Review Only

Table 4. Quantitative performance of representative nanoporous adsorbents for competitive ion capture

Target/competing ions	Adsorbent and selective site	Feed, pH and temperature	Capacity or partition metric	Competitive selectivity/working performance	Kinetics and testing mode	Desorption, regeneration and limitation	Refs.
Nd^{3+}; REE capture	DGA-postfunctionalized Ugi-COF; multidentate diglycolic-acid sites	50 ppm $Nd(NO_3)_3$; 10 mg in 50 mL; pH ≈6; 25 °C	qe≈203 mg g^{-1} under the stated condition; Langmuir qmax≈656 mg g^{-1}	Predominantly single-component capacity; no real-feed competitive working capacity	20 h batch equilibration; rapid initial uptake	Desorption with 2.0 M HNO_3; uptake/release largely retained over five cycles; strong-acid demand remains a process burden	[61]
Nd^{3+}, Dy^{3+}, Yb^{3+}, Eu^{3+}; Cd^{2+}, Ca^{2+}, Fe^{3+} and others	CA-BNMG-1 MOF/cellulose-acetate macrobeads; imidazole-N sites	Simulated mine wastewater/e-waste leachate; pH 5; 25 °C	Yb^{3+} and Eu^{3+} adsorption efficiencies ≈95–100%; absolute uptake feed-dependent	In simulated mine water: Nd/Cd=92.1, Dy/Cd=137.9, Nd/Ca=769.9, Dy/Ca=1152.9	24 h batch tests; Yb/Eu approach equilibrium within hours	Mild acid elution; >95% uptake retained over cycles; Cu leaching <1%; fixed-bed evidence remains limited	[62]
Tb^{3+} and multiple REEs; broad non-REE background	Lanmodulin-functionalized magnetic nanoparticles; protein recognition sites	Synthetic competition tests, coal-fly-ash leachate and geothermal brine	Tb adsorption activity 6.01±0.11 μmol g^{-1}	REE selectivity retained against diverse non-REEs; 967-fold increase in REE purity	Fast batch uptake; magnetic recovery	>90% desorption; ≈95% activity retained after eight cycles; relatively low gravimetric capacity	[63]
Y^{3+}, Gd^{3+}, Dy^{3+}; K^{+}, Mn^{2+}, Ca^{2+}, Mg^{2+}	ZIF-8; imidazole-N and hydrolysis-assisted REE–O interactions	Real REE-mining wastewater; pH and temperature as reported	Kd: Y 4.02×10^4, Gd 7.8×10^4, Dy 6.8×10^4 mL g^{-1}	Competing-ion Kd only 239–396 mL g^{-1}, giving orders-of-magnitude partitioning advantage	Batch adsorption plus 7 h column test	>40% desorption of heavy REEs; >40% column recovery; recovery remains below what equilibrium partitioning alone suggests	[64]
Li^{+}; Na^{+} and other brine ions	P-PAA granulated LMO; hierarchical pores and PAA carboxyl groups facilitate Li^{+} transfer	Real Puguang gas-field brine with high Na salts and organic contaminants	Li^{+} capacity 12.9 mg g^{-1}; Kd=1391.3 mL g^{-1}	Li/Na separation factor 718; Li recovery ≈98.4–98.5% from real brine	Granular adsorption with kinetic and intraparticle-transport analysis	No obvious salt crystals/internal cracks after extended cyclic use; cumulative bed volumes and regenerant consumption need fuller reporting	[65]
Hg(II); Cl^{-}, NO_3^{-}, Ca^{2+}, Na^{+} and NOM	Wood-based SWP700 biochar; sulfur-containing intraparticle sites	Hg-contaminated water; NOM up to 46.2 mg L^{-1}; varied ionic backgrounds; 48 h	log Kd=0.8–4.4 in complex matrices, spanning >3 orders of magnitude	Not a conventional ion-pair selectivity metric; NOM limits pore access, whereas Cl^{-} and Ca^{2+} can restore capture through speciation and bridging	48 h batch tests; speciation modelling plus EXAFS	Desorption/reuse not reported; demonstrates that real-water chemistry can reshape apparent capture performance	[66]

Note: maximum equilibrium capacity, competitive working capacity, distribution coefficient and breakthrough capacity are physically distinct. Single-component qmax values should not be used to infer practical recovery without competitive-feed or continuous-flow evidence.

3.4 Operational Stability and Process Performance

Peak flux, selectivity, or adsorption capacity obtained by selective ion-separation materials in ideal feeds and short-duration tests does not automatically extend to continuous operation. In an actual process, the material must withstand high ionic strength, compositional fluctuations, foulant deposition, mechanical loading, and repeated cleaning or regeneration. The resulting reconstruction of pore structure, changes in interfacial charge, and deactivation of recognition sites may gradually erode the initially established selective advantage. Operational stability should therefore be understood as sustained retention of the origin of selectivity and its corresponding separation function under practical conditions, rather than as preservation of material appearance or a single performance metric.

Such functional retention involves several interconnected but nonequivalent levels. Chemical stability concerns whether the framework, polymer chains, metal nodes, or active phase undergo hydrolysis, dissolution, or leaching. Structural stability concerns changes in operando pore size, interlayer spacing, membrane–support interfaces, and particle morphology. Functional-site stability involves irreversible occupancy, drift in protonation state, ligand loss, and response fatigue. These changes must ultimately be evaluated through target-ion flux, competing-ion leakage, working capacity, product purity, and recovery.[43,67–75] Structural preservation is only a necessary condition for stable operation; process-level stability can be discussed only when both separation function and process output are retained.

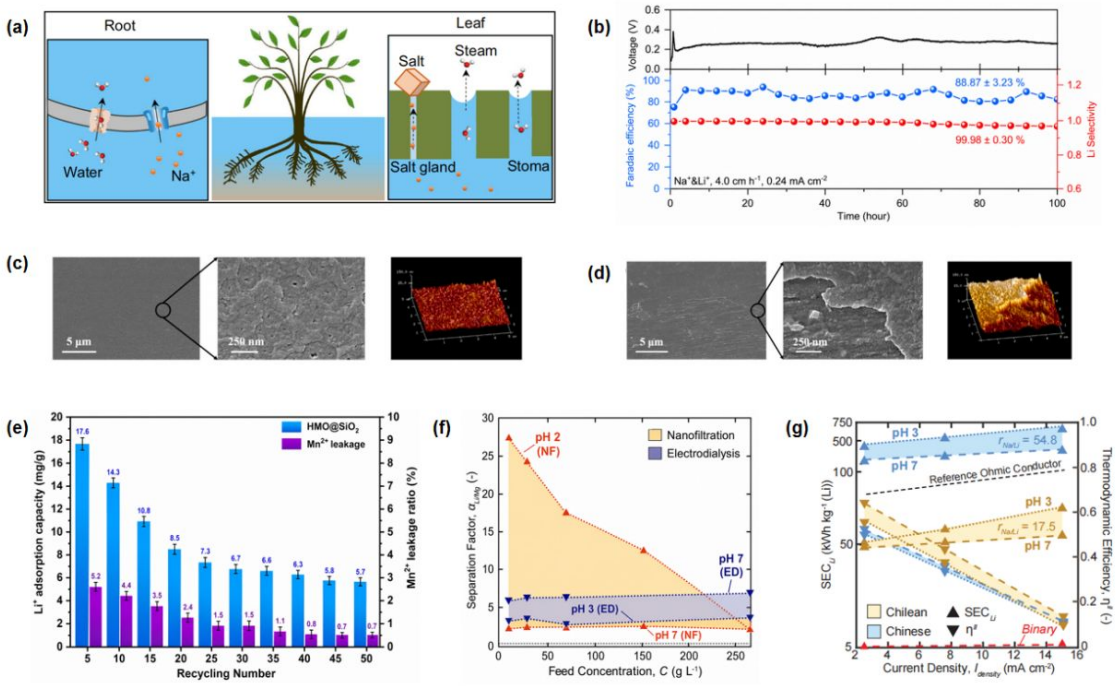


Figure 10 **Multilevel assessment of operational stability and process performance in selective ion separation.**
(a) A mangrove-inspired root–leaf transport architecture coupling selective ion exclusion at the root with evaporation-driven water transport at the leaf, illustrating the translation of material function into an integrated separation process. Adapted from Ref. [67]. (b) Operating voltage, Faradaic efficiency, and Li^+ selectivity during 100 h of continuous lithium extraction from a mixed Na^+/Li^+ feed, showing that operational stability requires the simultaneous retention of driving conditions, transport efficiency, and selectivity. Adapted from Ref. [68]. (c,d) FESEM and AFM images of CEM 0 and CEM 409 membranes, revealing surface roughening, delamination, and defect development under hypersaline-brine exposure and linking performance drift to structural degradation. Adapted from Ref. [69]. (e) The Li^+ working capacity and Mn^{2+} dissolution rate of HMO@SiO_2 over 50 adsorption-desorption cycles indicate that the apparent cycle plateau may be accompanied by initial capacity loss and active phase depletion. Adapted from Ref. [70]. (f) Li^+/Mg^{2+} separation factors of nanofiltration and electrodialysis as functions of feed concentration and pH, illustrating the coupled effects of ionic strength, interfacial charge, and operating mode on apparent selectivity. Adapted from Ref. [71]. (g) Specific energy consumption per unit Li recovered (SECLi) and second-law efficiency (ηII) as functions of current density for Chilean and Chinese salt-lake brines, revealing the energetic penalty associated with maintaining ion selectivity under hypersaline conditions. Adapted from Ref. [72].

3.4.1 From Operating Time to Cumulative Load

Existing studies often summarize stability using operating duration or cycle number, but neither metric represents the actual treatment load borne by the material. The same 100 h of operation may correspond to cumulative transported amounts differing by several orders of magnitude because of differences in membrane area, feed concentration, flow rate, and target-ion flux. Similarly, tens of cycles in low-concentration batch adsorption cannot be equated with operation of a fixed bed treating tens of bed volumes near breakthrough. Stability is therefore better described jointly by time and cumulative load, including treated volume per unit area, cumulative target-ion transport, number of bed volumes, regeneration count, and pressure or electric-field history.

Figure 10b shows the synchronous evolution of operating voltage, Faradaic efficiency, and Li^+ selectivity during continuous lithium extraction.[68] The value of this result lies not merely in operation for 100 h, but in the simultaneous tracking of several mutually constraining metrics. Voltage reflects device resistance and driving requirements, Faradaic efficiency measures charge utilization, and selectivity describes relative transport of the target and competing ions. Even when total current or target-ion flux remains stable, a gradual increase in competing-ion leakage indicates deterioration of separation function. Conversely, preservation of selectivity may be achieved at the cost of continuously increasing voltage and energy consumption. “Stability” should therefore not mean that an individual curve

remains approximately horizontal, but that the relationships among critical performance metrics do not undergo substantive drift within a specified load range.

Different testing modes also provide markedly different levels of stability evidence.[43,68–70] Static diffusion cells and batch adsorption are suitable for excluding rapid dissolution or initial deactivation of the material, but poorly reproduce concentration polarization, propagation of the mass-transfer zone, foulant accumulation, and local precipitation in continuous processes. Continuous-flow membrane cells, fixed beds, and cyclic electrochemical devices reveal performance evolution more realistically, but their effective area, flow-channel geometry, loading, and operating boundaries must still be specified. Long-duration laboratory operation can establish durability under a particular set of conditions, but cannot be directly extrapolated to module lifetime or replace validation using real feeds and enlarged systems.

3.4.2 Complex Feeds and Selectivity Drift

High-salinity backgrounds, organic ligands, colloids, and scaling precursors in practical feeds simultaneously alter target-species speciation, interfacial state, and mass-transfer resistance, causing selectivity to be reordered during operation.[71] The challenge posed by complex feeds is therefore not merely the presence of more competing ions, but also the temporal evolution of material state and the dominant transport mechanism.

Increasing ionic strength first compresses the electrical double layer and weakens Donnan exclusion, causing heterovalent-ion separation that relies on fixed charge to progressively lose its advantage. In Figure 10f, the nanofiltration membrane achieves a high Li^+/Mg^{2+} separation factor at low pH and low feed concentration, but selectivity decreases substantially as salt concentration increases. Electrodialysis, by contrast, maintains a relatively stable separation factor over a broader concentration range. This difference does not imply that electrodialysis is intrinsically unaffected by high salinity; rather, it shows that different processes depend differently on interfacial charge, transference number, and external driving force. Material performance cannot therefore be compared independently of feed concentration and mode of operation. An electrostatic mechanism dominant in a dilute system may be reconstructed by charge screening, ion correlations, and concentration polarization at high salinity.

The influence of pH likewise extends beyond regulation of surface charge.[72] It also changes metal-ion hydrolysis, complexation, and precipitation equilibria, as well as the protonation state of coordination sites. An increase in removal observed in some systems may arise because the target ion forms an insoluble phase or a complex that is more readily rejected, rather than because the affinity of a recognition site genuinely increases. Such speciation changes are particularly likely to confound selective adsorption with phase transformation for rare-earth, transition-metal, and uranyl ions. Complex-feed tests therefore need to combine solution speciation with characterization of solid products. Otherwise, apparent “resistance to pH fluctuations” may simply mean that similar endpoint concentrations are maintained through different chemical processes rather than through preservation of the same separation mechanism.

Organic matter and colloids exert more dualistic effects.[66,69] On the one hand, they may cover pore entrances or functional sites and reduce flux and working capacity. On the other hand, the resulting fouling layer may itself introduce new charge- and size-sieving effects, more strongly obstructing competing ions and temporarily increasing apparent selectivity. Such an apparent “performance improvement” does not indicate a superior material state, but may mean that the original selective layer has been replaced by an uncontrolled secondary mass-transfer layer.[75] Flux decline, selectivity increase, or capacity retention in a complex feed therefore cannot be interpreted in isolation, but must be assessed together with foulant-layer composition, reversible cleanability, and recovery of selectivity after cleaning.

3.4.3 Structural Degradation and Post-Operation Evidence

Performance degradation during operation generally arises from changes occurring at multiple scales. Lamellar membranes may undergo swelling, compaction, or nanosheet misalignment; polyelectrolyte selective layers may reorganize under high-salinity and multivalent-ion conditions; and delamination or nonselective bypass pathways may develop at the interface between a selective layer and its support. Adsorbent particles may experience abrasion, pulverization, pore blockage, and dissolution of active components. These changes do not necessarily occur synchronously and may not all be visible by conventional dry-state characterization.

The pronounced roughening, delamination, and defect formation observed on the membrane surfaces in Figures 10c and 10d under high-salinity conditions[69] demonstrate that long-term performance changes can be directly traced to structural degradation of the selective layer. The converse, however, is not valid: the absence of visible cracks does not prove preservation of transport pathways. Minor swelling of subnanometre pores, a decrease in fixed-charge density, or changes in local wettability may substantially alter ion partitioning while leaving the macroscopic morphology largely unchanged. For isovalent-ion separation that depends on precise pore size and coordination environments, such subtle changes may be more consequential than complete collapse of the framework.

Functional-site deactivation may also precede structural failure. Once high-affinity sites are irreversibly occupied by competing ions or impurities, total adsorption capacity may still be maintained by a large population of nonselective sites; capacity retention therefore does not necessarily mean selectivity retention.[9] A similar problem exists in membrane systems: total ionic conductivity may change only slightly even though the local coordination sites originally responsible for the target-ion advantage have undergone hydrolysis, screening, or reorganization. Stability evaluation should therefore target the origin of selectivity itself rather than merely determine whether the material remains porous or retains ion-exchange capacity.

The purpose of post-operation characterization is to establish this causal relationship. PXRD can determine whether long-range structural order is retained, but cannot prove that pore-entry dimensions and site chemistry remain stable. SEM can identify macroscopic defects, but provides little information on wet-state swelling or local coordination changes. More persuasive evidence should correlate changes in wet-state structure, surface charge, pore-size distribution, component leaching, residual occupying ions, and functional-group state before and after operation with performance drift. Characterization methods should be selected according to the hypothesized failure mechanism rather than applied as a routine collection of spectra.

3.4.4 Regeneration and Recovery of Function

Regeneration here refers not merely to eluting the target ion from the material, but to whether the material can recover and continuously retain its original separation function after desorption or cleaning. Section 3.3 considers whether a single capture–release process can be closed; this section examines whether the selective sites, mass-transfer pathways, and material

structure continue to operate in the same manner after the process is repeated. A high single-cycle desorption efficiency therefore proves only that the ion can be released, not that the material possesses long-term regeneration stability.

Regeneration conditions themselves may become an important source of material degradation. Strong acids or bases promote dissociation of target ions but may also cause ligand hydrolysis, metal-node leaching, and dissolution of inorganic active phases. Elution using high salt concentrations or competing ligands may be milder, but may leave new counterbalancing ions within the pores and alter the partition sequence in the next cycle. For membrane materials, chemical cleaning can remove a fouling layer but may simultaneously change the charge density, wetting state, and interfacial integrity of the selective layer. Regeneration is therefore not a neutral recovery step, but an additional chemical and structural perturbation experienced by the material in every cycle.

In Figure 10e, the Li^+ adsorption capacity of HMO@SiO_2 decreases rapidly during the initial cycles and then approaches a lower plateau, while Mn^{2+} continues to leach.[70] Such a result cannot simply be summarized as "the material remains usable after 50 cycles". The later plateau may indicate that the more soluble or highly active fraction was consumed during the early cycles, leaving the remaining material in a new, lower-performance steady state. A more meaningful analysis should quantify the working-capacity and selectivity losses between the first cycle and the steady-state regime, and identify the origin of performance decay through leaching of active components, mass loss, and post-operation structural changes.

Performance metrics after regeneration should directly correspond to the original source of selectivity. Adsorbents should report competitive working capacity, retention of target/competing-ion selectivity, loss of active components, and eluent consumption per unit amount recovered. Membrane materials should simultaneously measure target-ion flux, competing-ion leakage, selectivity, and structural changes after cleaning. Dynamic-gating materials should track switching amplitude, response time, hysteresis, and baseline drift. Separation function can be considered recovered only when these mechanism-relevant metrics are restored.[61–65]

The objective of regeneration is therefore not to return the system completely to its initial state after every cycle, but to keep it within a functional window that satisfies requirements for product purity, recovery, and productivity at acceptable material, chemical, and energy inputs. Evaluation should accordingly shift from cycle count to the decay of selectivity with cumulative load, while simultaneously quantifying the reagent and energy costs required to restore separation function.

3.4.5 Module Scale-Up and Process Boundaries

When a material is transferred from a small membrane coupon or powder to a continuous device, the factors controlling separation change. The biomimetic root–leaf architecture shown in Figure 10a extends local selective channels into a process coupling evaporation, transport, and salt management.[67] Such integrated designs can use spatial division of function to reduce the burden on a single separation layer, but also introduce new stability boundaries, including salt crystallization at the evaporation interface, ion backflow between functional regions, blockage of capillary channels, and unequal ageing rates among components. Conceptual process integration is genuinely superior to a single material unit only when these interfaces can operate cooperatively over the long term.

As membrane area increases, the probability of local defects increases, and a small number of bypass pathways may dominate competing-ion transport across the entire module. Velocity distributions and concentration polarization within the flow channel also invalidate the uniform mass-transfer conditions of laboratory membrane coupons. Fixed-bed scale-up faces nonuniform packing, channeling, particle compaction, and increased pressure drop.[43,75] Scale-up is therefore not a linear extrapolation of flux per unit area or capacity per unit mass, but a new problem involving coupled structure and fluid flow. Whether the material retains selectivity in a module must be evaluated in terms of effective area, flow distribution, stage recovery, and product composition.

Process stability is further constrained by the energy and material inputs required to maintain separation performance.[71] Figures 10f and 10g jointly reveal the intrinsic coupling between selectivity and energy efficiency under high-salinity conditions. As feed concentration increases, compression of the electrical double layer and weakening of Donnan exclusion cause the Li^+/Mg^{2+} separation factor of nanofiltration to decrease continuously. Electrodialysis can partly maintain differences in ion migration by increasing current density, but this increases the specific energy consumption per unit Li recovered and correspondingly decreases second-law efficiency, with the trade-off strongly dependent on brine composition.[72] Compensating for declining material selectivity by increasing the external driving force therefore does not eliminate the separation limitation, but may simply shift the bottleneck from intramembrane transport to system-level energy consumption. Operational stability should consequently consider not only whether selectivity is retained, but also whether the marginal energy required to maintain target purity and recovery continues to rise with feed concentration and operating load.

The endpoint of operational evaluation should therefore extend beyond the post-membrane solution concentration or ion loading on an adsorbent to include product purity, target-ion recovery, enrichment factor, regeneration-liquid volume, and net energy consumption per unit product. Pretreatment, pumping, cleaning, regeneration, concentration of eluates, and waste-liquid treatment all form part of the actual system boundary.[73] A material-level performance advantage is translated into a process advantage only when high selectivity produces a stable product stream at module scale and the energy, chemicals, and material replenishment required to maintain that state remain within a reasonable range.

For acidic battery leachates, the positively charged PA-TAG polyamide membrane expands ion-transport channels and enhances rejection of divalent cations, achieving a relative volumetric lithium recovery of 48.2% from a simulated feed. After two-stage nanofiltration, the Li^+/M^{2+} mass ratio in the second-stage permeate reaches 53.35, 445 times that of the feed.[76] This case demonstrates that process value depends not only on the rejection or separation factor of a single membrane stage, but also on whether the cascade configuration can translate differences in ion transport into an improved product-stream composition.

Overall, module scale-up places material selectivity under the combined constraints of flow-field distribution, defect statistics, energy consumption, and material circulation.[74] Process validation should centre on a stable product stream and simultaneously report product purity, target-ion recovery, productivity, cumulative treatment load, and energy and chemical inputs per unit product. Together, these metrics define the boundary within which material-level performance is converted into engineering process value.

For Review Only

Table 5. Operational stability and process-level validation of representative selective ion-separation systems

System and configuration	Feed and scale information	Operation/load	Performance retention or drift	Regeneration/fouling/post-operation evidence	Product and energy metrics	Evidence boundary	Refs.
PEI/PS-DVB monovalent-selective ion-exchange membrane	Real Llullaillaco salt-lake brine; TDS up to 409 g L^{-1}; membrane area NR	Exposure/operation up to 30 d	K^+/Mg^{2+} permselectivity decreased from 16.60 to 5.67	FESEM/AFM showed roughening, delamination and defects; charge functionality declined as ions disrupted PEI–PS-DVB ionic crosslinks	Product purity and energy not reported	High-value failure analysis, but not a complete industrial module test	[69]
Redox-couple electrodialysis (RCE) for continuous Li extraction	Li/Na or Li/K brine; linear flow 4.0 cm h^{-1}; current density 0.24 mA cm^{-2}	>100 h continuous operation; ≈0.25 V	Faradaic efficiency 88.87%; Li selectivity 0.9954 (≈99.54%)	Voltage and efficiency monitored over time; limited post-operation structural evidence	Specific energy 1.1 kWh $kgLi^{-1}$	Laboratory continuous device; effective area and real-brine load require scale-up validation	[68]
LSTH ceramic-membrane redox-mediated electrodialysis	Simulated Atacama, Taijinar and Bonneville brines plus seawater; area NR	50 h continuous simulated-seawater test; 5 V	Extraction rate retained 83% of its initial value; charge efficiency ≈60%; product Li purity >99%	Rate loss mainly attributed to declining feed Li concentration; limited structural-aging evidence	7–320 mmol m^{-2} h^{-1}; 0.14–0.34 kWh mol^{-1} depending on feed	Broad simulated resources, but real-seawater and long-term ceramic-interface validation remain needed	[73]
Rigid crystalline NCM-1 membrane for direct lithium extraction	Natural low-grade brine with large excesses of Na^+, K^+, Mg^{2+} and Ca^{2+}	Electrically driven; 13 repeated cycles	Li^+ flux 128–250 mmol m^{-2} h^{-1}; high separation factors retained across cycles	Feed-facing side developed fissures; XRD indicated Na^+ insertion associated with $NaGe_2(PO_4)_3$	Energy per unit Li not reported; direct extraction claimed within <10 h	Real-brine and post-operation evidence reveal the structural-lifetime risk of brittle inorganic membranes	[60]
Rigidly confined APV@GO anion-selective membrane	0.1 M $NaCl/Na_2SO_4$; 20 mL min^{-1}	108 h continuous-flow ED at 6 mA cm^{-2}; separate 10-cycle test	Cl^- flux 2.74 mol m^{-2} h^{-1} and Cl/SO_4 selectivity 125; APV@GO retained performance, whereas pristine GO retained only 26% selectivity after 10 cycles	Retention linked to swelling-resistant channels; quantitative post-operation chemistry remains limited	Product purity and energy not reported	Strong continuous-flow evidence, but still based on a simplified binary feed	[37]
Millimetre HMO@SiO_2/alginate beads; continuous-flow adsorption–desorption	Simulated Da Qaidam brine: Li 330.6, Na 11882.5, K 11737.5, Ca 9613.3, Mg 18825 mg L^{-1}	50 continuous-flow adsorption/acid-desorption cycles	Li capacity fell from 17.6 to a stable ≈6.22 mg g^{-1}; later Mn dissolution averaged 1.26% per cycle	Capacity and Mn dissolution declined together over the first 25 cycles, consistent with acid-induced spinel damage; SiO_2 reduced acid dissolution	Energy and eluate-concentration costs not reported	Many cycles were demonstrated, but the large early capacity loss precludes an unqualified claim of stability	[70]
λ-MnO_2/Purolite C100 composite cation-selective membrane in ED	Simulated brine containing 1% Li; membrane area and long-term duration NR	Electrodialysis process test	Li recovery 44.5%; current efficiency 57.9%	Limited cyclic, fouling and post-operation evidence	Energy consumption 0.185 kWh mol^{-1}	Useful process-level recovery/energy data, but insufficient for long-term stability claims	[74]

Note: The "evidence boundary" column defines the scope supported by the reported tests and should not be interpreted as certification of industrial stability.

4. From Mechanistic Inference to Verifiable Design

The preceding performance analysis shows that similar fluxes, rejection values, or separation factors may correspond to different controlling steps and that endpoint performance alone cannot provide reliable mechanistic attribution.[42–44] This section therefore turns to verifiable design and discusses how operando characterization, multiscale simulation, and data-driven methods can establish testable links among microscopic states, transport processes, and macroscopic performance.

The three approaches play complementary roles. Operando characterization determines wet-state structures, solvation states, site occupancy, and local concentrations under actual feeds and driving forces. Multiscale simulation converts these states into free-energy, diffusion, and multicomponent-transport parameters and connects them to membrane, fixed-bed, and device scales. Data-driven methods integrate material structures, operating conditions, and evidence quality to identify transferable relationships, quantify predictive uncertainty, and guide subsequent experiments.[77–81] This section is therefore organized around identification of operando variables, establishment of cross-scale transfer relationships, and validation of model extrapolation, forming a feedback loop of "mechanistic hypothesis–operando observation–model testing–data updating–material design".

4.1 Operando Characterization

The central task of operando characterization is to synchronously measure the wet-state pore structure, ion solvation, site occupancy, local concentration field, and separation performance under actual feed, driving-force, and flow boundaries.[77,78] The objective is not simply to add more characterization dimensions, but to provide mutually independent experimental constraints on competing mechanisms and to determine which state variables and transport steps generate selectivity.

4.1.1 Operando Pore Structure and Effective Transport Pathways

To validate the operando effective pore aperture proposed in Section 2.1, the channel structure must be measured directly in the presence of solvent filling, ion occupancy, and the actual driving force.[9,77] The objective is no longer merely to demonstrate that a material swells or reconstructs, but to determine where the structural change occurs, its magnitude and timescale, and whether it corresponds to synchronously measured changes in flux and selectivity.

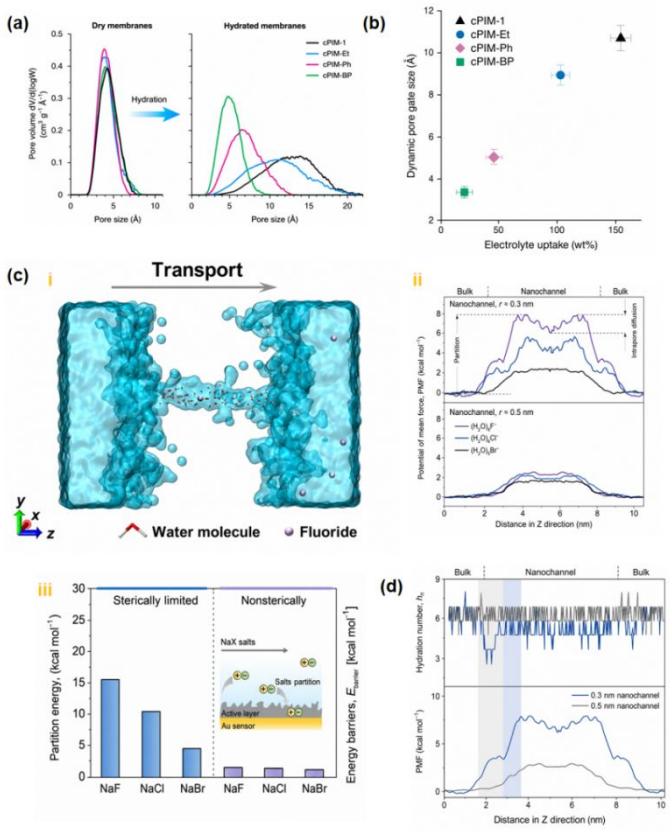


Figure 11 **Hydrated pore structure and ion dehydration jointly regulate transport through subnanometre channels.**
(a) Pore-size distributions of cPIM membranes in the dry and hydrated states, showing pronounced and chemistry-dependent restructuring upon hydration. Adapted from Ref. [9]. (b) Dynamic pore-gate size as a function of electrolyte uptake, demonstrating that the transport-limiting aperture cannot be inferred directly from the average dry-state pore size. Adapted from Ref. [9]. (c) Simulated water-filled polyamide nanochannels, together with the potentials of mean force and partition energies for hydrated F^-, Cl^- and Br^- transport through channels of approximately 0.3 and 0.5 nm. Strong confinement amplifies ion-dependent entry penalties, whereas these differences diminish in the wider channel. Adapted from Ref. [82]. (d) Hydration-number and free-energy profiles of F^- across the two channel sizes; the narrower channel induces more pronounced partial dehydration accompanied by a higher transport barrier. Adapted from Ref. [82].

The microporous polymer systems shown in Figures 11a and 11b illustrate this discrepancy. Different cPIM membranes exhibit similar pore-size distributions in the dry state but markedly different pore expansion and dynamic aperture sizes after hydration.[9] Increased electrolyte uptake does not simply correspond to enhanced transport. Excessive hydration enlarges percolated channels and weakens sieving, whereas insufficient hydration limits the formation of continuous aqueous pathways. The parameter more closely related to ion transport is the size and connectivity of local bottlenecks after hydration, rather than the dry-state mean pore size.

This understanding requires further differentiation among pore cavities, pore apertures, and percolated pathways. Cavities determine the local accommodation volume, apertures control the entry barrier between adjacent cavities, and percolated pathways determine whether long-range migration can persist.[9,77] These three structural features do not necessarily change synchronously in space. An unchanged mean interlayer spacing does not exclude contraction of local apertures or formation of a small number of bypass pathways; pronounced overall swelling does not mean that all transport pathways lose selectivity. For subnanometre separation, the tail of the structural distribution and local defects are often more consequential than the average structure.[9,77,83]

Operando structural analysis should therefore focus directly on effective transport pathways. In addition to wet-state pore size and interlayer spacing, the distribution of pore entrances, channel orientation, degree of percolation, and spatial location of structural changes should be examined. For responsive systems, it is further necessary to establish whether the structural response occurs at the entrance bottleneck or principal recognition region and whether its timescale is matched to ion migration. Demonstrating swelling, contraction, or conformational change alone is insufficient to support a selective-gating mechanism.[77,78]

4.1.2 Direct Evidence of Solvation and Coordination States

When an ion enters a subnanometre channel, its hydration shell generally undergoes continuous reorganization rather than an abrupt transition from a fully hydrated state to a bare ion.[5–7,82,84] Pore size, local electric field, and pore-wall chemistry jointly determine the extent of water removal, the lifetime of the coordination shell, and subsequent ion–pore-wall interactions.[82,84,85] Bulk hydrated radii and hydration free energies provide preliminary references but cannot fully describe the actual ion state under confinement.

Figures 11c and 11d show the relationship between hydration state and the free-energy pathway for anions entering polyamide nanochannels.[82] Narrower channels cause more pronounced partial desolvation and increase the free-energy costs of pore entry and intrapore migration. In wider channels, hydration-structure changes are weaker and differences in the barriers among anions decrease accordingly. Notably, water removal simultaneously changes effective charge screening and the distance over which the ion interacts with the pore wall. The consequences of desolvation are therefore not limited to a reduction in effective size, but also reconstruct subsequent electrostatic and short-range interactions.

This distinction is especially important when interpreting local spectroscopic and coordination data. A change in coordination number, a shift in a functional-group band, or intrapore ion enrichment establishes only that the local chemical environment has changed. A high intrapore concentration may reflect favourable partitioning or a long residence time; a strong coordination signal may represent a reversible transport intermediate or indicate that the ion is trapped at a high-affinity site.[24,79,82] Whether local binding is translated into steady-state migration must be assessed together with residence time, diffusion coefficient, and outlet-side release behaviour.[24,79,82,85]

For pH-sensitive or multicomponent systems, changes in solution speciation further complicate attribution. Ion hydrolysis, complexation, ion-pair formation, or local precipitation may all alter spectroscopic signals and solid-phase loading.[77,78,86,87] Without speciation analysis and a complete mass balance, a local coordination change may be mistaken for enhanced recognition by the material. Operando characterization must therefore resolve both ion state and site state and establish the temporal order in which they change.[77,78]

4.1.3 Local Concentration Fields and Transport Timescales

Steady-state flux and outlet concentration compress complex spatiotemporal processes into a single value. Interfacial enrichment, concentration polarization, transient occupancy, and propagation of a mass-transfer front may all be averaged out, causing different controlling steps to produce similar macroscopic outcomes. Time- and space-resolved measurements can recover information concealed by these global metrics.[88,89]

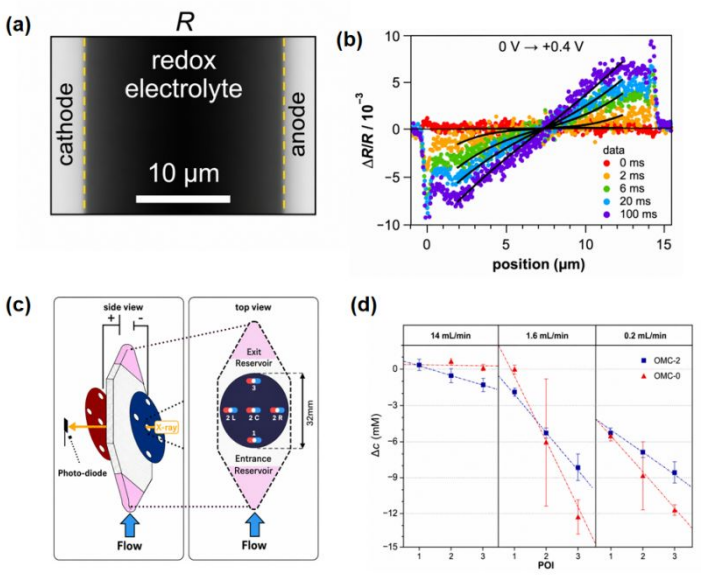


Figure 12 **Operando spatiotemporal mapping of local concentration fields during selective ion transport.**
(a) Microfluidic electrochemical channel and electrode configuration used for label-free optical imaging. Adapted from Ref. [88]. (b) Position-dependent reflectance changes at successive times following a potential step from 0 to +0.4 V, showing the millisecond-scale propagation of concentration gradients from the electrode interfaces into the electrolyte. Adapted from Ref. [88]. (c) Operando X-ray transmission cell and the measurement positions located near the inlet, centre and outlet. Adapted from Ref. [89]. (d) Final local concentration changes for two electrode materials at different flow rates, revealing pronounced axial heterogeneity and its dependence on hydrodynamic conditions. Adapted from Ref. [89].

The label-free optical imaging in Figures 12a and 12b records the evolution of ion concentration along a microfluidic channel after a potential step.[88] Concentration changes first appear near the electrodes and then propagate into the channel on the millisecond timescale, with different positions exhibiting different response amplitudes and characteristic times. Such data can distinguish interfacial response, bulk diffusion, and local accumulation, and can test whether a single diffusion model is sufficient to describe the observations. Endpoint current or average concentration, by contrast, provides only a global response and cannot locate the actual rate-limiting region.

In a flow device, the influence of local states on overall performance is even more pronounced. Operando X-ray transmission measurements in Figures 12c and 12d reveal substantial concentration differences among the inlet, centre, and outlet and show that these differences are jointly affected by flow rate and porous structure.[89] At lower flow rates, inadequate replenishment along the flow direction enlarges the axial concentration gradient, while different pore structures alter the extent of local counter-ion adsorption and release. Overall removal inferred from the outlet concentration may therefore simultaneously contain contributions from a rapid inlet response, intrapore mass-transfer limitation in the central region, and inadequate supply near the outlet.

Temporal sequence can also be used to test causality.[78,88,89] If structural changes precede selectivity drift, pore reconstruction may be a direct cause. If local ion accumulation appears first and structural changes follow, the latter are more likely to be induced by occupancy, charge accumulation, or local stress. For dynamic-gating materials, the response, migration, and recovery timescales must be measured separately. Structural differences between two steady states are insufficient to establish whether a material can switch rapidly enough under continuous feed fluctuations.

Site accessibility should also be understood within this dynamic framework. Endpoint occupancy cannot distinguish rapid enrichment at the external surface from gradual utilization of internal sites, nor can it establish whether high occupancy arises from favourable partitioning or slow dissociation. Pulse response, tracer exchange, breakthrough curves, and position-resolved concentration measurements can jointly constrain ion arrival, occupancy, displacement, and release,[77,78,88,89] thereby identifying which sites genuinely participate in effective separation.

4.1.4 Attribution Strength and Applicability Boundaries of Operando Evidence

In situ measurement generally refers to characterization of a material in a liquid phase or under an external field, although the conditions do not necessarily match those of the actual separation. Operando characterization requires the material state and separation performance to be recorded synchronously under actual feed, driving-force, and flow boundaries.[77,78] The distinction lies primarily in whether operating conditions are retained, whether structural and performance data are temporally correlated, and whether the measurements can distinguish competing mechanisms.

High-quality operando evidence must first preserve critical boundary conditions. Changes in feed composition, ion ratio, pH, pressure, current density, flow rate, or temperature may redefine the dominant transport step.[77,78] Substantially reducing salinity, eliminating flow, or changing the membrane-support configuration to accommodate a characterization cell may shift the observed system away from its actual working state. Corresponding structural and chemical signals should be acquired synchronously with target-ion flux, competing-ion leakage, or local concentration to avoid assembling data obtained from different specimens or operating stages into a single mechanistic chain.[78]

The characterization scale must also match the scale of the mechanism. An averaged scattering signal may fail to detect a small number of percolated defects, and surface-sensitive spectroscopy cannot represent the membrane interior. Second-scale temporal resolution may miss rapid solvation exchange, while nanoscale local observations may not explain concentration polarization in a millimetre-scale flow channel.[77,78] Connections among multiscale observations must be established through mass conservation, spatial correspondence, and temporal synchronization.

Interpretation of operando data is likewise constrained by measurement perturbations. Windows and probes may alter the flow field; high-energy beams can cause local heating or radiation damage; fluorescent labels may affect coordination and diffusion; and limited detection depth may overemphasize surface contributions.[78] Blank cells, measurements at different doses, label-free controls, and repeated operational tests should form part of data interpretation. Agreement among complementary methods is generally more important than the high resolution of a single instrument: scattering constrains wet-state structure, spectroscopy identifies local chemical states, imaging resolves concentration fields, and separation testing provides the overall mass balance.

Operando characterization should ultimately provide state variables that can be used for mechanistic testing and parameter constraints, rather than remaining at the level of phenomenological description. Figure 11 reveals how hydrated pore structure and solvation reorganization affect local free-energy pathways, whereas Figure 12 shows the spatially and temporally nonuniform evolution of concentration fields.[9,82,88,89] Together, these two forms of evidence constrain key factors including effective apertures, site occupancy, local migration, and boundary-layer mass transfer, thereby defining experimental boundaries for subsequent quantitative transport models.

4.2 Multiscale Simulation

The task of multiscale simulation is to convert experimentally constrained local structures and chemical states into free-energy, partitioning, diffusion, and multicomponent-migration parameters, and then determine whether these microscopic differences can continue to explain macroscopic performance when membrane thickness, feed composition, and driving force change.[79,83–87,90,91] Cross-scale connection does not mean successively inserting small-scale parameters into progressively larger models. Different models describe different physical objects, reference states, and approximations, and it is therefore first necessary to establish which parameters can be transferred across scales and which conclusions are valid only under specific boundary conditions.[79,80,83–87,90,91]

4.2.1 Local Interactions and Free-Energy Reference States

Electronic-structure calculations are suitable for comparing local coordination, proton transfer, and charge redistribution between ions and pore-wall groups, but binding energies in vacuum generally do not represent thermodynamic preference in aqueous separation.[24,79,84] Solvent competition, site protonation, counter-ion distribution, and interfacial polarization can all alter the relative stability of ions. Even when two ions exhibit a pronounced difference in binding energy in optimized configurations, the difference may be offset by desolvation penalties or configurational entropy. The basic output of local

For Review Only

calculations should therefore shift from a single binding energy to a free-energy difference in an explicit environment, while retaining the dependence on feed composition and chemical state

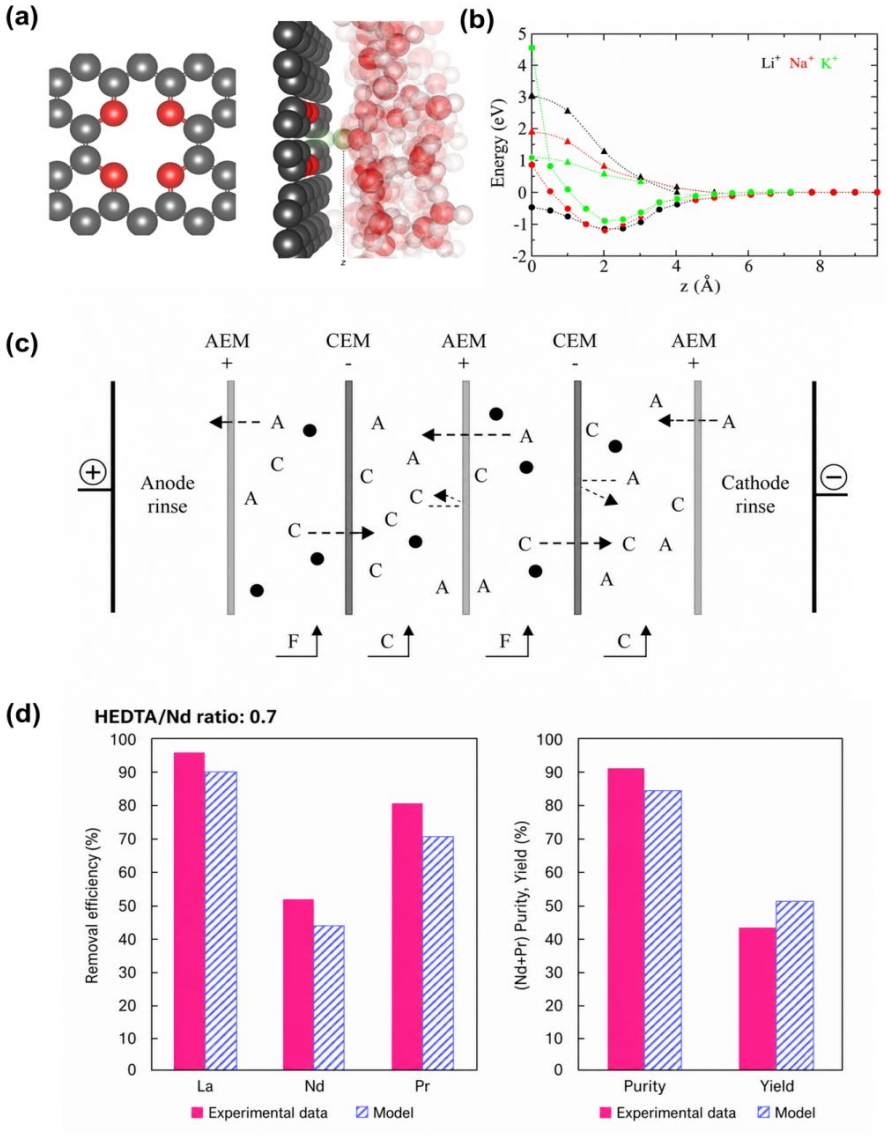


Figure 13 Multiscale modelling from molecular free energies to process-level performance.
(a) Top and side views of a crown-ether-functionalized graphene pore and the explicit-water simulation system used to calculate Li^+ translocation. Adapted from Ref. [79]. (b) Solvated energy, solvation-energy contribution and thermodynamic-integration solvation free energy for Li^+, Na^+ and K^+ along the membrane-normal coordinate, showing that ion selectivity reflects the coupled contributions of pore–ion interactions and solvent reorganization over the full transport pathway. Adapted from Ref. [79]. (c) Electrodialysis stack comprising alternating anion- and cation-exchange membranes, illustrating the partitioning and migration of anions, cations and neutral complexes across multiple compartments. Adapted from Ref. [86]. (d) Comparison of model predictions with experimental measurements at an HEDTA/Nd molar ratio of 0.7 for La, Nd and Pr removal efficiencies and for the purity and yield of the Nd+Pr product. Adapted from Ref. [87].

The first-principles framework shown in Figures 13a and 13b exemplifies this transition.[79] Machine-learning-accelerated molecular dynamics is used to explicitly represent the aqueous environment, correct capacitive effects in the finite simulation cell, and incorporate entropy and electrical-double-layer charging into the energy pathway for ions crossing a crown-ether pore. The resulting profiles for Li^+, Na^+, and K^+ are not isolated pore–ion interactions, but effective free energies jointly formed by pore chemistry, solvent reorganization, and interfacial charge. Only after microkinetics is introduced are these energetic differences translated into steady-state sieving results. Thus, even an accurately calculated free-energy profile must be embedded in a dynamic process subject to mass and charge constraints before comparable selectivities can be obtained.

Free-energy results also depend on whether the reaction coordinate represents the actual confinement process. Coordination number is convenient for describing water removal but may not reflect the geometric requirement for a hydrated complex to pass through an irregular pore entrance. Recent molecular simulations under high-salinity and high-pressure conditions show that salinity can alter cation decoordination free energies through ion association, whereas the effect of pressure is relatively limited.[84] The same study proposes that the maximum cross-sectional area of a hydrated complex can, in some cases, better represent the pore-entry constraint than the average coordination number. A potential-of-mean-force curve is therefore not a material property independent of the selected collective variable. Different migration coordinates, constraints, and reference states may yield different rate-limiting steps for the same system, and these choices and their sensitivities should be reported together with the model conclusions.

4.2.2 Molecular-Scale Transport and Multi-Ion Coupling

Molecular dynamics can resolve solvent exchange, intrapore residence, and diffusion, but barriers and diffusion coefficients obtained from single-ion trajectories are generally valid only for the corresponding concentration and occupancy state.[79,85,90] In a practical mixed feed, channel charge is compensated collectively by multiple ions, while target-ion migration is influenced by competitive occupancy, ion-pair formation, and cooperative motion. Selectivity is then no longer equal to the ratio of two independent single-ion rates, and the intrapore composition cannot be inferred directly from the bulk concentration.

Equilibrium partitioning and kinetic migration must be treated separately. Classical density-functional analysis shows that ion preference inside a nanopore can arise from coupling between excluded volume and electrostatic interactions and may vary nonmonotonically with pore size, concentration, and surface potential.[90] Such models are suitable for describing intrapore composition under multi-ion competition, but the result is an equilibrium occupancy and cannot be directly treated as a transmembrane permeation rate. Membrane-transport analysis additionally requires the mobility of each component under the corresponding occupancy state and cross-correlations among ions. Approximations based on fixed pore walls, fixed charge, and infinite dilution may underestimate structural fluctuations and collective diffusion. Conversely, indiscriminately increasing atomistic detail does not necessarily improve predictive ability, because force-field errors, finite sampling, and an excessively small simulation cell may exceed the ionic differences under investigation.

Molecular-scale models are therefore better suited to providing a set of condition-dependent quantities, including pore-entry free energy, intrapore partitioning, residence time, effective diffusion, and ion correlations, rather than a condition-independent "material selectivity".[79,84,85,90] These quantities should be cross-validated against the wet-state pore size, local coordination, and concentration distributions obtained in Section 4.1. If a simulation predicts strong enrichment of an ion inside the pore but no corresponding occupancy is observed experimentally, the protonation state, channel water content, and competing-ion settings should first be examined rather than merely adjusting the diffusion coefficient to preserve agreement with the macroscopic flux.

4.2.3 Transport Models at the Membrane and Process Scales

As the scale expands to complete membranes and flow devices, molecular free energies must be converted into partition coefficients, chemical potentials, and mobility coefficients and coupled to diffusion boundary layers, fluid transport, and potential distributions. The critical issue is not the name of the governing equation, but whether its assumptions are appropriate for the feed and membrane structure under study. Dilute-solution approximations may be used for low-concentration systems, whereas high-salinity mixtures require consideration of activity, ion association, and multicomponent friction. Homogeneous-membrane models describe average behaviour but cannot capture the disproportionate influence of a small number of large pores on competing-ion leakage.[83,86,87,91]

Pore-size-distribution models illustrate this point. Studies coupling the Poisson–Nernst–Planck and Navier–Stokes equations show that membranes with the same average pore size can exhibit different local flow rates and salt rejection because of differences in pore-size polydispersity and spatial arrangement. Cross-flow can reduce concentration polarization but cannot eliminate the loss of selectivity caused by large pores carrying a disproportionate fraction of the flow.[83] Barriers obtained from an ideal single pore therefore cannot simply be averaged according to pore number. Macroscopic flux is more accurately represented as parallel transport through different pathways weighted by flow, requiring the tail of the pore-size distribution, defect connectivity, and local hydraulic partitioning to be included in scale-up.

Process models must also explicitly represent solution species. Chelator-assisted electrodialysis of rare-earth ions provides a representative example: the species actually participating in membrane transport include free cations, charged complexes, and neutral species, whose proportions are jointly determined by pH, ligand concentration, and stability constants.[86,87] The models shown in Figures 13c and 13d connect solution selectivity, membrane selectivity, and Nernst–Planck transport, and separately validate their predictions against removal, product purity, and yield.[87] Agreement with one total concentration does not mean that the model correctly describes the flux of each species. Only when several independent process metrics are reasonably predicted are the species distribution and membrane-transport parameters sufficiently constrained.

Device-scale parameters are generally composite quantities incorporating several unresolved processes. An effective intramembrane diffusion coefficient inferred from experiments, for example, may simultaneously include pore tortuosity, interfacial partitioning, local defects, and boundary-layer resistance. After experimental calibration, a multi-ion reverse-electrodialysis model can be used to analyse flow-channel geometry and effective area, but the transferability of its parameters to new salt compositions, membrane batches, and flow states still requires independent validation.[91] Scale-up should therefore not seek to retain every microscopic parameter directly, but should identify the minimum parameter set that is both sensitive to the target output and experimentally constrainable.

4.2.4 Parameter Identifiability and Predictive Validity

Agreement between a model and experiment does not establish a unique mechanism.[86,87,91] A flux may be generated by high partitioning combined with slow diffusion or by low partitioning combined with rapid diffusion. Similar selectivity curves over a limited range of conditions do not imply that two parameter sets will have the same extrapolative behaviour. Such parameter compensation may persist even when target and competing ions are fitted simultaneously, particularly when the only observable is a steady-state outlet concentration.

An effective way to improve identifiability is to use different data types to cross-constrain the same parameter. Changes in membrane thickness can test whether bulk diffusion is dominant; feed concentration and ion ratio can constrain competitive partitioning; driving-force scans can identify assumptions of linear migration; and time-dependent responses can distinguish boundary-layer resistance from intramembrane resistance.[83,86,87,91] The operando structures, local occupancies, and concentration fields described in Section 4.1 provide independent constraints that reduce the multiplicity of solutions obtained by fitting macroscopic performance alone. Parameters should be distinguished as directly measurable physical quantities or empirical effective quantities, and the applicability range of the latter should be reported together with model results.

Validation should also shift from reproducing existing data to prediction outside the calibration conditions. Data used for parameter determination should not be reused as the principal validation set; more persuasive tests include new mixture ratios,

higher salinity, different membrane thicknesses, and continuous-flow conditions.[83,86,87,91] Systematic model bias under these conditions can expose missing species, structural changes, or transport coupling. For a material class, a shared conductivity–selectivity upper bound can provide a more stringent test than fitting an individual sample. A model that explains isolated data but not the trade-off exhibited by the material population remains of limited generality.[92]

Uncertainty should propagate across scales rather than being concealed after each modelling stage. Uncertainties in local protonation state, free energy, and pore-size distribution can be greatly amplified through exponential rate relations or flow weighting of large pores.[79,83,84] Sensitivity analysis can identify variables that merit priority measurement, while prediction intervals distinguish robust trends from parameter-dependent coincidences.[81,93] The maturity of a multiscale model ultimately depends on whether it can generate testable predictions under new conditions and specify which level of its assumptions should be revised when those predictions fail.

The value of simulation therefore lies not in adding a possible microscopic explanation to an experimental observation, but in establishing a quantitative mapping from local thermodynamics and multicomponent migration to process outputs. The cross-scale chain shown in Figure 13 can be used reliably for material screening and process design only when parameter sources are traceable, scale-conversion relationships are explicit, and predictions have been validated under independent operating conditions.[79,80,83,86,87,91,92]

4.3 Data-Driven Materials Design

Material composition, pore structure, feed chemistry, and operating parameters jointly create a design space far beyond the reach of exhaustive experiments or high-accuracy simulations.[80,81,94–96] Data-driven methods establish statistical relationships among existing experimental and computational results to screen candidate structures, identify important variables, and optimize operating conditions. Their effectiveness, however, depends on whether the data retain the specific evaluation boundaries associated with each performance value. A "material–selectivity" relationship stripped of feed composition, driving force, and testing mode can readily misidentify differences in operating conditions as intrinsic material behaviour.[81,94,95]

4.3.1 Data Objects and Independent Information Content

An independent data unit suitable for modelling should therefore contain at least four categories of information: material state, feed chemistry, operating boundary, and performance output.[81,94,95] For a membrane process, monomer structure, wet-state pore structure, surface charge, selective-layer thickness, and fabrication conditions describe the material state. The concentrations and ratios of target and competing ions, counter-ions, pH, and ionic strength define feed chemistry. Pressure, potential, flow rate, temperature, and operating time specify transport boundaries. Absolute fluxes of target and competing ions, rejection, separation factor, and energy consumption constitute the performance outputs. For adsorption, site density, material form, solid-to-liquid ratio, contact time, working capacity, elution conditions, and regeneration method must additionally be recorded. If only a material name and a single separation factor are retained, the model may incorrectly attribute differences arising from experimental boundaries to material structure.

Existing studies have demonstrated the practical impact of this problem. A database developed for ion transport through polyamide membranes contains membrane properties, ion characteristics, and operating parameters, from which a model can identify the statistical contributions of size exclusion and electrostatic interactions.[94] The study also shows, however, that inappropriate data splitting causes pronounced information leakage. Records derived from the same membrane or publication often share unreported fabrication details. Randomly assigning these records to training and test sets causes test performance to reflect recognition of related samples rather than predictive ability for new materials.

The problem is more pronounced in literature-derived adsorption data. A single lithium-ion sieve may generate many data rows at different initial concentrations, pH values, and coexisting-ion conditions, but these records do not constitute independent material samples. Grouping by source or material generally yields model performance more representative of genuine extrapolation than random splitting. Related studies further show that operating parameters can contribute more strongly to predictions of lithium adsorption than some material descriptors, indicating that a "high-capacity material" in the literature may sometimes simply have been tested under more favourable conditions.[95]

Data quality should therefore not be judged solely by the number of records. More meaningful measures include the number of independent materials, coverage of operating conditions, fraction of mixed systems, fraction of real feeds, and repeated validation across different sources.[81,94,95] Single salts, binary mixtures, and complex brines should be retained as distinct levels of evidence. Equilibrium capacity, breakthrough capacity, and post-regeneration capacity should likewise not be merged into a single label. Testing protocols and evidence quality should themselves be included as database fields, allowing a model to distinguish performance differences caused by material design from those caused by evaluation boundaries.

4.3.2 Physical Boundaries of Structural Representation and Model Interpretation

Before entering a model, a material must be converted into a machine-readable representation. For regular organic structures, molecular fingerprints, molecular graphs, and quantum-chemical descriptors can encode functional groups, local charge, and geometric features.[24,81,96] For amorphous membranes, porous composites, and defect-rich two-dimensional materials, representation solely by the monomer or ideal unit cell may omit crosslinking degree, wet-state reconstruction, and pore-size distribution.[81,96] The level of detail in the structural representation should match the prediction target: monomer descriptors may be used to screen synthetic precursors but cannot automatically represent the effective pore structure of the final membrane.

Figure 14a presents a data-driven concept for screening ion-specific sites. Candidate functional groups are first encoded as molecular graphs, fingerprints, or string representations. High-accuracy calculations on a subset then provide ion-binding data, allowing a surrogate model to be trained and used to screen a larger chemical space.[24] The rationale is to incorporate ion, site, and solvent jointly into design rather than empirically ranking classes of functional groups. The objective should likewise not be to identify the strongest-binding site. An interaction that is too weak cannot establish effective partitioning, whereas excessively strong binding may prolong residence and impede release; an appropriate site should balance selective partitioning against sustained migration.

Model interpretation can help determine whether an algorithm has learned an acceptable structural relationship. A study of polyamide nanofiltration membranes represented monomers using

For Review Only

molecular descriptors and fingerprints and used SHAP and partial-dependence analyses to investigate how different features affect water permeability and Li^+/Mg^{2+} selectivity.[96] Figure 14b presents both descriptor importance and the direction of correlation, avoiding the misinterpretation that "a variable frequently used by the model" means that "increasing the variable necessarily improves performance".

Interpretation remains a statistical attribution within the range of the training data. Highly correlated descriptors may substitute for one another, and the direction of a SHAP value may change with other variables and with the range of the descriptor.[81,96] Correlations of maximum partial charge, hydrophobicity, or molecular sphericity with selectivity do not mean that independently adjusting one of these parameters will reproduce the same result, because the descriptors are usually also correlated with reaction activity, crosslinked structure, and wet-state membrane morphology. The principal value of an interpretable model is to generate design hypotheses requiring further testing, rather than to replace mechanistic evidence.[81,94,96]

Hybrid physics–data models can reduce ambiguity arising from purely statistical correlations. Existing studies of ion separation have first used component and process models to generate physically consistent training data, then corrected a machine-learning surrogate with a small number of experimental results and simultaneously predicted separation efficiency and energy consumption.[80] Such frameworks are suitable for systems in which experimental samples are limited but fundamental conservation relationships are clear. Their reliability still depends on whether the underlying model includes the actual species and dominant resistances. Machine learning can correct systematic bias, but cannot automatically restore physical processes excluded from the underlying model.[80,81]

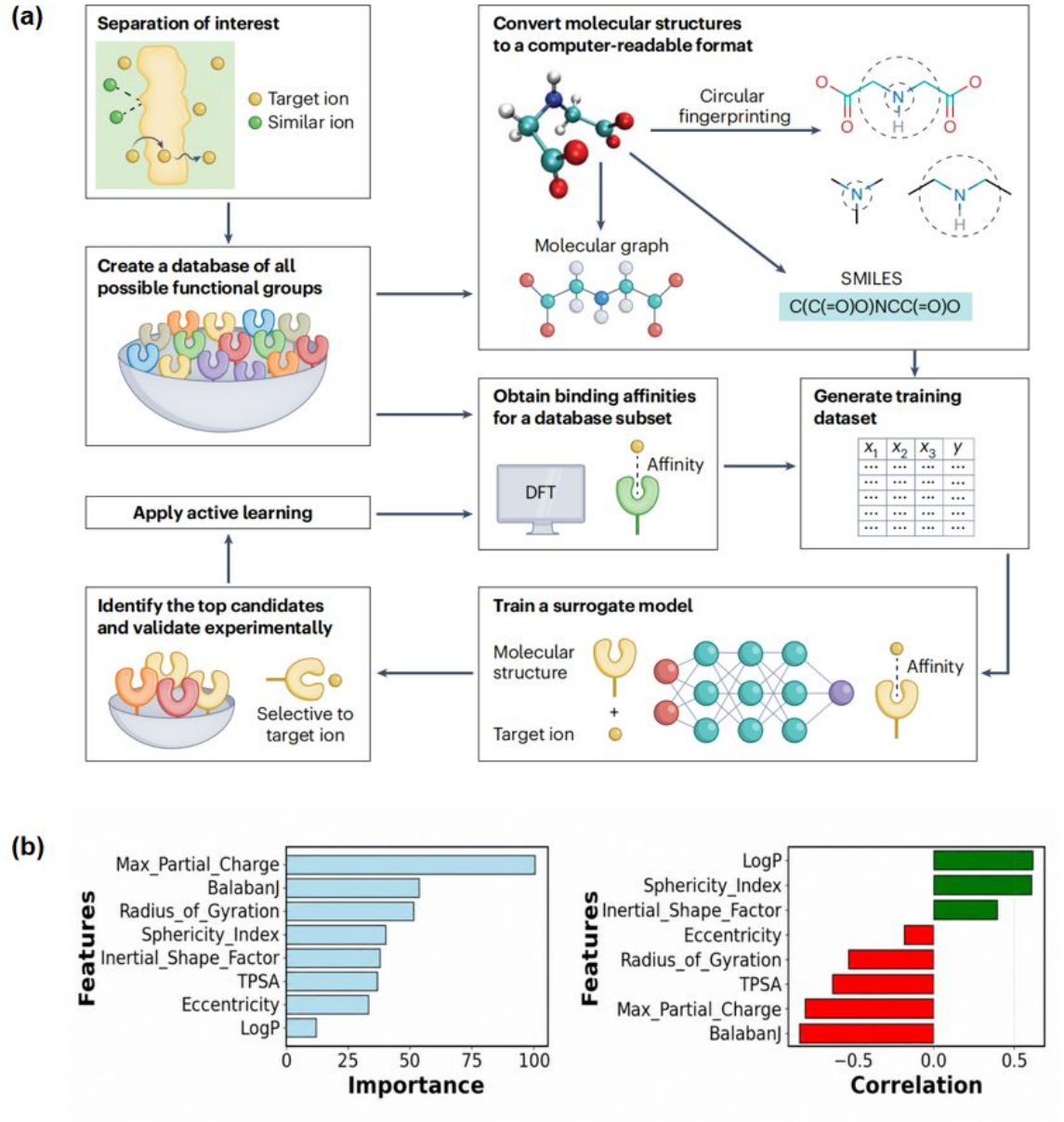


Figure 14 **Data representation and interpretable prediction for selective ion separation.**

(a) Data-driven workflow for a targeted separation problem. A library of candidate functional groups is first constructed for discriminating a target ion from similar ions. Molecular structures are then converted into machine-readable descriptors (e.g., molecular graphs, fingerprints, and SMILES), while binding affinities for a representative subset are generated by high-throughput quantum-chemical calculations to form the training set. A surrogate model is subsequently trained and iteratively refined through active learning, enabling the identification and experimental validation of top candidate binding sites. Adapted from Ref. [24]. (b) Interpretable machine-learning results for Li^+/Mg^{2+} selectivity, including the relative importance of key molecular descriptors and the direction of their correlations with selectivity. This panel highlights that the value of data-driven design lies not only in predictive accuracy, but also in identifying which structural features govern selectivity and whether they promote or suppress separation performance. Adapted from Ref. [96].

4.3.3 Candidate Screening and Multiobjective Decision-Making

An effective test of data-driven design is not whether a model can reproduce high-performing samples already present in the database, but whether it can propose candidates absent from the training set and independently verify their synthesizability and separation performance. Figure 15a presents an example in which monomers are screened by machine learning and used to fabricate polyamide membranes.[96] The candidate monomers exhibit different trade-offs between permeability and Li^+/Mg^{2+} selectivity, showing that structural screening cannot stop at a single predicted ranking. Polymerization, membrane integrity, and actual pore structure continue to affect performance beyond the molecular features represented by the model.

This also constrains the choice of optimization objectives. If only the separation factor is maximized, an algorithm may favour candidates that reduce the fluxes of both ions, but suppress the competing ion more strongly.[80,96] In adsorption systems, maximizing equilibrium capacity alone may identify high-affinity materials that are difficult to regenerate. A more rational objective set should, depending on process type, simultaneously include target-ion flux or working capacity, mixed-system selectivity, product purity and recovery, stability, and energy consumption. Because these metrics generally cannot all be optimized at a single point, candidates should be compared along a Pareto frontier rather than compressed into a composite score lacking a physical basis.

To prevent a single separation factor from obscuring the origin of performance, model outputs should separately retain the absolute flux, partition coefficient, or dynamic capacity of the target and competing ions and calculate selectivity from these values.[80,94,96] This output structure can determine whether a performance change arises from preservation of the target component, reduced leakage of the competing component, or simultaneous changes in both, and can be directly connected to the partition–diffusion and multicomponent-transport models in Section 4.2.

Failed candidates are also informative. A material predicted to perform well but found experimentally to perform poorly may expose limitations in synthetic feasibility, structural stability, or descriptor coverage. If such results are not incorporated into subsequent datasets, the model will continue to propose candidates in the same infeasible region.[81,93] Data-driven studies should therefore record negative results such as failure to form a membrane, structural collapse, low flux, and regeneration failure, rather than retaining only successful samples.

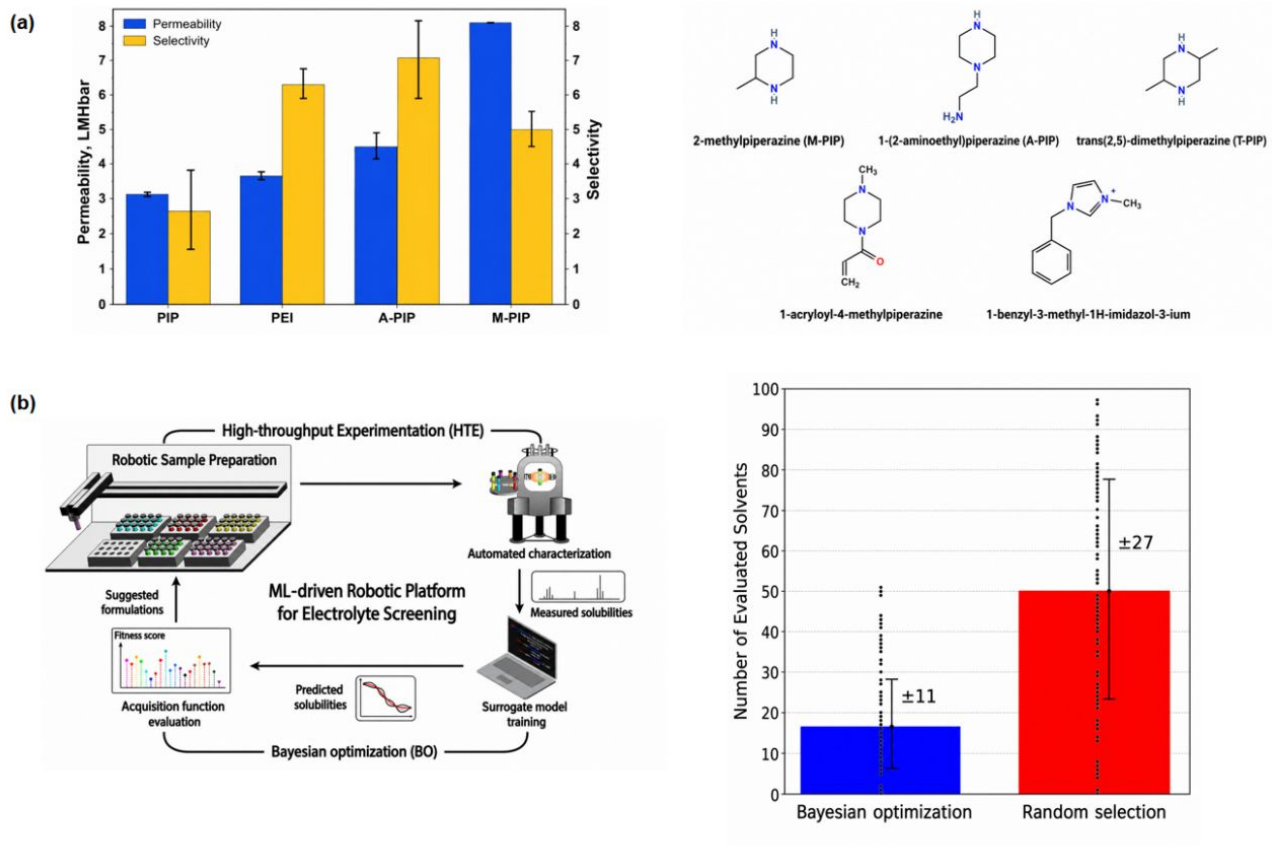


Figure 15 **Candidate validation and active-learning loops in data-guided design.**
(a) Molecular structures of machine-learning-screened monomer candidates and experimentally measured permeability and Li^+/Mg^{2+} selectivity of representative polyamide membranes. The distinct permeability–selectivity responses demonstrate that model rankings must be tested through membrane fabrication and separation experiments using previously untested chemical structures. Adapted from Ref. [96]. (b) Machine-learning-guided high-throughput experimentation and Bayesian optimization workflow. Automated preparation and characterization generate new data, while the surrogate model proposes subsequent formulations using predicted performance and uncertainty; Bayesian optimization identifies the optimum with fewer experiments than random selection. Adapted from Ref. [97].

4.3.4 Extrapolative Uncertainty and Active Learning

The principal application scenarios for selective separation generally lie outside the training distribution, including transitions from single salts to mixed salts, from low concentration to hypersaline brines, from ideal solutions to real feeds, and from small membrane coupons to continuous devices. A randomly selected test set cannot evaluate these extrapolation tasks.[81,94,95] More rigorous validation includes grouped holdout according to material family, literature source, ion system, or feed type, followed by testing of predictions for unseen chemical classes and unseen combinations of operating conditions. Systematic reviews of machine learning in membrane science likewise regard grouped validation, public availability of data and code, and explicit reporting of the training domain as basic requirements for evaluating model reproducibility and transferability.

Extrapolative predictions should also report uncertainty. A high predicted value accompanied by high uncertainty may represent a promising new structure or merely a numerical artefact far from the training data.[81,93] Distance metrics, ensemble models, and conformal prediction can be used to identify candidates outside the applicability domain, but such statistical intervals have practical meaning only when the data have been split appropriately and experimental error has been retained. The absence of failed results and long-duration operating data in the literature can also cause systematic overoptimism in predictions of performance and stability.

Active learning converts uncertainty from a risk indicator into an experimental decision variable. In the high-throughput platform shown in Figure 15b, automated experiments generate data, a surrogate model predicts candidate performance, and an acquisition function selects the next experiment by combining potential benefit and uncertainty.[97] The study concerns electrolyte formulations, and Bayesian optimization substantially reduces the number of experiments required to identify preferred candidates relative to random search; the methodology can be transferred to joint screening of separation materials and operating conditions. For ion separation, the most valuable next experiment may not be the sample with the highest predicted selectivity, but a condition that distinguishes two competing mechanisms, supplements the high-salinity region, or reduces uncertainty along the Pareto frontier.

The value of data-driven design should therefore not be assessed solely by test-set accuracy or candidate ranking, but by whether it proposes the next experiment with genuine discriminatory power. Active learning can balance potential performance, predictive uncertainty, and experimental cost, prioritizing samples and operating conditions that expand the applicability domain, distinguish competing mechanisms, or reduce uncertainty along a multiobjective frontier.[93,97] As new results are continually used to revise data representations and model assumptions, material screening can evolve from a one-off database prediction into a verifiable and updatable iterative design process.

5. Summary and Outlook

The central conclusion of this Review is that ion selectivity is a property of the transport pathway rather than an isolated function of pore size, surface charge, or binding energy.[5,13,24] Nanoconfinement can amplify limited differences in ion solvation and coordination, but a locally established advantage can be translated into a separation outcome with meaningful productivity only if it is retained through interfacial partitioning, intrapore migration, and outlet-side release.[5,9,13,24,79] Material design should therefore not stop at obtaining smaller pores or stronger sites, but should coordinate the free-energy and kinetic resistances of different transport steps.[5,13,24]

Correspondingly, performance evaluation should shift from individual maximum values to paired metrics with explicitly defined conditions.[42,43] Membranes and nanochannels should simultaneously report the absolute fluxes of target and competing ions, the selectivity definition, and performance under mixed feeds. Adsorbent materials should emphasize competitive working capacity, breakthrough behaviour, product concentration, and regenerant consumption.[42,43,61,62,65] Quantitative comparisons among materials have physical meaning only when the ion system, feed composition, driving force, and testing mode are explicitly defined.[42,43]

A deeper challenge for the field is to translate nanoscale recognition into a stable product stream under complex feeds and cumulative operating loads.[3,43,68,69,72,75] Increasing membrane area, shaping particles, and integrating devices introduce defect statistics, concentration polarization, channeling, structural wear, and additional energy consumption, preventing linear extrapolation of laboratory performance.[43,68–75] Future studies should use product purity, recovery, productivity, and cost per unit product as process endpoints, while incorporating material deactivation, cleaning and regeneration, and waste-stream treatment within the same evaluation boundary.[3,43,72,75]

Operando characterization, multiscale simulation, and data-driven methods can jointly support this transition. Experiments provide structural and chemical constraints under actual operating conditions; simulations test whether local states quantitatively explain multicomponent transport; and data-based methods identify applicability domains, organize uncertainty, and select subsequent experiments with the greatest discriminatory value.[78,79,81,94] Transferable design rules can be established only when both successful and failed results are retained and predictions are independently validated using unseen materials and operating conditions.[81,93–95,97] Nanoporous materials may thereby evolve from objects of empirical screening into quantitative separation platforms designed for specific ions, feeds, and process conditions.[5,13,24,43,79,81,93]

REFERENCES

1 Zhao Y, Gao H, Yu L, *et al*. Versatile heavy metal ion separation via biological ion-channel-inspired membranes. Nat Nanotechnol, 2026, 21: 680–688

2 Yang S, Wang Y, Pan H, *et al*. Lithium extraction from low-quality brines. Nature, 2024, 636: 309–321

3 Kim SJ, Ko SH, Kang KH, *et al*. Direct seawater desalination by ion concentration polarization. Nat Nanotechnol, 2010, 5: 297–301

4 Liu Q, Yan Z, Gao J, *et al*. Ion sieving membrane for direct seawater anti-precipitation hydrogen evolution reaction electrode. Chem Sci, 2023, 14: 11830–11839

5 Epsztein R, DuChanois RM, Ritt CL, et al. Towards single-species selectivity of membranes with subnanometre pores. Nat Nanotechnol, 2020, 15: 426–436

6 Esfandiar A, Radha B, Wang FC, *et al*. Size effect in ion transport through angstrom-scale slits. Science, 2017, 358: 511–513

7 Goutham S, Keerthi A, Ismail A, *et al*. Beyond steric selectivity of ions using ångström-scale capillaries. Nat Nanotechnol, 2023, 18: 596–601

8 Iddya A, Zarzycki P, Kingsbury R, *et al*. A reverse-selective ion exchange membrane for the selective transport of phosphates via an outer-sphere complexation–diffusion pathway. Nat Nanotechnol, 2022, 17: 1222–1228

9 Wang A, Breakwell C, Foglia F, *et al*. Selective ion transport through hydrated micropores in polymer membranes. Nature, 2024, 635: 353–358

10 Wang H, Zhai Y, Li Y, *et al*. Covalent organic framework membranes for efficient separation of monovalent cations. Nat Commun, 2022, 13: 7123

11 Mo RJ, Chen S, Huang LQ, *et al*. Regulating ion affinity and dehydration of metal-organic framework sub-nanochannels for high-precision ion separation. Nat Commun, 2024, 15: 2145

For Review Only

12 Hu QH, Song AM, Gao X, *et al*. Rationally designed nanotrap structures for efficient separation of rare earth elements over a single step. Nat Commun, 2024, 15: 1558
13 Shen J, Liu G, Han Y, *et al*. Artificial channels for confined mass transport at the sub-nanometre scale. Nat Rev Mater, 2021, 6: 294–312
14 Abraham J, Vasu KS, Williams CD, *et al*. Tunable sieving of ions using graphene oxide membranes. Nat Nanotechnol, 2017, 12: 546–550
15 Chen L, Shi G, Shen J, *et al*. Ion sieving in graphene oxide membranes via cationic control of interlayer spacing. Nature, 2017, 550: 380–383
16 Ma H, Wang S, Yu B, *et al*. Bioinspired nanochannels based on polymeric membranes. Sci China Mater, 2021, 64: 1320–1342
17 Chen L, Tu B, Lu X, *et al*. Unidirectional ion transport in nanoporous carbon membranes with a hierarchical pore architecture. Nat Commun, 2021, 12: 4650
18 Qiu M, Liu L, Ling Q, *et al*. Biochar for the removal of contaminants from soil and water: a review. Biochar, 2022, 4: 19
19 Werber JR, Osuji CO, Elimelech M. Materials for next-generation desalination and water purification membranes. Nat Rev Mater, 2016, 1: 16018
20 Denny MS Jr, Moreton JC, Benz L, *et al*. Metal–organic frameworks for membrane-based separations. Nat Rev Mater, 2016, 1: 16078
21 Dou H, Xu M, Wang B, *et al*. Microporous framework membranes for precise molecule/ion separations. Chem Soc Rev, 2021, 50: 986–1029
22 Srimuk P, Su X, Yoon J, *et al*. Charge-transfer materials for electrochemical water desalination, ion separation and the recovery of elements. Nat Rev Mater, 2020, 5: 517–538
23 Sheng F, Ge L, Li X, *et al*. Covalent organic framework membranes for selective ion separation. Commun Mater, 2026, 7: 33
24 Violet C, Ball A, Heiranian M, *et al*. Designing membranes with specific binding sites for selective ion separations. Nat Water, 2024, 2: 706–718
25 Zuo P, Ye C, Jiao Z, *et al*. Near-frictionless ion transport within triazine framework membranes. Nature, 2023, 617: 299–305
26 Lu J, Zhang H, Hou J, *et al*. Efficient metal ion sieving in rectifying subnanochannels enabled by metal–organic frameworks. Nat Mater, 2020, 19: 767–774
27 Tan R, Wang A, Malpass-Evans R, *et al*. Hydrophilic microporous membranes for selective ion separation and flow-battery energy storage. Nat Mater, 2020, 19: 195–202
28 Ye T, Gao H, Li Q, *et al*. Highly selective lithium transport through crown ether pillared angstrom channels. Angew Chem Int Ed, 2024, 63: e202316161
29 Villalobos LF, Zhang J, Lee J, *et al*. Ultrathin crown ether-based polyamide membrane for ion-ion separations. Nat Commun, 2026, 17: 4263
30 Li C, Li S, Zhong Y, *et al*. Supramolecular-based ion separation membranes for direct separation of concentrated mixed-salt solutions. J Am Chem Soc, 2026, 148: 6116–6124
31 Wang X, Zhang H, Wei G, *et al*. Comediation of voltage gating and ion charge in MXene membrane for controllable and selective monovalent cation separation. Sci Adv, 2024, 10: eado3998
32 Zhou S, Ai F, Song Z, *et al*. TASK2-inspired pH-gating polymeric nanochannels with multiple interconvertible permeability states by synergistic regulation of conformation and charge. Angew Chem Int Ed, 2025, 64: e202512145
33 Sun Y, Ma J, Zhang F, *et al*. A light-regulated host–guest-based nanochannel system inspired by channelrhodopsins protein. Nat Commun, 2017, 8: 260
34 Yu X, Li C, Chang J, *et al*. Gating effects for ion transport in three-dimensional functionalized covalent organic frameworks. Angew Chem Int Ed, 2022, 61: e202200820
35 Liang C, Wang D, He S, *et al*. Bioinspired cation-gated dynamic liquid film nanochannel for controlled transport of ions and molecules. Sci China Mater, 2024, 67: 2523–2531
36 Xu T, Qi H, Zhong J, *et al*. Bioinspired voltage-gated multi-state ion channels in MXene nanoconfinement for emulating synaptic plasticity. Sci China Mater, 2026, 69: 3514–3522
37 Jia R, Ji Z, Li X, *et al*. Reconfiguring hydration shells by rigidly confined interaction within graphene oxide membranes for ultra-efficient anion separation. Sci China Mater, 2026, 69: 481–491
38 Meng QW, Li J, Lai Z, *et al*. Optimizing selectivity via membrane molecular packing manipulation for simultaneous cation and anion screening. Sci Adv, 2024, 10: eado8658
39 Zhang H, Xing J, Wei G, *et al*. Electrostatic-induced ion-confined partitioning in graphene nanolaminate membrane for breaking anion–cation co-transport to enhance desalination. Nat Commun, 2024, 15: 4324
40 Zhang Z, Kong Y, Li R, *et al*. COF scaffold membrane with gate-lane nanostructure for efficient Li^+/Mg^{2+} separation. Nano-Micro Lett, 2026, 18: 126
41 Lu G, Zhao Y, Van der Bruggen B. Ion association in nanoconfinement for precision separation. Sci China Mater, 2026, 69: 2973–2974
42 Wang R, Zhang J, Tang CY, *et al*. Understanding selectivity in solute–solute separation: definitions, measurements, and comparability. Environ Sci Technol, 2022, 56: 2605–2616
43 Wang R, He R, He T, *et al*. Performance metrics for nanofiltration-based selective separation for resource extraction and recovery. Nat Water, 2023, 1: 291–300
44 Zhang J, Shocron AN, Meola V, *et al*. New methodology for characterizing ion permeability and selectivity of ion-exchange membranes. Environ Sci Technol Lett, 2025, 12: 1082–1088
45 Xu Z, Michos I, Cao Z, *et al*. Proton-selective ion transport in ZSM-5 zeolite membrane. J Phys Chem C, 2016, 120: 26386–26392
46 Ding D, Yaroshchuk A, Bruening ML. Electrodialysis through Nafion membranes coated with polyelectrolyte multilayers yields >99% pure monovalent ions at high recoveries. J Membr Sci, 2022, 647: 120294
47 Xin W, Fu J, Qian Y, *et al*. Biomimetic KcsA channels with ultra-selective K^+ transport for monovalent ion sieving. Nat Commun, 2022, 13: 1701
48 Li Y, Gao L, Lu Z, *et al*. Enhanced removal of heavy metals from water by hydrous ferric oxide-modified biochar. ACS Omega, 2020, 5: 28702–28711
49 Peng Q, Wang R, Zhao Z, *et al*. Extreme Li-Mg selectivity via precise ion size differentiation of polyamide membrane. Nat Commun, 2024, 15: 2505
50 Meng QW, Zhu X, Xian W, *et al*. Enhancing ion selectivity by tuning solvation abilities of covalent-organic-framework membranes. Proc Natl Acad Sci USA, 2024, 121: e2316716121
51 Huang D, Ge X, Chen Q, *et al*. Acid-base pairs engineering enables ultra-selective lithium-magnesium separation via sulfonated polybenzimidazole membranes. Sci China Mater, 2025, 68: 3359–3367
52 Bao S, Ma Z, Yu L, *et al*. Randomly oriented covalent organic framework membrane for selective Li^+ sieving from other ions. Nat Commun, 2025, 16: 3896
53 DuChanois RM, Heiranian M, Yang J, *et al*. Designing polymeric membranes with coordination chemistry for high-precision ion separations. Sci Adv, 2022, 8: eabm9436
54 Cao L, Chen IC, Li Z, *et al*. Switchable Na^+ and K^+ selectivity in an amino acid functionalized 2D covalent organic framework membrane. Nat Commun, 2022, 13: 7894
55 Teng X, Sheng D, Wang J, *et al*. Ion selectivity mechanism of the MgtE channel for Mg^{2+} over Ca^{2+}. iScience, 2022, 25: 105565
56 Shan W, Liang M, Zan J, *et al*. Separation of Ni and Co from lithium-ion batteries through chloride coordination and electrodialysis. Sep Purif Technol, 2025, 379: 134838
57 Xin J, Wang L, Wang X, *et al*. Selective separation of $Ni^{2+}/Co^{2+}/Mn^{2+}$ enabled by tunable intrapore sulfonic acid group content in covalent organic framework membranes via EDTA-chelation-assisted process. J Membr Sci, 2025, 732: 124252
58 Otaki M, Suominen T, Suorsa V, *et al*. The effect of phosphonates on lanthanide separation for surface-grafted porous zirconia. Mater Adv, 2023, 4: 551–560
59 Song AM, Yang MJ, Wu Z, *et al*. Efficient separation of adjacent rare earths in one step by using ion-microporous metal–organic frameworks. Adv Funct Mater, 2025, 35: 2419093
60 Fan F, Ren Y, Zhang S, et al. A bioinspired membrane with ultrahigh Li^+/Na^+ and Li^+/K^+ separations enables direct lithium extraction from brine. Adv Sci, 2024, 11: 2402898
61 Chatterjee P, Volkov A, Mi J, *et al*. Efficient capture and release of the rare-earth element neodymium in aqueous solution by recyclable covalent organic frameworks. J Am Chem Soc, 2024, 146: 20468–20476
62 Bhadane P, Dhumal P, Brun E, *et al*. Safe and sustainable by design MOF beads for selective entrapment and recovery of rare earth elements. Environ Sci Technol, 2025, 59: 16379–16391
63 Ye Q, Jin X, Zhu B, *et al*. Lanmodulin-functionalized magnetic nanoparticles as a highly selective biosorbent for recovery of rare earth elements. Environ Sci Technol, 2023, 57: 4276–4285
64 Wu R, Hong B, Xue C, *et al*. ZIF-8 used for the selective recovery of heavy rare earth elements from mining wastewater. Environ Sci Technol, 2024, 58: 9612–9623
65 Zhao M, Luan J, Zhao C, *et al*. Highly selective granulation adsorbents for lithium recovery from gas field brine: selectivity, kinetics and mechanism. Desalination, 2024, 583: 117699
66 Chaudhuri S, Sigmund G, Bone SE, *et al*. Mercury removal from contaminated water by wood-based biochar depends on natural organic

For Review Only

matter and ionic composition. Environ Sci Technol, 2022, 56: 11354–11362
67 Zhang S, Wei X, Cao X, *et al*. Solar-driven membrane separation for direct lithium extraction from artificial salt-lake brine. Nat Commun, 2024, 15: 238
68 Xu R, Xiao X, Zhang G, *et al*. Continuous lithium extraction from brine by efficient redox-couple electrodialysis. Matter, 2024, 7: 3876–3890
69 Ying J, Lin Y, Zhang Y, *et al*. Mechanistic insights into the degradation of monovalent selective ion exchange membrane towards long-term application of real salt lake brines. J Membr Sci, 2022, 652: 120446
70 Su J, Fan Q, Hu X, *et al*. Continuous flow extraction of lithium from brine using silica-coated LMO beads. Mater Adv, 2025, 6: 2202–2210
71 Foo ZH, Rehman D, Bouma AT, *et al*. Lithium concentration from salt-lake brine by Donnan-enhanced nanofiltration. Environ Sci Technol, 2023, 57: 6320–6330
72 Foo ZH, Thomas JB, Heath SM, *et al*. Sustainable lithium recovery from hypersaline salt-lakes by selective electrodialysis: transport and thermodynamics. Environ Sci Technol, 2023, 57: 14747–14759
73 Xie R, Sun D, Tang J, *et al*. Ecofriendly, highly selective lithium extraction by redox-mediated electrodialysis. ACS Cent Sci, 2024, 10: 2119–2124
74 Mojtahedi B, Askari M, Dolati A. Development of selective cationic membranes for lithium recovery from brines using electrodialysis processes. ACS Sustain Chem Eng, 2025, 13: 3107–3118
75 Foo ZH, Liu S, Kanias L, *et al*. Positively-coated nanofiltration membranes for lithium recovery from battery leachates and salt-lakes: ion transport fundamentals and module performance. Adv Funct Mater, 2024, 34: 2408685
76 Zhu Z, Qian Y, Yu W, *et al*. Positively charged polyamide membranes with expanded ion passage channels enabling exceptional lithium extraction from battery leachate. Sci China Mater, 2026, 69: 473–480
77 Petersen H, Weidenthaler C. A review of recent developments for the in situ/operando characterization of nanoporous materials. Inorg Chem Front, 2022, 9: 4244–4271
78 Prajapati A, Hahn C, Weidinger IM, *et al*. Best practices for in-situ and operando techniques within electrocatalytic systems. Nat Commun, 2025, 16: 2593
79 Bonnet N, Marzari N. Ion sieving in two-dimensional membranes from first principles. ACS Nano, 2025, 19: 8552–8560
80 Rall D, Schweidtmann AM, Kruse M, *et al*. Multi-scale membrane process optimization with high-fidelity ion transport models through machine learning. J Membr Sci, 2020, 608: 118208
81 Ignacz G, Bader L, Beke AK, *et al*. Machine learning for the advancement of membrane science and technology: A critical review. J Membr Sci, 2025, 713: 123256
82 Lu C, Hu C, Chen Z, *et al*. Dehydration-enhanced ion-pore interactions dominate anion transport and selectivity in nanochannels. Sci Adv, 2023, 9: eadf8412
83 Hsu MH, Tsou TY, Hsu JP, *et al*. Influence of pore size distribution and applied cross-flow on ion rejection and separation. Sep Purif Technol, 2025, 352: 128248
84 Schwindt NS, Epsztein R, Straub AP, *et al*. Molecular details of ion de-coordination at elevated salinity and pressure and consequences for membrane separations. J Membr Sci, 2025, 734: 124358
85 Liao S, Liu Y, Li L, *et al*. Theoretical framework for confined ion transport in two-dimensional nanochannels. Nat Commun, 2025, 16: 6675
86 Azimi G, Ding L, Mosadeghsedghi S, *et al*. Separation of rare earth elements using chelating agent-assisted electrodialysis: Phenomenological modeling and comparison with experimental data. Hydrometallurgy, 2024, 224: 106252
87 Azimi G, Mosadeghsedghi S, Dashtban Kenari SL, *et al*. Class II three-layer system phenomenological model based on limiting current density and dynamic chelation chemistry for separation of rare earth elements using electrodialysis. Sci Rep, 2024, 14: 18340
88 Utterback JK, King AJ, Belman-Wells L, *et al*. Operando label-free optical imaging of solution-phase ion transport and electrochemistry. ACS Energy Lett, 2023, 8: 1785–1792
89 Rauscher MV, Kohns R, Seyffertitz M, *et al*. Beyond global metrics in capacitive water deionization: Position-resolved ion concentration from operando X-ray transmission. Desalination, 2026, 623: 119849
90 Cui L, Liu Y, Liu H. Classical density functional analysis of ion selectivity in nanopores: The coupling between hard-sphere and electrostatic interactions. Chem Eng J, 2022, 444: 136673
91 Cho H, Kim J, Han CS. Multi-ion transport in reverse electrodialysis: A validated model for design and optimization. Desalination, 2024, 586: 117746
92 Kitto D, Kamcev J. Predicting the conductivity–selectivity trade-off and upper bound in ion-exchange membranes. ACS Energy Lett, 2024, 9: 1346–1352
93 Ren Z, Ren Z, Zhang Z, *et al*. Autonomous experiments using active learning and AI. Nat Rev Mater, 2023, 8: 563–564
94 Jeong N, Epsztein R, Wang R, *et al*. Exploring the knowledge attained by machine learning on ion transport across polyamide membranes using explainable artificial intelligence. Environ Sci Technol, 2023, 57: 17851–17862
95 Xu Z, Ding Y, Han SC, *et al*. Predicting the performance of lithium adsorption and recovery from unconventional water sources with machine learning. Water Res, 2024, 266: 122374
96 Dangayach R, Jeong N, Chen Y. Machine learning analysis and monomer screening of polyamide nanofiltration membranes for lithium separation. ACS EST Engg, 2025, 5: 3039–3050
97 Noh J, Doan HA, Job H, *et al*. An integrated high-throughput robotic platform and active learning approach for accelerated discovery of optimal electrolyte formulations. Nat Commun, 2024, 15: 2757

For review only

Acknowledgements This work was supported by the National Key R&D Program of China (2024YFB3612600), the National Natural Science Foundation of China (22375100, 22275098 and 62288102), the Basic Research Program of Jiangsu (BK20243057), and the Jiangsu Province College Students Innovation Training Program (202610293144Y).

Author contributions Chaoyang Dai contributed to conceptualization, literature curation, writing-original draft and visualization. Zhicheng Xu contributed to literature curation and writing-review and editing. Hao Luo contributed to writing-review and editing. Tianyang Zhou contributed to literature curation and visualization. Yinzi Shao contributed to writing-review and editing. Haotian Wu contributed to literature curation. Linghai Xie contributed to supervision, funding acquisition and writing-review and editing. Quanyou Feng contributed to supervision, project administration, funding acquisition and writing-review and editing. All authors have read and approved the final manuscript.

Conflict of interest The authors declare that they have no conflict of interest.

Ethical approval This review did not involve studies with human participants or animals performed by any of the authors.

AUTHOR BIOGRAPHIES



Chaoyang Dai is an undergraduate student at the College of Electronic and Optical Engineering & College of Flexible Electronics (Future Technology), Nanjing University of Posts and Telecommunications. His research interests include nanoporous materials for ion separation, machine-learning-assisted materials design and optoelectronic materials.



Linghai Xie is a professor at Nanjing University of Posts and Telecommunications (NJUPT). He received his Ph.D. degree from Fudan University in 2006 and joined the Institute of Advanced Materials of NJUPT. His research focuses on organic and polymer optoelectronic materials for organic/plastic electronics and molecular electronics.



Quanyou Feng received his Ph.D. degree from Fudan University in 2014. From 2015 to 2017, he conducted postdoctoral research at Virginia Tech. Now he is an associate professor in Institute of Advanced Material (IAM), Nanjing University of Posts and Telecommunications. His research focuses on organic/polymer wide-bandgap semiconductor materials and optoelectronic devices.

中文摘要

纳米多孔材料中的选择性离子分离：限域筛分、化学识别与动态门控

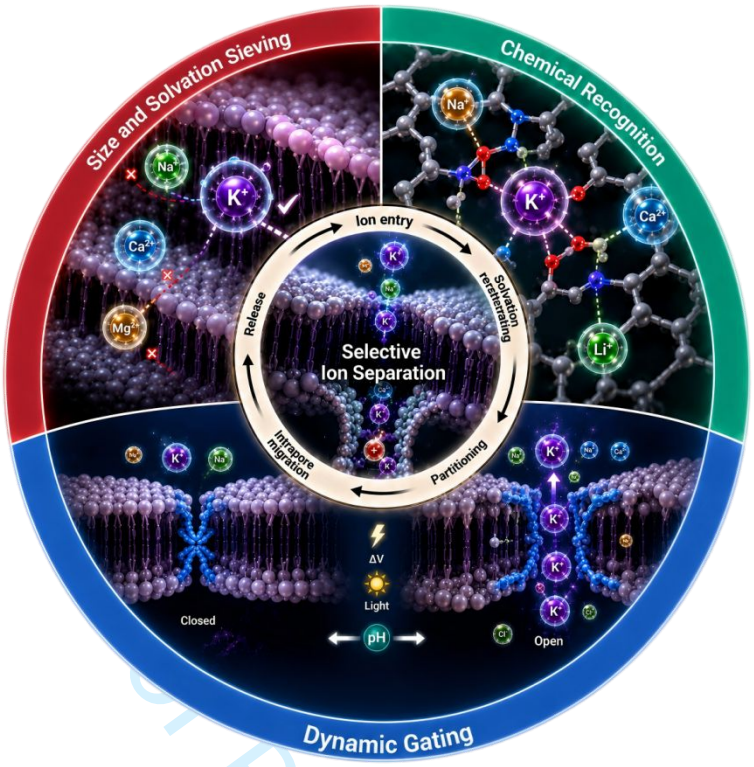
戴朝阳[2]，徐志成[1]，骆浩[3]，周天阳[2]，邵音子[4]，吴昊天[1]，解令海[1]*，冯全友[1]*

选择性离子分离对于资源回收、水处理、盐湖提锂和核废物管理具有重要意义，但不同离子在尺寸、溶剂化结构和配位行为上的差异往往十分有限，且其分离过程还受到价态、界面电荷和竞争离子共同影响。纳米多孔材料具有可调的亚纳米孔道和化学活性界面，可用于调节离子进入、溶剂化重组、界面分配、孔内迁移与释放。本文从限域传输和离子−孔道相互作用出发，综述了尺寸与溶剂化筛分、化学识别和动态门控三类机制，并比较其在同价单价、同价二价、异价及化学性质相近的多价离子体系中的作用及耦合关系。在此基础上，进一步区分选择性吸附、膜内富集与跨膜传输，讨论选择性定义、离子通量、进料组成、驱动力和运行时间对性能评价的影响。现有研究仍面临三方面问题，即不同测试条件下的性能数据缺乏可比性，运行状态下的离子溶剂化、位点占据与迁移过程缺少直接证据，以及复杂进料和长期运行中的功能稳定性不足。针对这些问题，本文总结了原位/工况表征、多尺度模拟和数据驱动方法的进展，并提出将湿态孔道结构、界面化学、传输动力学与过程性能相联系的研究思路，为发展高选择性、高通量且长期稳定的纳米多孔分离材料提供参考。

关键词：选择性离子分离；纳米多孔材料；限域筛分；化学识别；动态门控

For Review Only

Table of Contents graphic



For Review Only